AFRPL-TR-72-26

ELECTROLYTIC IGNITION SYSTEM FOR A MILLIPOUND THRUSTER

(CONTRACT FO4611-70-C-0070)

FINAL REPORT
JUNE, 1972

by

C.T. BROWN

UNITED AIRCRAFT RESEARCH LABORATORIES
UNITED AIRCRAFT CORPORATION
EAST HARTFORD, CONNECTICUT

"Approved for public release; distribution unlimited."

AIR FORCE ROCKET PROPULSION LABORATORY
DIRECTOR OF LABORATORIES
AIR FORCE SYSTEMS COMMAND
UNITED STATES AIR FORCE
EDWARDS, CALIFORNIA 93523

187

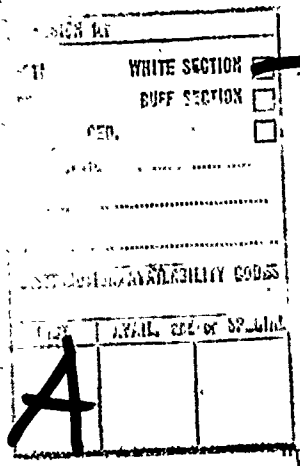

"When U. S. Government drawings, specifications, or other data are used for any purpose other than a definitely related Government procurement operation, the Government thereby incurs no responsibility nor any obligation whatsoever, and the fact that the Government may have formulated, furnished, or in any way supplied the said drawings, specifications, or other data, is not to be regarded by implication or otherwise, or in any manner licensing the holder or any other person or corporation, or conveying any rights or permission to manufacture,use, or sell any patented invention that may in any way be related thereto."

DOCUMENT CONTROL DATA - R&D

(Security classification of title, body of abstract and indexing annotation must be entered when the overall report is classified)

1. ORIGINATING ACTIVITY (Corporate author)	2a. REPORT SECURITY CLASSIFICATION
United Aircraft Research Laboratories	Unclassified
	2b. GROUP --

3. REPORT TITLE

Electrolytic Ignition System for A Millipound Thruster

4. DESCRIPTIVE NOTES (Type of report and inclusive dates)
Final Report

5 AUTHOR(S) (Last name, first name, initial)
Brown, Charles T.

6. REPORT DATE	7a. TOTAL NO. OF PAGES	7b. NO. OF REFS
June, 1972	168	12

8a. CONTRACT OR GRANT NO.	9a. ORIGINATOR'S REPORT NUMBER(S)
F04611-70-C-0070	
b. PROJECT NO.	AFRPL-TR-72-26
c.	9b. OTHER REPORT NO(S) (Any other numbers that may be assigned this report)
d.	

10. AVAILABILITY/LIMITATION NOTICES
Approved for public release; distribution unlimited

11. SUPPLEMENTARY NOTES	12. SPONSORING MILITARY ACTIVITY
	Air Force Rocket Propulsion Laboratory Edwards Air Force Base Edwards, California 93523

13. ABSTRACT

The United Aircraft Research Laboratories have conducted a research program under Contract F04611-70-C-0070, which had as its objective the development of an electrolytic ignition system for monopropellant-fueled millipound thrusters. The total program included: (a) the study of the mechanism of electrolytic decomposition of two hydrazine-based monopropellants; (b) optimization of electrolysis cell design based on data from (a);(c) electrolysis cell fabrication based on the design in (b); and (d) life tests on a millipound thruster incorporating the electrolysis cell.

The electrochemical decomposition of hydrazine-based monopropellants was studied as a function of propellant composition and electrode materials. It was found that a 77% hydrazine-23% hydrazine azide composition yielded the highest heat output with the lowest power input provided platinum was used as an anode and either platinum or 304SS was used as the cathode. The power requirements are a function of the electrical conductivity of the propellant.

Performance data was obtained on prototype engines incorporating the electrolytic ignition concept. Measurements were made at atmospheric pressure using both steady-state and pulsed ignition modes with 77% hydrazine-23% hydrazine azide as the propellant. The final test engine was run for a period exceeding one

14. KEY WORDS	LINK A		LINK B		LINK C	
	ROLE	WT	ROLE	WT	ROLE	WT
Electrolytic Ignition Monopropellants Hydrazine Hydrazine Azide Millipound Thrusters						

INSTRUCTIONS

1. ORIGINATING ACTIVITY: Enter the name and address of the contractor, subcontractor, grantee, Department of Defense activity or other organization *(corporate author)* issuing the report.

2a. REPORT SECURITY CLASSIFICATION: Enter the overall security classification of the report. Indicate whether "Restricted Data" is included. Marking is to be in accordance with appropriate security regulations.

2b. GROUP: Automatic downgrading is specified in DoD Directive 5200.10 and Armed Forces Industrial Manual. Enter the group number. Also, when applicable, show that optional markings have been used for Group 3 and Group 4 as authorized.

3. REPORT TITLE: Enter the complete report title in all capital letters. Titles in all cases should be unclassified. If a meaningful title cannot be selected without classification, show title classification in all capitals in parenthesis immediately following the title.

4. DESCRIPTIVE NOTES: If appropriate, enter the type of report, e.g., interim, progress, summary, annual, or final. Give the inclusive dates when a specific reporting period is covered.

5. AUTHOR(S): Enter the name(s) of author(s) as shown on or in the report. Enter last name, first name, middle initial. If military, show rank and branch of service. The name of the principal author is an absolute minimum requirement.

6. REPORT DATE: Enter the date of the report as day, month, year; or month, year. If more than one date appears on the report, use date of publication.

7a. TOTAL NUMBER OF PAGES: The total page count should follow normal pagination procedures, i.e., enter the number of pages containing information.

7b. NUMBER OF REFERENCES: Enter the total number of references cited in the report.

8a. CONTRACT OR GRANT NUMBER: If appropriate, enter the applicable number of the contract or grant under which the report was written.

8b, 8c, & 8d. PROJECT NUMBER: Enter the appropriate military department identification, such as project number, subproject number, system numbers, task number, etc.

9a. ORIGINATOR'S REPORT NUMBER(S): Enter the official report number by which the document will be identified and controlled by the originating activity. This number must be unique to this report.

9b. OTHER REPORT NUMBER(S): If the report has been assigned any other report numbers *(either by the originator or by the sponsor)*, also enter this number(s).

10. AVAILABILITY/LIMITATION NOTICES: Enter any limitations on further dissemination of the report, other than those imposed by security classification, using standard statements such as:

(1) "Qualified requesters may obtain copies of this report from DDC."

(2) "Foreign announcement and dissemination of this report by DDC is not authorized."

(3) "U. S. Government agencies may obtain copies of this report directly from DDC. Other qualified DDC users shall request through _____."

(4) "U. S. military agencies may obtain copies of this report directly from DDC. Other qualified users shall request through _____."

(5) "All distribution of this report is controlled. Qualified DDC users shall request through _____."

If the report has been furnished to the Office of Technical Services, Department of Commerce, for sale to the public, indicate this fact and enter the price, if known.

11. SUPPLEMENTARY NOTES: Use for additional explanatory notes.

12. SPONSORING MILITARY ACTIVITY: Enter the name of the departmental project office or laboratory sponsoring *(paying for)* the research and development. Include address.

13. ABSTRACT: Enter an abstract giving a brief and factual summary of the document indicative of the report, even though it may also appear elsewhere in the body of the technical report. If additional space is required, a continuation sheet shall be attached.

It is highly desirable that the abstract of classified reports be unclassified. Each paragraph of the abstract shall end with an indication of the military security classification of the information in the paragraph, represented as *(TS)*, *(S)*, *(C)*, or *(U)*.

There is no limitation on the length of the abstract. However, the suggested length is from 150 to 225 words.

14. KEY WORDS: Key words are technically meaningful terms or short phrases that characterize a report and may be used as index entries for cataloging the report. Key words must be selected so that no security classification is required. Identifiers, such as equipment model designation, trade name, military project code name, geographic location, may be used as key words but will be followed by an indication of technical context. The assignment of links, roles, and weights is optional.

hour using sixty cold starts. No degradation in performance was noted. The engine thrust was in the range 35-50 millipounds and characteristic velocities in the range 3800-4100 ft/sec were achieved. Ignition delay times were on the order of 30-70 msec, and the specific impulse was in the range of 190-205 sec. The energy requirement for ignition (cold start) is 15-30 watt-sec using a peak power of 100-130 watts.

AFRPL-TR-72-26

ELECTROLYTIC IGNITION SYSTEM FOR A MILLIPOUND THRUSTER

FINAL REPORT
(Contract F04611-70-C-0070)

June, 1972

by
C. T. Brown
United Aircraft Research Laboratories

"Approved for public release; distribution unlimited"

Air Force Rocket Propulsion Laboratory
Director of Laboratories
Air Force Systems Command
United States Air Force
Edwards, California 93523

id

FOREWORD

The work described in this report was performed at the United Aircraft Research Laboratories, East Hartford, Connecticut, for the Air Force Rocket Propulsion Laboratory under Contract F04611-70-C-0070 initiated July 15, 1970 and ending June 15, 1972.

Those who participated in the performance of the work under this contract were: Dr. C. T. Brown, Principal Investigator; Mr. D. G. McMahon, Program Manager and Chief, Chemical Sciences Section: Mr. S. Russell; Mr. T. Fondrk; and Mrs. I. Reed of UARL.

This work was conducted under the technical management of Captain Douglas D. Huxtable and Captain Ronald J. Meetin AFRPL/LKDP, of Edwards Air Force Base, Edwards, California. This technical report has been reviewed and is approved.

Ronald J. Meetin, Captain, USAF
Project Engineer

ABSTRACT

The United Aircraft Research Laboratories have conducted a research program under Contract F04611-70-C-0070, which had as its objective the development of an electrolytic ignition system for monopropellant-fueled millipound thrusters. The total program included: (a) The study of the mechanism of electrolytic decomposition of two hydrazine-based monopropellants; (b) optimization of electrolysis cell design based on data from (a); (c) electrolysis cell fabrication based on the design in (b); and (d) life tests on a millipound thruster incorporating the electrolysis cell.

The electrochemical decomposition of hydrazine-based monopropellants was studied as a function of propellant composition and electrode materials. It was found that a 77% hydrazine-23% hydrazine azide composition yielded the highest heat output with the lowest power input provided platinum was used as an anode and either platinum or 304SS was used as the cathode. The power requirements are a function of the electrical conductivity of the propellant.

Performance data was obtained on prototype engines incorporating the electrolytic ignition concept. Measurements were made at atmospheric pressure using both steady-state and pulsed ignition modes with 77% hydrazine-23% hydrazine azide as the propellant. The final test engine was run for a period exceeding one hour using sixty cold starts. No degradation in performance was noted. The engine thrust was in the range 35-50 millipounds and characteristic velocities in the range 3800-4100 ft/sec were achieved. Ignition delay times were on the order of 30-70 msec, and the specific impulse was in the range of 190-205 sec. The energy requirement for ignition (cold start) is 15-30 watt-sec using a peak power of 100-130 watts.

(THIS PAGE IS BLANK)

TABLE OF CONTENTS

LIST OF TABLES

LIST OF TABLES (CONTINUED)

LIST OF FIGURES

LIST OF FIGURES(CONTINUED)

LIST OF FIGURES (CONTINUED)

LIST OF FIGURES (CONTINUED)

LIST OF FIGURES (CONTINUED)

LIST OF SYMBOLS

A_t	Area of Throat (in^2)
C_F	Thrust coefficient
C^*	Characteristic Velocity (ft/sec)
ΔE	Activation Energy (kcal/mole)
F	Thrust (lbs) or (mlbs)
I_{sp}	Specific Impulse (sec)
I	Current (amps)
i	Current Density (ma/cm^2)
P_c	Chamber Pressure (psia)
R	Gas Constant (cal/°K/mole)
T_c	Chamber Temperature (°F)
T	Absolute Temperature (°K)
t_{90}	Pressure rise time (msec)
t_{10}	Pressure tail-off time (msec)
η	Overpotential (mv)
κ	Specific conductivity ($ohms^{-1}cm^{-1}$)
$\dot{\omega}$	Mass Flow rate (lbs/sec)

SECTION I
INTRODUCTION

The advantages of monopropellants over bipropellants for specific rocket engine applications have long been recognized. These advantages include the simplicity and reliability of the system resulting from elimination of problems and inefficiencies associated with residual fuel or oxidizer at other than the design mixture ratio for bipropellant systems. Consequently, a considerable amount of research and development has been carried on during the past fifteen years to develop suitable monopropellants. This work has included studies of the quaternary ammonium salts (cavea-type (compounds), hydrogen peroxide, n-propyl nitrate, tetranitromethane, hydrazine and a variety of other materials. In most instances, however, the simultaneous requirements of high performance and low shock sensitivity have eliminated many candidate propellants.

Among the various candidate monopropellants, hydrazine was recognized early in its use as presenting a good compromise between the requirements of performance and safety. Initial work was hampered by the need for relatively high bed temperatures to initiate the hydrazine decomposition in a reaction chamber. Interest consequently lagged. However, the development of spontaneous low-temperature catalysts for monopropellant hydrazine has stimulated a considerable resurgence of interest during the past decade in the use of hydrazine and hydrazine-based mixtures as monopropellants for various applications in thrusters and gas generators and has lead to the recent successful use of hydrazine monopropellant thrusters for satellite station-keeping operations.

One major problem remaining with the low-temperature catalyst for hydrazine-based monopropellants is the present requirement for substantial amounts of critical noble metals in systems which must achieve multiple cold starts. A number of alternatives to the use of noble metal catalysts for ignition have been suggested. In particular, the need for rapid ignition with high reliability over a wide range of temperatures and engine sizes has resulted in interest in the development of an electrochemical means of ignition for hydrazine-based monopropellants in small thrusters. The development of an electrochemical ignition system circumvents problems associated with catalyst degradation caused by spallation, sintering, crystallite formation, and poisoning. In addition, such an ignition method has a potential advantage of reduced chamber volume. An ignition system of this general type has been demonstrated on a small scale (Ref. 1), but substantial design information was still needed before an optimized system could be fabricated and tested.

A more complete technical program directed toward obtaining such design information has been completed during the past year and a half at UARL under Contract F04611-70-C-0070. The program had as its objective, the development of a millipound thruster using electrolytic decomposition of the propellant as the ignition device. The program comprised three phases which are: Phase I, Study of the mechanism of electrochemical decomposition of the propellants; Phase II, Design and Optimization of an

electrolytic cell based on the data obtained in Phase I; and Phase III, Fabrication and evaluation of an electrolytically ignited millipound thruster designed for propellant flow rates in the range 1 to 4 x 10^{-4}lbs/sec. The results for these Phases are discussed in the following sections of this report.

SECTION II

PHASE I: MECHANISM OF ELECTROCHEMICAL DECOMPOSITION

The Phase I experimental program comprised three basic studies: (1) the evaluation of the ohmic losses that result from the resistivity (conductivity) of the propellants used; (2) the determination of polarization effects on various electrode materials as a function of the propellant/electrolyte used; and (3) electrolysis of propellant/electrolyte in order to determine the decomposition products formed and thus provide a basis for evaluating the theoretical heat output arising from the electrolysis.

1. ELECTRICAL CONDUCTIVITY OF CANDIDATE ELECTROLYTES

The electrolytic ignition concept is based on providing the heat for ignition by utilizing the heat of decomposition of the propellant. The rate of decomposition is a direct function of the current flow through the propellant; that is,current is the driving force for the process.

In order to achieve rapid ignition and at the same time minimize power it is necessary to have an electrolyte with as high an electrical conductivity as possible. Ohmic heating can represent a large power loss in the cell, and low conductivity severely limits the current available for direct-low temperature decomposition of the electrolyte.

Since the specific conductivity of pure hydrazine is on the order of 10^{-6} $ohms^{-1}$ cm^{-1} (ie, a resistivity of one million ohms per centimeter) (Ref. 2), it obviously cannot be used directly in an electrolytic cell. In order to raise the conductivity, it is necessary to use hydrazine-salt mixtures. Since little or no conductivity data was available on hydrazine-salt mixtures, this parameter was determined for electrolytes of interest.

a. Experimental Approach

(1) Materials

For the determination of electrolytic conductance, platinum electrodes were used. The electrodes consisted of two parallel sheets of platinum foil (each approximately one cm^2); in order to aid in eliminating polarization effects due to the current, the electrodes were coated with a layer of finely divided platinum black.

The specific conductances of the following materials were determined: propellant grade hydrazine, hydrazine + 2% ammonium nitrate, and two solutions of hydrazine and hydrazine azide, one containing 23% hydrazine azide and the other containing 2% hydrazine azide. The nitrate solution was prepared by adding two weight percent of ammonium nitrate to propellant grade hydrazine. The 2% hydrazine azide solution was prepared by dilution of 23% hydrazine azide solution.

(2) Apparatus

The study of the conductance of hydrazine and hydrazine-based solutions was accomplished by the use of a conductance bridge in which the essential component was a precision impedance comparator (General Radio Company). The other components were an adjustable resistance standard and a set of balancing capacitors. Capacitance decade boxes (Electronic Instrument Company) connected in parallel with the resistance standard provided an auxiliary variable capacitor.

A constant temperature bath (Precision Scientific Company) containing oil was used to maintain the solutions at the prescribed temperature.

Two H-shaped conductivity cells were used - one with an electrode spacing of 1.0 cm and one with a spacing of 7.0 cm -in order to accommodate a wide range of resistances.

(3) Procedure

The conductivity cells were calibrated using a 0.01 Demal solution of KCl of known specific conductance. A cell constant(K)was calculated from resistance measurements using the KCl solution according to the equation $\kappa = K R$ where κ is the specific conductance of the KCl and R is the measured resistance. This constant is then used to calculate the specific conductance of the hydrazine solutions. The resistance was measured at four frequencies, 1KC, 2KC, 5KC, and 20KC and plotted against $1/\sqrt{f}$. The true resistance was found by extrapolating the plot to infinite frequency. The specific conductance of each solution was found at three temperatures, 25°C, 35°C, and 45°C.

b. Results

The conductivity data for four propellants at three temperatures are summarized in Table I. It is apparent from these results that a small addition of a hydrazine salt has a large effect on the conductivity of the propellant. There is an increase of about two orders of magnitude for 2% nitrate and 2% azide . The use of the 23% azide provides another order of magnitude increase in the conductivity.

The fact that both the nitrate and azide mixtures have similar conductivities at similar concentrations indicates that the mechanism of conduction may be the same (i.e., both are completely ionized and the major conducting species is the $N_2H_5^+$ ion). The activation energies for the conduction process were determined from the equation:

$$\ln \kappa = \ln A - \frac{\Delta E}{RT}$$

where ΔE is the energy of activation for conduction in cal/mole, κ is the specific conductivity in ohm^{-1} cm^{-1}, and R is the gas constant expressed in cal/deg K/mole, A is an empirical constant, and T is the temperature in deg K. A plot of log κ versus 1/T yields a slope of $-\Delta E/2.303$ R and thus ΔE can be calculated. The values for the energies of activation obtained from plots of log κ versus 1/T using data from Table I and illustrated in Fig. 1 are 10.0, 1.6, 2.9, and 1.3 kcal/mole for N_2H_4, N_2H_4 - 2% NH_4NO_3, N_2H_4 - 2% N_5H_5 and N_2H_4 - 23% N_5H_5, respectively. Although the high value of 2.9 for the 2% N_5H_5 is unexplained, it is apparent that the values for the energies of activation for the propellants containing the two additives studied are all substantially smaller than the value of 10 kcal/mole measured for N_2H_4. These results add further credence to the premise that the conduction mechanisms are similar for these additives. It is not necessary to screen a further large group of additives for the sole purpose of finding one which will greatly increase the conductivity of the propellant.

The use of the azide additive is preferred over the nitrate, since the azide decomposition products should be the same as those for neat hydrazine. Other additives such as nitrates would be expected to yield a wide variety of products.

Thus the use of an electrolyte such as the 77% N_2H_4 - 23% N_5H_5 mixture can be expected to conduct sufficiently to maximize the current flow for a given applied voltage and minimize the ohmic losses in the cell.

The second major factor that can contribute to an increase in power requirements is the extra voltage that must be used to increase polarization effects at the electrode-electrolyte interface where current is flowing. The following section of the report describes studies that were performed in this important area .

2. POLARIZATION OF ELECTRODES

Electrode polarization or voltage loss (overvoltage) due to electrode-electrolyte effects becomes important as the internal resistance effects are minimized. The polarization effects are due to a slow step in the electron transfer reaction in the vicinity of the electrode surface (activation polarization) or to slow diffusion of a reacting species into the electrolyte-electrode zone (diffusion polarization). The latter case is usually important when the reacting species is present in low concentrations in an electrochemically inert solvent. This solvent can be an electrolyte whose ionic species are not discharged in the normal range of applied potentials. Since the source of reactants in this case is hydrazine azide, which is present in excess, there should be little or no diffusion polarization.

The preferred methods for electrode reaction studies are based on potentiostatic (controlled potential) or galvanostatic (controlled current) techniques. In either case, a noncurrent-carrying reference electrode is used to monitor potential changes at the anode and cathode separately. In the studies reported herein, a stable reversible reference electrode developed earlier at UARL was used.

Potentiostatic devices are used to maintain a set potential between the reference electrode and the electrode under study and provide the current necessary to maintain this potential. The system can be rapidly scanned and it is particularly applicable to anode polarization studies where, for example, the presence of an oxide film or other protective films on the anode is easily detected as a plateau in the current-voltage curves. The applied voltage in excess of the natural voltage of the system can thus be measured in terms of the current flow through the cell. This excess voltage may be termed the voltage loss due to reactions at the electrode surface. Another voltage loss which may also be present near the electrode surface is due to pseudo-resistances that occur because of films that form on the surface of the electrode or the layers of non-reacting ions that may build up near the electrode surface.

Measurements of pseudo-resistance effects were accomplished in this program by applying a known constant current to the cell (galvanostatic techniques). The circuit is opened by means of a mercury-wetted reed switch and the potential decay is noted as a function of time using an oscilloscope as a recorder. Since transition times for resistance effects are on the order of 10^{-5} sec, while decay of the potential due to capacitance effects in the electrolyte layer near the electrode surface and/or diffusion of reactant species requires times of the order of 10^{-4} to 10^{-3} sec, both effects are determined in the same experiment.

Descriptions of both the potentiostatic and constant current devices are contained in subsequent paragraphs.

a. Experimental Approach

(1) Materials

The electrolytes used were propellant grade hydrazine, 77% hydrazine - 23% hydrazine azide and two dilutions of the latter containing 12% hydrazine azide and 4.8% hydrazine azide. Hydrazine with additions of 5% and 6% ammonium nitrate was also used.

The first set of electrodes tested were flat plate electrodes of known surface area (approximately 2 cm^2). Each was spot welded to a wire of the same material. Electrode materials used were platinum; the stainless steels, AM350, 304SS and 17-7PH; two aluminum alloys, AA1100 and AA6061-T6; HS1414, a gold-nickel brazing alloy; nickel; and Inconel 600. (The latter two materials were tested in 77% hydrazine - 23% hydrazine azide only).

The second set of electrodes were rods of varying diameters. They were adjusted in the cell so that a surface area of 2 cm^2 was obtained in all cases. Materials for these electrodes were the three stainless steels cited above and two grades of graphite-pyrolytic and spectrographic.

(2) Apparatus

The cell used in polarization experiments is shown in Fig. 2 (Item 1). This cell consists of three compartments, and was designed to eliminate electrolyte resistance effects through the use of a Luggen probe, which consists of a capillary tube extending from the center compartment to one of the side compartments. Thus, problems due to the wide range in conductivity of electrolytes should not effect the results of polarization experiments. A fritted disk below the center chamber allows nitrogen to be bubbled constantly through the solution in the cell. Three electrodes are used: (1) the test or working electrode in the center chamber; (2) the counter-electrode which was always a spectrographic grade graphite rod located in one side chamber; and (3) a saturated calomel reference electrode in the other side chamber which fixes the potential of the electrode with respect to the hydrazine-containing electrolyte. The solution in the cell was maintained at a constant temperature, 28°C,by immersion in an oil bath [Precision Scientific Company (Fig. 2,Item 10)

Current-voltage relationships were measured by means of a Wenking potentiostat (Fig. 2, Item 8), a Wavetek Model 116 Function Generator (Fig. 2, Item 7) and a DC Offset Device (Fig. 2 Item 6). A triangular wave output from the function generator was fed to the potentiostat to provide the control signal between the referencing and working electrodes. The initial voltage of the triangular wave output was set by means of the DC offset device. The voltage range and sweep rate were set by means of the function generator amplitude and frequency controls, respectively. The potentiostat automatically provides the current flow between the working and counter electrode necessary to maintain the potential difference between the reference and working electrodes. The reference versus working potential was monitored using a Kiethly Model 200B Vacuum Tube Voltmeter (Fig. 2, Item 5) and the current-voltage relationships were recorded using a Tektronix Type 536, X-Y oscilloscope using Type G differential plug-in units (Fig. 2, Item 9). Permanent records of the traces were made using a C-12 Polaroid camera assembly.

Potential-time relationships were made using a regulated power supply [Dressen and Barnes model 62-112 (Fig. 2, Item 4)] in conjunction with a decade resistor [General Radio (Fig. 2, Item 2)] to maintain a constant cell current. A mercury-wetted reed switch (Fig. 2, Item 3) was used as a triggering device for the current output. The oscilloscope was used to record the voltage-time relationship using the Type G differential plug-in unit for voltage, and a Type T, time base generator, plug-in unit for time.

(3) Procedure

(a) Current-voltage

The cell was filled with 40 ml of the electrolyte solution and placed in the oil bath at 28 C. The electrodes were immersed in the electrolyte to the proper depth and connected to the potentiostat and voltmeter. The function generator was always set to give a triangular wave pattern, a span of one volt, and a frequency of 0.03 cycles per second equivalent to a scanning rate of 400 mv/min. The initial voltage was set to the rest potential of the cell using the DC offset device. Once vertical and horizontal

adjustments on the oscilloscope had been made, a five-minute picture was taken for both the anodic and cathodic process.

From the pictures, points were plotted of the overpotential versus the logarithm of the current density (milliamps/cm^2) to provide a direct comparison of the different electrodes and electrolyte solutions.

(b) Potential-Time

The cell was set up in the same manner as for the current-voltage runs, and leads were connected from the electrodes to the voltmeter and regulated power supply. The leads from the power supply were connected to the working and counter electrodes with polarity appropriately adjusted to make either anodic or cathode runs. Currents of 10 ma, 50 ma, 75 ma, and 100 ma were set by the power supply and a resistance box for each of the currents used. The horizontal time control on the oscilloscope was set at 0.05 millisec/cm or less in order to give a smooth curve. The mercury-wetted reed switch assembly is provided with a time delay which first triggers the oscilloscope and after 0.8 milliseconds connects the power supply to the cell. Pictures of the traces wereusing a 10-second exposure.

(c) Potentiostatic Results

(1) Preliminary Survey

The potentiostatic technique, described above, is a rapid method for determining the voltage losses of a given electrode-electrolyte combination due to reactions taking place at the electrode surface. Effects of the bulk electrolyte such as electrical conductivity, are eliminated since the experiments are run very rapidly and the potential is measured very close to the electrode surface.

These experiments were designed to determine the best electrode-electrolyte combinations in term. of voltage losses for both the anodic (oxidation) and cathodic (reduction)processes.

The anodic polarization curves for the eight materials and three electrolytes used in the initial studies are illustrated in Figs. 3-10. Later data obtained for Inconel 600 and nickel in 77% hydrazine-23% hydrazine azide are shown in Fig. 11. Using the criterion that the best electrode-electrolyte combination is the one that provides the maximum current at the minimum overpotential (applied voltage) it is possible to draw several general inferences in terms of both the electrolyte and the electrode material. The current density achieved at an applied potential of one volt (1000mv) was used in order to compare the relative merits of candidate anode materials for each electrolyte studied. This data is summarized in Table II.

With only one or two exceptions the materials fall into three distinct groups; first Pt, HS1414, Ni and graphite; second, the stainless steels (17-7PH, AM350, and 304SS) and Inconel 600; and, third, the two aluminum alloys. The first group represent metals with good polarization characteristics as anodes in all three electrolytes. (The only exception to this is graphite in propellant grade hydrazine.) The remaining two groups of metals do not appear to have good anodic properties. This is especially true of the aluminum alloys.

With respect to the electrolyte used, the anodic polarization increases in the order hydrazine - 23% hydrazine azide; hydrazine - 5% hydrazine nitrate; and propellant grade hydrazine. Exceptions to this effect are noted for the polarization of the aluminum alloys which show very little difference in all three electrolytes. (Figs. 9 & 10) It also appears that 17-7PH is less polarized in the nitrate propellant than in the azide. (Fig. 3)

The general shape of the polarization curves provides information on the effect of the electrode surface on the electrochemical processes. The formation or dissolution of films on the electrode surface is usually indicated when current plateaus or peaks are noted. The relative smoothness of the anodic polarization plots in hydrazine azide and hydrazine nitrate indicates a lack of surface inhibitation of the anodic decomposition process. Slight dips exist in the hydrazine curves for 17-7PH (Fig. 3) and graphite (Fig. 8) at an overpotential of about 500 mv indicating the formation of an intermediate species on these surfaces. A pronounced double oxidation peak is noted on AA6061-T6 in hydrazine nitrate (Fig. 10) indicating very complex reaction on this surface. The process on AA1100 also appears to be highly inhibited since there is a sharp break in the plots at an overpotential of about 400 mv. The presence of slight dips in the polarization curves, even at relatively high current densities, causes doubt as to the usefulness of the material under study, since the film formation indicated may become more pronounced over long periods of use.

The cathodic polarization curves for the materials studied in the three electrolytes are illustrated in Figs. 12-20 and include the results for nickel and Inconel. A summary of the cathodic current densities at an overpotential of 1000mv is shown in Table III. The data in Table III indicates that the cathodic process is in general less inhibited in hydrazine 23% - hydrazine azide than in the other two electrolytes with the exceptions of 17-7PH (as previously noted) and AM350.

The grouping of material in a given electrolyte is much different than in the case of anodic polarization. For instance the polarization of the stainless steels and the aluminum alloys may now be grouped together in the case of hydrazine - 23% hydrazine azide. The current densities at 1000 mv are also much higher when these materials are used as cathodes rather than anodes. It should also be noted that graphite as a cathode is no better than the stainless steels, while it

exhibits much smaller polarizations effects than these materials when used as an anode. Platinum, nickel, and Inconel 600 (Fig. 20) all exhibit low cathodic polarizations.

The shapes of the polarization curves in hydrazine - 23% hydrazine azide indicate a marked inhibiting effect at lower current densities for 17-7PH (Fig. 12), HS1414 (Fig. 15) and graphite(Fig. 17) and a definite plateau for AA1100 (Fig. 18). Less pronounced dips in the polarization curves are also present in the case of 304SS (Fig. 13) and AM350 (Fig. 14). As mentioned above the presence of these variations in the polarization curves indicates that there may be some difficulties involving the long-term usefulness of these materials even though the overall polarization is low.

The materials that may be useful as cathodes include platinum and, with some qualifications, 17-7PH, AM350 and 304SS. The aluminum alloy AA6061-T6 has not been considered since its melting point (i.e., 1200°F) is probably too low for use in an engine. The aluminum alloys were primarily used in these studies for comparison with the precious metals and the iron and nickel base alloys. Materials with pronounced plateaus were eliminated since the presence of strongly adhering surface films was felt to be undesirable.

As a result of the preliminary survey, further testing was limited to hydrazine-23% hydrazine azide as the electrolyte and platinum, the stainless steels and graphite as the electrode materials. Platinum consistently exhibited the best characteristics as both anode and cathode, but it is an expensive material. The stainless steels may be good cathode materials if the surface effects noted above are not pronounced. Graphite may be a good alternative to platinum as an anode.

The stainless steels and graphite were investigated in more detail by comparing electrode geometry and surface cleaning effects and by using pyrolytic graphite as well as spectrographic grade graphite. The former material has a more regular surface than the spectrographic grade.

All materials were cleaned with fine emery paper followed by detergent cleaning, rinsing with deionized water, and air drying.

(2) Stainless Steel: Surface and Geometry Effects

Current voltage polarization data was obtained using rod electrodes in a 23% hydrazine azide solution in the same manner as previously described. Comparison of the data between cleaned rod and flat plate electrodes show that anodic polarization of 304SS and AM350 is similar in the two cases, but that the 17-7PH rod stock was much less polarized than flat plate stock. The polarization plots shown in

Fig. 21 for 17-7PH include data for the flat plate stock cleaned in the same manner as the rod stock as described above. The initial polarization of the 17-7 PH rod stock is very high up to an overpotential of about 600 mv . Following this point, there is an abrupt rise in current which accounts for the improved behavior. This curve indicates existence of a passive film which is removed at high overpotentials. Repeated runs yielded erratic results. In some cases the passive state was retained up to overpotentials of 1200 mv, while in others a high current was obtained after 600 mv. Apparently, there is a condition of unstable passivity in this electrode-electrolyte combination which makes the usefulness of 17-7 PH doubtful.

Cathodic polarization of stainless steel rod electrodes in 77% hydrazine -23% hydrazine azide indicates similar behavior for 304SS compared to the flat plate stock but erratic results for 17-7 PH. The polarization on AM350 showed slight improvement when the flat plate stock, previously used, was cleaned in the same manner as the rod. The cathodic polarization curves for AM350 are shown in Fig. 22. The shapes of the three curves are similar, but the rod stock indicates a limiting current at 88 ma.

The data for AM350 and 17-7 PH rod stock was repeated many times and in most cases inconsistent data was obtained. The cathodic data for AM350 varied over a fairly limited range (i.e., from 50-90 ma/cm^2 at η = 1000 mv) with no regular pattern. However, the anodic AM350 data fell into two distinct groups, one set at about 17 ma/cm^2 and the other at about 50 ma/cm^2. A summary of this data is shown in Table IV. Typical current-voltage curves for the two cases taken directly from the oscilloscope traces are shown in Fig. 23B. Traces similar to these were also obtained for 17-7 PH in both the anodic and cathodic case. It was found that cleaning of AM350 prior to use could, in most cases, yield a much lower polarization, but 17-7 PH yielded inconsistent results in spite of the use of cleaning procedures. Therefore, 17-7 PH was eliminated from future studies.

(3) Pyrolytic versus Spectrographic Graphite

The anodic and cathodic polarization curves for spectrographic grade and pyrolytic graphite in 23% azide solution are shown in Figs. 24 and 25, respectively. The anodic polarization of the two types of graphite are similar, but pyrolytic graphite indicates a 35 percent improvement in current density at an overpotential of 1000 mv.

The cathodic polarization is extremely high for both graphites and shows a definite "passivation" plateau in each case. (The more regular surface of pyrolytic graphite is more strongly affected than is that of spectrographic grade.) Because of this behavior, graphite has been eliminated as a candidate cathode material.

(4) Effect of Azide Concentration

The polarization curves of 304SS, AM350, platinum and pyrolytic graphite were measured as a function of azide concentration to ascertain if there is an optimum concentration in which polarization and conductivity effects can be traded off. The optimization of these effects would be important in a practical ignition cell configuration where resistance effects will play an important part in determining the power necessary to achieve ignition.

The anodic polarizations of 304SS, AM350, platinum and pyrolytic graphite as a function of azide concentration are shown in Figs. 26 through 29. The anodic current densities achieved at an overpotential of 1000 mv for each material at the three azide concentrations studied are summarized in Table V. The anodic data indicate that the polarization of pyrolytic graphite compares favorably with platinum and that pyrolytic graphite can probably be used as an anode material in an electrolytic cell. It is also apparent that the anodic polarization is a much stronger function of azide concentration for platinum and pyrolytic graphite than for either 304SS or AM350 and that the polarization for the latter two materials are linear functions of azide concentration. This behavior is shown in Fig. 34, which is a plot of current density at an overpotential of 1000 mv versus azide concentration.

It is also interesting to note that AM350 as an anode exhibits (Fig. 27) a crossover point where the polarization is independent of azide concentration (about 8 ma/cm^2 at η = 700 mv) and that the reaction is strongly inhibited at higher azide concentrations at overpotentials less than 700 mv.

It was also found that the anodic behavior of AM350 was considerably different in 23% azide than previously measured (compare data in Table V with data in Table IV). The latter case was due to passivity, as previously shown in Fig. 23B. However, proper cleaning of AM350 surface using the procedure described above followed by repeated runs yielded consistent current densities on the order of 50 ma/cm^2 at η = 1000 mv. The same anodic polarization behavior for AM350 was also observed in 12% and 4.8% azide, as shown in Fig. 23A.

The cathodic polarization of 304SS, AM350, and platinum as a function of azide concentration is shown in Figs. 30 through 32. The cathodic current densities achieved at an overpotential of 1000 mv for each material at the three azide concentrations studied are summarized in Table VI, and plots of the current density data versus azide concentration are shown in Fig. 33. The data for 304SS and AM350 are almost linear functions of azide concentration. The data for platinum indicate an irregular behavior as evidenced by the extremely low value at an azide concentration of 12%. The cathodic data for platinum at 12% azide was repeated many times and found to be between 35 and 40 ma/cm^2 at η = 1000 mv in each case. If the

data at 12% azide is ignored, however, the slopes of linear plots for all three electrode materials are identical (i.e., $\simeq$ 4 ma/cm^2/% azide) indicating a similar concentration-controlled process in each case. It is apparent from the above data that the 304SS and AM350 are comparable to platinum as a cathode for the electrolytic cell and that there is no optimum azide concentration below 23%. Even though there is some irregular behavior as a function of azide concentration, none is beneficial. It appears that the most promising electrolyte would be 23% azide, the concentration corresponding to the lowest melting point of any hydrazine-hydrazine azide solution.

As a corollary to this investigation, an evaluation of the relative merits of a nitrate and azide electrolyte was also made. Polarization data was obtained for platinum, pyrolytic graphite, 304SS and AM350 in hydrazine - 6% hydrazine nitrate. This nitrate concentration is equivalent on a mole basis to a 4.8% hydrazine azide concentration. Since the cathodic process is expected to be the same for both azide and nitrate electrolytes (i.e., the discharge of the $N_2H_5^+$ ion), the cathode polarization should be similar in both cases. The polarization for the anodic process should be different, since the N_3^- ion is being discharged in the case of the azide and the NO_3^- ion in the case of the nitrate.

The anodic polarization curves are illustrated in Figs. 35 through 38 for 304SS, AM350, platinum, and pyrolytic graphite. A comparison of the current densities at an overpotential of 1000 mv is summarized in Table VII. On the basis of this data, it is apparent that the anodic polarization of all of the materials except platinum is significantly different in the two electrolytes. Evidently, platinum can catalyze the reaction of both the azide and nitrate anions equally well. The AM350 is less polarized in the azide propellant, while 304SS and pyrolytic graphite are less polarized in nitrate.

Cathodic polarization curves for 304SS, AM350, and platinum are illustrated in Figs. 39 to 41. The current densities at an overpotential of 1000 mv are summarized in Table VII. The cathodic polarization of AM350 and platinum were similar in both electrolytes as anticipated, since the $N_2H_5^+$ ion is involved in the cathodic reaction in both cases. The cathodic polarization of pyrolytic graphite was not included, since it has been shown to be highly polarized in all cases. The cathodic polarization in the two electrolytes was somewhat different for 304SS, but not enough to rule out the likelihood that both cathodic processes are the same.

There does not seem to be any clear-cut advantage for either propellant at these concentrations levels. No consistant pattern for $N_2H_5^+$ and either N_3^- or NO_3^- discharge was demonstrated by these experiments. However, it is known that propellants with high nitrate concentrations are quite unstable and would probably not have an advantage over the 23% azide. (For example, a 20% nitrate solution could not be used in the conductivity experiments because of its rapid decomposition in the presence of platinum).

c. Potential-Time Results at Constant Current

The potentiostatic current-voltage data previously discussed were obtained by rapidly scanning over a voltage range and, therefore, primarily indicates transient effects. This technique is most applicable to the characterization of surface effects and provides a rapid means of surveying a large number of electrode materials.

An alternative approach, the steady-state constant-current experiment, employing potential-time measurement at constant applied current more closely represents actual conditions of propellant electrolysis. By measuring the rapid potential rise upon application of the constant current and also determining the total steady-state over-potential, it is possible to obtain data in three important areas: (a) an initial rapid ($<10^{-5}$ sec) rise in potential corresponds to resistance effects uncompensated by the Luggen Probe (i.e., surface resistances as opposed to electrolyte resistivity); (b) the slope of the succeeding potential time curve yields information on the sequence of processes taking place as the electrode-electrolyte interface is charged; and (c) the true resistance-free total polarization at constant current can be obtained.

Potential-time measurements at constant applied current were taken for the original eight electrode materials in the hydrazine azide and hydrazine nitrate electrolytes. The measurements were obtained in less than 0.1 msec by rapidly applying a fixed current to the experimental cell and recording the potential-time relationship on an oscilliscope. Potential-time data was obtained at 1, 5, 10, 25, and 50 ma in hydrazine-23% hydrazine azide and hydrazine-5% hydrazine nitrate. Subsequent runs with the rod electrodes were made at 10, 50, 75, and 100 ma. The resulting maximum current densities were approximately 25 ma/cm^2 in the azide and nitrate.

The total resistance-free polarization data at constant current was adjusted for variation in electrode surface area. The order of preference of materials as both anodes and cathodes is based on $mv/ma/cm^2$ since all materials were run at a constant current in spite of differences in electrode surface area. The relative order of preference for cathode and anode materials based on this parameter is summarized in Table VIII and IX for azide and nitrate. The data for the anodic potential-time function is generally the same as the anodic current-voltage data in Table II. However, the cathodic potential-time data is considerably different than the current-voltage data in Table III. Graphite, HS1414 and the stainless steels, with the exception of 17-7PH, show about the same performance level at constant current. That is the cathodic surface effects previously noted on these materials do not have as much effect on the performance of graphite operated at steady-state while 17-7PH is considerably reduced in performance compared to the other materials tested under these conditions. These results confirm the suspicion that 17-7PH may become completely passivated when used on a prolonged basis, while this effect was not noted for AM350, 304SS and graphite.

Typical potential-time traces are shown in Fig. 42 for AM350, 304SS and pyrolytic graphite in 23% azide. During anodic polarization, no uncompensated resistance effects were noted for any material studied in the azide or nitrate electrolytes. Resistance effects in propellant grade hydrazine were so large that it was impossible to use this technique and obtain reliable data.

Cathodic resistance effects were noted in the case of 304SS only. In the example shown in Fig. 42, half of the total overpotential at 100 ma (50 ma/cm^2) is due to uncompensated resistance. Cleaning techniques were applied to 304SS to no avail; the resistance effect was always present.

In most cases, the potential transients were found to have a simple logarithmic relationship with time. On occasion, a curve similar to that shown for the anodic polarization of 304SS (Fig. 42) was obtained where the initial portion of the potential-time curve is linear. This portion of the curve may be due to charging of the electrode-electrolyte interface or removal of species adsorbed on the electrode surface and represents a voltage loss in addition to those due to electrolyte resistivity and the actual electrochemical discharge of a reacting ionic species. This effect was always present in the case of the anodic polarization of 304SS and could not be eliminated. It was found that this linear portion of the curve was sometimes present for AM350 and 17-7PH.

A series of experiments were run in 23% azide to determine the IR drop and polarization characteristics of several materials using the oscillographic recording technique. A summary of this data for both the anodic and cathodic process is shown in Table X. Experiments in which cathodic and/or anodic deposits were electrolytically placed on the surface prior to anodic and cathodic polarization, respectively, show that these deposits result in abnormally high polarizations due to the extra current necessary to remove these deposits before normal polarization sets in. This effect is particularly evident for anodic polarization of AM350 and 17-7PH. (The overpotential value of 1100 mv for 17-7PH shown in Table X is apparently due to a cathodic deposit, even though it was not deliberately placed on the surface). These materials seemed to yield inconsistent results. It is now evident that these results were due to the prior polarization history of the electrodes. In each case the initial linear portion of the potential-time curve was present when this high overpotential was noted for AM350 and 17-7PH. However, it has been found that platinum, 304SS, both anodic and cathodic, and pyrolytic graphite during anodic polarization only, are not subject to this prior history and are, therefore, more reliable electrodes (pyrolytic graphite as an anode only) for use in an electrolytic cell.

Constant-current total-overpotential data were also obtained as a function of azide and nitrate concentrations and are summarized in Tables XI and XII. In general, those results confirm the current-voltage data. Platinum and pyrolytic graphite are superior to the stainless steel as anodes at all concentrations, but the difference

diminishes as the concentration is lowered. There is little difference between platinum, AM350 and 304SS as cathodes; however, based upon the equilibrium data platinum is best at both 12% and 4.8% azide. This latter data does not confirm the current-voltage results which show high platinum polarization at 12% azide, but the constant current data is considered more reliable for the purpose of designing an electrolytic cell.

The polarization data for the 6% nitrate and the 4.8% azide is summarized in Table XII for a constant current of 50 ma (25 ma/cm^2). The cathodic polarization is similar in both electrolytes for Pt, 304SS, and AM350, but the data for pyrolytic graphite indicates a somewhat higher polarization in hydrazine nitrate. The latter is not surprising, since the cathodic process on graphite has always been highly inhibited. It is possible that both azide and nitrate are preferentially adsorbed on the graphite surface or even react chemically with the graphite. The cathodic process is expected to be the same in both cases since both electrolytes contain the $N_2H_5^+$ ion.

The anodic data indicates a large polarization difference in the two electrolytes for both platinum and pyrolytic graphite. The anodic process for 304SS and AM350 is similar for both electrolytes, indicating that the anodic process in this case is independent of the anodic species involved in the reaction or that only one anodic species is present in both electrolytes.

The above anodic data does not correspond to the current-voltage results summarized in Table VII. In the latter case, the anodic polarization of platinum was almost the same in azide and nitrate, while the rest of the electrodes indicated large anodic differences.

The polarization studies indicated that materials such as platinum and graphite are only slightly polarized when used as anodes and that 304SS and platinum are only slightly polarized when used as cathodes. All other materials either indicated a high polarization or, under certain circumstances, were passivated. It was also determined that the lowest polarization effects were achieved when the 77% N_2H_4-23% N_5H_5 was used as the electrolyte.

Since heat production is a function of the decomposition products of the electrolysis reaction, electrolysis experiments were performed to determine the composition of these products as a function of the electrode material used. The following section describes these experiments.

3. ELECTROLYSIS AND PRODUCT ANALYSIS

Electrolysis experiments were performed using a dual-column chromatograph to analyze gaseous and liquid products from both anode and cathode compartments for specially constructed cells. On the basis of this product analysis, the relative proportions of nitrogen, hydrogen, and ammonia were determined.

The electrochemical reactions for the decomposition of hydrazine azide (N_5H_5) may be written as follows:

Ionization of N_5H_5:

$$N_5H_5 \rightarrow N_2H_5^+ + N_3^- \quad (1)$$

Anode:

$$2N_3^- \rightarrow 3N_2 + 2e^- \quad (2)$$

Cathode with no NH_3 decomposition:

$$2N_2H_5^+ + 2e \rightarrow 2NH_3 + N_2 + 2H_2 \quad (3)$$

Cathode with complete NH_3 decomposition:

$$2\ N_2H_5^+ + 2e \rightarrow 2N_2 + 5H_2 \quad (4)$$

Overall with no NH_3 decomposition:

$$2\ N_5H_5 \rightarrow 2NH_3 + 4N_2 + 2H_2 \quad (5)$$

Overall with complete NH_3 decomposition:

$$2N_5H_5 \rightarrow 5N_2 + 5H_2 \quad (6)$$

A generalized overall reaction for the decomposition of N_5H_5 may be written as:

$$2N_5H_5 \rightarrow 2(1 - x)NH_3 + (4 + x)N_2 + (2 + 3x)H_2 \quad (7)$$

where x is the fraction of NH_3 decomposed. This equation is analogous to the generalized N_2H_4 decomposition reaction which is:

$$3N_2H_4 \rightarrow 4(1 - x)NH_3 + 6x\ H_2 + (1 + 2x)N_2 \quad (8)$$

The difference between the two decomposition reactions is the cathodic discharge of the $N_2H_5^+$ ion in N_5H_5 which requires the formation of H_2 in all cases, even if there is no catalytic decomposition of NH_3. For N_2H_4 the overall reaction can yield NH_3 and N_2 as the only products.

These equations indicate that four moles of gas should be formed per Faraday passed (assuming 100 percent Faradaic efficiency) if no ammonia is decomposed. This case corresponds to a 2/1 ratio of N_2/H_2. Five moles of gas will be produced per Faraday if all the ammonia is decomposed, corresponding to a 1/1 ratio of N_2/H_2.

Reactions other than those above can be written. J. J. Lander has postulated a large number of possible reactions for the electrolytic decomposition of hydrazine, hydrazine-water, hydrazine-hydrazine nitrate, and hydrazine-hydrazine azide in a series of three reports (Refs. 3 - 5). Some of the more attractive reactions in Ref. 5, involving hydrazine-hydrazine azide mixtures, are as follows:

$$N_5H_5 \rightarrow N_2H_4 + 3/2\ N_2 + 1/2\ H_2 \qquad (9)$$

where the cathodic reaction is:

$$N_2H_4 \cdot H^+ + e \rightarrow 1/2\ H_2 + N_2H_4 \qquad (10)$$

and

$$2N_5H_5 \rightarrow 2NH_3 + 3N_2 + N_2H_4 \qquad (11)$$

where the cathodic reaction is:

$$N_2H_4 \cdot H^+ + e \rightarrow NH_3 + 1/2\ N_2H_4 \qquad (12)$$

In the above reactions (9 and 11) the total moles of gas per Faraday would be 2.0 for the case where hydrogen was the only cathodic product, corresponding to a 3/1 N_2/H_2 ratio and 2.5 for the case where ammonia is the only cathodic product and is not further decomposed. If all the NH_3 is decomposed the total number of moles per Faraday would be 3.5 corresponding to a 1.33/1 ratio of N_2/H_2. Thus all the more practical reactions that involve the direct electrolysis of azide result in a total of more than one mole of gas per Faraday and N_2/H_2 ratios in excess of one.

If it is assumed that the reactions that take place are primarily due to the hydrazine (and water contained in the propellant) and that the azide ion is not discharged, but only provides high electrical conductivity, then the following reactions may be used:

Anodic

$$N_2H_4 + 4OH^- \rightarrow N_2 + 4H_2O + 4e \qquad (13)$$

Cathodic $\qquad 4H_2O + 4e \rightarrow 2H_2 + 4OH^- \qquad (14)$

Overall $\qquad N_2H_4 \rightarrow 2H_2 + N_2 \qquad (15)$

The total moles per Faraday is only 0.75 and the nitrogen/hydrogen ratio will be 0.5.

a. Experimental Approach

(1) Materials

Rod type electrodes of stainless steel and graphite and flat plate platinum electrodes previously described were used in these experiments.

In addition to the test electrolyte, 77% N_2H_4-23% N_5H_5 several standard solutions were used to calibrate the chromatograph. These were: hydrazine, hydrazine plus 1%, 5%, and 10% water; and hydrazine plus 1%, 5%, and 10% ammonia.

(2) Apparatus

The cell used for electrolysis is shown in Fig. 43. It consists of two cells joined by a glass frit (Fig. 43, Item 5), each cell having a gas inlet (Fig. 43, Item 8) located at the bottom. A rubber septem (Fig. 43, Item 4) for taking liquid samples, a reference electrode (Fig. 43, Item 3), and a working electrode (Fig. 43, Item 2) are fitted into the three openings of each cell. Lines from anode and cathode compartments of the cell are connected to a chromatograph by means of a special valving system. This system permits gas samples to be taken from one compartment while the other compartment is being vented.

The gas chromatograph used in these tests (Fig. 44) was developed at United Aircraft Research Laboratories and consists of two adsorption columns connected in series. One column separates gaseous ammonia, water, and hydrazine. The other column separates the permanent gases - H_2, N_2, and O_2.

The carrier gas used in this chromatograph is 91.5% He - 8.5% H_2 at a pressure of 50 psig and a flow rate of 170 cc/min. The carrier gas flows through a heat exchanger coil which serves to equilibrate its temperature with that of the hot-wire detectors before flowing through the reference chambers. From there the carrier gas flows through a heated inlet which is used to vaporize liquid samples and then through a 10 cc sample loop section of an automatic gas sampling valve(Beckman 102396). The sample is swept through the first column maintained at a temperature of 110-115 C. At this temperature, H_2, N_2, and O_2 are not retained, while ammonia, water, and hydrazine are separated in that order. Each component gives rise to a separate peak on the recorder corresponding to the output of the first detector.

After the gases have emerged from the sample side of the detector, they enter a second column which separates the H_2, O_2, and N_2 into its components at 30-32 C.

The oven (Fig. 44, Item 1) is a Blue-M model OV8A modified with a circulating fan and a themistor-Triac-IC temperature controller.

The control unit of the chromatograph (Fig. 44, Item 2) consists of a power supply and attenuators for the detector output. The recorder is a Hewlett-Packard Model 7100 B dual-pen strip chart recorder with built-in integrator.

A Kiethly Model 600 B vacuum tube volt meter is used to measure rest potential of the cell and operating potential during electrolysis. The power supply (Harrison Labs Model 6201 A) provides a constant current to the cell in conjunction with a General Radio decade resistor.

(3) Procedure

Calibration curves for liquid and gas samples were obtained using standard solutions for liquid samples and flowmeter calibrations for gas samples.

For any liquid a one microliter sample was taken with a Hamilton microliter syringe and injected into the rubber septum of the heated inlet; the plunger was depressed and withdrawn after five seconds. The peaks were recorded on the strip chart recorder and peak heights or areas calculated. Gas samples consist of mixtures of either nitrogen or hydrogen and the helium-hydrogen carrier gas.

In taking a gas sample, the gas mixtures were passed through the cell valving system (Fig. 40, Item I) and then through the 10 cc sample loop section of the automatic gas sampling valve. The sample switch on the chromatograph control unit opens the sample loop to the chromatograph. Peaks corresponding to nitrogen, hydrogen and ammonia are recorded, and areas and peak heights are calculated. Calibration curves were constructed by plotting the known percent of water, ammonia, or N_2 and H_2, versus peak height and peak area.

During actual test operations, each compartment of the cell was filled with 20 ml of 77% hydrazine - 23% hydrazine azide. The electrodes were set in place and lines were connected from the valving system to the cell.

First, a liquid blank sample was taken with the microliter syringe. The helium-hydrogen carrier gas was then bubbled through the cell in order to remove all air. Gas samples from the cathode compartment were taken by means of the automatic gas sampling valve until the nitrogen and oxygen peaks had gone down sufficiently to insure replicate runs. The last run before electrolysis was the cathode gas blank. Leads were then connected from the power supply and voltmeter to the electrodes, and rest voltages for anode and cathode were recorded. A current of 30 ma with a resistance of 200 Ω was set by means of the power supply. After the onset of electrolysis, gas samples from the cathode compartment were taken at 10 minutes, 25 minutes, and 40 minutes and from the anode compartment at 55 minutes, 70 minutes, and 85 minutes. Then, liquid samples were taken from anode and cathode compartments just prior to termination of electrolysis. Cell voltages during electrolysis were also recorded.

The percents of ammonia, nitrogen, and hydrogen for blank and electrolysis runs were determined from the calibration curves. From these results, the percent increase for each component was found and the total percents of ammonia, nitrogen and hydrogen produced were determined. This procedure was followed for each of the following electrodes: platinum, pyrolytic graphite rod, 304SS rod, and AM350 rod.

b. Results

The gas analysis and the polarization of each electrode couple are summarized in Tables XIII and XIV, respectively. The gas analyses show that the value for the fraction of ammonia decomposed, x, using the equations derived earlier in this section is zero for 304SS, AM350, and pyrolytic graphite, and is unity for platinum. The relative proportions for H_2, N_2, and NH_3 (where applicable) are in good agreement with the values predicted using the overall azide reaction (7). Apparently platinum catalyzes the thermal decomposition of NH_3 while the remainder of the materials do not. The total over-potentials (Table XIV) using identical materials for both anode and cathode indicate that platinum would be the best electrode material. If platinum were excluded, the best electrode couple would be pyrolytic graphite as an anode and 304SS as a cathode for a total cell voltage of 1.01v at 30 ma/cm^2. If platinum were used as a cathode with a pyrolytic graphite as an anode, the total polarization would be 0.97v.

The differences in potential between the Pt couple, and 304SS as a cathode with graphite as an anode are not large enough to be significant. The choice of electrode combinations using these three materials must be based on physical and corrosion characteristics in actual use as the electrodes in a working device.

The heat release will be the highest if 304SS is used as a cathode and platinum or graphite as an anode since these combinations provide the lowest over-potential and the largest proportion of ammonia during electrolysis.

SECTION III
PHASE II - DESIGN AND OPTIMIZATION OF THE ELECTROLYTIC CELL

The most promising electrode materials and propellant compositions selected as a result of the electrochemical measurements of Phase I were studied further in Phase II. These are Platinum, Pyrolytic graphite and 304 stainless steel as electrode materials and 77% hydrazine-23% hydrazine azide as the propellant. The objective of this second (and longest) phase of the experimental program was to design an engine/electrolytic cell combination that would provide rapid ignition, require low power input, and yield high combustion efficiency

The design goals for the electrolytic engine as stated in the contract were:

(a)	chamber pressure during steady state	±6%
(b)	ignition delay	50 msec (max)
(c)	tail-off	25 msec(max)
(d)	chamber pressure	40-200 psia
(e)	cold start	40 F
(f)	characteristic velocity	4000 ft/sec
(g)	mass flow rate	1-4 $x10^{-4}$ lbs/sec
(h)	thrust level	20-80 millipounds

Ignition delay is defined as the time required to go from 10% of equilibrium chamber pressure to 90% of equilibrium pressure. Tail-off is defined as the time required to go from 90% of equilibrium chamber pressure to 10% of equilibrium chamber pressure. The cold start temperature is defined as the initial bed (electrolytic cell) and propellant temperatures which are the same unless otherwise specified.

In order to meet these objectives, the experimental program for the second phase was devoted to: (1) preliminary measurement of heat release using different electrode combinations with the hydrazine - 23% hydrazine azide propellant, and the evaluation of the compatibility of several materials with the azide propellant, (2) the design of several different electrode configurations, (3) the incorporation of these designs into an engine-like device for testing, and (4) preliminary testing of each design for the evaluation of the power required, the sequence of fuel injection and power application, the combustion efficiency achieved in each device, and the effect of propellant temperature. Also included in item (3) were the evaluation of thermal beds and the use of catalysts in conjunction with these electrode designs.

The following paragraphs summarize the results of these studies which led to an optimum engine design that would be applicable to an extended testing cycle.

1. PRELIMINARY EVALUATION OF HEAT RELEASE AND MATERIAL COMPATIBILITY

a. Heat Release as a Function of Electrode Material

In order to evaluate the electrode materials in terms of heat release, hydrazine-

23% hydrazine azide was electrolyzed at high currents in an insulated (lucite) cell having a capacity of 10 cc and an electrode spacing of 1.4 cm. Heating rates and polarization characteristics were determined for the following electrode combinations at cell currents up to 8 amps (i.e., up to 1 amp/cm^2):

Anode	Cathode
Graphite	Platinum
Graphite	304SS
Graphite	Graphite
Platinum	304SS
Platinum	Platinum

The tests run with this cell were designed to determine the relative heating efficiencies of the above electrode combinations and to determine the relative contribution of N_5H_5 decomposition heating and of resistance heating in the cell. The cell configuration was such that large resistance effects were present. Polarization data was acquired in order to determine possible interaction between the anode and cathode processes under physical conditions much different from those used in the earlier electrode polarization studies. These interactions coupled with the much higher current densities to be used in a practical cell design would influence the ultimate selection of electrode materials for the electrolytic decomposition engine.

The heating rates, as determined by the temperature rise of the electrolyte, for the various electrode combinations at a constant electrolysis current of 6 amps are illustrated in Fig. 45. Even though these rates do not begin to approach those required for a practical ignition system, the relative rates are extremely important in determining the proper electrode combinations to be used in a practical cell design. It is apparent that the most rapid heating is achieved when platinum is used in the cell. The platinum-platinum combination appears to yield the best heating rates, but shows little advantage over the platinum-304SS or graphite-platinum combinations.

The possibility was considered that the difference in heating rates illustrated in Fig. 45 might be due to the difference in the heat capacities of the materials used. Platinum has a heat capacity of 0.03 cal/g/°C as compared to 0.12 cal/g/°C for 304SS and 0.25 cal/g/°C for graphite. The electrodes used were 0.005 in. thick platinum foil weighing about 3 grams, 0.05 in. thick 304SS weighing about 18 grams, and 0.125 in. thick graphite weighing about 17 grams. Thus the total cal/°C required for each of the electrodes used is 4.2, 2.1, and 0.09 for graphite, 304SS and platinum, respectively. Since the Pt-C, Pt-304SS and Pt-Pt combinations show a similar heating rate, it is difficult to ascribe the differences to heat capacity effects. Therefore, electrolysis efficiency appeared to be a major consideration in the rate at which the electrolyte is heated.

The heat released due to hydrazine azide decomposition is based on a calculated value of 619 cal/gram N_5H_5. Chromatographic analysis was used to determine the amount of hydrazine azide consumed during each run. These results were then used to calculate the amount of heat that should have been released by electrolysis of that amount of hydrazine azide. The efficiency of the electrolytic process can also be determined by comparing the analytical results with the amount of N_5H_5 that should have been decomposed using a value of 1290 ampere-seconds/g N_5H_5, and assuming a 100 percent current efficiency. This value is based on reactions confirmed by electrolysis at low currents as reported in Section II of this report. The heat release data is summarized in Table XV. The current efficiency of the decomposition process is also included in this table. In the cases where Pt was used for both electrodes or where the Pt-C combination was used, an apparent or indicated efficiency on the order of 400 percent was achieved. Much lower efficiencies were achieved for the other combinations, the worst case being C-C.

I^2R heating was calculated from the IR voltage drop for each electrode-combination at the current levels studied. These values, expressed in calories, are also include in Table XV. In each case where platinum was used, the I^2R heating was of the same order of magnitude as the decomposition heating - about 50 percent of the total heat evolved. Thus the real heating efficiency for N_5H_5 decomposition is about 50 percent. The trends should be enhanced when a cell configuration is used which more closely approximates an actual engine configuration. That is, the heating efficiency should increase in a smaller cell and the I^2R losses should be decreased.

The polarization characteristics of each electrode combination are summarized in Table XVI. The resistance-free polarization, polarization due to IR drop and the total polarization are tabulated for each electrode and for the whole cell. The IR drop is 60-80 percent of the total polarization of the cell. Thus, the major factor in reducing power requirements is minimization of this effect. For an electrode gap of 0.040 in. (0.1 cm) and a surface area of 5 cm^2 the resistance of the cell will be about 0.1 ohm rather than the 0.9 to 1.2 ohm experienced in the large cell. Since the IR drop can be adjusted by adjusting cell dimensions, the most important parameter remaining is the IR-free polarization of the cell. For convenience, the IR-free polarization of each electrode combination is summarized in Table XVII. The experimental results (as shown in Table XVII) indicate that the Pt anode-304SS cathode is the electrode combination which experiences the least electrode polarization as a function of cell current. It appears that in a cell with close electrode spacing, as opposed to the larger cells used in the polarization studies summarized in Section II of this report, there is a large interaction between the two electrodes. This interaction is magnified at higher currents. The results indicate that the electrochemical restrictions on this system are different than

those concerned with heat production, and a trade-off exists between the electrode combination that yields the maximum heat output (Pt-Pt) and the combination that requires the least power as a function of current (Pt-304SS). The Pt-304SS combination appeared to be the most attractive since its heat output is not much lower than that for Pt-Pt.

Thermodynamic calculations were also carried out in an attempt to predict the power necessary to raise the electrolyte (propellant) to the self-ignition temperature of approximately 900 F. According to the equation for the decomposition of hydrazine azide:

$$2N_5H_5 \rightarrow 2(1 - x)\ NH_3 + (4 + x)\ N_2 + (2 + 3x)\ H_2$$

(where x is the fraction of NH_3 decomposed) the heat release on decomposition of azide will be 46.4 kcal/mole if x = 0 and 35.4 kcal/mole if x = 1. The theoretical heat output will thus be 619 cal/g of N_5H_5 decomposed assuming no NH_3 decomposition. The heat necessary to bring the propellant temperature from ambient to 900 F is estimated to be 495 cal/g. This value is based on the heat capacity of hydrazine since heat capacity data is not available for the 77% hydrazine-23% hydrazine azide mixture. The heat necessary to bring one gram of propellant to 900 F is equivalent to the passage of approximately 0.800 Faradays/mole or 1,030 amp-sec/g through the cell. This requirement may also be expressed in terms of power needed using the conversion factor that 860 cal is equivalent to one watt-hour. Thus, 0.52 w-hrs/g is required to heat the propellant to 900 F.

This power requirement does not take into account any resistance heating and is based on standard heats of formation at 298 K so that it does not reflect the additional heat produced as the temperature increases. Also by using small cell volumes, it is possible to reduce the actual power to levels about a factor of 100 less than that given above, (i.e., about 180 watt-sec).

b. Material Compatibility

Besides evaluating materials for use as electrodes for the electrolytic process (Phase I), it was also necessary to evaluate the compatibility of materials to be used for other engine parts. In this case materials that indicate a high polarization using the hydrazine- hydrazine azide propellant are desirable.

The ability of a material to accelerate or retard the decomposition of hydrazine- based propellant on its surface can be measured electrochemically by determining the equilibrium rate of decomposition on an electrode surface during long-term, steady-state measurements. Potentiostatic techniques, previously described can be used for these measurements. During these measurements is it also possible to estimate the rates at which metals or alloys are dissolved in the propellant.

This technique has been used with propellant grade hydrazine with results that compare favorably with longer term gas evolution data.

Equilibrium polarization data as opposed to fast voltage sweeps have been obtained for platinum, pyrolytic graphite, 304SS, AM350, and 17-7PH in the temperature range 27-107 C (1-225 F). The linear portion of the log i versus overpotential plots at high overpotentials were extrapolated to zero overpotential to obtain the catalytic decomposition currents for each material as a function of temperature. Since it has been established that one Faraday is required to decompose one mole of N_5H_5 it is possible to calculate a decomposition rate in terms of weight per unit surface area per unit time for each combination of variables. The data thus obtained is summarized in Table XVIII.

Data for the decomposition rate for propellant grade hydrazine is also included for comparison in Table XVIII. It will be noted that the decomposition rates on Pt and graphite are about an order of magnitude greater for the azide than for propellant grade hydrazine. However, the decomposition rates on the stainless steels (which may be used for construction material) are not very different in the two propellants.

The validity of this method was established by comparing the UARL results (where possible) with literature values of decomposition based on long-term gas evolution data. This comparison is shown in Table XIX, where Ref. 6 and 7 are the UARL data. The general agreement is quite good with the exception of the Au-Ni brazing alloy where the UARL data is about an order of magnitude greater than the literature value obtained in Ref. 9.

The decomposition rates were plotted against reciprocal temperature and the slopes were used to calculate the activation energies. The anodic plots yielded a good straight line function for 304SS, 17-7PH platinum, and pyrolytic graphite, but erratic results were obtained for AM350 at higher temperatures. The erratic anodic behavior of AM350 is consistent with previous experience with this alloy. The cathodic plots were all reasonably good straight line functions. The values for anodic and cathodic activition energies are summarized in Table XX. Anodic activation energies derived from previous measurements in propellant grade hydrazine in the temperature range 120-140 F are included in Table XX for comparison. The activation energies are consistent with the anodic and cathodic polarization results reported in Section II of this report and are surprisingly low for the cathodic process (with the exception of 304SS). The anodic activation energies are also very low for platinum and pyrolytic graphite. The "catalytic" effect of platinum and graphite in hydrazine azide and the lack thereof on 304SS suggest that the latter may not be the best cathodic material to use in the electrolytic cell but is a good candidate as a material for other cell parts. The compatibility of the azide does not appear to be much worse than that of propellant grade hydrazine for the stainless steels, indicating that materials used for engine construction with hydrazine as a fuel may also be practical for use with hydrazine azide.

On the basis of qualitative results for the dissolution of metals in hydrazine and hydrazine-hydrazine azide it appears that the stainless steels and nickel are attacked and form a pink to red colored complex in hydrazine-based propellants. This is only true if they are used as anodes however. Analysis of the solutions after electrolysis has shown that nickel is preferentially dissolved from the stainless steels and is the cause of the pink to red color. This effect is not noted if the material is used as a cathode. The same results were obtained when Inconel 600 was used as a cathode. It thus appears that the stainless steels and Inconel 600 can be used as construction materials in the engine provided they are not exposed to anodic currents.

Heating rates as a function of electrode material appear to be maximized when the Pt-Pt combination is used for both anode and cathode; however, the platinum-graphite and platinum - 304SS combinations also indicate good heating rates when platinum is used as the cathode in this first case and as an anode in the second.

Polarization characteristics are such that the platinum-304SS combination requires the least power. However, the differences between the heat output and power requirement is not that much different for the two combinations. The platinum-graphite combination requires more power than the other combinations mentioned above and will not be further considered.

The material compatibility studies have shown that the stainless steels and Inconel 600 react similarly in the presence of both neat hydrazine and the 77% hydrazine - 23% hydrazine azide propellants. The more active materials such as platinum indicate propellant decomposition rates in the presence of the azide propellant at least an order of magnitude greater than in the presence of neat hydrazine. Inconel 600 and 304SS will probably be satisfactory materials of construction provided they are not exposed to anodic currents. This condition can be achieved if the chamber and nozzle are connected to the cathode side of the electrolytic cell.

2. ELECTRODE CONFIGURATIONS AND PRELIMINARY ENGINE DESIGN

a. Electrolytic Cell Design Requirements

Design concepts for several electrode configurations were generated prior to fabrication of an electrolytic cell. All the configurations were designed to fulfill certain basic requirements that were felt to be necessary to achieve rapid and sustained ignition. These requirements were:

(1) a large ratio of electrode surface area to propellant volume
(2) immediate and uniform dispersion of the propellant through the volume between the electrodes
(3) maximum thermal insulation of the cell from the engine body
(4) a finite and steady pressure drop across the electrode chamber

The maximum current per unit of applied voltage will flow through a cell of minimum electrode spacing. Maximum electrode area results in a low effective current

density (i.e., low polarization) for a given current flow. A cell design that will satisfy those requirements will result in a minimum power requirement from both the electrochemical and thermal aspects of the ignition process since the amount of heat released depends on the amount of flow per unit time, and the heat required to achieve ignition is minimized at low propellant volumes. Therefore, propellant volume must be limited in accord with achievable electrode current densities and attainable electrode surface areas. It is also evident that the amount of metal in the electrode must be kept small to avoid an additional undesirable heat sink. Utilization of fine wire screens or other large-surface structures that can be closely spaced is thereby indicated. Isolation of the electrodes from the body of the engine is also necessary in order to minimize heat loss due to conduction.

To prevent flooding of one region of the electrolytic cell and starving of another, it is necessary to ensure a uniform distribution of propellant across the entering face of the electrode structure. Uniform dispersion makes most efficient use of available electrode surface area and contributes to a smooth flow of propellant through the electrode structure. These factors afford the possibility for most rapid propellant ignition. Uniform propellant distribution can be enhanced through the use of a porous matrix that is also an insulator. Dispersion may also be accomplished with porous metal plates which act as part of one or more electrodes.

In order to provide suitable, steady flow rates of propellant under desired fluid driving pressures it is necessary to control the overall porosity of the electrode structure. This can be regulated by the choice of mesh and gauge sizes for electrodes, insulators, etc. Open-gas passages through the electrode structure must be sustained at all times in order to prevent the blowing out of raw fuel with the out-rushing gases. Both these design critiera should provide a steady-state back pressure that will provide smooth combustion of the propellant.

b. Basic Electrode Configurations

Several electrode configurations were designed and constructed. Four of these configurations are illustrated in Figs. 46-49. In the electrode configurations shown, electrode surface area was kept high and electrode bulk was minimized by using fine screens and wires and hollow tubes. Spacing between the electrodes was kept to a minimum. Electrical insulating materials were used to insure positive separation of electrodes, as well as to help limit the volume of entrained propellant. In the first configuration, Fig. 46 fine metal screen or thin metal felt was spirally coiled with glass cloth interlayers. In the second configuration, Fig. 47, small-gauge platinum wire which served as one electrode was isolated by a fence of fine ceramic rods from a hollow nickel tube which served as the other electrode. In addition, a glass liner was used to minimize heat loss to the outer metal shell in this configuration.

The third electrode configuration, shown schematically in Fig. 48, comprised 100-mesh nickel screen electrodes which were flame sprayed with porous alumina. The alumina insluation was found to be very adherent and did not spall when the screens were bent. A small piece of nickel metal felt 0.020 inch thick was pressed into the lower screen and was positioned directly over the fuel inlet tube. The felt thus forces the fuel to spread in a horizontal plane as it enters the electrode assembly.

A stacked screen or parallel plate configuration using alumina insulators is illustrated in Fig. 49. The fuel dispersion configuration (lower left-hand corner of the figure) is basically the same as that used previously (Fig. 48). However, the plate configuration has the advantage of ease of construction as well as providing a simple means of varying bed length by using plates of different lengths. The electrodes may also be connected in series and parallel combinations to accomodate various available voltages and current requirements.

c. Preliminary Engine Design and Testing

(1) Coiled Screens

Initial evaluation of the design concepts was performed using the coiled screen concept shown in Fig. 46. The test engines incorporating variations of the coiled screen concepts are shown in Figs. 50 and 51 and are designated CS-1, CS-2TB, and CS-3.

Platinum screens were used in combination with glass cloth insulation in the first of the three engines (CS-1). In the second and third engines, nickel screens were used with Refrasil cloth. The design of the second (CS-2TB) engine differed slightly from the others in that provisions were incorporated for a packed granular bed immediately after the electrolysis chamber. Its function was to serve as a thermal bed to enforce the complete decomposition of fuel droplets or vapors should these get beyond the electrolysis chamber. The third engine, CS-3, differed in that the cloth insulation was chemically pre-treated with partially reduced molybdenum trioxide and ruthenium metal. These catalytic materials were used to study the relative effects of treated and non-treated cloth insulators on the ignition properties of the propellant.

In order to perform ignition tests on these engines, it was necessary to construct a propellant delivery system, provide for automatic data acquisition and provide power to the electrolysis unit. The propellant delivery system is shown in schematic form in Fig. 52. Propellant is delivered by means of nitrogen pressure. Flow rate is monitored using a calibrated sight glass. The volume of this device was sufficient for several seconds of running time and was reloaded from the fuel tank between runs. All materials in the system were 304SS, glass or nylon tubing. Two filters are used to protect the inlet tube to the engine. The latter had an ID of 0.023 in. or 0.010 in. depending on the engine use. The upstream filter was capable of removing particles down to 70 microns in diameter and the downstream filter was effective down to 10 microns. The solenoid valve was especially designed for continuous duty for hydrazine and operates from a 28 volt-DC supply. All data were recorded on a Visicorder equipped with seven input channels. These input channels were used to record chamber pressure, engine current, engine voltage, chamber and outer wall temperatures and solenoid valve actuation (i.e., time of propellant flow). A 40-volt, 10 amp D.C. power supply was used to provide power to the cell. In all configurations, the body of the engine was the electrical connection for the cathode,

and the fuel inlet was the electrical connection for the anode. The fuel delivery system, engine mount and data recording system are shown in Fig. 53.

The first successful engine ignition was achieved using the electrode configuration shown in Fig. 46 which was incorporated in engine CS-1 (Fig. 50). Current, voltage, and chamber pressure were recorded on a high-speed visicorder, but for these tests no provision was made for internal temperature measurement. In order to effect rapid vaporization of the propellant, voltage was applied to the cell prior to initiation of propellant flow. For the first test, an applied potential of 5 volts was chosen. About 30 sec after initiation of propellant flow, the current rose to 8 amps (40 watts). At this point, hydrazine vapors were seen at the engine exhaust. The voltage and propellant flow were terminated and the system was held in this condition for 2.5 minutes. Voltage was again applied by slowly raising the voltage from zero in 0.5 volt steps, but in the absence of propellant flow. At 2v the current rose suddenly to 4 amps (8 watts) and ignition occurred. Ignition was sustained for about 30 sec until all the residual propellant in the engine was exhausted. During ignition, the chamber pressure rose rapidly to 80 psia followed by a slower rise to 110 psia. Because ignition occurred in the absence of propellant flow, it was not possible to determine the true mass flow rate. The delay in ignition after the initiation of propellant flow was probably due to flooding of the internal structure of the electrode assembly. The onset of ignition after a "soaking" period was probably due to a redistribution of the propellant in the electrode structure so that maximum vaporation could occur, coupled with the fact that the engine was, in effect, preheated by the initial power application.

A second set of engine tests were run using the original electrode configuration but with the following modifications:

(a) A screen was added to the top of the electrode assembly just below the combustion chamber since some glass cloth was injected into the throat during the first test.

(b) A glass (later nickel) porous plate was inserted at the inlet, or lower side of the electrode assembly, to help disperse the fluid flow (and thus prevent flooding).

This new configuration was tested and short ignition bursts were achieved, but a major problem was encountered through improper control of propellant flow which alternately flooded and starved the cell. Flooding was associated with ejection of vapor from the throat followed by good vaporization which resulted in ignition followed by ignition cut-off and then a repeat of the flooding condition. The short ignition periods were encouraging because they were accompanied by rapid pressure rise. The power requirement for this configuration was 16 watts (2v at 8 amp).

Another series of tests was run using the platinum wire configuration of Fig. 47 which was designed to elimiinate construction problems with the screen and glass cloth. The performance during these tests was similar to the second series of tests (described in the preceding paragraph) indicating that this configuration also had problems due to inadequate control of propellant flow. Since the coiled screen configuration used in the earlier engine test was simpler to construct, the platinum wire configuration of Fig. 47 was not used in subsequent tests. Tests were also conducted with an engine comprising a coiled screen electrolytic cell followed by a thermal bed composed of alumina granules (engine configuration CS-2TB, Fig. 51). It was determined that the use of a thermal bed (alumina granules) in engine CS-2TB (Fig. 48) did not significantly improve the performance of this general type of engine. It was also noted that there were no differences in performance when either nickel or platinum screens were used.

As these preliminary tests progressed, it became more apparent that ignition was instantaneous only when the engine was in a pre-heated condition (in excess of 200 F). This heat was probably derived from prior electrolysis or a previous ignition that had been slowly achieved. In a new engine configuration (CS-3, Fig. 47) it was then demonstrated that instantaneous ignitions could be obtained at room temperature if the glass cloth insulation used in this configuration was pre-impregnated with a partially reduced form of molybdenum trioxide or the incorporation of other catalytic materials such as ruthenium metal. (The amount of metal added was sufficiently small that the cloth retained its electrical insulating properties). Under these circumstances no ignition occurred without power on; delayed ignition (1-2 secs) occurred if power was turned on after the bed was pre-soaked with propellant; instantaneous ignition occurred when power was turned on before or simultaneously with propellant flow. The burn continued in all cases after power was turned off as long as fuel was supplied.

Preliminary data was also obtained on C* versus propellant flow for engine configuration CS-3. This data is summarized in Table XXI, and is shown graphically in Fig. 54. It will be noted that C* appears to approach a maximum at about 2×10^{-4} lb/sec propellant flow, which corresponds to a 40 millipound thruster.

The ignition delay and tail-off for the preceding engine designs were very long. Ignition delays were on the order of 200-300 milliseconds (Table XXI) whereas the target was 50 milliseconds. In general, the performance was encouraging, but these engine designs were such that maximum combustion efficiency could only be obtained at low mass flow rates and correspondingly low thrust.

The use of coiled screen concepts resulted in several difficulties. Shorting of electrodes became a common problem due to distortion of the entire assembly at higher temperatures. It was also found that only the lower part of the coils near the inlet were effective electrically since almost all the heat was produced in this lower zone. The remainder of the coils functioned more like a thermal bed. The use of high surface area was negated by the fact that the only effective current (at low current density) was over a very small portion of the entire assembly. Fuel distribution was therefore correspondingly poor since this concept depended on vertical wicking

of the propellant in the glass cloth insulation.

(2) Flat Plate Configurations

After the tests described in the preceding paragraphs, electrode assemblies and engines were built on a flat plate concept in an attempt to avoid the fuel distribution and low effective current problems. The basic flat plate concept shown in Fig. 48 was incorporated into the basic engine shell as shown in Figs. 55 and 56, and these configurations were designated FP-1TB and FP-2. Configuration FP-1TB was a combination of a flat plate and coiled screen design, while the FP-2 was a simple 2-plate electrolysis cell with the bottom plate insulated from the engine body. The coiled screens acted as a thermal bed. No impregnated catalyst was used in these engines.

A series of eight runs were made using the engine configuration FP-1TB, four of which yielded sufficient data to be reported. The results of these runs are summarized in Table XXII. Runs 24-3 and 24-5 yielded C* values in excess of 3,000 ft/sec at mass flow rates of 1.3×10^{-4} and 1.2×10^{-4} lbs/sec respectively. Plots of chamber pressure vs time and C* vs flow rate are shown in Figs. 57 and 58 respectively. The rise times were at least a factor of two less than any previously measured. These data indicated that good fuel dispersion was being achieved resulting in much more efficient combustion and rapid ignition. The structural integrity of the electrode assemblies was also maintained. Cold starts were achieved in all cases without the use of catalytic materials.

These results represented a distinct improvement over those achieved using the coiled screen concept and consequently the remaining development work was concentrated on variations of the flat plate concept. The combustion efficiency was still low at this point and it was also necessary to operate at very low flow rates which resulted in thrust levels on the order of 20 millipounds. The low combustion efficiency was tentatively attributed to excessive thermal losses in the bed above the plates and subsequent engines were designed to minimize these heat losses.

Engine configuration FP-2 (Fig. 56) and a further modification designated FP-3 were constructed to evaluate the effectiveness of thermal beds and also to provide cells that were more structurally sound. The flame-sprayed alumina used in configuration FP-1TB was abandoned since the alumina had a tendency to spall off at high temperatures. The use of nickel as an electrode material was also abandoned because of excessive corrosion.

Engine modification FP-2 (Fig. 56) was constructed with the bottom of the engine threaded for ease of assembly. A threaded retaining ring was used to secure the two electrode screens (304SS) and the Refrasil insulators. With this type of construction electrical shorts and degradation of the insulators were eliminated even after many engine firings.

In the modification of this engine design designated FP-3(Fig. 59),a cone-shaped pressure plate was used to minimize thermal losses from the screens. Also

as many screens as desired could be stacked to provide a thermal bed configuration.

The retaining ring used in these configurations allowed the adjustment of compression on the refrasil separator so that the fuel could disperse evenly throughout the cell volume.

A series of over thirty runs were made using engine configuration FP-2 and ten runs were made using engine configuration FP-3. (The latter engine was used without the thermal screens in order to obtain base line data for comparison with FP-2 which had a flat pressure plate). Selected data from the two series of runs are shown in Table XXIII. A plot of C* versus mass flow rate is illustrated in Fig. 60.

In general, the data is similar to that achieved in earlier tests using engine FP-1TB (Table XXII). However, with the FP-2 and FP-3 configurations cold starts were obtained and rapid pulsing was possible without loss of performance. In some cases as many as ten pulses were made with no appreciable degradation in performance. For instance, Run 6-5-1, the first pulse (2 sec) of a series indicates a C* of 2200 ft/sec run 6-5-10 (not shown in Table XXIII) indicates a C* of 2000 ft/sec. In some cases an improvement in performance during successive pulses was noted. For example, runs 5-3A-1 and 5-3A-3 shown in Table XXIII represent the first and third pulses each of about 2 sec duration for the FP-2 engine which was started cold. The third pulse indicates an improvement in performance. In most cases the duty cycle was 2 sec on and 6 sec off.

The plot shown in Fig. 58 indicates a high performance level at low flow rates. The basic engine size using two screens is equivalent to about a 20 millipound engine which can be operated at efficiency levels on the order of 90-95 percent. The data for engine FP-1TB is also included in Fig. 60 for comparison at flow rates on the order of 2×10^{-4} lbs/sec. This engine (with the thermal bed) did not provide as high an efficiency as did the FP-2 or FP-3 configurations, but at flow rates near 1×10^{-4} lbs/sec its performance was on a par with FP-2. FP-3 was not run at lower flow rates, but the data at the higher flow rates indicate better performance than the other configurations. Thus the change in design resulted in a higher C* at higher flow rates and it appears that some of this increase in C* occurred because the cone-shaped pressure plate reduced heat losses in the cell.

d. Advanced Engine Design and Testing

All the flat plate designs used screen electrodes that allowed the product gases to pass vertically through the cell possibly carrying undecomposed propellant into the chamber before the self-decomposition temperature was achieved. Low performance at higher propellant flows would be explained in this way. As a result a new cell design was used, which made it necessary to eliminate the conical support for structural purposes. This cell configuration (FP-4) is shown in Fig. 61. In this configuration the fuel inlet is brazed to a platinum plate, and serves as the anodic electrical connection to the cell. The anode is electrically and thermally insulated from the body of the engine by a nonporous alumina disc and an alumina tube in the inlet

pressure fitting. The cathode is a stainless steel screen which is wide enough to make good annular contact with the engine body. Thus the engine body serves as the cathode electrical contact. The nonporous alumina disk on top of the screen forces the hot gases to travel laterally through the cell and thus increases the residence time in the engine. The gases then pass along the engine wall, through the holes in the retainer and into the chamber.

(1) Optimization of Cell Dimensions

In configuration FP-6 the propellant had to spread in a lateral direction, and the volume of the free space in the matrix was a limiting factor to effective propellant distribution. [In earlier configurations (FP-1 through FP-3) the propellant could easily pass right through the entire cell]. Because of these new considerations, the effect of the matrix (i.e., Refrasil) on the resistivity of the cell was studied since the resistivity in the matrix is the factor which primarily controls the current flow and thus the heat production in the cell.

An AC bridge was used for determining the resistance so that resistance could be measured without simultaneously decomposing the electrolyte. Propellant was added to two cells of different diameters by means of a micro-burette that could be read to the nearest 0.01 cc. Resistances were measured and plotted as a function of propellant volume. A distinct break in the curve indicated when the cell was just filled. The resistance at this point is at a minimum value without the cell being flooded. (In the flooded condition, excess propellant is present which is not in the direct current path between the electrode and through the pores of the matrix).

The matrix in each cell was 0.016 in. thick Refrasil. The diameters of the two cells used were 1.0 in. and 0.5 in., respectively. The data obtained from the experiments are summarized in Tables XXIV and XXV. By knowing the free volume in the cell (measured as described above) the equivalent volume in the absence of the Refrasil it was possible to calculate the porosity of the Refrasil - i.e., 29% (Table XXV). When the measured resistance of the filled cell was compared to the resistance of the electrolyte in the total cell volume (again in the absence of the Refrasil) resistance factor for Refrasil of given thickness and diameter was obtained (i.e., 52.5 for the 1.0 in. cell, but only 17.5 for the 0.5 in. cell).

In addition to the above resistance factors (which decrease with cell diameter), the mass of propellant which must be heated was also reduced by a factor of four in going from a 1.0 in. to 0.5 in. cell diameter, and the time to fill the cell was reduced by the same factor. This last parameter coupled with the rate at which the resistance changes with the volume of the propellant in the cell may be the primary factor governing the igntion delay. As shown in Table XXV, the resistance of the 1.0 in. cell is more than ten ohms when the cell is nearly full and approaching the flooded condition of 0.06 cc of propellant. Thus the current is limited to a little over two amps if a 28v DC power source is used. When the resistance has dropped to less than 2 ohms (i.e., the current is greater than 14 amps at 28v DC), the cell is flooded. However, the 0.5 in. diameter cell has a resistance of 4.4 ohms when it is only two-thirds full

(i.e., 0.01 cc). The current flow at 28v at this point is 6.5 amps. This current level has been found to be sufficient to achieve the ignition provided the cell is not in a flooded condition.

The experiments and results described in the preceding paragraphs provide important design criteria for the electrolytic cell. The cell diameter must be small enough to reduce the resistance factor of the matrix to a point where low resistances (and thus high current flow) can be achieved before the cell is flooded. The minimum diameter to be used is determined by the ability to control propellant flow to prevent flooding prior to ignition. If the inherent ignition delay is 50 msec, the cell volume must be 0.01 cc for a propellant flow rate of 5×10^{-4} lbs/sec.

These results indicate that the volume of the electrolytic cell must be matched to the mass flow rate used.

The smaller cell diameters in the engines used previously (FP-1 through FP-3) were 0.25 in. to 0.30 in. and at the mass flow rate of 2×10^{-4} lbs/sec are flooded in less time than it takes for ignition to occur. The optimum cell diameter for this flow rate is 0.5 in.

(2) Evaluation of Heat Losses

Based on the foregoing evaluation of effect of cell dimensions, a 0.5 in. diameter engine was constructed and tested for performance. Details of this engine design (FP-4) are illustrated in Fig. 62. This design incorporates the cell shown in Fig. 61. This particular test cell was constructed to provide ease of access to the electrolytic cell by the use of a threaded pressure cap and a base of one-piece construction. The electrolytic cell was held in place by means of a threaded cap, beveled at the bottom. The beveled portion of the cap was provided with four holes to allow the hot gases to reach the chamber.

The mass of the engine was much larger than would be used in a flight-weight configuration; however, the high heat capacity (i.e., large heat loss) provided a means for separating effects of low chamber pressure as a result of heat losses from the effects of actual combustion efficiency in the cell.

Performance data was obtained using the FP-4 engine described above for a variety of mass flow rates, and is summarized in Table XXVI. The engine started easily with little or no condensed vapors at the nozzle. The pressure response was smooth. It was also noted that the rise time was strictly a function of the height of the current peak at ignition. The power input was limited to 8 amps and 40 volts by the power supply used in these experiments. Using the FP-4 configuration the current dropped to a nominal level of 0.2 to 0.5 amps. However, the engine continued to function after the power has been turned off. The duration of the current pulse was of the order of 200-300 msec. The rise time of the current peak could be correlated with the rise time of the pressure. If the engine was pulsed on a short duty cycle, it was not necessary to apply power again. The minimum off-time before

power must be used again was not determined since this particular experimental engine had a high heat capacity.

It will be noted from Table XXVI that the apparent performance of the engine incorporating the FP-4 cell is much less than desired. However, with the exception of runs at very high flow rates, the efficiency of the engine appears to be constant over a flow range from about 1.5×10^{-4} to almost 5×10^{-4} lbs/sec. Both the low values of C* and the apparent small dependence of C* on mass flow rate are due to large thermal losses in the cell. This fact was confirmed by adding thermal beds and a catalyst bed downstream from the cell and operating the engine at the same flow rate (Table XXVII). The most striking information was obtained through the use of an active catalyst bed downstream of the electrolytic cell. The fact that the characteristic velocity is the same with and without a catalyst (Runs 1-4 and 3-1, Table XXVII) indicates that the complete conversion of N_2H_4 to product gases had been achieved in the electrolysis process and that the low pressures were due to tremendous heat losses across the electrolysis cell itself.

The temperature profile of the FP-4 engine was measured using two configurations. The data is summarized in Table XXVIII and illustrated in Fig. 63. In the first configuration the thermocouple was placed directly above the cathode screen by drilling holes in the bottom of the retainer and the alumina disk. The presence of the thermocouple thus effects the residence time in the bed since the hot gases can pass directly through the cell without lateral motion toward the sides. Thus a decrease in performance is expected. It will be noted that, at this point, the temperature was 1500 F, even though the engine was firing erratically and condensed vapors were present at the nozzle. The remainder of the temperature measurements were taken using the normal cell configuration with the thermocouple positioned as shown in Fig. 62. The temperature profiles were encouraging since extrapolation of the curve in Fig. 63 to the center of the bed (i.e., the bottom of the porous separator) indicates combustion temperatures on the order of 1800 F in an engine in which the geometry of the bed had been disturbed due to the presence of the thermocouple. The temperature measurements in the chamber indicate a smooth profile except at the top of the engine where additional heat losses occurred. The temperature at the top of the bed (i.e., on top of the retainer) in the normal engine was between 800 and 1000°F depending on flow rate, while only about 200 to 300°F in the chamber itself. These measurements confirm the fact that very efficient combustion was taking place in the electrolytic cell and the major problem was heat loss across the cell itself due to the high heat conduction in the engine.

(3) Analysis of Power Requirements

An analysis was made of the power requirements for ignition using engine configuration FP-4. It was found that the area of the current-time curves for the cell could be used to accurately determine the number of coulombs (ampere-sec) passed through the cell during the ignition process. This information coupled with applied voltage data yields the total energy required for the ignition process.

Typical current and pressure-time traces are shown for runs 2-1A, 27-9A, and 5-9B in Figs. 64-66, respectively. Fig. 64 illustrates the case in which the propellant flow rate is too low for the engine size, resulting in a broad current peak and an initial pressure spike considerably higher than the equilibrium pressure. The latter effect is due to a flow surge when the propellant feed valve is opened. Fig. 65 illustrates the case when the propellant flow is too high. A large residual current is noted after ignition indicating excess propellant in the cell at all times. Proper flow and rapid ignition is shown in Fig. 66. The total energy required is low and there is almost no residual current. It is possible then to determine optimum flow by monitoring current as a function of time for any size engine.

The energy and power data for several runs on engine configuration FP-4 are summarized in Table XXIX. When the flow rate of the propellant is closely matched to the capacity of the cell, the current pulse width and the residual current after ignition (voltage on) both decrease resulting in a reduction of the energy required. At flow rates on the order of 4.0 to 4.5 x 10^{-4} lbs/sec the total ignition energy requirements are only 30 to 40 watt-sec. The peak power in most cases is in the 300-400 watt range.

The total ignition energy requirements of the electrolytic engine are quite low compared to the electrothermal engine concept as described, for example, in Ref. 12. In the latter case a one-minute warmup is required at a continuous drain of 5 watts prior to initiation of propellant flow resulting in a total energy requirement of 300 watt-sec. Thus the electrolytic system is an order of magnitude better on an energy basis.

(4) Final Engine Evaluation

Because of the high thermal losses in the FP-4 engine configuration a new engine was built (FP-5) which incorporates the same electrolytic cell design as shown in Fig. 4, but has a much smaller total mass (Fig. 67). The cell is encased in a stainless steel shell with 0.03 in. walls and an outside diameter of 0.5 in. The upper alumina disk of the cell contacts the top of the engine so that the combustion chamber has an annular configuration. The nozzle is offset near one edge of the engine top. The height of the engine exclusive of the fuel inlet is 0.2 in. which is essentially the height of the cell itself. However, the diameter of the cell is about 0.4 in. so that the cell capacity and thus the optimum flow rate is slightly smaller than the FP-4 configuration.

Performance and power requirement data for the new engine are summarized in Table XXX. The characteristic velocity of the engine (using the same cell configuration as FP-4) rose to the 3800-4100 ft/sec range at a mass flow rate of about 2 x 10^{-4} lbs/sec (40 millipound thrust). Thus, the low apparent efficiencies experienced with the FP-4 configuration were, as expected due to excessive thermal losses.

The energy requirements for the FP-5 engine were slightly higher than those for

engine FP-4 but were still in the 50-60 watt-sec range. The rise time was poor,but this effect was traced to poor fuel distribution in the cell due to uneven pressure of the top alumina disk (lucalox) on the cathode screen and thus on the Refrasil. Failure of the top alumina disk was also noted. Even compression on the Refrasil is required to eliminate the fuel pockets that allow excess fuel in the cell. This condition appeared to be the major cause of excessive rise-times.

Because of the difficulties outlined above, engine configuration FP-5 was modified by replacing the alumina insulators with fused quartz. This material has much better thermal characteristics than the alumina and is less prone to failure from thermal shock. In addition, the fuel inlet was shortened so that the fitting which seals and insulates the inlet tube from the rest of the engine (not shown in Fig.67) was only 0.25 in. from the bottom of the cell. This was done to decrease the residual fuel volume between the solenoid valve and the cell. This residual fuel is wicked into the Refrasil after the valve is closed and contributes to the long pressure tail-off times. In the previous design this fitting was located about 1.5 in.from the cell. The remainder of the parts were identical to those used in engine configuration FP-5. A series of over thirty runs was made on the modified engine (FP-5A) using mass flow rates in the range of 1.0 to 3.5 x 10^{-4} lbs/sec and engine operating times of 100 msec to 30 sec. No degradation in performance was noted and there were no part failures. The total accumulated firing time was 13 minutes. The performance data for the engine configuration FP-5A is summarized in Table XXXI. Although the tail-off time improved considerably (averaging about 130 msec), it was still greater than desired. The rise time was somewhat improved, but the data was scattered with the exception of the data at the high end of the flow rate range where several runs indicated rise times of less than 100 msec. In the mass flow rate range of about 1.0 to 3.0 x 10^{-4} lbs/sec, the characteristic velocity (C*) was, with a few exceptions, nearly constant in the range 2700-2900 ft/sec. As noted previously, this type of performance has been traced to excessive heat loss which is apparently very critical for these small thrust engines.

In order to minimize heat loss a second modification, FP-5B, was made to the basic FP-5 configuration. The design was changed by placing the insulated fitting for the inlet tube 1.0 in. from the bottom of the engine and reducing the thickness of the engine wall from 0.030 in. to 0.010 in. The fuel inlet valve was also placed to within 2.0 in. of the bottom of the engine.

The results of the tests on this engine configuration are summarized in Table XXXII. Data were obtained in the mass flow range of about 1.0 to 2.0 x 10^{-4} lbs/sec. In this flow range the characteristic velocity was in the range 3800-4100 ft/sec for room temperature starts. The C* versus $\dot{w}$ data is included in Fig. 60 for comparison with the other configurations. The rise time was improved in some cases but in general the tail-off time was poor (probably due to excessive inlet volume). However, the improvement in combustion efficiency (to about 90-95% of theoretical)substantiates the fact that excessive heat losses were the cause of the low combustion efficiency in the previous engine designs.

(5) Effect of Propellant and Bed Temperatures

The data accumulated using engine FP-5B was also used to evaluate the effect of reduced propellant and cell temperatures on rise time and combustion efficiency. Tests were also run under conditions where the cell temperature was considerably different from room temperature.

The results of these tests are summarized in Table XXXIII. The data have been arranged in order of increasing cell temperature and includes four tests at initial cell temperatures in the -55 to -15 F range, four tests at room temperature (72).

There is a trend toward lower rise times as the bed temperature is increased. The scatter in the rise time data and variations in the mass flow rate used make it difficult to draw quantitative conclusions, but the increase in propellant temperature from 32 F to 72 F when the bed temperature was raised from -15 F to 72 F did not appear to have a significant effect on the rise time. It is difficult to separate the two effects (i.e., bed temperature from propellant temperature) but in general, it appears that the heat transfer from the engine has a significant effect on the rise time.

A comparison of two typical pressure-time traces is shown in Fig. 68. The upper trace, run at an initial engine and propellant temperature of 72 F is that of run 1-11-3C (Table XXX); the lower trace (Run 1-11-4) was run at a propellant temperature of 32 F and a cell temperature of -15 F. The major difference in the two traces are the longer rise time at reduced temperature (130 msec) compared to room temperature (60 msec) and the gradual increase in pressure after the initial pressure rise at low initial temperature. The latter effect can be directly correlated with the initial cell temperature (i.e., the lower the temperature the longer the time required to reach the final equilibrium pressure). This effect would not be as extreme under normal operating conditions, since the cell temperatures used in these experiments were extremely low.

As a result of the Phase II effort it was found that a flat plate electrolytic cell concept was the most reliable. Mechanical difficulties were minimized and the flat plates coupled with a glass cloth separator provided the means for proper fuel distribution in the cell. By reducing the mass of the engine it was possible to minimize heat losses which were the major contributor to low combustion efficiency. As a result it was possible to repeatedly achieve rapid ignition (50-70 msec ignition delay) and characteristic velocities in the 3900-4100 ft/sec range. Total ignition energy requirements were in the 30-40 watt-sec range at 40v. Peak power was in the 300-400 watt range with a power pulse duration of about 100 msec. The basic design parameters using the flat plate concept described above were incorporated into a more sophisticated engine to be used in durability tests as described in the following paragraphs.

SECTION IV

DESIGN, FABRICATION, AND EVALUATION OF A PROTOTYPE MILLIPOUND THRUSTER

The results of the tests on the experimental engine described in Section III established the feasibility of the electrolytic ignition concept. The test series leading to the development of the FP-5B configuration demonstrated that this design is capable of sustained, efficient propellant combustion at a thrust level of 40 millipounds. The FP-5B design was consequently used as the basis for a more advanced prototype engine that could be used for extensive testing for reliability and endurance. The assembly procedure outlined below was developed by assembling and testing six experimental engines of the same basic design.

1. PROTOTYPE DESIGN AND FABRICATION

The prototype engine design differs from the FP-5B configuration in that a conical nozzle has been added. An annular perforated retainer ring was also added for cell compression and as a mount for the top quartz insulator and platinum electrode. A sketch of this design is shown in Fig. 69. As mentioned above, the design is based on the flat plate electrolytic cell concept using platinum electrodes and Refrasil (woven-high temperature glass cloth) as the electrolyte matrix. The top and bottom insulators are fused quartz. The latter material has been shown to withstand thermal cycling without cracking. The insulators serve a dual purpose in that they electrically insulate the electrodes and provide thermal isolation of the electrolytic cell from the body of the engine. The top insulator is also used to maintain an even pressure on the cell so that the Refrasil is compressed equally over its entire area. This even distribution of pressure is necessary to provide proper fuel distribution throughout the volume of the cell. If this condition is not achieved, pockets develop between the Refrasil and the electrodes and uneven fuel combustion results. The top insulator is held in a center position by a retainer ring which is provided with holes for gas passage from the outer circumference of the cell to the engine chamber. The nozzle is of standard conical design with a 60:1 expansion ratio. The throat diameter is .024 in.

The inlet portion of the engine design is comprised of a standard A/N fitting with insulated ferrules (not shown in Fig. 69). An alumina tube insulator separates the injector tube from an outer tube which is welded to the fitting body and the bottom of the chamber. The alumina tube serves to minimize heat losses through the fitting which is large compared to the size of the engine. This insulating device is necessary since the inlet tube is brazed directly to the bottom platinum electrode and is, at present, the electrical connection for this electrode.

Originally the top electrode was to be spot-welded to the inner chamber wall as shown in Fig. 69. However, the final design was changed so that the platinum electrode was spot-welded in four places to the retainer ring. The support plate shown in Fig.69 was eliminated.

The disassembled engine is shown in Figs. 70A and B. Subassemblies are also shown with their constituent parts. The inlet section of the engine is composed of the inlet tube (.010 in. ID Inconel 600)which is gold-nickel brazed into a hole in the bottom platinum electrode (70-9, 70-11, and 70-3). The inlet fitting and stand-off tube (70-13) is gold-nickel brazed to the bottom of the chamber (70-1). The alumina tube insulator (70-12) is inserted in the inlet stand-off, and the lower electrode assembly is inserted through the lower quartz insulator (70-2), which in turn fits into the bottom of the chamber. The inlet tube extends through the bottom fitting. An adaptor tube (70-10) is gold-nickel brazed to the inlet tube to match the ID of the inlet fitting. The tube is sealed in the fitting using a high temperature silicone ferrule. The inlet tube and lower electrode are thus insulated from the body of the engine. The lower electrode is 0.080 in. smaller in diameter than the lower quartz insulator.

The 0.016 in. thick glass cloth electrolyte matrix (70-4) is placed on the lower electrode and is held in place and compressed 0.002 in. by the upper electrode assembly (70-5). This assembly comprises the Inconel retainer ring which is grooved to fit the upper quartz insulator (70-6). The upper platinum electrode (70-7) is spot-welded in four places to the retainer ring for electrical contact to the engine body. The four contact points are sufficient for structural integrity and minimize thermal paths from the upper electrode to the engine body. The entire assembly is positioned with proper compression and is then spot-welded to the inside of the chamber walls. The nozzle (70-8) is inserted in the chamber so that it rests on the retainer ring and is welded in position. The nozzle flange is 0.0625 in. above the top of the chamber to protect the nozzle during the welding process.

2. PRELIMINARY ENGINE EVALUATION

Each assembled engine was tested both manually and by means of a programmer which automatically actuated the inlet valve according to the duty cycle prescribed in the contract. The duty cycle is shown in Table XXXIV. The duty cycle was designed to provide testing data that would include a large number of cold starts, fast pulse operation as well as longer steady-state runs and a total engine time of at least one hour. A close-up of the third experimental engine mounted on the test stand is shown in Fig. 71. A platinum/platinum-10% rhodium thermocouple was used to measure chamber temperature (above the upper quartz insulator and retainer ring) and a chromel-alumel thermocouple was used to measure the outer skin temperature of the chamber opposite the electrolytic cell. The recording instrumentation for the two temperatures, pressure, current, and voltage is shown in Fig. 53. The tape unit, programmer, and power supplies are shown in Fig. 72.

a. Prototype Engines No. 1 through No. 3

The first prototype engine was assembled and welded according to the sketch shown in Fig. 69. Engine No. 1 was constructed using a fusion weld to fasten the nozzle piece to the main engine chamber. The inlet tube was 0.010 in. ID. The

engine could not be operated due to blockage in the cell which prevented propellant flow. The blockage was not in the inlet tube itself, but was due to excessive compaction of the glass fiber matrix which blocked the inlet at its junction with the lower platinum electrode. Engine No. 2 was constructed in the same manner as Engine No. 1, but a 0.023 in. ID inlet was used. The same problem of inlet blockage occurred in this engine. On inspection of the engine it was determined that the problem was not a function of the inlet diameter, but was due to shrinkage of the chamber walls because of the excessive heat during the fusion welding process. Independent experiments on the compression properties of the glass cloth indicated that complete blockage of the cloth was obtained when original 0.016 in. thickness was reduced to 0.012 in.

Engine No. 3 was also fusion welded. Rather than preloading the nozzle piece to achieve a slight compaction of the glass cloth, the nozzle piece was raised 0.010 in. above the retainer ring prior to welding to allow for material shrinkage. Successful ignitions were obtained on this engine but pressure fluctuations were noted during steady-state operation indicating a loose fit which allowed pockets of propellant to form between the glass cloth and the electrodes. However, the engine was tested using several steady-state manual runs and several runs using portions of the duty cycle. Twenty-seven cold starts and 11.6 min. on-time were accumulated on this engine.

The performance data for the manual runs is summarized in Table XXXV. In the mass flow rate range 1.7 to 3.2 x 10^{-4} lbs/sec the characteristic velocity ranged from about 3000 ft/sec to 3800 ft/sec. These preliminary runs indicated that the best flow rate for the engine was about 2.3 x 10^{-4} lbs/sec (Run 2-13-3). At this flow a characteristic velocity of 3600 ft/sec was obtained indicating a combustion efficiency of 83 percent based on a theoretical value of 4340 ft/sec.The rise time for (70°F) cold starts were generally long, but a rise time of 70 msec was obtained for the optimum run.

The engine tests were continued using the duty cycle. The inlet pressure was 95 psia and the resulting chamber pressures were generally in the range of 49-53 psia indicating a pressure drop of about 40 to 45 psia across the inlet and the electrolytic cell. The duty cycle data is summarized in Table XXXVI. In this case no attempt was made to run through the entire duty cycle. Checks were made using each part of the duty cycle and the operation of the engine was further checked by periodically repeating the base point runs.

The performance of the engine improved during the running of the first two base points, and cycle #1 (50 msec on-50 msec off). However,when cycle #2 (100 msec on-6 sec off) was tried ignition occurred in the inlet tube resulting in a failure of the seal in the inlet fitting. The propylene-ethylene seal melted due to excessive heat in the inlet tube. The heat was the result of heat transfer from the hot engine during the six-second periods when there was no propellant flow to cool the inlet. As a result, combustion takes place in the inlet tube causing a choking effect. The heat of combustion in the tube eventually destroys the inlet system. This thermal soak-back behavior is due to poor heat transfer away from the inlet tube during the long off time. The experimental engine is not provided with a heat sink and the inlet

tube is thermally insulated by the alumina tubing which electrically isolates the inlet and lower electrode from the engine chamber. The inlet seal was replaced with silicone which has a higher softening point, but this also melted during the second test using cycle #2. This part of the duty cycle was thus not used during the additional tests.

The engine was also tested using cycles #5, 7, and 8. The performance was good in these cases, but after the first eight runs using cycle #7 the rise-times were longer than desired. However, good performance with a short rise-time was obtained when the base point (#4) was repeated after these runs. After a two-week period the engine was tested manually (Runs 3-2-1 through 3-2-3) but ignition was difficult to achieve. Another base point (#5) was then run, but it was obvious that performance had deteriorated to the point where further testing was not warranted.

Upon engine disassembly it was noted that arcing had occurred from the point where the inlet tube is brazed into the lower platinum electrode. The center of the glass matrix and the upper platinum electrode had been melted so that good fuel dispersion was no longer possible. The engine failure was probably due to increased loss of fuel dispersion as the center portion of the glass matrix eroded away during each firing.

The improvement in engine performance found in the earlier runs and the subsequent degradation in performance can be seen from Fig. 73 by examining the 1st and 100th of the 250-msec pulses of the five base-points run using engine #3. It is apparent that performance was improved in the base-point series #1 through #3, the chamber pressure was reduced somewhat in base-point #4 and the pressure response was very poor in base-point #5. In a given run the 100th pulse shows a higher pressure, smoother equilibrium pressure and a faster rise time than the first pulse in the series. The tail-off time was about the same in all cases.

b. Prototype Engines No. 4 through No. 6.

The assembly procedure for prototype engines No. 4 through No. 6 was changed to minimize the cell matrix compression problem encountered in the previous engines. Proper compression was achieved by positioning the retainer ring upper electrode assembly under the proper load and spot welding it to the inner chamber wall. The matrix, under proper compression, was thus fixed in place prior to the final welding of the nozzle assembly to the chamber. The latter operation was accomplished by means of electron beam welding in order to minimize the thermal expansion and subsequent contraction of the chamber.

Engine #4 was an immediate failure. No propellant flow could be obtained. The problem was traced to electrical arcing across the cell which melted the upper platinum electrode at its center opposite the injector tube. The molten platinum plugged the inlet. The arcing apparently occurred due to the protrusion of the inlet tube and the center portion of the lower electrode. The electrode gap at this point was so reduced that arcing occurred at 40 v in the absence of propellant. The lower

tube is thermally insulated by the alumina tubing which electrically isolates the inlet and lower electrode from the engine chamber. The inlet seal was replaced with silicone which has a higher softening point, but this also melted during the second test using cycle #2. This part of the duty cycle was thus not used during the additional tests.

The engine was also tested using cycles #5, 7, and 8. The performance was good in these cases, but after the first eight runs using cycle #7 the rise-times were longer than desired. However, good performance with a short rise-time was obtained when the base point (#4) was repeated after these runs. After a two-week period the engine was tested manually (Runs 3-2-1 through 3-2-3) but ignition was difficult to achieve. Another base point (#5) was then run, but it was obvious that performance had deteriorated to the point where further testing was not warranted.

Upon engine disassembly it was noted that arcing had occurred from the point where the inlet tube is brazed into the lower platinum electrode. The center of the glass matrix and the upper platinum electrode had been melted so that good fuel dispersion was no longer possible. The engine failure was probably due to increased loss of fuel dispersion as the center portion of the glass matrix eroded away during each firing.

The improvement in engine performance found in the earlier runs and the subsequent degradation in performance can be seen from Fig. 73 by examining the 1st and 100th of the 250-msec pulses of the five base-points run using engine #3. It is apparent that performance was improved in the base-point series #1 through #3, the chamber pressure was reduced somewhat in base-point #4 and the pressure response was very poor in base-point #5. In a given run the 100th pulse shows a higher pressure, smoother equilibrium pressure and a faster rise time than the first pulse in the series. The tail-off time was about the same in all cases.

b. Prototype Engines No. 4 through No. 6.

The assembly procedure for prototype engines No. 4 through No. 6 was changed to minimize the cell matrix compression problem encountered in the previous engines. Proper compression was achieved by positioning the retainer ring upper electrode assembly under the proper load and spot welding it to the inner chamber wall. The matrix, under proper compression, was thus fixed in place prior to the final welding of the nozzle assembly to the chamber. The latter operation was accomplished by means of electron beam welding in order to minimize the thermal expansion and subsequent contraction of the chamber.

Engine #4 was an immediate failure. No propellant flow could be obtained. The problem was traced to electrical arcing across the cell which melted the upper platinum electrode at its center opposite the injector tube. The molten platinum plugged the inlet. The arcing apparently occurred due to the protrusion of the inlet tube and the center portion of the lower electrode. The electrode gap at this point was so reduced that arcing occurred at 40 v in the absence of propellant. The lower

electrode assembly of Engine No. 5 was redesigned so that the inlet tube and center portion of the electrode were recessed in a tapered hole in the center of the bottom quartz insulating disk. This engine was run for a total on-time of 13.7 minutes and 47 cold starts were obtained.

During the 26 preliminary runs (Table XXXVII) the engine performance improved considerably. Rise times decreased from about 250 msec to around 50-70 msec. The characteristic velocity improved from about 2400 ft/sec to 3300-3500 ft/sec. The mass flow rate was varied between 1.0 to 3.0 x 10^{-4} lbs/sec and run times were varied from 3 to 20 sec. The optimum flow rate was about 2 x 10^{-4} lb/sec which gave a thrust of 40 millipounds.

Duty cycle runs included two base points and ten runs each of cycle #1 and #3. Cycle #2 was deleted because of previous thermal soak-back problems. As shown in Table XXXVIII, the performance was very stable and, in fact, improved slightly during the runs. Characteristic velocities in the 4100-4200 ft/sec range (92-95% efficiency) were consistently achieved as well as rise times as low as 20 msec. (Rise times are not reported in many cases due to programmer malfunction.) The chamber temperatures reported in Table XXXVIII are substantially below the actual combustion temperature due to heat losses near the nozzle where the thermocouple was placed. The outside wall temperature near the combustion zone was about 1500 F indicating an internal temperature in the 1800-1900 F range. The estimate of the temperature profile across the chamber wall was based on the internal temperature measurements taken during Phase II of the program as shown in Table XXVIII and Fig. 63.

The engine performed consistently until the last run of cycle #3 when a slight reduction in the characteristic velocity was noted. During the second base point run large pressure fluctuations occurred in the 44th-250 msec pulse near the end of the cycle. When cycle #5 was run (50 msec on - 450 msec off) the engine was hot at the bottom of the chamber below the electrolytic cell, and the cell developed an open circuit preventing further ignition. The failure was due to melting of the gold-nickel braze (m.p. 1740 F) between the inlet tube and the lower platinum electrode which resulted in the open circuit since the inlet tube is one of the external electrical connections.

The power requirements for engine No. 5 were evaluated and are summarized in Table XXXIX. The peak power is about one-third of that required with the preliminary engines used during the Phase II portion of the work (i.e., 100-130 watts). The initial energy peak required is only 15-35 watt-sec. The total energy is larger due to current tail-off in the first one or two seconds of operation corresponding to the current-time relationship shown in Fig. 65. This higher energy requirement can be eliminated by turning the voltage off just after the initial current peak. However, the voltage was left on during the entire run.

The first and last 250 msec pulses are shown in Fig. 74 for the two base points run using Engine No. 5. The performance characteristics are similar to

those for Engine No. 3, but the rise times were shorter in most cases. The engine failure prevented accumulation of a large total on-time, so a sixth engine was constructed for testing.

Engine No. 6 was constructed in the same manner as engine No. 5, but a gold-platinum braze (20% Pt) was used to join the inlet tube to the lower platinum electrode. The melting point for this braze material is 2170 F or about 100 F above the maximum theoretical combustion temperature.

Engine No. 6 was run successfully for a total on-time of 3650 sec. These runs were accomplished over a period of five days and were terminated only because the supply of azide propellant was exhausted. The engine was subjected to sixty (60) cold starts at 70 F using both manual runs (for preliminary testing) and portions of the programmed duty cycle. The only portion of the duty cycle not used was cycle #2 in which thermal soak-back occurred. Cold starts at 70 F were used for convenience (essentially room temperature) since the contract requirements for ignition at 40 F had already been established (p.39) and little difference was seen between ignition at 40 F and 70 F propellant temperatures.

The data for Engine No. 6 is summarized in Table XL. The majority of the time on the engine was accumulated using cycle #7 (10 sec on-100 sec off). Every fifth run using this cycle was reported, since 173 runs were made and the performance data did not change to any appreciable extent.

The base point cycle was run periodically with little noticable change in performance. The first and one-hundreth pulses in selected base point runs and the associated data are illustrated in Fig. 75. The only variation in performance noted was the appearance of relatively large pressure fluctuations during base point runs 2 and 3. These fluctuations were also apparent in some runs using cycle #3 (30 sec runs) and cycle #6 (3 sec runs) which were run during the total on-time period of about 400-700 sec. These fluctuations did not occur in subsequent runs, as Fig. 75 indicates for base point runs 4 and 9. The total time on the engine at each base point illustrated in Fig. 75 is: base point 1B, 40 sec; base point 2, 440 sec; base point 3, 720 sec; base point 4B, 2450 sec; and base point 9, 3600 sec.

There is a slight downward trend in the equilibrium pressure as time is built up on the engine. This effect is a direct result of a decrease in propellant flow rate (i.e., the combustion efficiency has not changed) due to increased back pressure in the engine. The inlet pressure was 75 psia for all the runs reported in Table XL, so the pressure drop across the engine increased from 26 psia to 31 psia indicating compaction of the glass cloth separator in the electrolytic cell. This 5 psia change is very low, but is the only significant change noted during the entire test period.

The temperatures measured during the engine test are not a true indication of engine performance. The chamber thermocouple is considerably removed from the engine "bed", which in this case is the electrolytic cell. At equilibrium the chamber temperature is essentially the same as the outside wall temperature near the combustion zone, i.e., the cell matrix. Thus the temperature drop across the chamber wall is essentially the same as the gas temperature drop from the cell, through the annular retainer ring to the chamber. Previous measurements reported in Section III of this report have shown that the temperature drop through the cell is on the order of 400-600 F so the actual combustion temperature must be in the 1800-2000 F range.

The power requirements for the engine are identical to those shown for Engine No. 5 (Table XXXIX). The peak power is on the order of 100-120 watts while the peak energy requirement is on the order of 15-30 watt-sec. In some cases there is a residual current after the main current peak which results in an increase in the total energy requirement to about 100-170 watt-sec. As pointed out earlier, this effect can be avoided by terminating the applied voltage immediately after ignition. This lack of applied voltage at this point in no way effects engine performance. The voltage was terminated during runs 8-9 and 8-10 (Table XL) and the data from these runs is similar to those obtained with the voltage applied throughout the entire run (i.e., runs 8-1 through 8-4 as well as 8-11 and 8-12).

The termination of the voltage with no effect on performance is an important concept in that the actual energy requirements are then very low. The effect also shows that the engine is actually operating in a thermal mode immediately after the current pulse. and can be pulsed without further application of power as long as the cell temperature is sufficiently high. It has been determined that this particular engine design is capable of restart without power application up to six minutes if the engine has previously reached an equilibrium temperature. This off-period allows ample time to charge a capacitor at a low power level. Capacitor discharge can then be used without using the main power supply for the 100-120 watts peak power required for ignition.

Engine No. 6 represents a completely successful test for durability and performance. The engine was run for a total on-time of one hour using sixty cold (70 F) starts. The ignition delay time was on the order of 30-70 msec; the characteristic velocity was 3800-4000 ft/sec which is 90-95% of theoretical. Power requirements were 100-120 watts peak and the total energy required was 15-30 watt-sec. The engine ran at a thrust level of 40 millipounds using a mass flow rate of 2×10^{-4} lb/sec. Pressure fluctuations were at a minimum in all cases.

SECTION V

SUMMARY AND CONCLUSIONS

1. PHASE I

In the course of the work done on Phase I of Contract F04611-70-C-0070, experimental investigations were carried out on selected propellants as candidate electrolytes and on various electrodes to determine their usefulness in an electrolytic ignition system for millipound thrusters.

Electrical conductivity data was obtained as a function of temperature between 25 C and 45 C, for propellant grade hydrazine, hydrazine-2% hydrazine nitrate, hydrazine-2% hydrazine azide, and hydrazine-23% hydrazine azide. This data is quite important since ohmic losses due to poor electrolyte conductivity in the electrolytic cell is one of the primary factors in cell design.

Voltage losses due to slow electrochemical processes at the electrode-electrolyte interface also effect the design and performance of the electrolytic ignition cell. For this reason polarization studies (measurements of voltage losses under conditions of current flow) were carried out on platinum, pyrolytic, and spectrographic grade graphite, three types of stainless steel; AM350, 17-7PH, and 304SS, two aluminum alloys, AA1100, and AA6061-T6; a gold-nickel brazing alloy, HS1414, nickel; and Inconel 600. The electrolytes used in these studies included propellant grade hydrazine, hydrazine-5%, hydrazine nitrate, and hydrazine-23% hydrazine azide.

Preliminary electrolysis experiments (at low currents) were carried out and an analysis was made of the products of the electrolysis reaction. These experiments were designed to determine the theoretical heat output. Hydrazine-23% hydrazine azide was the only electrolyte used in these studies.

The results of the conductivity studies showed that the addition of small amounts of hydrazine-based salts enhances the conductivity of propellant grade hydrazine by at least two orders of magnitude. Both 2% hydrazine nitrate and 2% hydrazine azide additions showed conductivities of 3.0×10^{-2} and 3.5×10^{-2} $ohms^{-1}cm^{-1}$ at 25 C compared to 1.6×10^{-4} $ohms^{-1}cm^{-1}$ for propellant grade hydrazine at the same temperature. The addition of 23% hydrazine azide yielded a conductivity value of 1.8×10^{-1} $ohm^{-1}cm^{-1}$, another factor of ten better than obtained with the low percentage additions.

The polarization results were evaluated in terms of both transient and steady-state effects. The former studies were designed to determine if any films were formed on the surface of the electrodes that would impede or stop the electrochemical process. The cell used in the experimental apparatus was designed to

eliminate any effects due to differences in the conductivities of the electrolytes used. It was found that all electrodes were highly polarized in propellant grade hydrazine and that the aluminum alloys performed very poorly as anodes in all the electrolytes studied. Almost without exception the best performance of all electrodes, anodic or cathodic, was obtained using the 23% hydrazine azide solution.

In hydrazine-23% hydrazine azide, platinum was found to be the least polarized material, as both an anode and a cathode. However, pyrolytic graphite behaved in a similar manner to platinum as an anode.

The three stainless steels were relatively poor anodes but good cathodes with some notable reservations. The anodic and cathodic behavior of 17-7PH was unpredictable and often indicated very high polarization. The cathodic behavior of AM350 was similar, although not to as great an extent. 304SS was the only low cost cathodic material that showed consistent performance.

Steady-state experiments were designed to evaluate electrode surface resistance effects which are independent of electrolytic resistivity and to compare total voltage losses at a steady current input to the cell. In general, the steady-state results confirmed those obtained in the transient studies. The only true electrode resistance effects obtained were found under conditions of cathodic polarization of 304SS.

The effect of hydrazine azide concentration was also studied in the range of 2 to 23 weight percent azide to determine whether there was an optimum concentration at which minimum polarization could be attained. However, the lowest polarization was always found at the 23% hydrazine azide level. The polarizations of the stainless steels were found to be linear functions of azide concentration while the relationship between polarization and azide concentration for platinum and graphite was irregular.

The products of electrolysis of hydrazine-23% hydrazine azide were determined using platinum, pyrolytic graphite, AM350, and 304SS. In all cases nitrogen was the only anodic product. The cathodic products for graphite, AM350, and 304SS were ammonia, nitrogen, and hydrogen in proportions consistent with the reaction:

$$2N_2H_5^+ + 2e \rightarrow N_2 + 2H_2 + 2NH_3$$

indicating no ammonia decomposition, and thus producing the highest heat output possible for the reaction. The cathodic process on platinum yielded nitrogen and hydrogen only, indicating catalytic decomposition of ammonia on the platinum surface, and thus a lower heat output.

The power input data for the cell indicates that the lowest polarization is achieved using platinum as either an anode or a cathode, 304SS as a cathode and

graphite as an anode. Any combination of these materials yield about the same results. Thus final selection of materials from this group depends on physical and corrosion properties.

On the basis of the above results, the following conclusions have been reached:

(a) Hydrazine-23% hydrazine azide is the best electrolyte studied.

(b) Either platinum or pyrolytic graphite should be used as the anode of the electrolytic cell.

(c) 304 Stainless steel or platinum should be used as the cathode for the cell.

2. PHASE II

In the course of the work done in Phase II, four different electrode configurations were developed and three of these were tested in preliminary engine designs. The design requirements for the electrolytic cell design included thrust levels in the 20-80 millipound range, mass flow rates in the range 1-4 x 10^{-4} lbs/sec, chamber pressure of 40-200 psia, a cold start temperature of 40 F minimum, a 50 millisecond ignition delay time, a 25 millisecond tail-off time and a characteristic velocity of 4000 ft/sec.

The mechanical design requirements necessary to achieve the above performance parameters include:

(a) A large ratio of electrode surface area to propellant volume.

(b) Immediate and uniform dispersal of the propellant through the volume between the electrodes.

(c) Maximum thermal isolation of the cell from the engine body

(d) A finite and steady pressure drop across the electrode chamber.

Two of the original electrode configurations were extensively evaluated. These were coiled screen electrodes using a woven glass cloth as an electrolyte matrix and electrode separator, and flat plate configurations using the same glass cloth separator material. Variations of these configurations included the use of thermal beads, flame sprayed alumina electrodes, and the use of MoC_3 or ruthenium promotors impregnated in the glass cloth separators.

Using the coiled screen concept it was possible to obtain a characteristic velocity (C*) of about 3800 ft/sec, but only at a flow rate of about 2 x 10^{-4} lbs/sec. Cold starts could only be achieved using glass cloth separators impregnated with a promotor. The rise-times and tail-off times were also large and averaged about

250 msec and 500 msec respectively. Shorting of electrodes was also a common problem, and the use of thermal beds had little or no effect on engine performance.

Flat plate configurations were found to be much more structurally reliable than the coiled screens. The use of insulated electrodes considerably improved the rise times. The use of a simple two-plate cell resulted in characteristic velocities up to 4100 ft/sec at flow rates of about 1 x 10^{-4} lbs/sec and rise times on the order of 150 msec. Cold starts were achieved without the use of any catalytic materials. The construction of the cell was modified to include alumina disks above and below the cell for thermal isolation and to ensure that the propellant would flow toward the sides of the engine. A retainer ring was used to compress the glass cloth evenly and thus ensure even fuel distribution. The alumina disks were eventually replaced with quartz which has better thermal shock resistance.

This flat-plate cell design was used to determine the optimum cell dimensions and to evaluate the heat losses and power requirements. It was found that the cell volume was a critical factor in determining optimum mass flow rates and the power that can be achieved. The latter determines the rate of heat input. The optimum cell diameter for a 0.016 in. electrode spacing and a flow rate of about 2 x 10^{-4}lb/sec was found to be 0.50 in.

By measuring the temperature profile in a preliminary engine incorporating the cell design described above, it was determined that heat losses in the chamber and the top of the engine were primary causesof low characteristic velocities. The final engine design incorporated the same cell configuration but the engine itself was reduced in mass using 0.010 in. to 0.020 in. walls with a total engine height of 0.040 in. This engine was run at a flow rate of 2 x 10^{-4} lbs/sec with characteristic velocities in the range of 3900-4100 ft/sec and rise times in the 50-70 msec range.

The power requirements of the preliminary engine are minimized when the mass flow rate and cell volume are matched so that filling occurs in a time less than the ignition delay time. Voltage is applied prior to initiation of fuel flow. When fuel is introduced a current pulse of about 100 msec duration occurs just prior to ignition. The energy required for ignition was about 30-40 watt-sec at 40 v and peak currents of 8-10 amps. Peak power was in the 300-400 watt range.

The final engine design incorporated a flat-plate design using two platinum electrodes, a glass cloth separator, and two quartz disks to insulate the cell from the engine body. The cell was slightly compressed using the top of the engine as a retainer. The fuel inlet tube was brazed into the bottom platinum electrode so that fuel would impact the glass cloth separator and spread throughout the cell prior to and during the ignition process. Once ignition was achieved further application of power was not necessary and was needed for cold starts only. The engine ran at a combustion efficiency of 90-95% and the chamber pressure was smooth with fluctuations less than ±10%.

This basic engine concept was used to design an engine for extensive testing using the duty cycle prescribed in the AFRPL contract.

3. PHASE III

Six engines were constructed for testing during this phase of the program. The major problem areas encountered during test were associated with the degree of compaction of the glass cloth electrolyte matrix, electrical arcing between the electrodes at the point where the inlet tube is brazed to the lower electrode, melting of the braze at the same point due to high combustion temperatures, and thermal soak-back when using short ignition pulses and long off-times with a hot engine.

Excessive compaction of the glass cloth was avoided by placing a slight stress on the glass cloth using the upper electrode assembly and then spot welding the retainer ring to the inside of the chamber wall prior to welding of the nozzle assembly to the chamber. The maximum compaction was set at 0.002" in. for maximum fuel distribution and minimum back pressure.

Electrical arcing was eliminated by recessing the center of the lower electrode in a tapered hole in the bottom quartz insulating disk. The increased spacing at the junction of the inlet tube with the lower electrode (about 0.003 in.greater than the rest of the electrode) was sufficient to prevent arcing up to an applied voltage of at least 42 volts.

Efficient engine operation resulted in cell temperatures in the 1800-1900 F range. These temperatures are above the melting point of the gold-nickel braze (20% Ni) initially used to fasten the inlet tube to the lower platinum electrode (mp 1740 F). Failure of this braze was corrected through the use of a gold-20% platinum braze which melts at 2060 F.

Of the six engines constructed, only one incorporated all the modifications noted above. This engine ran for a total of one hour on-time using sixty cold starts. The pressure rise time was on the order of 30-70 milliseconds, the characteristic velocity range was 3800-4000 ft/sec, while the peak power requirement for cold starts was 100-120 watts. The energy requirement was 15-30 watt-sec during ignition. This engine was run at a thrust level of 35-38 millipounds using a throat area of 4.94×10^{-4} in^2 and a thrust coefficient of 1.6. The specific impulse was in the range 190-205 sec.

The tests show that the electrolytic ignition concept can be successfully applied to low thrust level engines at performance levels comparable to those of catalytic engines, with no degradation in performance over the time period tested.

Further development of this concept is recommended in the areas of (1) improvement of heat-transfer characteristics, (2) further reduction of power requirements, (3) alternate cell design in order to achieve higher thrust levels, and (4) adaptation to other monopropellants.

REFERENCES

1. Breen, B.P., M. Gerstein and M. A. McLain: Electrolytic Ignition System for Monopropellants. AFRPL-TR-69-247 Final Report, January, 1970.

2. Andrieth, L.F., and B. A. Ogg: The Chemistry of Hydrazine. John Wiley & Sons, Inc., New York, 1951.

3. Lander, J. J.: Analysis of Electrolytic Hydrazine Decomposition. Report to AFRPL, June, 1970.

4. Lander, J.J.: Electrolysis of Hydrazine Solutions. Report to AFRPL, September, 1970.

5. Lander, J.J.: Electrolysis of Hydrazine-Hydrazine Azide. Report to AFRPL, February, 1971.

6. Brown, C.T.: Electrochemical Measurement of Corrosion in Hydrazine, UARL Report UAR-H214, September, 1969.

7. Brown, C.T.: Electrochemical Measurement of the Decomposition of Hydrazine on Selected Materials. UARL Report UAR-H282, November, 1969.

8. Axworthy, A.E., et.al: Research on Hydrazine Decomposition. Technical Report AFRPL-TR-68-138, July, 1968.

9. Dee, L.A. et.al: The Catalytic Decomposition of Hydrazine on Gold, Nickel, and a Gold-Nickel Brazing Alloy. Technical Report AFRPL-TR-69-77, 1969,

10. Hollywood, L.P., et al: Storage tests of Nitrogen Tetroxide and Hydrazine in Aluminum Containers. NASA Technical Report 32-1-39, January, 1967.

11. Rockenfeller, J.D.: Materials Compatibility with Hydrazine-Based Monopropellants. CPIA Pub. No. 176, Vol. 1, pp 457-466, October, 1968.

12. Pugmire, T.K.,et.al: Electrothermal Hydrazine Engine Performance. AIAA/SAE 7th Propulsion Joint Specialist Conference, June, 1971. Paper No. 71-760.

TABLE I

SPECIFIC CONDUCTANCE OF SELECTED HYDRAZINE-BASE PROPELLANTS

Sample	Temperature (°C)	Specific Conductance (OHM^{-1} CM^{-1})
Propellant Grade Hydrazine	25°	0.000163
" " "	35°	0.000260
" " "	45°	0.000477
98% N_2H_4 + 2% NH_4NO_3	25°	0.02861
" " "	35°	0.03038
" " "	45°	0.03201
77% N_2H_4 + 23% N_5H_5	25°	0.19711
" " "	35°	0.20022
" " "	45°	0.22191
98% N_2H_4 + 2% N_5H_5	25°	0.03124
" " "	35°	0.03562
" " "	45°	0.04086

TABLE II

ORDER OF ANODIC POLARIZATION AT AN OVERPOTENTIAL OF 1000mv

N_2H_4 - 23% N_5H_5		N_2H_4 - 5% $N_2H_5NO_3$		N_2H_4	
Material	c.d.(ma/cm^2)	Material	c.d.(ma/cm^2)	Material	c.d.(ma/cm^2)
Pt	150	HS1414	70	HS1414	1.2
HS1414	120	Pt	35	Pt	1.0
Nickel	100	-	-	-	-
C	66	C	24	17-7PH	0.40
304SS	19	17-7PH	24	AM350	0.35
AM350	16	304SS	8.0	C	0.28
17-7PH	5.5	AM350	7.4	304SS	0.13
Inconel 600	3.4	-	-	-	-
AA6061-T6	0.11	AA6061-T6	0.019	AA1100	0.052
AA1100	0.012	AA1100	0.016	AA6061-T6	0.043

TABLE III

ORDER OF CATHODIC POLARIZATION AT AN OVERPOTENTIAL OF 1000mv

N_2H_4 - 23% N_5H_5		N_2H_4 - 5% $N_2H_5NO_3$		N_2H_4	
Material	c.d.(ma/cm^2)	Material	c.d.(ma/cm^2)	Material	c.d.(ma/cm^2)
Pt	170	HS1414	103	C	0.56
HS1414	125	17-7PH	102	17-7PH	0.34
Nickel	125	-	-	-	-
Inconel	120	-	-	-	-
17-7PH	86	AM350	70	HS1414	0.19
304SS	70	Pt	33	Pt	0.19
AA6061-T6	50	C	16	AM350	0.17
AA1100	48	304SS	6.2	AA1100	0.13
AM350	48	AA1100	1.5	304SS	0.08
C	32	AA6061-T6	0.88	AA6061-T6	0.08

TABLE IV

COMPARISON OF ANODIC AND CATHODIC POLARIZATION OF STAINLESS STEELS IN 77% HYDRAZINE - 23% HYDRAZINE AZIDE

	Current Density (ma/cm^2) at $\eta = \pm 1000$ mv					
	304SS		AM350		17-7PH	
Material Condition	Anode	Cathode	Anode	Cathode	Anode	Cathode
Rod-Cleaned	18	85	17	88	44	78
Plate-Uncleaned	19	70	16	48	5.5	86
Plate-Cleaned	19	70	17	68	5.5	20

TABLE V

ANODIC POLARIZATION OF AM350, 304SS, PYROLYTIC GRAPHITE AND PLATINUM AS A FUNCTION OF AZIDE CONCENTRATION

Current density (ma/cm^2) at η = 1000mv

% Azide	304SS	AM350	Pt	PyC
23	18	54	100	92
12	4.9	32	78	70
4.8	1.3	21	27	26

TABLE VI

CATHODIC POLARIZATION OF AM350, 304SS AND PLATINUM AS A FUNCTION OF AZIDE CONCENTRATION

	Current density (ma/cm^2) at η = -1000 mv		
% Azide	304SS	AM350	Pt
23	85	90	95
12	45	47	39
4.8	13	18	27

TABLE VII

COMPARISON OF ANODIC AND CATHODIC POLARIZATION IN AZIDE AND NITRATE PROPELLANTS

	Current Density (ma/cm^2) at η = ±1000 mv			
	92.5% N_2H_4 - 4.8% N_5H_5		94% N_2H_4 - 6% $N_2H_5NO_3$	
Material	Anodic	Cathodic	Anodic	Cathodic
AM350	21	18	7.4	15
304SS	1.3	13	7.5	24
Pyrolytic Graphite	26	--	55	--
Platinum	27	28	24	23

TABLE VIII

ORDER OF CATHODIC POLARIZATION AT A CONSTANT CURRENT OF 50ma

N_2H_4 - 23% N_5H_5			N_2H_4 - 5% $N_2H_5NO_3$		
Material	c.d. (ma/cm^2)	Total Polarization ($mv/ma/cm^2$)	Material	c.d. (ma/cm^2)	Total Polarization ($mv/ma/cm^2$)
Pt	31.8	11.3	Pt	31.8	18.9
C	25.0	18.8	HS1414	22.6	23.9
304SS	20.0	19.0	304SS	20.0	24.0
AM350	20.0	19.0	C	25.0	27.2
HS1414	22.5	19.5	17-7PH	24.7	32.4
17-7PH	23.6	26.6	AM350	19.4	36.0
AA6061-T6	21.0	88	AA1100	15.8	177
AA1100	17.0	127	AA6061-T6	21.8	179

TABLE IX

ORDER OF ANODIC POLARIZATION AT A CONSTANT CURRENT OF 50ma

N_2H_4 - 23% N_5H_5			N_2H_4 - 5% $N_2H_5NO_3$		
Material	c.d. (ma/cm^2)	Total Polarization ($mv/ma/cm^2$)	Material	c.d. (ma/cm^2)	Total Polarization ($mv/ma/cm^2$)
Pt	31.8	14.8	Pt	31.8	18.2
C	25.0	23.2	C	25.0	26.4
HS1414	22.5	24.1	HS1414	22.6	28.8
304SS	20.0	40.0	304SS	20.0	38.0
17-7PH	23.6	46.6	17-7PH	24.7	52.6
AM350	20.0	47.5	AM350	19.4	53.6
AA6061-T6	21.0	95	AA6061-T6	21.8	229
AA1100	17.0	135	AA1100	15.8	247

TABLE X

TOTAL OVERPOTENTIAL AT 50 ma/cm^2
IN 77% HYDRAZINE - 23% HYDRAZINE AZIDE

Anodic				Cathodic			
Material	η (mv)	IR (mv)	IR-Free η (mv)	Material	η (mv)	IR (mv)	IR-Free η (mv)
AM350	900	-		AM350	510	-	
	900	-			600	-	
	980	-					
	1200	-	} with cathodic		780	-	} with anodic
	1250	-	} deposit				} deposit
Pryolytic Graphite	590	-		Pyrolytic Graphite	1200	-	
	500	-			1600	-	
304SS	1500	-		304SS	800	320	480
	1550	-			800	320	480
17-7PH	1100	-		17-7PH	720	-	
	840	-					
	1120	-	with cathodic deposit				
Platinum	540	-		Platinum	800	-	
	560				680	-	

TABLE XI

POLARIZATION AS A FUNCTION OF AZIDE CONCENTRATION AT 50ma

mv/ma/cm^2

Cathodic

Material	23% Azide	12% Azide	4.8% Azide
Pt	12.6	16.0	24.8
Py C	--	--	45.6
304SS	17.0	24.8	35.2
AM350	19.1	21.6	26.4

Anodic

Material	23% Azide	12% Azide	4.8% Azide
Pt	21.5	22.8	35.2
Py C	15.8	27.2	21.2
304SS	51.8	50.0	57.5
AM350	37.0	30.0	41.5

TABLE XII

COMPARISON OF POLARIZATION IN HYDRAZINE-HYDRAZINE AZIDE AND HYDRAZINE-HYDRAZINE NITRATE AT A CONSTANT CURRENT OF 50ma

Cathodic

Material	4.8% Azide η (mv)	4.8% Azide mv/ma/cm^2	6.0% Nitrate η (mv)	6.0% Nitrate mv/ma/cm^2
Pt	620	24.8	540	21.6
PyC	1140	45.6	1550	62.0
304SS	880	35.2	920	36.8
AM350	660	26.4	720	28.8

Anodic

Material	4.8% Azide η (mv)	4.8% Azide mv/ma/cm^2	6.0% Nitrate η (mv)	6.0% Nitrate mv/ma/cm^2
Pt	880	35.2	350	14.0
PyC	530	21.2	1020	40.9
304SS	1440	57.5	1550	62.0
AM350	1040	41.5	1050	42.0

TABLE XIII

ELECTROLYSIS OF HYDRAZINE AZIDE-GAS ANALYSIS

	Electrode	Electrolyte	% NH_3 Produced	% H_2 Produced	% N_2 Produced	% NH_3 Decomposed
Anodic	Pyrolytic graphite	77% N_2H_4 23% N_5H_5	0	0	100	
	304SS	77% N_2H_4 23% N_5H_5	0	0	100	
	AM350	77% N_2H_4 23% N_5H_5	0	0	100	
	Platinum	77% N_2H_4 23% N_5H_5	0	0	100	
Cathodic	Pyrolytic graphite	77% N_2H_4 23% N_5H_5	42	41	17	0
	304SS	77% N_2H_4 23% N_5H_5	44	31	25	0
	AM350	77% N_2H_4 23% N_5H_5	50	36	14	0
	Platinum	77% N_2H_4 23% N_5H_5	0	75	25	100
	Theoretical - No NH_3 decomposed	cathodic	40.0	40.0	20.0	
	Theoretical - NH_3 decomposed	cathodic	0	72.4	28.6	

TABLE XIV

POLARIZATION DATA
ELECTROLYSIS CELL

Electrode		Rest Voltage	Current	Power Supply Voltage	Resistance	Electrolysis Voltage	η	Total Cell η
AM350	Anodic	+ 0.94 v	30 ma	15 v	200 Ω	- 0.36 v	+1300 mv	2.00 v
AM350	Cathodic	+ 0.95 v	30 ma	15 v	200 Ω	+ 1.65 v	- 700 mv	
Pyrolytic graphite	Anodic	+ 0.69 v	30 ma	15.8 v	200 Ω	+ 0.20 v	+ 490 mv	1.51 v
Pyrolytic graphite	Cathodic	+ 0.70 v	30 ma	15.8 v	200 Ω	+ 1.72 v	-1020 mv	
304SS	Anodic	+ 1.02 v	30 ma	15 v	200 Ω	- 0.16 v	+1180 mv	1.70 v
304SS	Cathodic	+ 1.03 v	30 ma	15 v	200 Ω	+ 1.55 v	- 520 mv	
Platinum	Anodic	+ 0.98 v	30 ma	17 v	200 Ω	+ 0.30 v	+ 680 mv	1.46 v
Platinum	Cathodic	+ 0.98 v	30 ma	15 v	200 Ω	+ 1.46 v	- 480 mv	

TABLE XV

EFFICIENCY OF HEAT PRODUCTION BASED ON THE AMOUNT OF N_5H_5 DECOMPOSED

Anode	Cathode	Actual N_5H_5 Decomposed (g)	Theoretical N_5H_5 Decomposed (g)	Current (amps)	Efficiency (%)	Heat (cal) (N_5H_5 decomp)	Heat I^2R (cal)	Total Heat Released (cal)
Pt	Pt	1.16	0.28	6	420	718	713	1431
Pt	Pt	1.39	0.31	8	450	860	619	1479
C	Pt	1.49	0.33	6	450	922	725	1647
C	Pt	1.46	0.36	6	410	904	838	1760
Pt	304SS	1.14	0.37	6	310	705	659	1364
C	304SS	1.23	0.70	6	180	767	1671	2438
C	C	1.01	4.19	6	24	625	-	-

TABLE XVI

POLARIZATION CHARACTERISTICS OF SEVERAL ELECTRODE COMBINATIONS

Anode	Cathode	Current (amps)	Cathode Polarization (Volts)			Anode Polarization (Volts)			Cell Polarization (Volts)		
			IR-Free	IR	Total	IR-Free	IR	Total	IR-Free	IR	Total
Platinum	Platinum	3.0	0.40	2.00	2.40	0.25	2.00	2.25	0.65	4.00	4.65
Platinum	Platinum	6.0	1.00	3.00	4.00	0.70	3.30	4.00	1.70	6.30	8.00
Platinum	Platinum	8.0	1.30	3.00	4.30	2.00	3.00	5.00	3.30	6.00	9.30
Graphite	Platinum	3.0	0.70	2.80	3.50	0.25	1.70	1.95	0.95	4.50	5.45
Graphite	Platinum	6.0	1.15	5.00	6.15	1.00	3.40	4.40	2.15	8.40	10.55
Graphite	Platinum	8.0	2.00	5.50	7.50	1.20	4.00	5.20	3.20	9.50	12.70
Platinum	304SS	3.0	0.50	1.60	2.10	0.25	1.90	2.15	0.75	3.50	4.25
Platinum	304SS	6.0	0.60	2.80	3.40	0.55	3.00	3.55	1.15	5.80	6.95
Platinum	304SS	8.0	0.80	4.00	4.80	0.70	3.60	4.30	1.50	7.60	8.30
Graphite	304SS	3.0	0.40	2.00	2.40	0.55	2.50	3.05	0.95	4.50	5.45
Graphite	304SS	6.0	0.70	3.70	4.40	0.80	3.50	4.30	1.50	7.20	8.70
Graphite	304SS	8.0	0.80	4.60	5.40	1.60	5.00	6.60	2.40	9.60	12.00

TABLE XVII

RESISTANCE-FREE POLARIZATION OF SEVERAL ELECTRODE COMBINATIONS

Anode	Cathode	IR-Free Polarization (Volts) 3 amps	6 amps	8 amps
Pt	304SS	0.75	1.15	1.50
C	304SS	0.95	1.50	2.40
C	Pt	0.95	2.15	3.20
Pt	Pt	0.65	1.70	3.30

TABLE XVIII

EQUILIBRIUM DECOMPOSITION RATES
OF 77% HYDRAZINE-23% HYDRAZINE AZIDE AT 300°K

Material	i_{decomp} for N_5H_5 (ma/cm^2)	N_5H_5 Decomposition Rate At 300°K ($g/cm^2/year$)	N_2H_4 Decomposition Rate at 322°K ($g/cm^2/year$)
Pt	12.0	276.5	26.1
Graphite	4.0	91.0	7.84
AM350	0.094	0.214	0.112
304SS	0.14	0.320	0.020
17-7PH	0.019	0.043	0.015

TABLE XIX

COMPARISON OF COMPATIBILITY DATA

(Electrochemical vs. Storage and Gas Evolution Methods)

Material	Temp. (°F)	Time of Exposure (hr)	Decomposition Rate $mgN_2H_4/cm^2/year$	Reference
304SS	288	75.5	22.2	8
304SS	160	1	62.5	6&7
304SS	160	24	67.5	6&7
304SS	140	1	31.2	6&7
304SS	140	5	11.2	6&7
304SS	120	1	19.8	6&7
304SS	120	5	9.1	6&7
304SS	120	24	2.6	6&7
Au-Ni (HS1414)	140	24	409	9
Au-Ni	140	1	3350	6&7
Au-Ni	140	24	3300	6&7
Au-Ni	120	1	2080	6&7
Au-Ni	120	24	2060	6&7
AA6061-T6	85	1440	0.32	10
AA6061-T6	120	1	0.88	6&7
AA6061-T6	120	5	0.065	6&7
AA6061-T6	160	1	0.78	6&7
AA6061-T6	160	20	0.26	6&7
AA6061-T6	160	67	0.34	6&7
AA1100	140	72	1.17	11
AA1100	140	1	8.85	6&7
AA1100	140	5	1.60	6&7
AA1100	120	1	10.9	6&7
AA1100	120	24	0.95	6&7

TABLE XX

INDICATED ACTIVATION ENERGIES FOR HYDRAZINE
AND HYDRAZINE AZIDE DECOMPOSITION

(Kcal/mole)

Material	77% N_2H_4-23% N_5H_5 Cathodic	77% N_2H_4-23% N_5H_5 Anodic	N_2H_4 Anodic
304SS	3.4	7.3	5.1
AM350	0.8	7.6	5.0
17-7PH	1.4	9.0	-
Platinum	0.5	0.6	-
Pyrolytic Graphite	-	2.3	-
HS1414	-	-	4.3

ΔE_a applies over the following temperature range:

77% N_2H_4-23% N_5H_5 Temperature Range 27 - 107 C
300 - 380 K
81 - 225 F

N_2H_4 Temperature Range 49 - 71 C
322 - 344 K
120 - 140 F

TABLE XXI

ELECTROLYTIC ENGINE PERFORMANCE DATA (CS-3)

Run#	Applied Voltage	Applied Current	Peak Power (watts)	P_c (psia)	C* (ft/sec)	F (lbs)	t_{90} (msec)	t_{10} (msec)	$\dot{\omega}$ (lbs/sec) x 10^{-4}
1-1	15	6	90	60	3850	.035	260	-	2.6
2-1	15	8	120	60	1440	.035	310	270	4.9
2-2	15	8	120	75	2270	.044	230	440	3.9
3-9	15	8	120	28	700	.016	210	630	4.7
3-10	15	8	120	35	450	.020	650	850	9.2
3-11	15	8	120	52	450	.030	190	410	13.7
3-22	10	8	80	50	1440	.029	230	770	4.1
3-23	20	1	20	50	1950	.029	230	750	3.0
3-24	28	0.5	14	50	1550	.029	270	510	3.8

Runs # 1-1 through 2-2 - MoO_3 Catalyst

Runs #3-9 through 3-24 - Ru Catalyst

Cold Start Temp. = 70°F for engine and propellant

TABLE XXII

ELECTROLYTIC ENGINE PERFORMANCE DATA
(FP-1-TB)

Run#	Applied Voltage (Volts)	Applied Current (Amps)	Power (Watts)	P_c (psia)	C* (ft/sec)	F (lb)	t_{90} (msec)	$\dot{\omega}$ (lbs/sec) x 10^{-4}
24-2	5	8	40	48	1400	.014	50	2.08
24-3	5	8	40	75	3500	.022	130	1.3
24-5	5	8	40	63	3200	.0188	150	1.2
24-7	5	8	40	63	1700	.019	100	2.2

Cold Start Temp.: 70 F

TABLE XXIII

ELECTROLYTIC ENGINE PERFORMANCE DATA FOR ENGINES (FP-2) AND (FP-3)

Run #	P_c (psia)	C^* (ft/sec)	I_s (lb-sec/lb)	F (mlb)	t_{90} (msec)	t_{10} (msec)	$\dot{\omega}$ (lb/sec) x10^{-4})
5-1A-2	39	1966	98	23	250	900	2.21
5-2A-1	33	3014	150	18	1500	900	1.22
5-3A-1	30	3755	187	16	150	1800	0.69
5-3A-3	33	4131	205	18	100	2200	0.69
5-4A	27	2296	114	15	100	2100	1.31
5-5A	48	2571	128	27	200	150	2.08
5-8A	63	1475	73	35	250	400	4.76
6-4-1	39	1889	94	22	150	400	2.30
6-5-1	42	2176	108	23	200	300	2.15
10-3 *	64	2580	128	35.4	50	700	3.0
10-4 *	43	2600	129	23.6	300	400	2.0
10-5A *	46	2520	125	25.4	250	400	2.2

All runs made at 24 volts and 0.5 amp

*These runs made with engine configuration FP-3.

Cold Start Temperature: 70 F

TABLE XXIV

RESISTANCE MEASUREMENTS IN ELECTROLYTIC IGNITION CELLS

1.0 Inch Cell

Volume of Propellant added (cc)	Resistance (ohms)
0.01	1570
0.02	162.0
0.04	12.5
0.045	8.1
0.050	5.5
0.055	3.2
*0.06	2.1
0.08	1.4
0.10	1.1
0.12	0.7

* Volume of propellant in flooded cell

0.5 Inch Cell

Volume of Propellant added (cc)	Resistance (ohms)
0.005	290.1
0.01	4.4
*0.015	2.5
0.02	2.8
0.06	2.1
0.12	1.8

* Volume of propellant in flooded cell

TABLE XXV

RESULTS OF RESISTANCE MEASUREMENTS IN ELECTROLYTIC IGNITION CELLS

1.0 Inch Cell		
Total Volume	=	0.206 cm^3
Fuel Volume	=	0.06 cm^3 (65 mg propellant)
Porosity	=	29%
Resistance of electrolyte in open cell (at 2 x 10^{-1} ohm^{-1} cm^{-1})	=	0.04 ohm
Resistance of full cell (with matrix)	=	2.1 ohms
Resistance Factor	=	52.5
Time to fill cell at 5 x 10^{-4} lbs/sec (0.20 cc/sec)	=	300 msec
0.5 Inch Cell		
Total Volume	=	0.0515 cm^3
Fuel Volume	=	0.015 cm^3 or 16 mg propellant
Porosity	=	29%
Resistance of electrolyte in open cell (at 2 x 10^{-1} ohm^{-1} cm^{-1})	=	0.16
Resistance of full cell (with matrix)	=	2.8 ohms
Resistance Factor	=	17.5
Time to fill cell at 5 x 10^{-4} lbs/sec	=	75 msec

TABLE XXVI

FP-4 ENGINE PERFORMANCE DATA

Run No.	P_c (psia)	$\dot{\omega}$ (lb/sec x 10^{-4})	C* (ft/sec)	t_{90} (m_{sec})
27-3	35	1.50	2650	300
27-4	32	1.70	2120	350
28-2	37	1.80	2300	250
29-3	46	2.30	2230	300
29-10	46	2.40	2150	400
27-8	76	4.20	2030	400
27-7	86	4.70	2050	350
29-8	80	6.20	1450	200
27-9	113	8.50	1490	150

Cold Start Temp.: 70°F

TABLE XXVII

PERFORMANCE OF FP-4 ENGINE AS A FUNCTION OF ENGINE MODIFICATION

Run #	P_c (psia)	$\dot{\omega}$ (lb/sec x 10^{-4})	C* (ft/sec)	t_{90} (msec)	
29-10	46	2.40	2150	400	Refrasil Thermal Bed - Above & Below Cell
1-3	48	2.16	2590	400	Refrasil Thermal Bed - Above Cell
1-4	43	2.36	2040	200	Shell 405 Bed Above Cell
2-1	43	2.38	2020	100	Insulated Engine
3-1	40	2.22	2020	300	No Modification

Cold Start Temp: 70°F

TABLE XXVIII

FP-4 ENGINE TEMPERATURE PROFILE

Run #	Distance of Thermocouple From Cell (mm)	$\dot{\omega}$ (lb/sec x 10^{-4})	Equilibrium Temperature (°F)	P_c (psia)	Total Run Time (sec)	C* (ft/sec)
3-1	In cell	2.2	1500	40	8.4	2020
5-3	0	2.3	820	43	10.2	2100
5-8	0	3.8	990	80	8.1	2360
5-4	3	2.2	860	46	17.2	2340
5-5	10	2.2	610	43	15.6	2190
5-6	15	2.2	610	43	17.0	2190
5-9	15	4.3	650	92	4.7	2400
5-7	17	2.0	300	40	16.8	2240

TABLE XXIX

ENERGY AND POWER REQUIREMENTS
(ENGINE CONFIGURATION FP-4)

Run #	$\dot{\omega}$ (lbs/sec x 10^{-4})	I_{peak} (amps)	Pulse Width (msec)	Total Ignition Energy (watt-sec)	Peak Power (watts)
27-9A	8.50	8.4	570	105	320
27-9C	8.50	9.2	500	100	360
29-8A	6.20	7.0	300	19	280
2-1A	2.38	5.8	530	56	240
5-8B	3.80	8.8	220	41	360
5-9B	4.60	10.4	130	27	400

TABLE XXX

PERFORMANCE DATA AND ENERGY REQUIREMENTS
(ENGINE CONFIGURATION FP-5)

Run #	$\dot{w}$ (lbs/sec x 10^{-4})	P (psia)	t_{90} (msec)	t_{10} (msec)	C* (ft/sec)	I_{peak} (amps)	Pulse Width (msec)	Ignition Energy (watt-sec)	Peak Power (watts)
19-6	6.30	87	300	200	1550	8.8	450	48	320
19-5	3.10	92	350	400	3300	10.4	500	80	420
23-3	1.63	60	410	400	4120	10.6	300	58	425
23-4	1.75	60	370	500	3840	12.3	300	48	490

TABLE XXXI

PERFORMANCE DATA
(ENGINE CONFIGURATION FP-5A)

Run#	$\dot{\omega}$ (lbs/secx10^{-4})	P_c (psia)	C* (ft/sec)	t_{90} (msec)	t_{10} (msec)
29-10B	1.10	29	2910	240	120
26-5B	1.10	28	2810	280	180
29-10A	1.10	29	2890	100	160
30-1B	1.20	37	3340	-	-
30-1A	1.30	33	2940	-	-
29-4B	1.30	33	2850	360	110
29-4A	1.30	33	2760	110	270
29-5B	1.40	37	2890	330	120
29-11B	1.40	37	2870	410	140
29-11A	1.40	37	2850	160	120
28-7B	1.40	35	2700	170	200
28-7A	1.50	33	2460	310	100
29-5A	1.50	37	2720	460	110
28-11	1.60	37	2520	160	130
28-13B	1.70	40	2660	380	130
20-3B	1.70	44	2860	160	120
29-3A	1.70	45	2900	-	-
29-6B	1.70	46	2960	350	110
28-12	1.80	44	2760	190	130
29-6A	1.80	42	2620	130	160
29-3C	1.80	42	2550	160	130
30-2	1.90	50	2970	100	220
28-13C	1.90	44	2580	560	140
28-14C	2.00	54	3010	500	230
26-14A	2.00	49	2720	-	120
28-14B	2.10	50	2620	310	180
29-8B	2.20	60	3040	270	120
29-8A	2.30	55	2700	80	130
29-9B	2.40	60	2820	50	130
29-9C	2.40	60	2820	60	120
29-2	2.60	65	2830	-	-
29-1B	2.80	67	2660	150	110

TABLE XXXII

PERFORMANCE DATA
(ENGINE CONFIGURATION FP-5B)

Run#	$\dot{\omega}$ (lbs/secx10^{-4})	P_c (psia)	C* (ft/sec)	Isp (sec)	t_{90} (msec)	t_{10} (msec)	Cold Start Temp °F
11-12(HS)	1.02	37	4060	202	10	120	156
10-5B	1.14	41	4030	200	110	420	72
12-1(CS)	1.46	46	3550	176	170	320	-55
11-11	1.46	49	3720	185	180	180	77
11-13(HS)	1.74	62	3990	198	35	140	173
12-2	1 79	68	4210	209	130	-	72
11-10B(HS)	1.88	70	4140	206	170	200	296
11-9B(CS)	1.92	68	3950	196	80	210	-15
11-10(CS)	1.97	67	3800	189	120	200	-25
10-5(CS)	1.99	73	4110	204	80	-	113
11-5(CS)	2.03	68	3750	186	170	200	-15
11-7	2.08	73	3890	193	60	220	72
11-3C	2.08	74	3980	198	60	240	72
11-4(CS)	2.08	68	3630	180	130	210	-15
11-6	2.11	73	3860	192	160	320	72
11-15(HS)	2.42	69	3190	159	90	420	134

Theoretical Characteristic Velocity (C*)= 4340 ft/sec

Theoretical Specific Impulse (Isp) = 246 sec

TABLE XXXIII

ENGINE PERFORMANCE DATA
(IN ORDER OF INITIAL CELL TEMPERATURE)
(ENGINE CONFIGURATION FP-5B)

Run #	Initial Bed Temperature(^{o}F)*	$\dot{\omega}$ (lbs/sec x 10^{-4})	P_c (psia)	t_{90} (msec)	C* (ft/sec)
1-12-1	-55	1.46	46	170	3550
1-11-10	-25	1.97	67	120	3800
1-11-5	-15	2.03	68	170	3740
1-11-4**	-15	2.08	68	130	3630
1-10-5B	72	1.14	41	110	4030
1-12-3	72	1.79	68	110	4210
1-11-3C**	72	2.08	74	60	3980
1-11-7	72	2.08	73	60	3930
1-10-5C	113	1.99	73	80	4110
1-11-12	156	1.02	37	10	4060
1-11-13	173	1.74	62	40	3990

* Propellant temperature was 32 F for all starts at bed temp. less than 72 F and 72 F for all other runs

** Pressure - Time Relationships shown in Fig. 68

TABLE XXXIV

DURABILITY TESTS - DUTY CYCLE

Run #	On Time (sec)	Off Time (sec)	No. of Pulses	No. of Pulse Trains
*Base Point	---------- see below ----------			1
1	0.050	0.050	200	
2	0.100	6	20	10
3	30	1200	1	
4	3	--	1	
*Base Point	---------- see below ----------			1
5	0.050	0.450	100	25
*Base Point	---------- see below ----------			1
6	3	--	1	10
*Base Point	---------- see below ----------			
7	10	100	100	3
*base Point 8	---------- see below ----------			1
8	60	--	1	3
*Base Point	---------- see below ----------			

*Base Point Pulse Train is as follows:

Run #	On Time (sec)	Off Time (sec)	No. of Pulses
1	3	0.050	1
2	0.050	0.050	100
3	0.250	0.250	100

**All repeat pulse trains run after cooling to cold start temperature

TABLE XXXV

PERFORMANCE DATA-PROTOTYPE ENGINE #3
(MANUAL RUNS)

Run #	$\dot{\omega}$ (lbs/sec x 10^{-4})	P_c (psia)	Engine On-time (sec)	t_{90} (msec)	t_{10} (msec)	C* (ft/sec)	Temp* (°F)
2-15-1	2.06	33	6.20	100	400	2530	-
2-15-2	1.72	34	10.27	210	470	3120	-
2-15-3	2.34	53	7.25	70	520	3580	-
2-15-4	2.58	53	9.14	310	540	3240	-
2-15-5	3.24	65	6.30	260	440	3170	-
2-16-1	2.95	50	6.20	---	---	2680	1200
2-16-2	2.19	50	8.35	100	450	3020	1240
3-2-1	2.50	53	10.85	230	---	3350	1500
3-2-2	2.10	50	20.8	---	---	3760	1590
3-2-3	2.52	46	7.6	---	---	2890	1370

*Temperatures are those of the outside chamber wall opposite the electrolyte matrix.

Cold Start Temperature: 70 F

TABLE XXXVI

PERFORMANCE DATA PROTOTYPE ENGINE #3

(DUTY CYCLE RUNS)

Run #	$\dot{\omega}$ (lbs/sec x 10^{-4})	P_c (psia)	Engine On-time (sec)	C* (ft/sec)	t_{90} (msec)	t_{10} (msec)	Temp* (^oF)
Base Pt. #1	2.15	50	50.5	3680	50	--	1640*
Base Pt. #2	2.10	53	50.5	3980	60	200	1550*
1-1	2.95	53	20	2800	180	--	1330
2-1	No data - failure due to thermal soak-back						
Base Pt. #3	2.01	55	50.5	4330	50	100	1290
1-2	2.10	50	20	3760	--	--	1370
2-2	No data - failure due to thermal soak-back						
5-1	2.06	37	5	3840	60	130	1160
7(1-8)	2.20	46	80	3300	50	500	1030
7(1-5)	2.12	51	50	3800	250	500	1330
7(6-14)	2.20	51	90	3660	250	500	1330
1-3	2.06	49	20	3760	250	400	1400
3-1	1.93	53	30	4340	220	520	1400
8-1	1.96	52	60	4200	260	--	1400
Base Pt. #4	2.06	53	50.5	4060	80	--	1350
Base Pt. #5	2.28	49	50.5	3400	--	--	1460

*Internal temperatures - all others are outside chamber wall temperatures.

Cold Start Temperature: 70 F

TABLE XXXVII

PERFORMANCE DATA PROTOTYPE ENGINE #5
(MANUAL RUNS)

Run #	$\dot{\omega}$ (lbs/sec x 10^{-4})	P_c (psia)	Time (sec)	C* (ft/sec)	t_{90} (msec)	t_{10} (msec)	Temp* (°F)
3-10-2	1.40	23	4.65	2400	--	220	--
3-10-3	1.80	23	3.33	1870	--	300	440
3-10-4	1.25	23	9.30	2680	260	230	680
3-10-5	2.05	37	8.29	3050	260	270	939
3-10-6	2.55	55	9.62	3140	200	320	1180
3-10-7	2.44	54	9.00	3230	200	220	1180
3-10-9	1.76	37	10.00	3070	160	330	1130
3-10-10	1.92	35	8.00	2660	160	270	1130
3-13-1	2.51	50	7.85	2900	110	210	1130
3-13-2	2.36	50	8.90	3100	160	360	1240
3-13-3	3.02	67	7.10	3220	50	300	1140
3-13-4	1.05	24	20.04	3340	60	420	1130
3-13-5	1.44	33	14.75	3360	90	320	1160
3-13-6	1.83	42	11.40	3340	110	540	1180
3-13-7	2.16	49	10.20	3300	80	370	1240
3-13-8	2.64	56	8.05	3100	70	210	1180
3-13-9	2.56	55	8.10	3120	60	420	1180
3-13-10	2.62	55	8.10	3060	80	320	1180
3-13-11	2.64	55	8.20	3050	70	340	1180
3-13-12	3.06	66	6.95	3170	70	320	1130
3-13-14	1.83	44	12.30	3500	70	220	1180
3-13-15	2.32	51	9.02	3200	50	340	1180
3-13-17	1.69	42	12.65	3430	50	220	1160
3-13-18	1.78	42	11.90	3320	80	470	1150
3-13-19	1.97	47	10.80	3470	50	370	1180
3-14-1	2.26	51	9.35	3300	--	---	1160

*All temperatures are those of the outside chamber wall
Cold Start Temperature: 70 F

TABLE XXXVIII

PERFORMANCE DATA PROTOTYPE ENGINE #5
(DUTY CYCLE RUNS)

Run #	$\dot{\omega}$ (lbs/sec x 10^{-4})	P_c (psia)	Engine On-time (sec)	C* (ft/sec)	t_{90} (msec)	t_{10} (msec)	T_c (^oF)	Peak Current (amps)	Peak Powers (watts)
Base Pt#1	2.00	53	50.5	3870	30	220	1330	2.5	105
1-1	1.98	53	20	3910	--	270	1330	3.0	126
1-2	2.01	51	20	3710	--	420	1380	1.75	74
1-3	1.80	52	20	4210	--	320	1380	---	---
1-4	1.86	53	20	4160	--	290	1380	3.0	126
1-5	2.00	53	20	3870	--	380	1380	2.5	105
1-7	1.85	53	20	4180	--	350	1380	2.5	105
1-8	1.92	52	20	3960	--	320	1380	2.0	84
1-9	1.79	51	20	4160	--	300	1380	2.5	105
1-10	2.01	52	20	3780	40	280	1380	3.0	126
3-1	1.85	54	30	4260	--	370	1380	3.0	126
3-2	1.95	54	30	4040	--	520	1440	3.0	126
3-3	1.92	54	30	4100	--	470	1440	2.5	105
3-4	1.86	54	30	4240	--	520	1440	---	---
3-5	1.90	54	30	4150	--	370	1440	---	---
3-7	1.86	53	30	4160	--	510	1440	2.5	105
3-8	1.85	53	30	4180	--	500	1440	3.0	126
3-9	1.81	53	30	4270	--	490	1450	---	---
3-10	1.98	53	30	3910	20	410	1450	2.5	105
Base Pt#2	2.16	49	50.5	3310	50	220	1453	3.1	131
5-1	No data - thermal soak back								

*All temperatures are those of the outside chamber wall
Cold Start Temperature: 70 F

TABLE XXXIX

PROTOTYPE ENGINE #5 POWER AND ENERGY REQUIREMENTS

Run #	Peak Current (amps)	Peak Power (watts)	Total* Energy (watt-sec)	Ignition Energy (watt-sec)
1 - 1	3.0	126	88	32
1 - 4	3.0	126	149	15
1 - 5	2.5	105	108	23
1 - 10	3.0	126	169	30
3 - 1	2.5	105	133	16
3 - 10	2.5	105	173	28
Base Pt. #2	3.1	131	130	34

* Based on applied voltage of 42 volts

TABLE XL

PERFORMANCE DATA
PROTOTYPE ENGINE #6
(DUTY CYCLE RUNS)

Run #	$\dot{\omega}$ (lbs/sec x 10^{-4})	P_c (psia)	Engine On-time (sec)	C* (ft/sec)	t_{90} (msec)	t_{10} (msec)	T_c (°F)	Peak Current (Amps)
4-3-1	2.28	44.5	8.0	3270	120	380	1070	6.4
4-3-2	2.11	47.5	13.6	3550	-	460	1316	6.6
4-3-3A	1.49	37.0	7.2	3880	-	410	930	5.7
4-3-3B	1.73	41.5	14.5	3820	-	550	1385	hot start
4-4-1	1.78	44.0	14.2	3670	-	450	1316	residual current
4-4-2	1.79	40.0	13.7	3560	-	410	1249	6.3
4-4-3	2.06	44.5	12.2	3440	120	530	1333	7.6
Base Pt #1A	2.08	37(3sec)		2830	110	-	-	3.0
		43(1 pls)	13.0	3280	80	400	1280	
		49(100pls)	50.0	3750	50	340	1450	
Base Pt #1B	1.95	38.5(3sec)		3140	80	-	-	2.4
		46(1 pls)	13.0	3760	40	240	1280	
		48.5(100pls)	50.0	3960	40	260	1450	
3-1	1.91	47.5	30.0	3960	-	440	1450	1.9
3-2	1.93	47.5	30.0	3910	100	520	1440	2.7
3-3	1.95	47.5	30.0	3870	100	500	1440	2.8
3-4	1.95	47.5	30.0	3870	110	560	1440	2.8
3-5	1.96	47.5	30.0	3860	90	560	1440	3.0
3-6	1.95	47.5	30.0	3870	100	600	1440	2.8
3-7	1.96	48.0	30.0	3900	100	560	1440	2.8
3-8	1.95	47.5	30.0	3870	-	580	1440	3.2
3-9	1.96	47.5	30.0	3860	-	590	1440	2.9
3-10	1.96	47.5	30.0	3860	80	610	1440	2.7
Base Pt #2	2.06	40(3sec)	13.0	3080	-	-	-	2.6
		44.5(1pls)		3440	40	170	1280	
		47.5 (100 pls)	37/50	3670	40	310	1430	

*Manual Runs - all rest duty cycle runs

TABLE XL CONTINUED

Run #	$\dot{\omega}$ (lbs/sec x 10^{-4})	Pc (psia)	Engine On-time (sec)	C* (ft/sec)	t_{10} (msec)	t_{10}	Tc (°F)	Peak Current (amps)	Starting Temperature (°F)
6-1	2.56	39.5	3	2460	--	460	740	residual current	
6-2	2.66	39.5	3	2360	80	440	705	3.1	
6-3	2.69	40	3	2360	100	350	720	3.2	
6-4	2.60	40	3	2440	90	430	725	3.0	
6-5	2.64	40	3	2410	80	460	720	3.1	
6-6	2.66	40	3	2390	80	520	670	3.1	
6-7	2.68	40	3	2380	50	400	715	3.1	
6-8	2.68	40	3	2380	80	460	705	3.1	
6-9	2.68	40	3	2380	--	420	650	3.6	
6-10	2.66	39.5	3	2360	80	420	670	3.0	
7-1	2.18	44.5	10	3250	400	550	1125	3.0	70
7-2	2.18	46	10	3350	120	580	1265	0.2	385
7-6	2.16	47	10	3460	100	480	1280	0.2	385
7-11	2.18	47.5	10	3460	80	530	1300	--	360
7-15	2.15	47.5	10	3520	70	540	1280	0.1	360
7-19	2.14	47.5	10	3460	50	440	1270	0.2	340
Base Pt #3	1.98	37(3sec)	13	2980	180	--	---	residual current	
		40(1stpls)	-	3210	50	340	1250		
		46(100pls)	37	3700	50	400	1420		
7-1(cs)	1.99	42.5	10	3400	140	510	1110	3.0	70
7-5	2.04	45.5	10	3550	70	460	1300	0.1	360
7-10	1.94	44.5	10	3650	80	340	1250	0.1	340
7-14	2.02	45.5	10	3580	100	360	1265	0.1	450
7-25	1.99	46	10	3680	70	380	1300	--	385
7-30	1.96	46	10	3750	60	340	1280	0.1	360
7-34	1.95	46	10	3750	60	340	1280	0.1	360
7-40	1.95	46	10	3750	50	350	1300	0.1	385
7-44	1.97	46	10	3720	40	310	1280	0.1	385

TABLE XL CONTINUED

Run #	$\dot{\omega}$ (lbs/sec x 10-4)	P_c psia)	Engine On-Time (sec)	C* (ft/sec)	t_{90} (msec)	t_{10} (msec)	T_c (°F)	Peak Current (amps)	Starting Temperature (°F)
8-2	1.78	46	60	4110	150	500	1470	3.2	
8-3	1.75	46	60	4180	120	120	1470	3.0	
8-4	1.76	46	60	4160	90	540	1470	3.0	
Base Pt #8	1.83	34.5(3sec) - 41.5(1st pls)	13	3000	100	--	---	2.6	
		44.5(100 pls)	50	3610	50	240	1230		
8-9	1.68	44.5	60	3950	40	220	1450		
8-10	1.70	45	60	4210	180	460	1435	residual current	
8-11	1.70	46	60	4210	60	440	1450	3.1	
8-12	2.04	46	60	4300	50	410	1450	residual current	
5-1	1.95	21(1pls)	--	3590	180	430	1450	2.0	
		41(50pls)	--	1710	50	100	---	2.8	
		41(100pls)	5	3340	50	210	1210		
5-2	1.80	29(4pls)	--	3340	30	160	1330	--	
		40.5 (50pls)		2560	20	100	---	residual current	
		41(100pls)	5	3580	20	150	1180		
5-3	1.65	27(4pls)		3620	40	110	1280		
		40(50pls)	--	2600	20	90	---	residual current	
		40.5(100 pls)	5	3860	30	110	1140		
1-1	1.70	43	10	3900	30	110	1280		
Base Pt #9	1.71	31.5(3sec)	--	4020	60	210	1390	residual current	
		42(1pls)	13	2930	70	--	---	residual current	
		44.5(100 pls)	50	3900	50	240	1300		
				4140	50	180	1470		

TABLE XL CONTINUED

Run #	$\dot{\omega}$ (lbs/sec x 10-4)	P_c (psia)	Engine On-Time (sec)	C* (ft/sec)	t_{90} (msec)	t_{10} (msec)	T_c (°F)	Peak Current (amps)	Starting Temperature (°F)
7-50	1.96	46	10	3750	50	310	1280	0.1	385
7-55	2.04	46	10	3580	50	260	1370	--	385
7-59	1.92	45.5	10	3770	60	260	1280	0.1	360
7-65	2.06	46	10	3550	60	270	1280	0.1	370
7-70	1.96	46	10	3740	130	270	1320	0.1	385
7-80	2.01	45.5	10	3600	140	270	1280	0.1	365
7-90	2.03	47	10	3680	50	260	1450	0.1	385
7-95	1.95	45	10	3680	50	280	1300	0.1	385
7-100	1.94	44.5	10	3650	60	340	1280	0.1	365
7-105	2.04	45.5	10	3540	40	510	1350	0.1	365
7-110	2.00	45.5	10	3610	70	380	1330	0.1	365
7-115	2.01	46	10	3640	70	460	1315	0.1	365
7-120	1.94	46	10	3770	60	320	1350	0.2	385
7-125	2.02	46	10	3630	70	280	1315	0.2	370
7-130	2.00	46	10	3660	180	410	1330	--	510
7-135	2.06	46	10	3550	80	270	1350	0.2	360
7-145	2.02	44.5	10	3500	80	430	1335	0.1	360
7-150	2.01	45	10	3560	90	400	1335	0.1	360
7-155	2.00	44.5	10	3540	100	440	1335	0.1	360
7-160	2.01	44	10	3520	60	370	1300	0.3	360
7-165	1.99	44	10	3520	60	370	1300	0.3	360
7-171	1.97	44	10	3550	90	310	1300	0.2	350
Base Pt #4	1.77	34(3sec)	--	3050	80	--	---	3.0	
		43(1stpls)	13	3860	30	160	1280	--	
		45.5(100pls)	50	4090	30	210	1450	--	
Base Pt #5	1.97	30.5(3sec)	--	2460	150	--	---	residual current	
		40(1stpls)	13	3230	40	--	1330		
		46(100 pls)	50	3720	30	340	1485		
8-1	1.75	46	60	4180	80	560	1485	residual current	

FIG. 1

TEMPERATURE DEPENDENCE OF ELECTRICAL CONDUCTIVITY IN HYDRAZINE SOLUTION

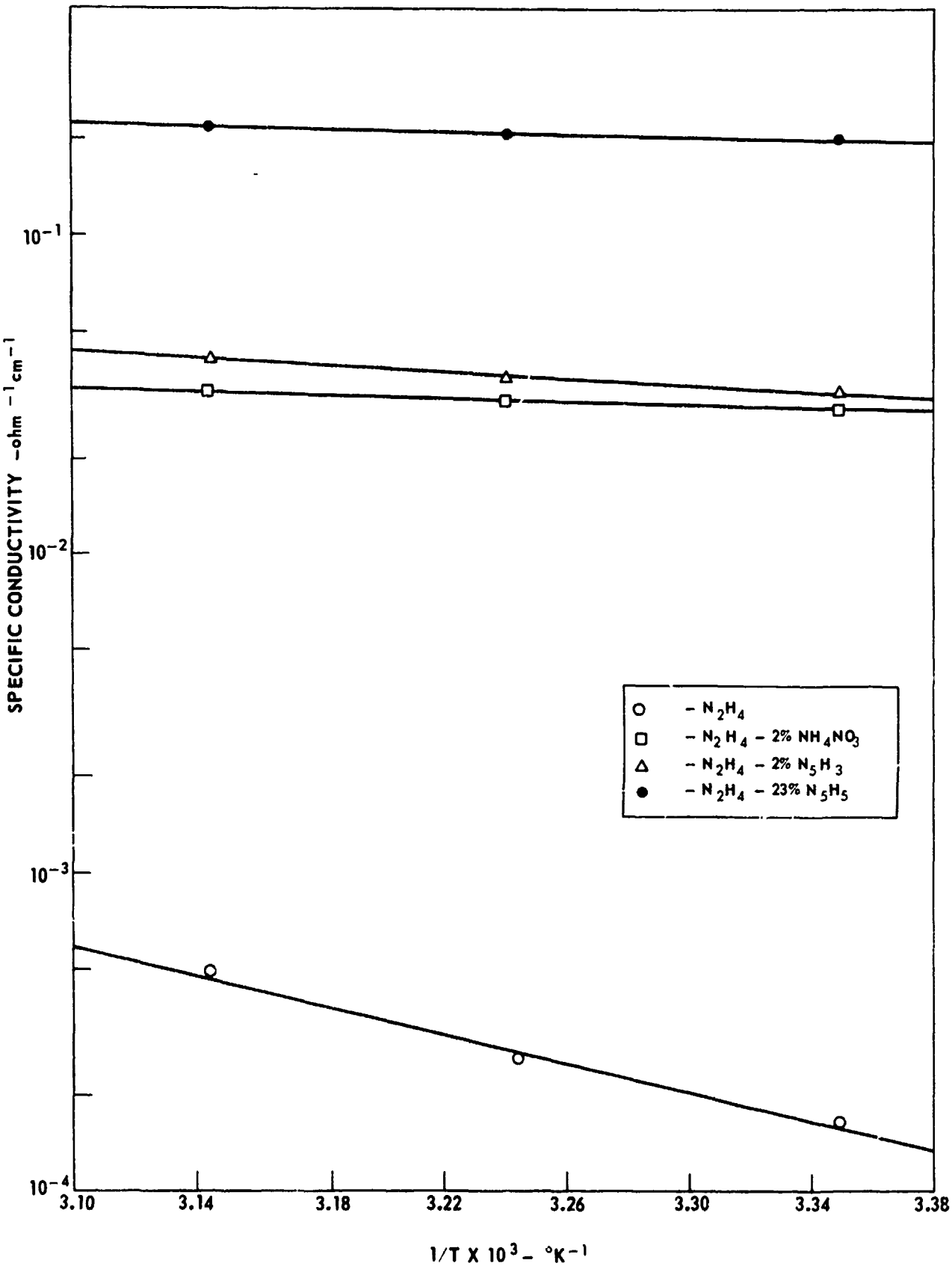

FIG. 2

ELECTRODE POLARIZATION APPARATUS

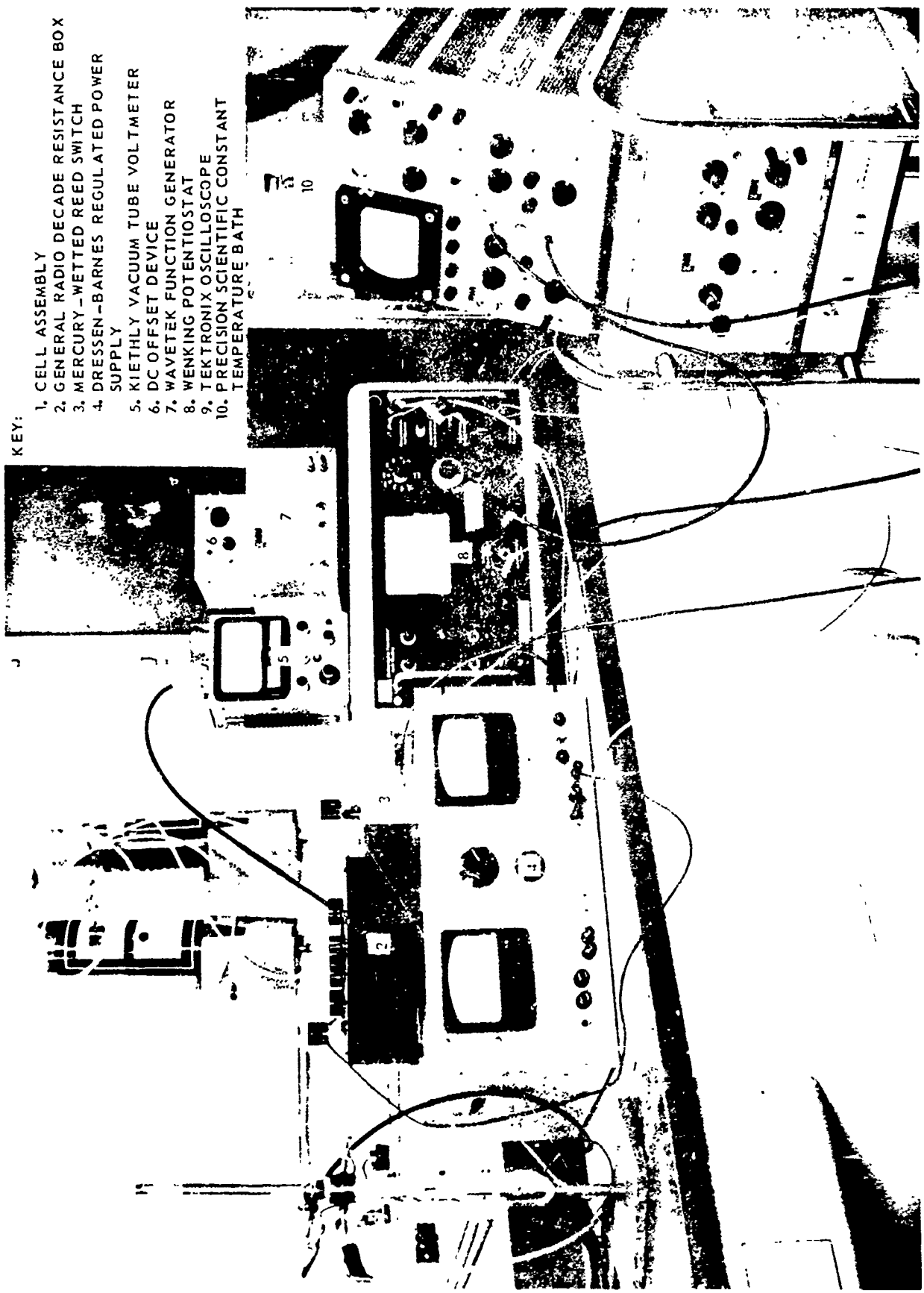

RL-70-291-A

FIG. 3

ANODIC POLARIZATION OF 17-7 PH IN HYDRAZINE-BASE PROPELLANTS

○ = N_2H_4 - 23% N_5H_5
△ = N_2H_4
□ = N_2H_4 - 5% $N_2H_5NO_3$

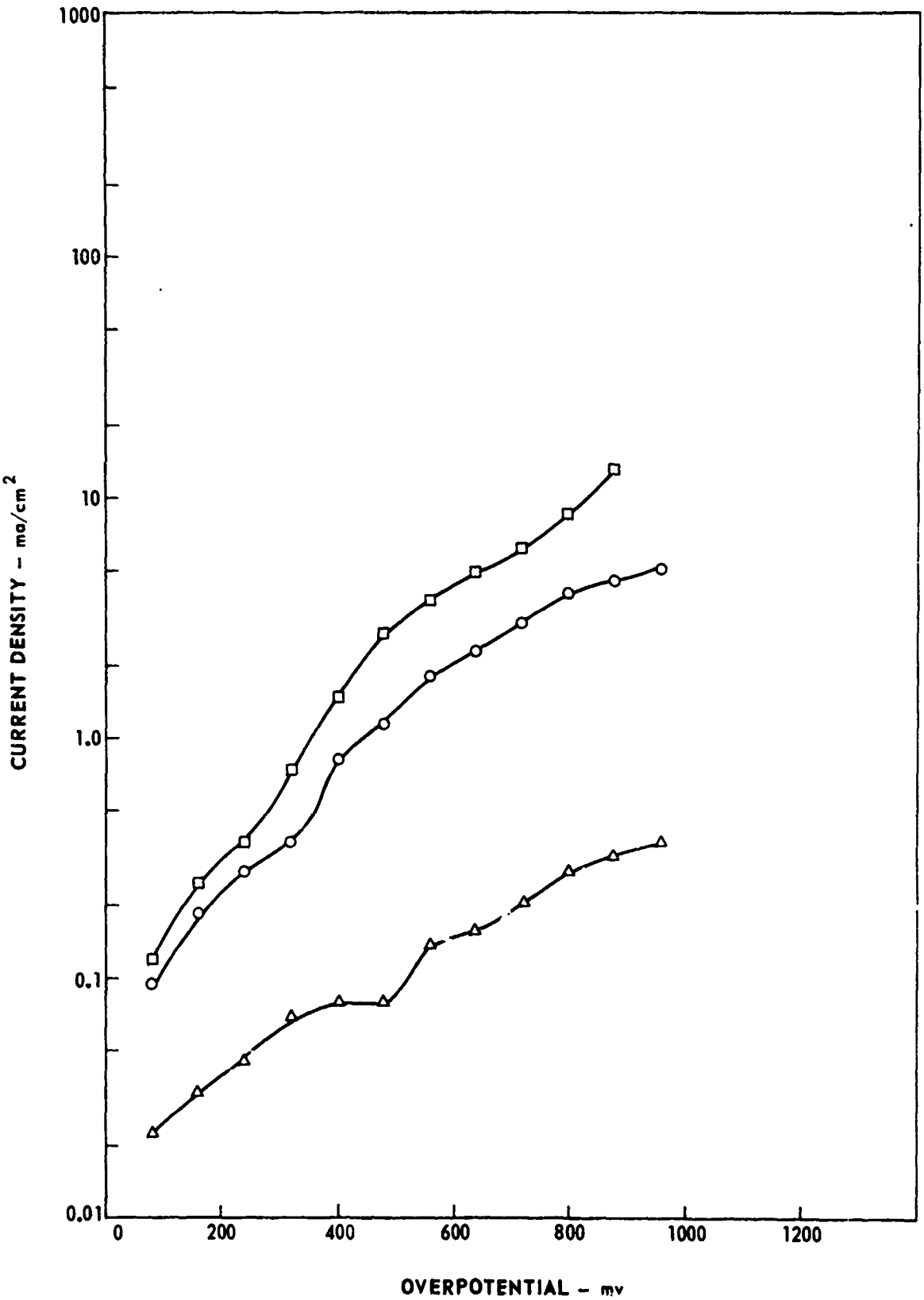

FIG. 4

ANODIC POLARIZATION OF 304SS IN HYDRAZINE-BASE PROPELLANTS

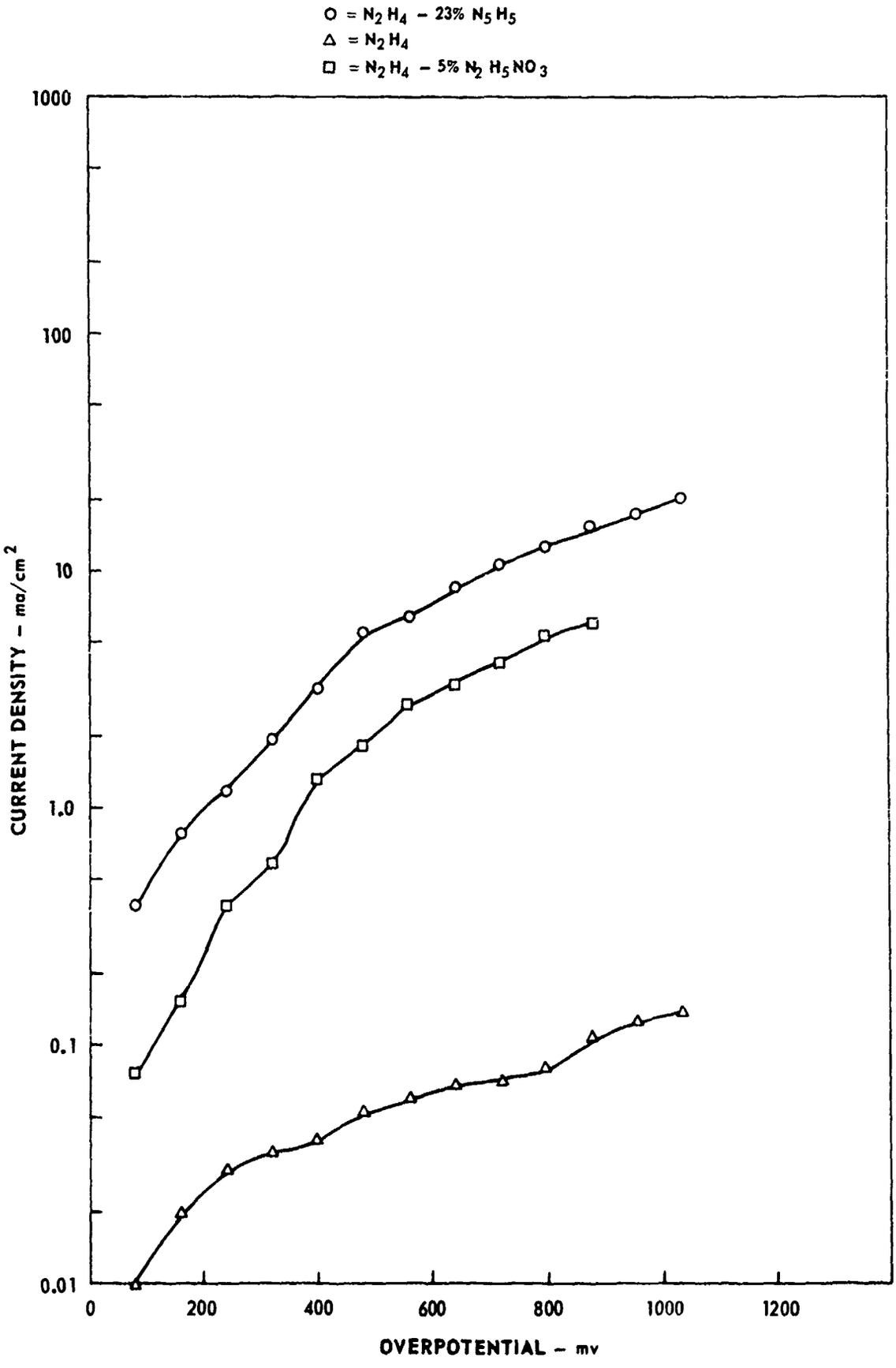

FIG. 5

ANODIC POLARIZATION OF AM 350 IN HYDRAZINE-BASE PROPELLANTS

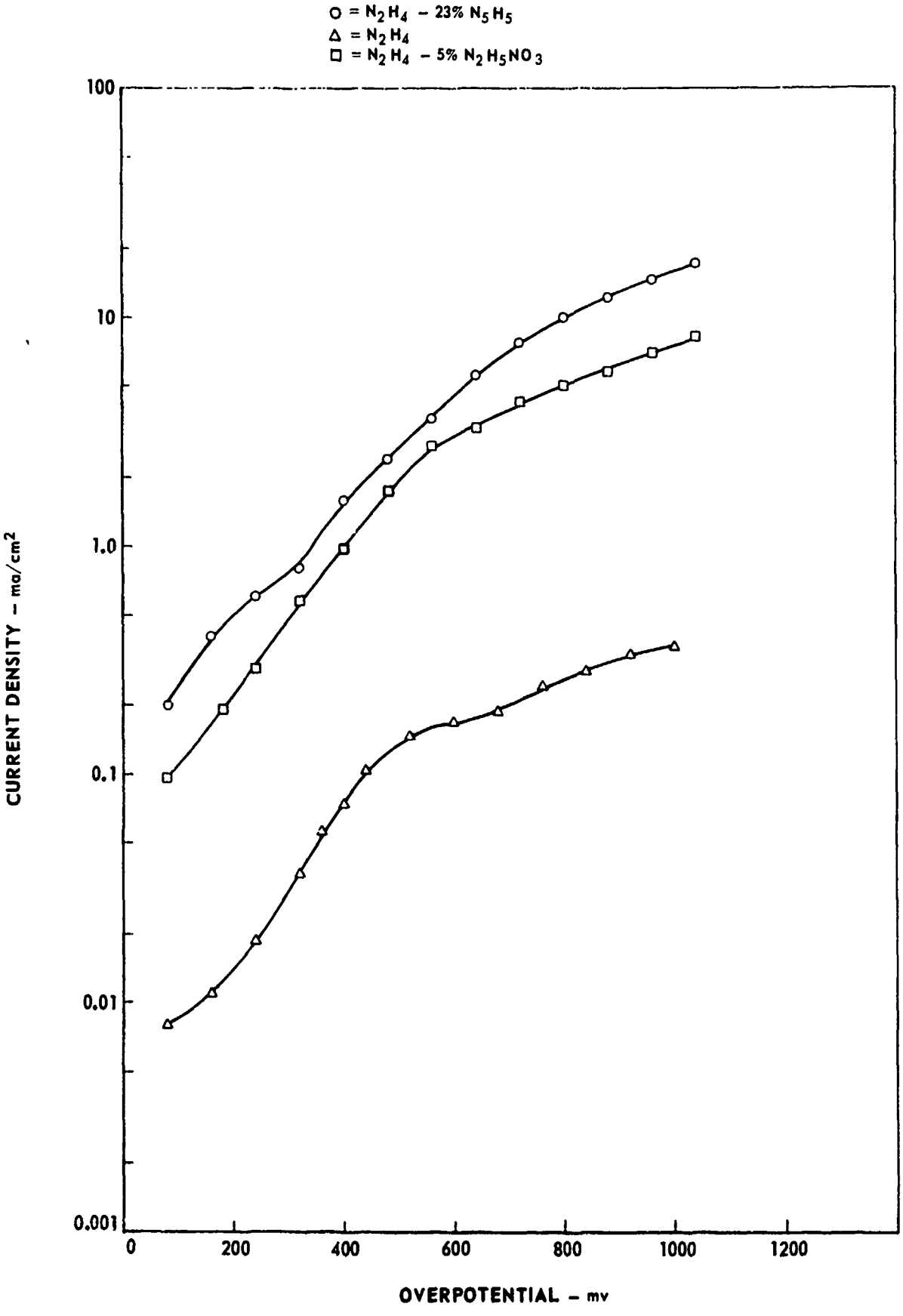

ANODIC POLARIZATION OF HS 1414 IN HYDRAZINE-BASE PROPELLANTS

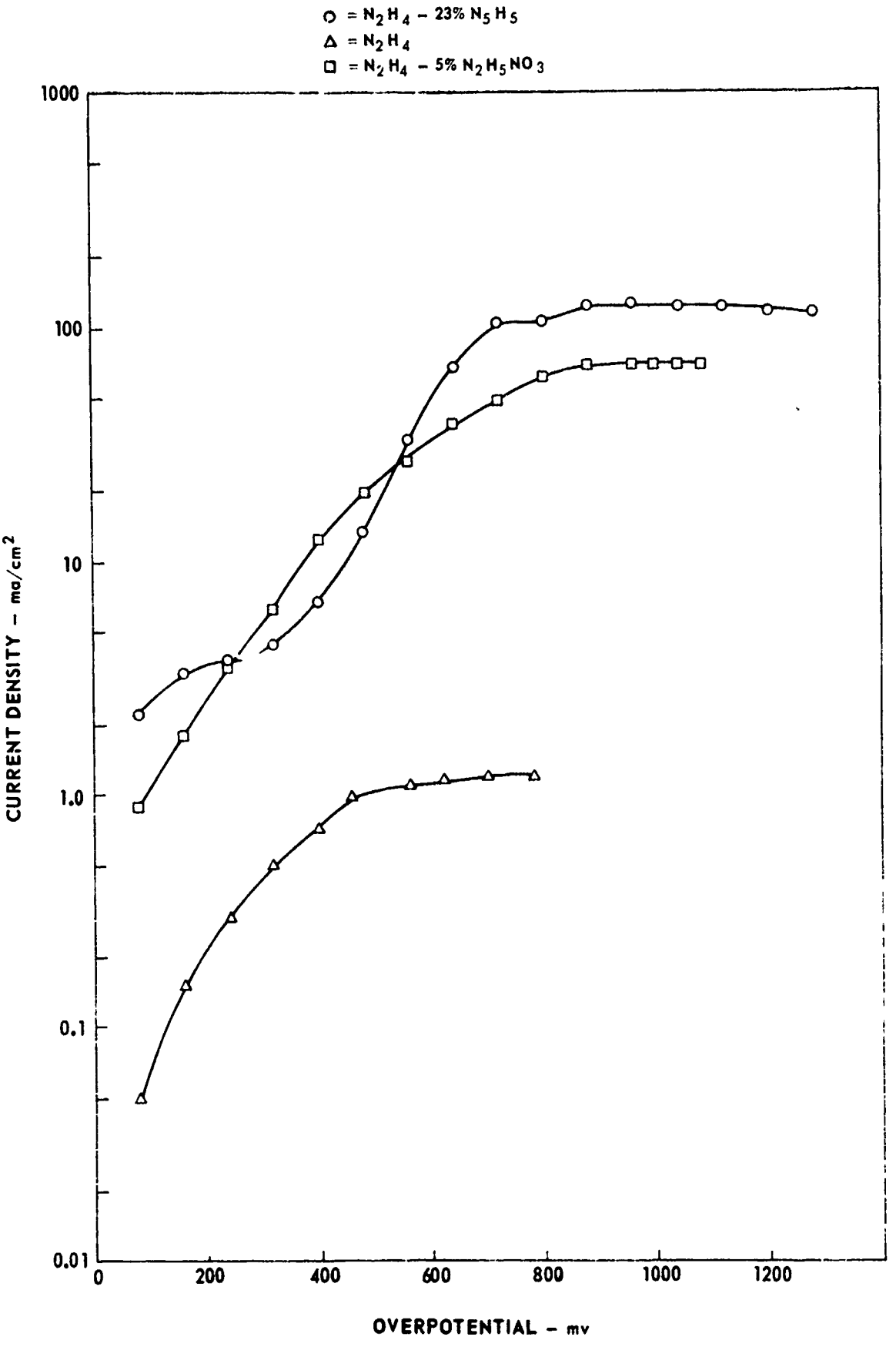

FIG. 7

ANODIC POLARIZATION OF PLATINUM IN HYDRAZINE-BASE PROPELLANTS

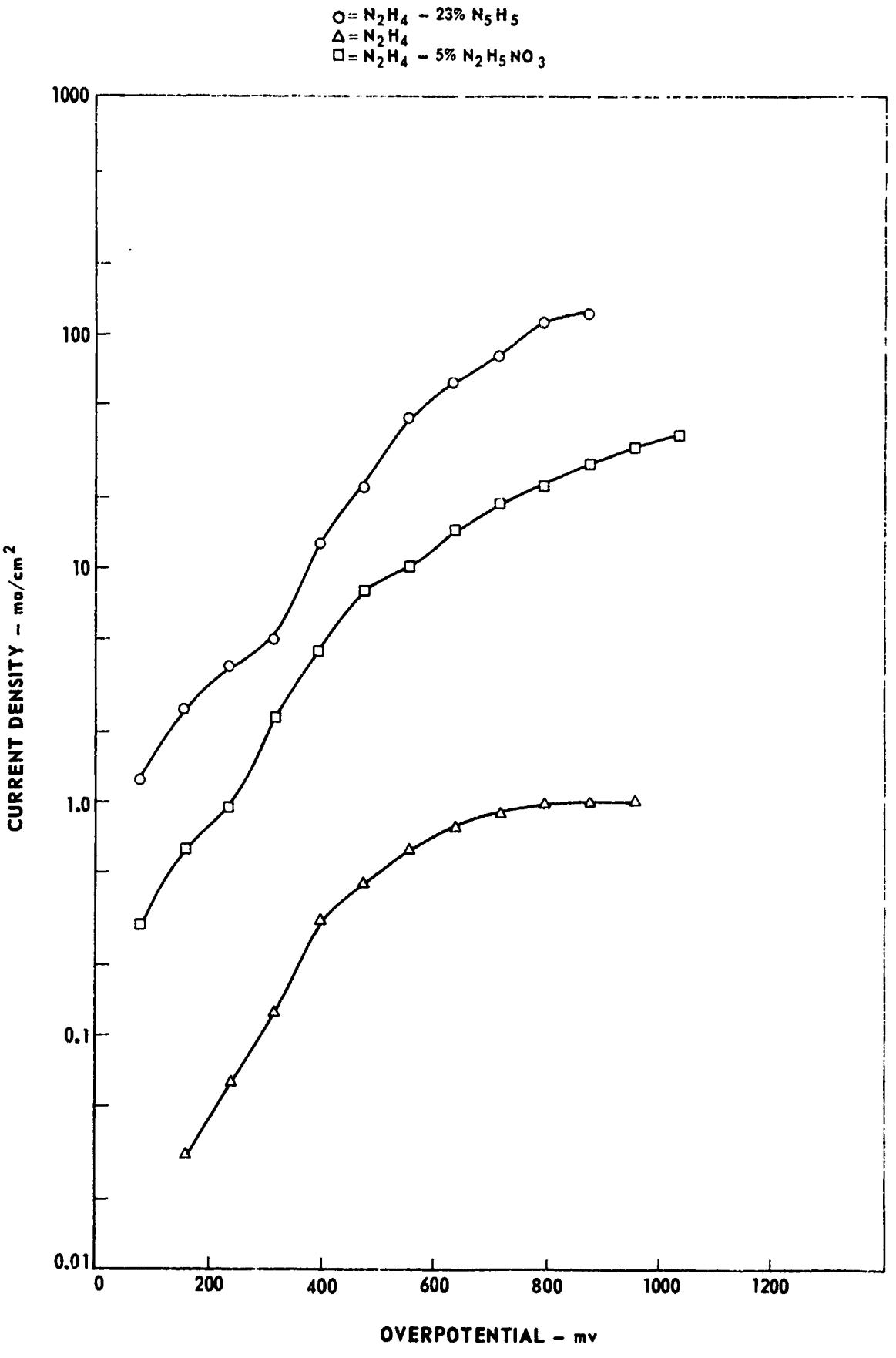

ANODIC POLARIZATION OF GRAPHITE IN HYDRAZINE-BASE PROPELLANTS

FIG. 8

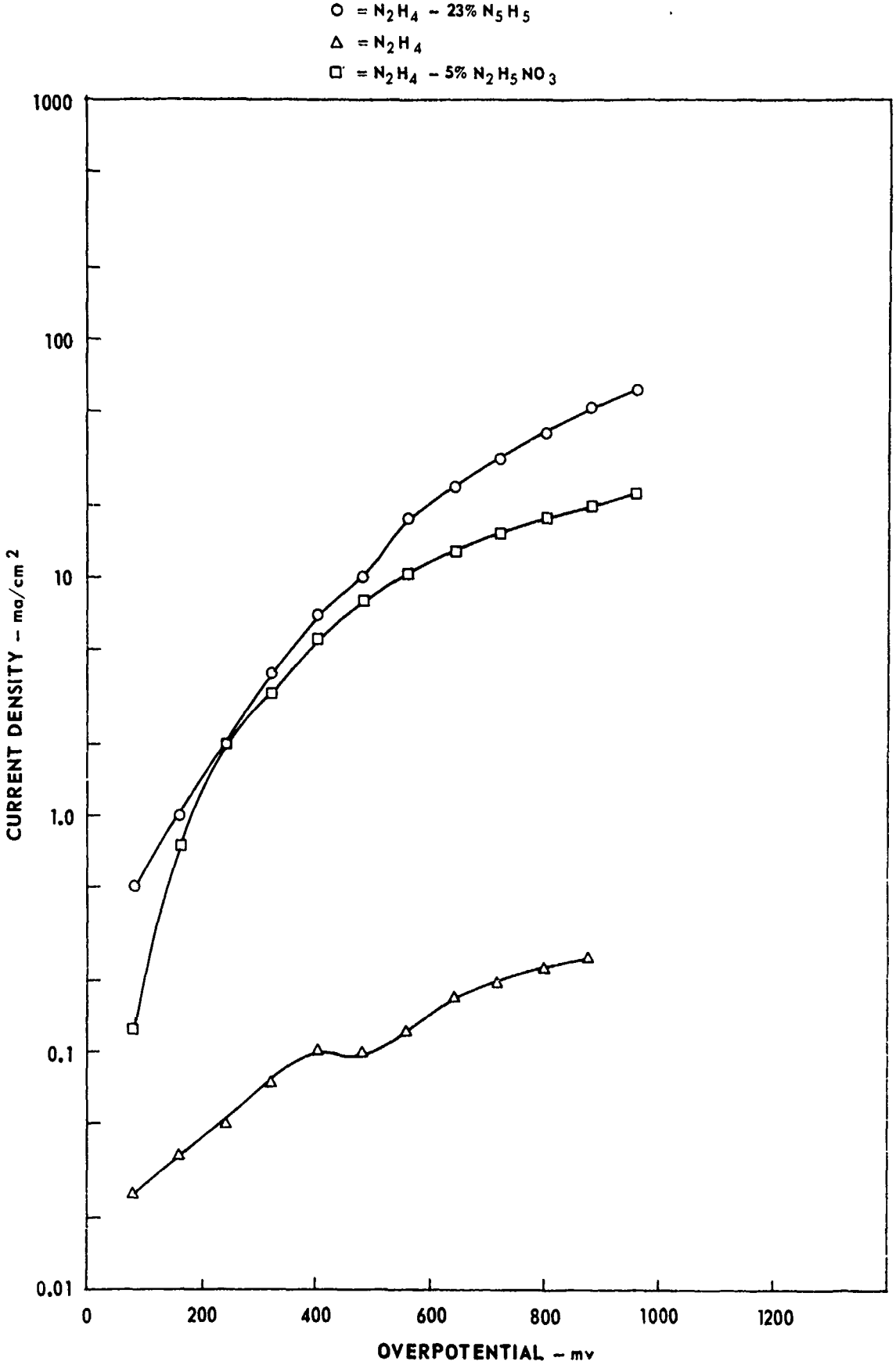

FIG. 9

ANODIC POLARIZATION OF AA 1100 IN HYDRAZINE-BASE PROPELLANTS

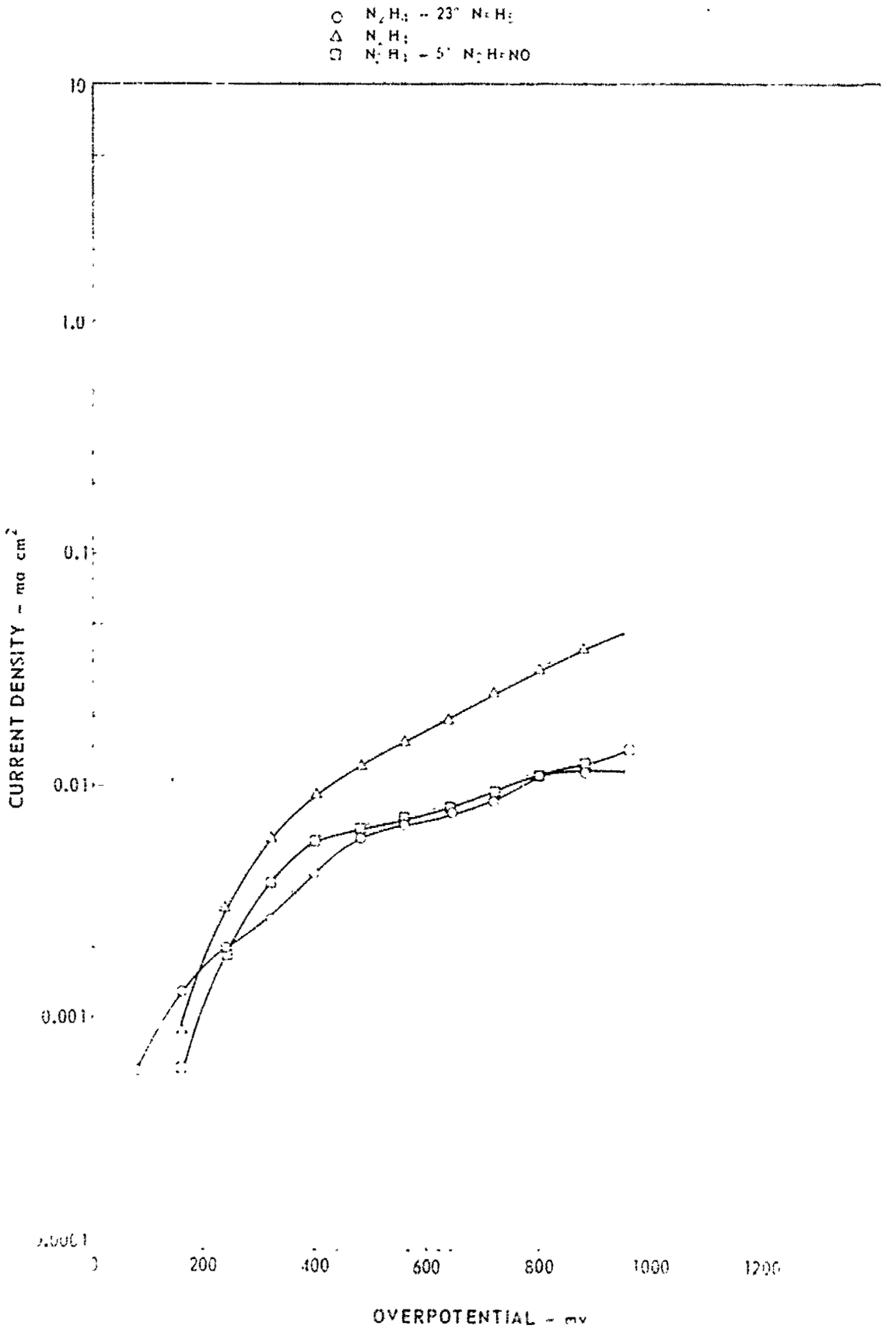

FIG. 10

ANODIC POLARIZATION OF AA 6061-T6 IN HYDRAZINE-BASE PROPELLANTS

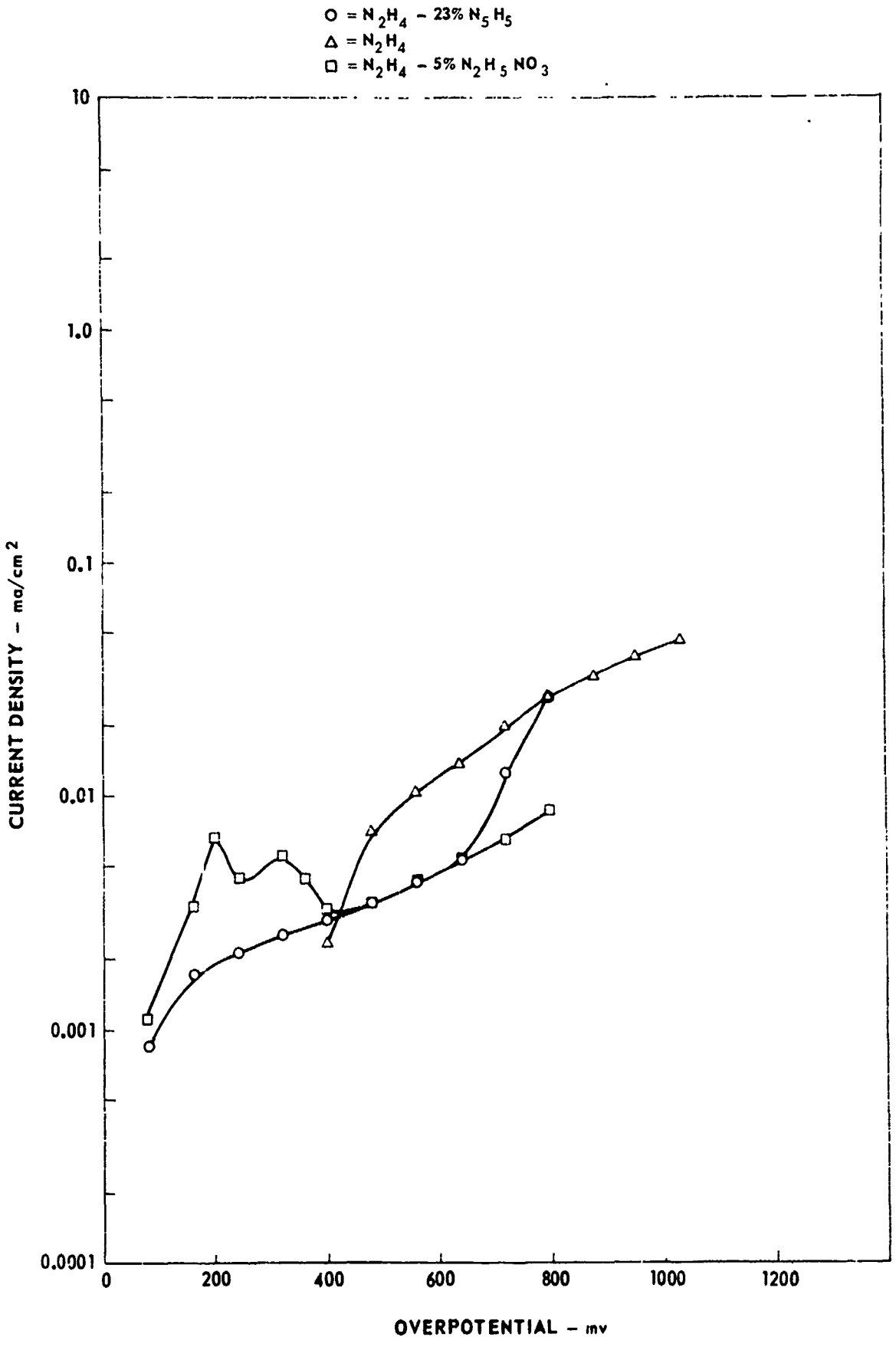

FIG. 11

ANODIC POLARIZATION OF NICKEL, PLATINUM, AND INCONEL IN 77% HYDRAZINE-23% HYDRAZINE AZIDE

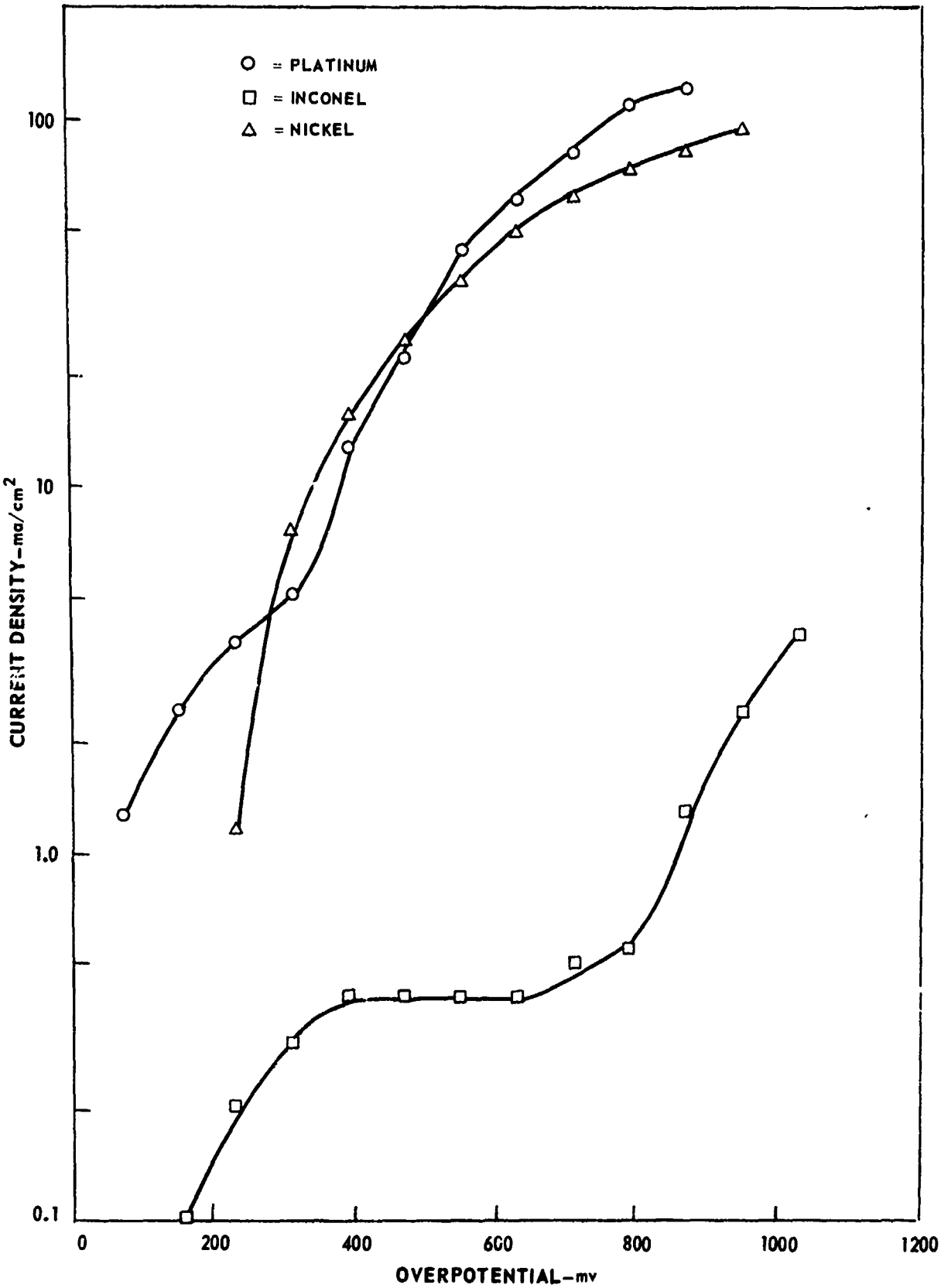

FIG. 12

CATHODIC POLARIZATION OF 17-7 PH IN HYDRAZINE-BASE PROPELLANTS

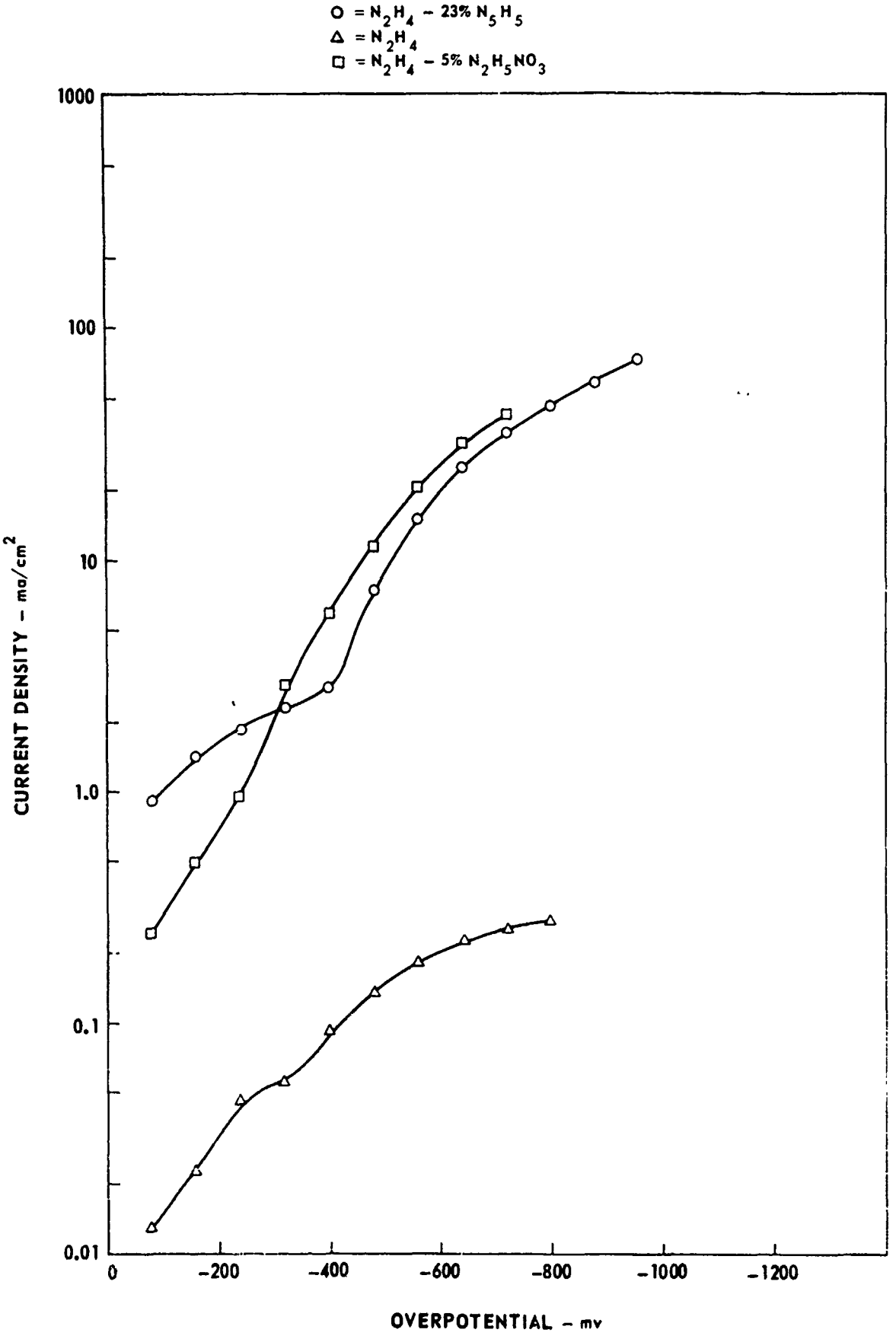

FIG. 13

CATHODIC POLARIZATION OF 304 SS IN HYDRAZINE-BASE PROPELLANTS

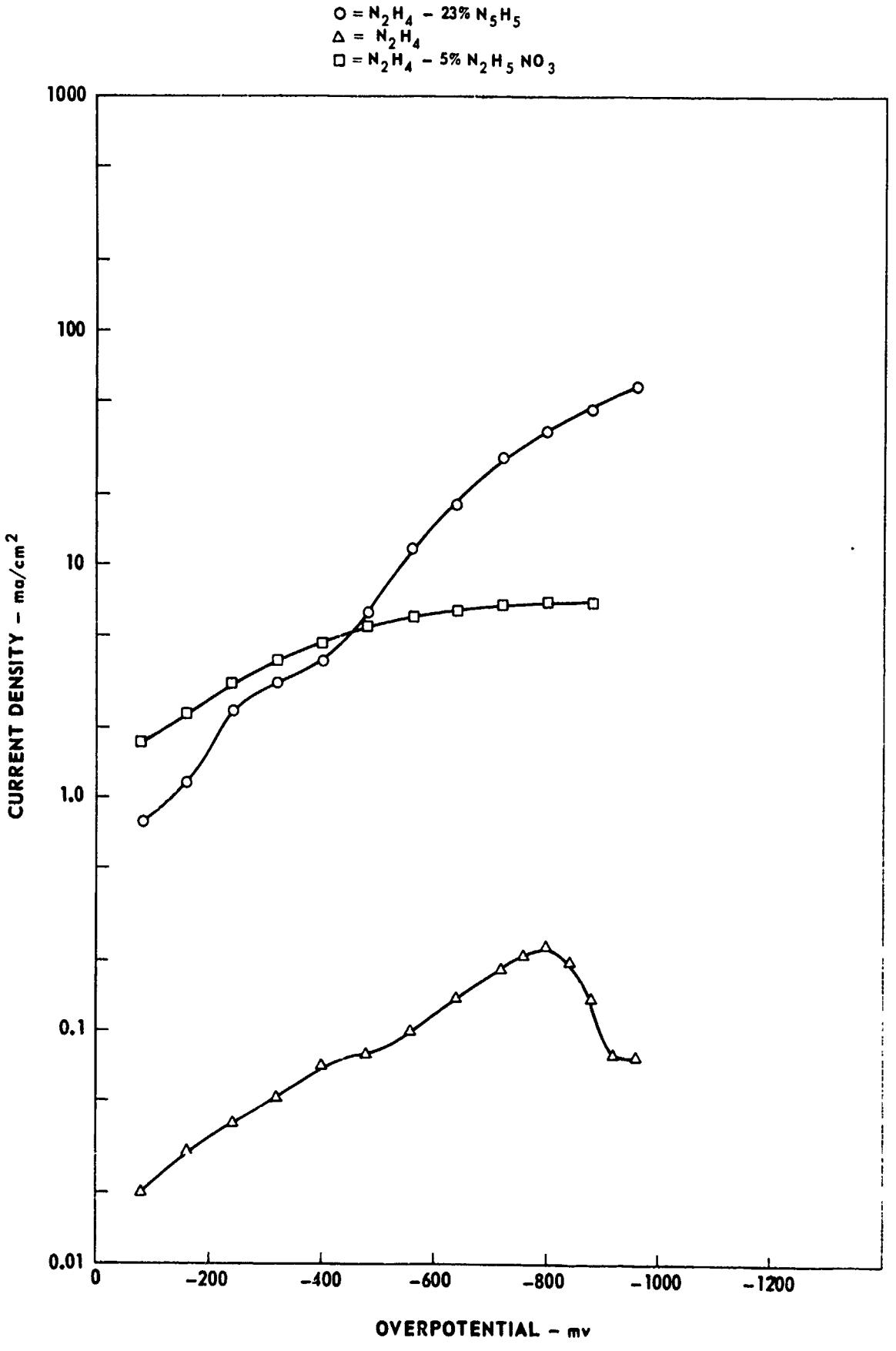

FIG. 14

CATHODIC POLARIZATION OF AM 350 IN HYDRAZINE-BASE PROPELLANTS

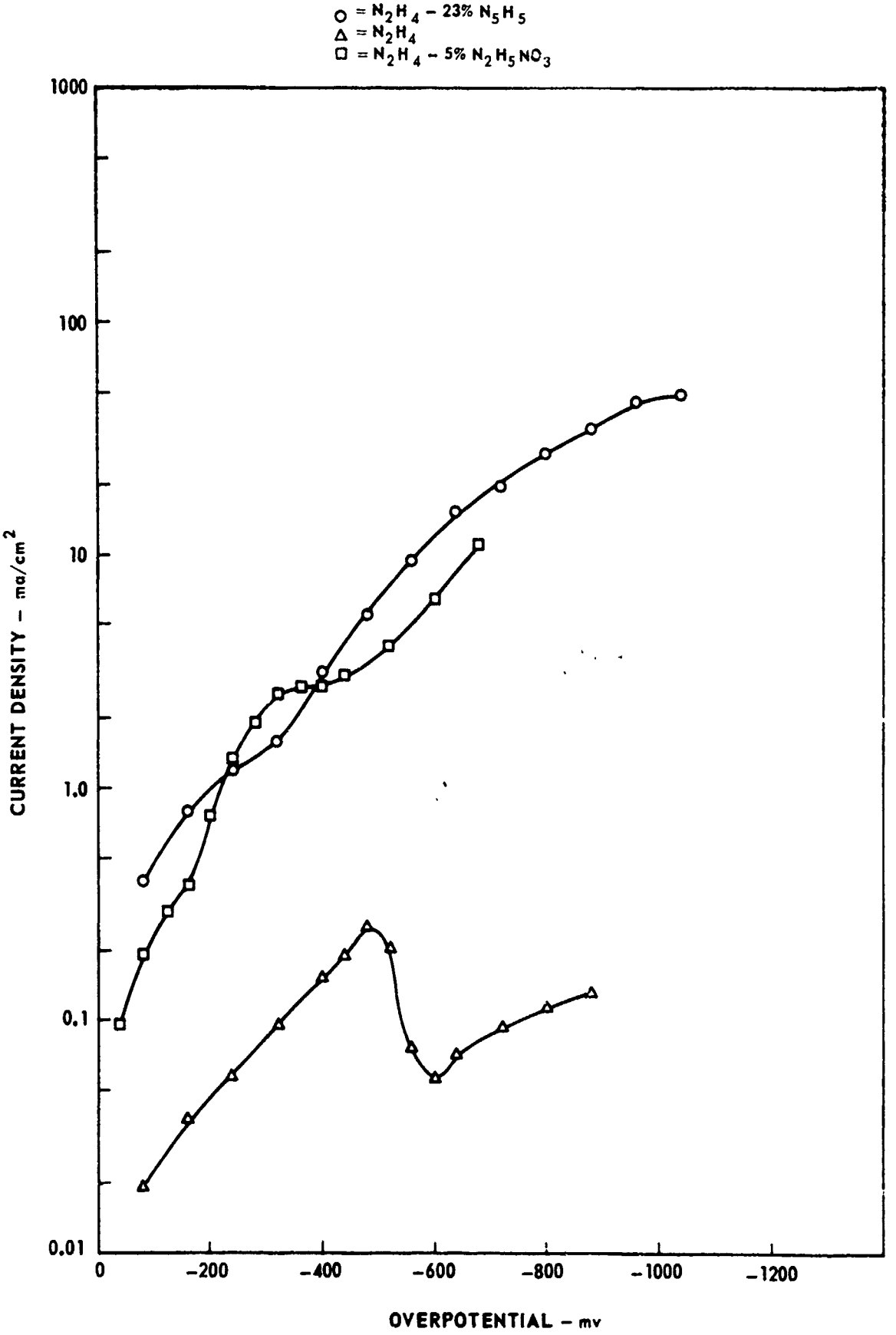

FIG. 15

CATHODIC POLARIZATION OF HS 1414 IN HYDRAZINE-BASE PROPELLANTS

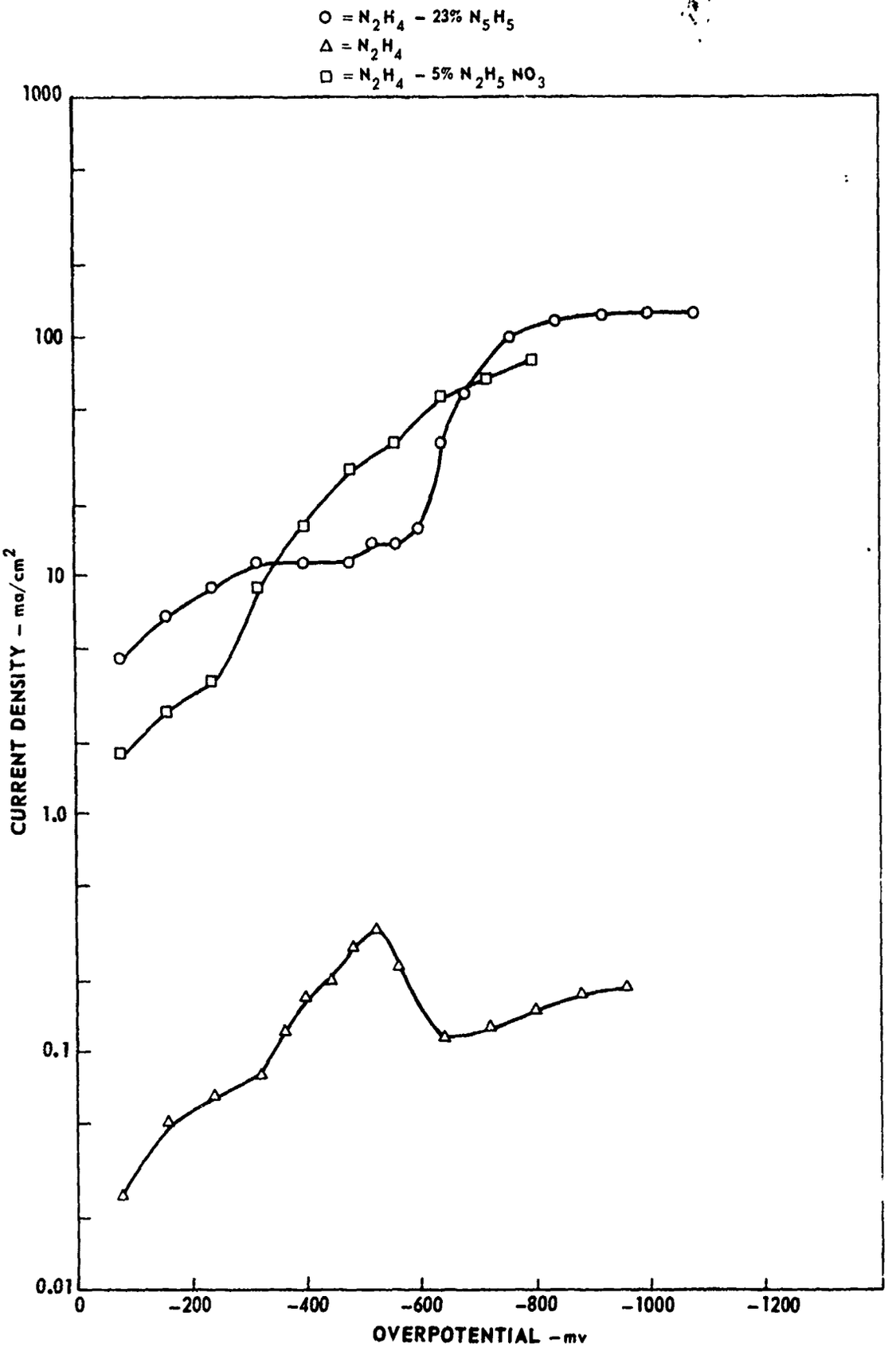

FIG. 16

CATHODIC POLARIZATION OF PLATINUM IN HYDRAZINE-BASE PROPELLANTS

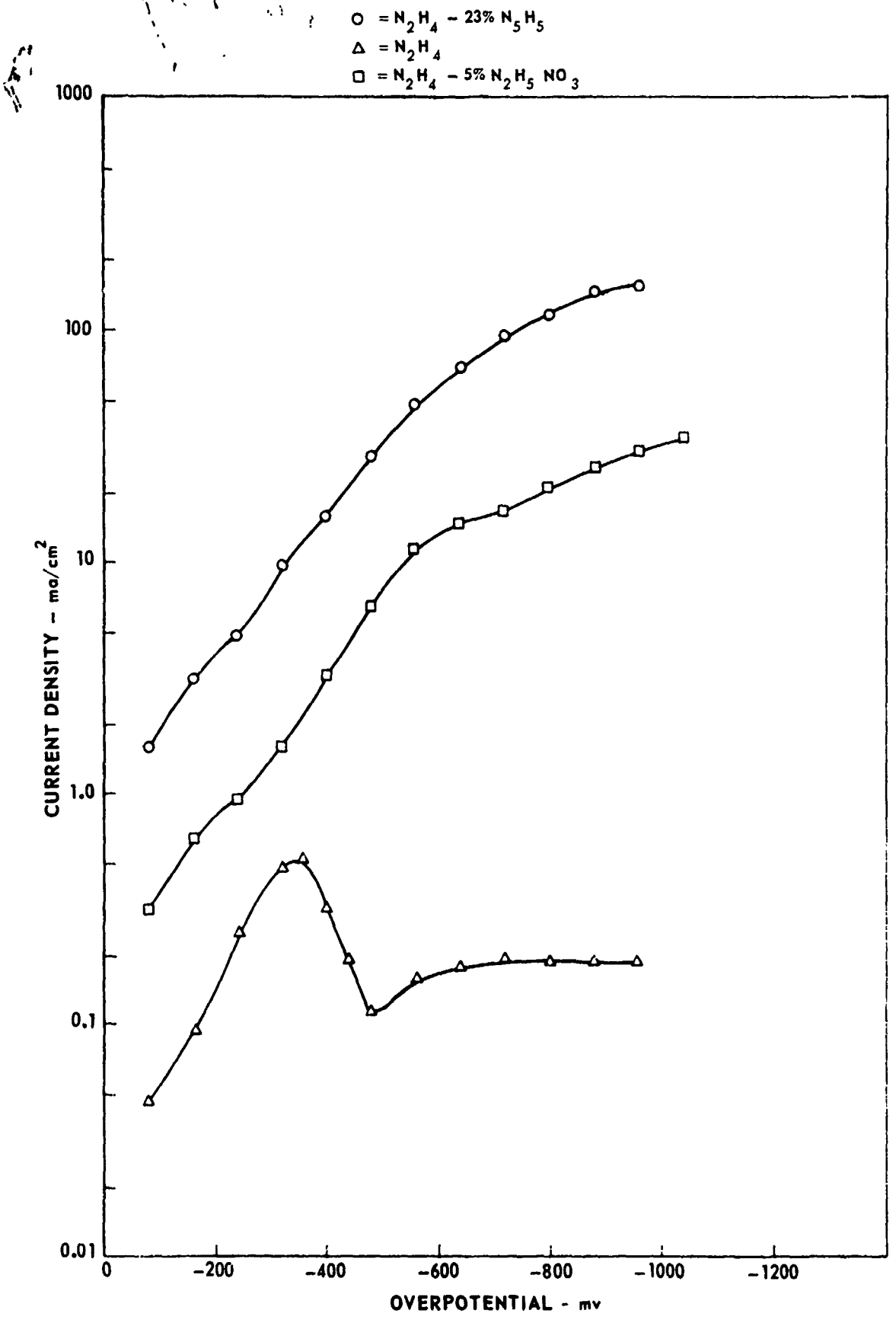

FIG. 17

CATHODIC POLARIZATION OF GRAPHITE IN HYDRAZINE-BASE PROPELLANTS

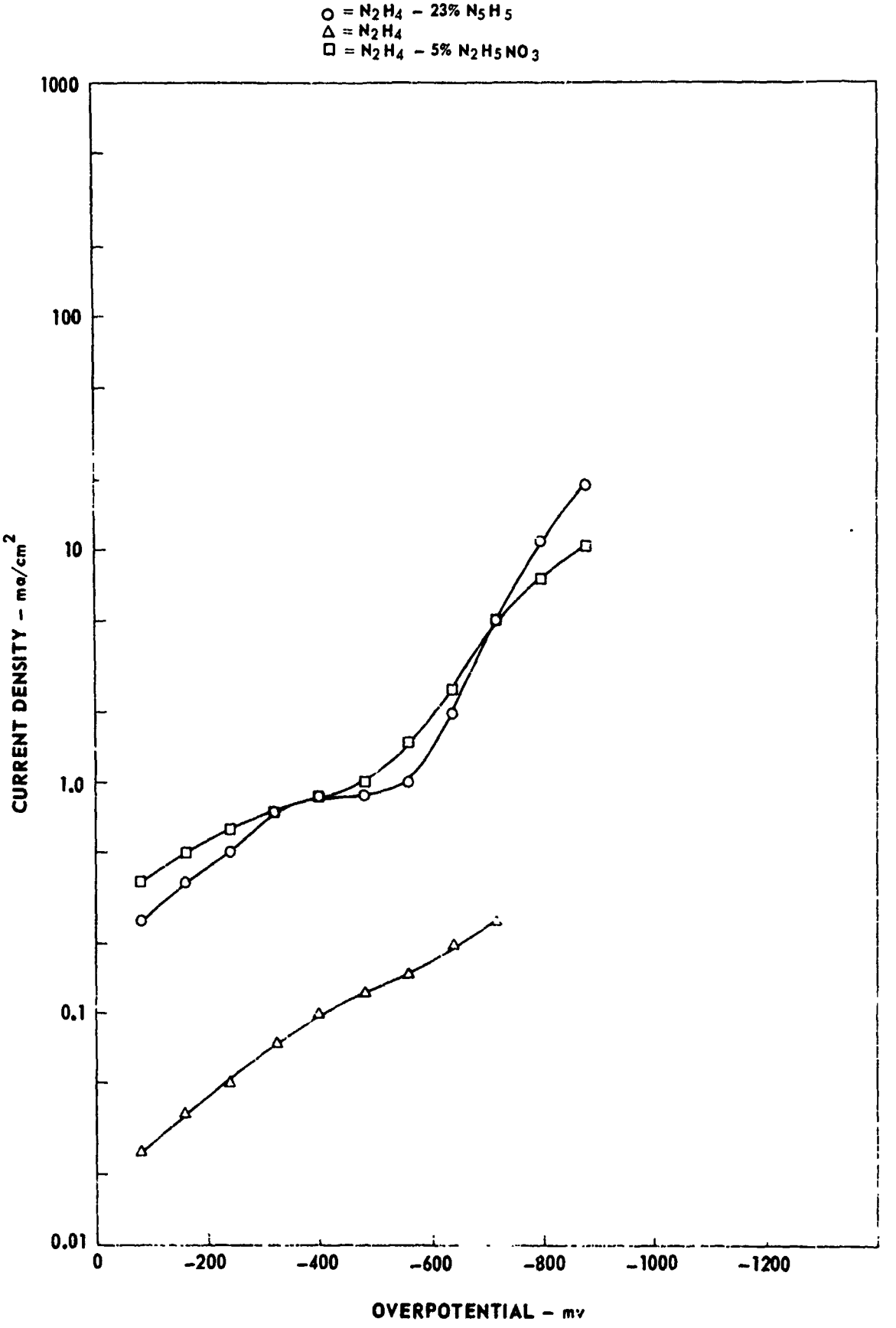

FIG. 18

CATHODIC POLARIZATION OF AA 1100 IN HYDRAZINE-BASE PROPELLANTS

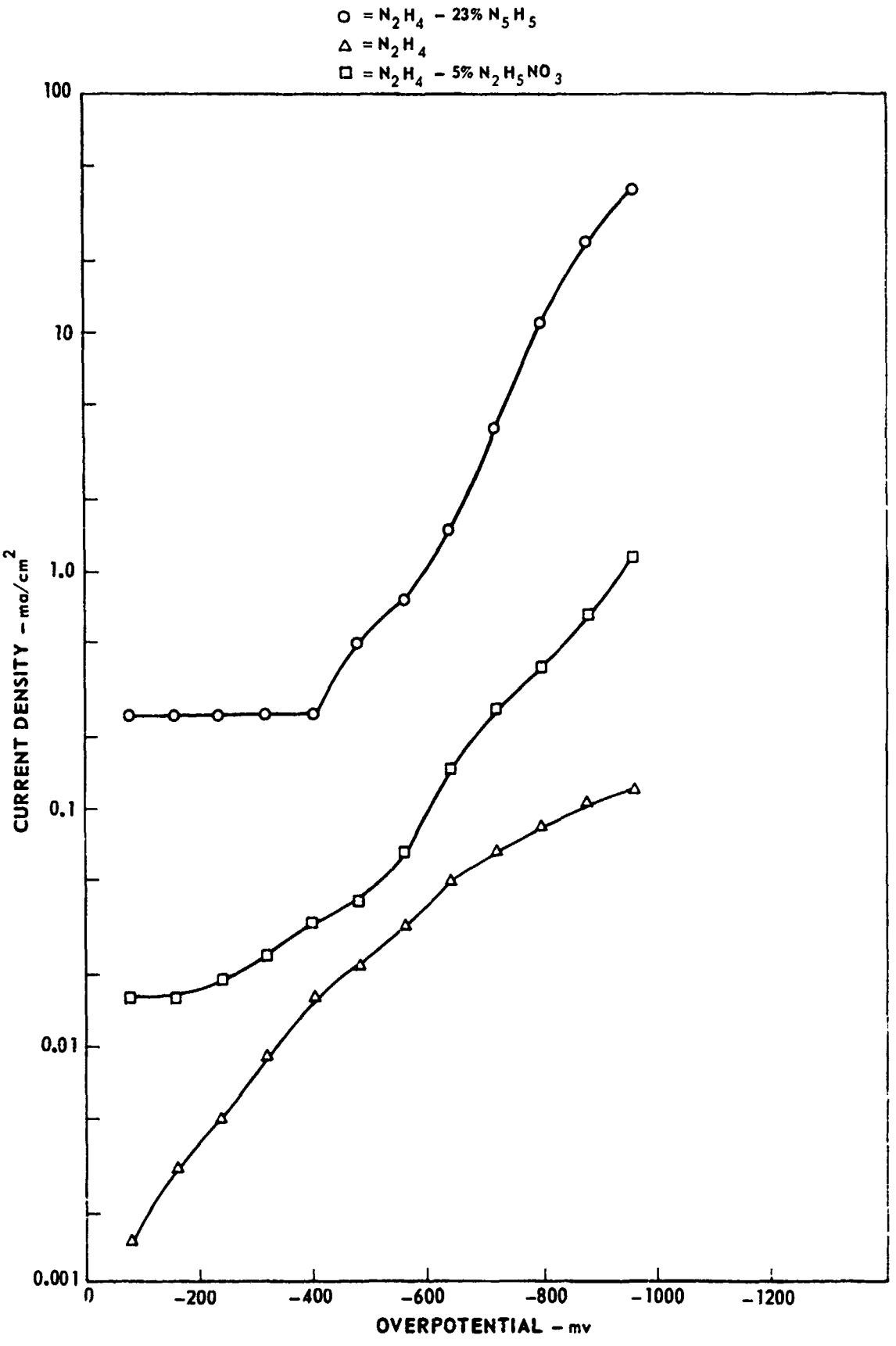

FIG. 19

CATHODIC POLARIZATION OF AA6061-T6 IN HYDRAZINE-BASE PROPELLANTS

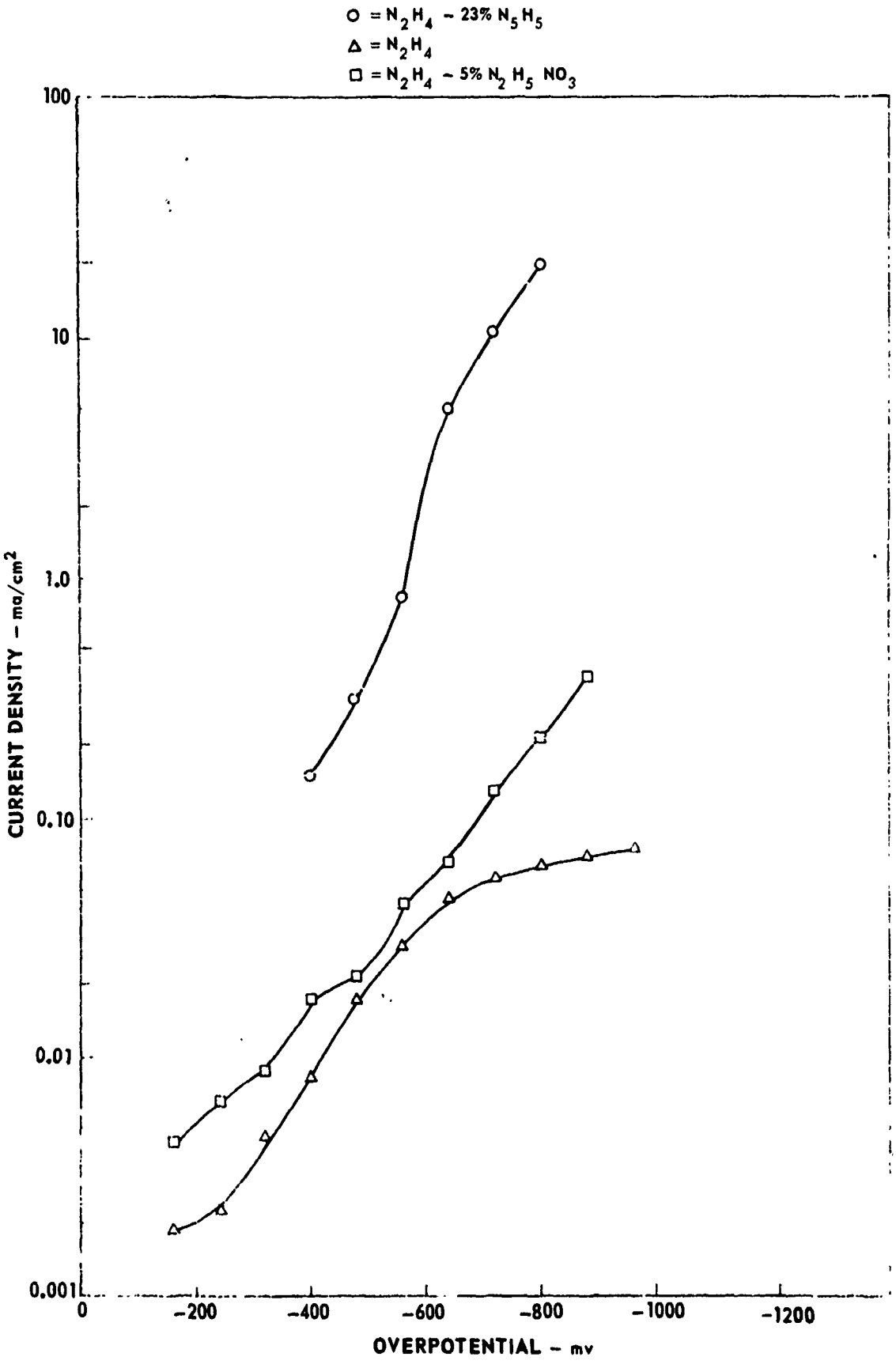

FIG. 20

CATHODIC POLARIZATION OF NICKEL, PLATINUM, AND INCONEL IN 77% HYDRAZINE–23% HYDRAZINE AZIDE

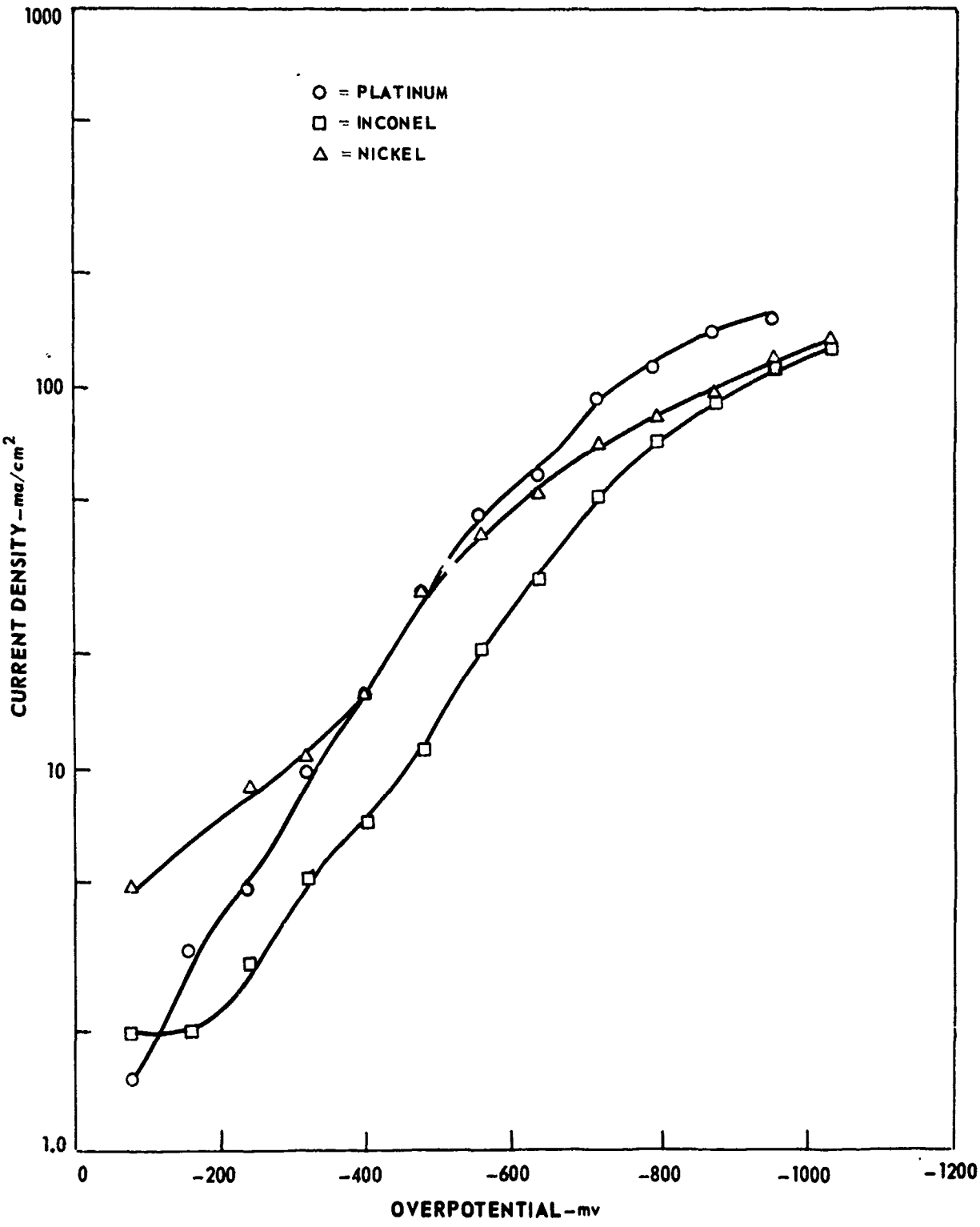

FIG. 21

ANODIC POLARIZATION OF 17-7PH IN 77% HYDRAZINE-23% HYDRAZINE AZIDE

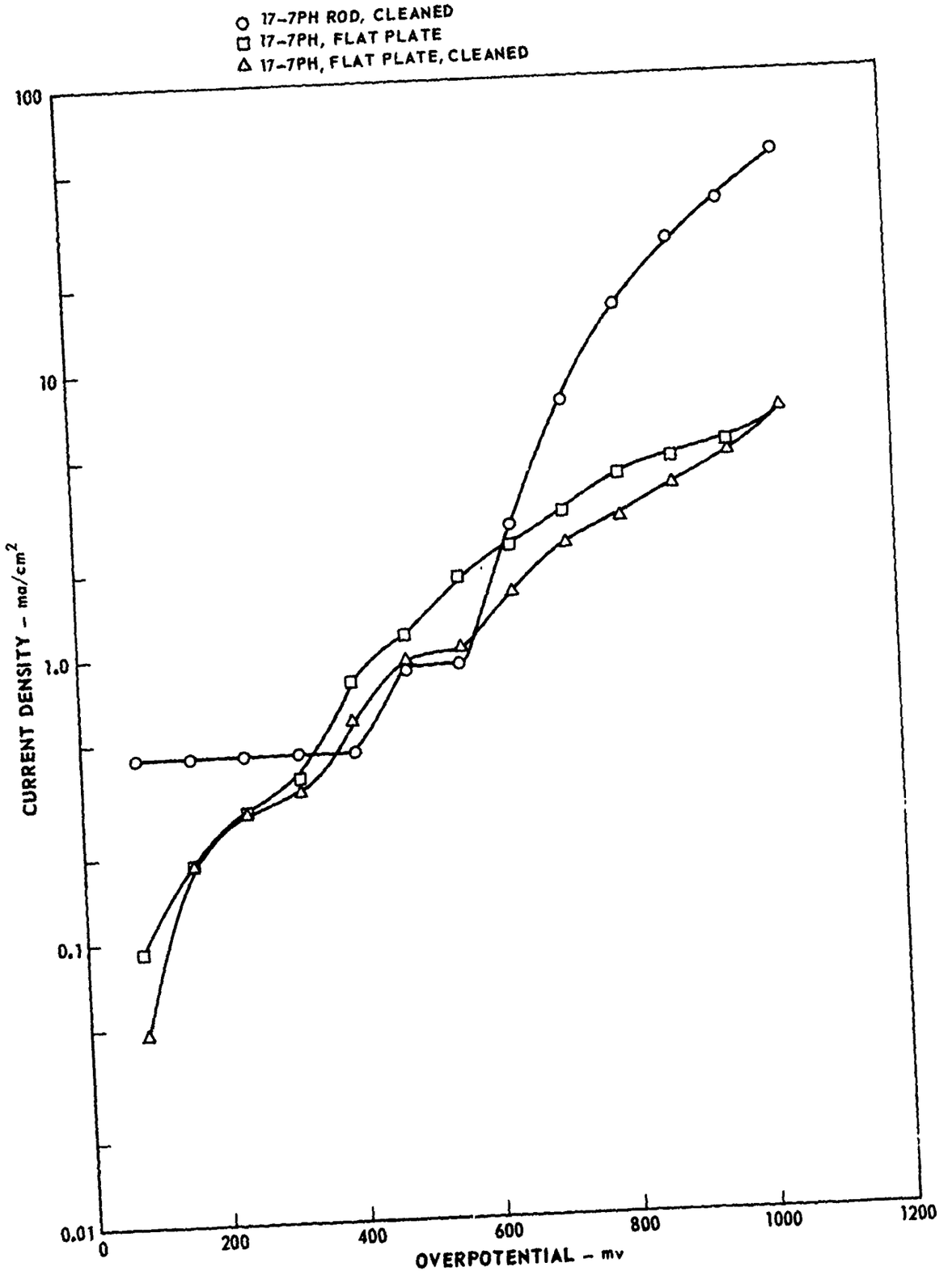

FIG. 22

CATHODIC POLARIZATION OF AM 350 IN 77% HYDRAZINE-23% HYDRAZINE AZIDE

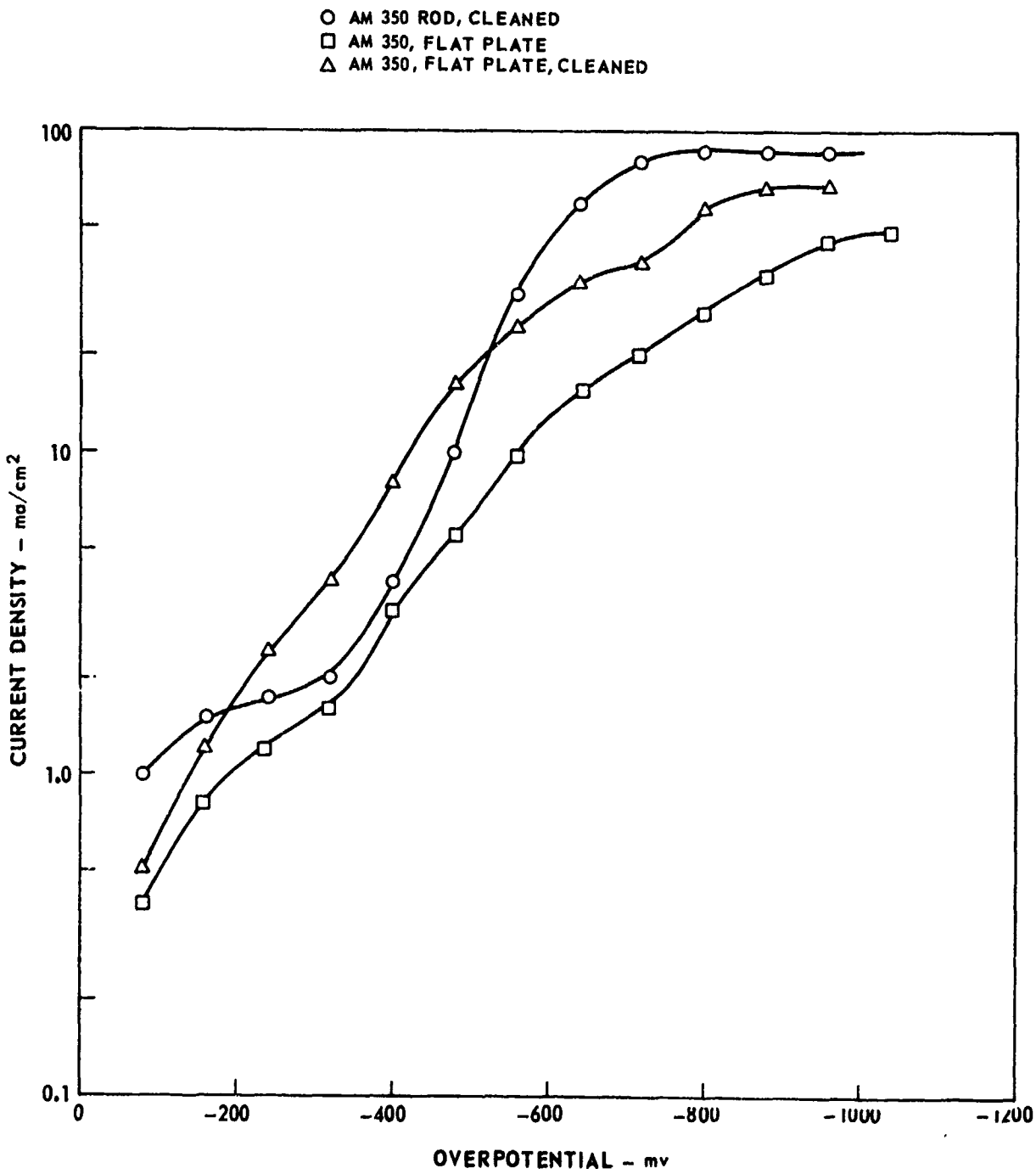

ANODIC POLARIZATION OF AM350 IN 77% N_2H_4–23% N_5H_5 AND 88% N_2H_4–12% N_5H_5

12% AZIDE–PASSIVATED

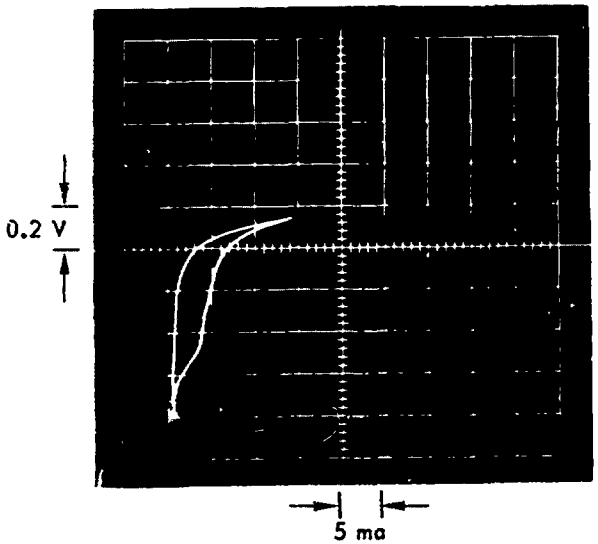

23% AZIDE–PASSIVATED

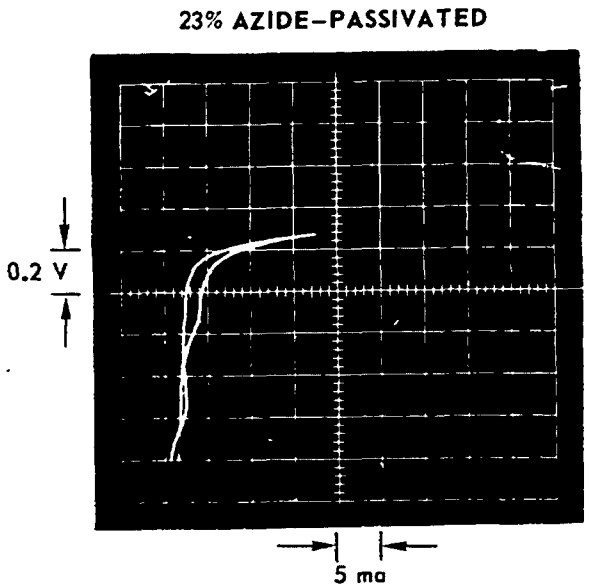

12% AZIDE– ACTIVE

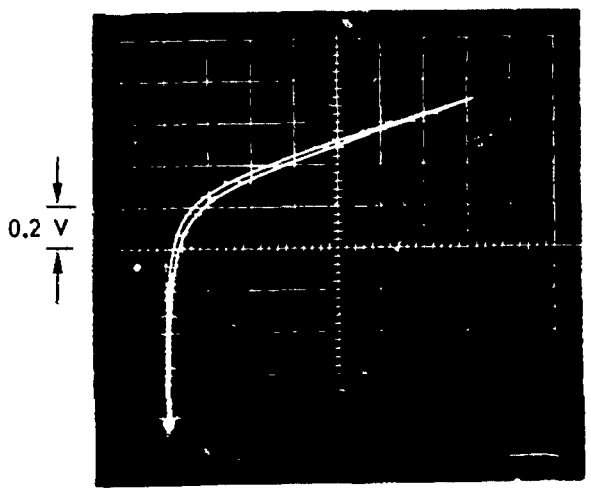

23% AZIDE– ACTIVE

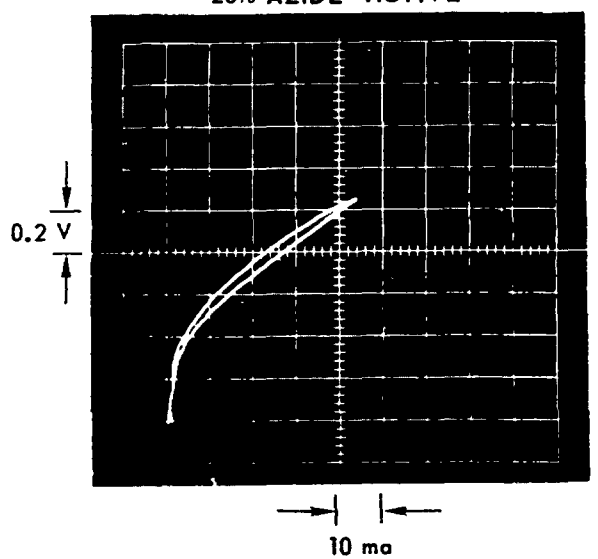

FIG. 23

FIG. 24

ANODIC POLARIZATION OF GRAPHITE IN 77% HYDRAZINE-23% HYDRAZINE AZIDE

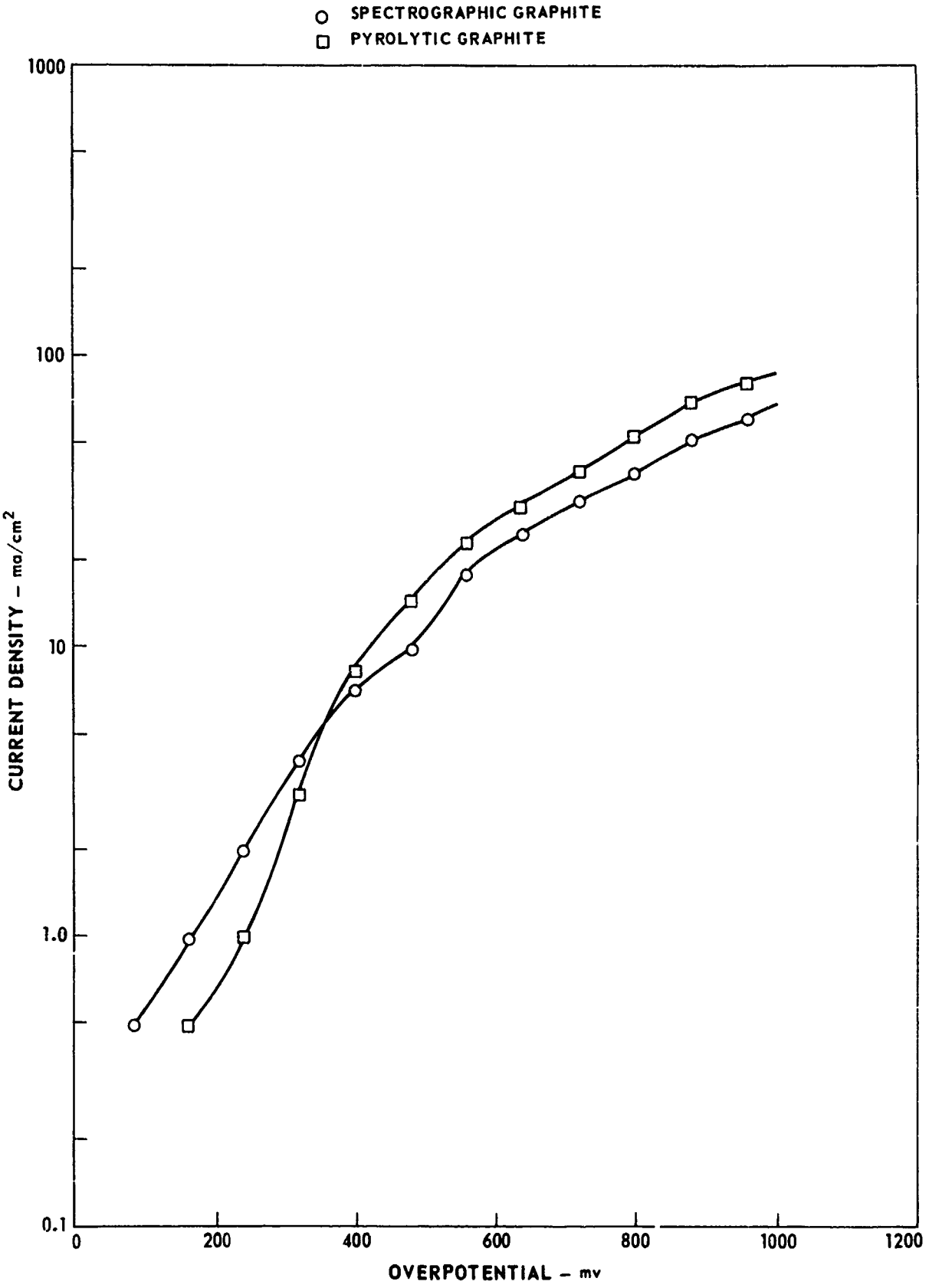

FIG. 25

CATHODIC POLARIZATION OF GRAPHITE IN 77% HYDRAZINE-23% HYDRAZINE AZIDE

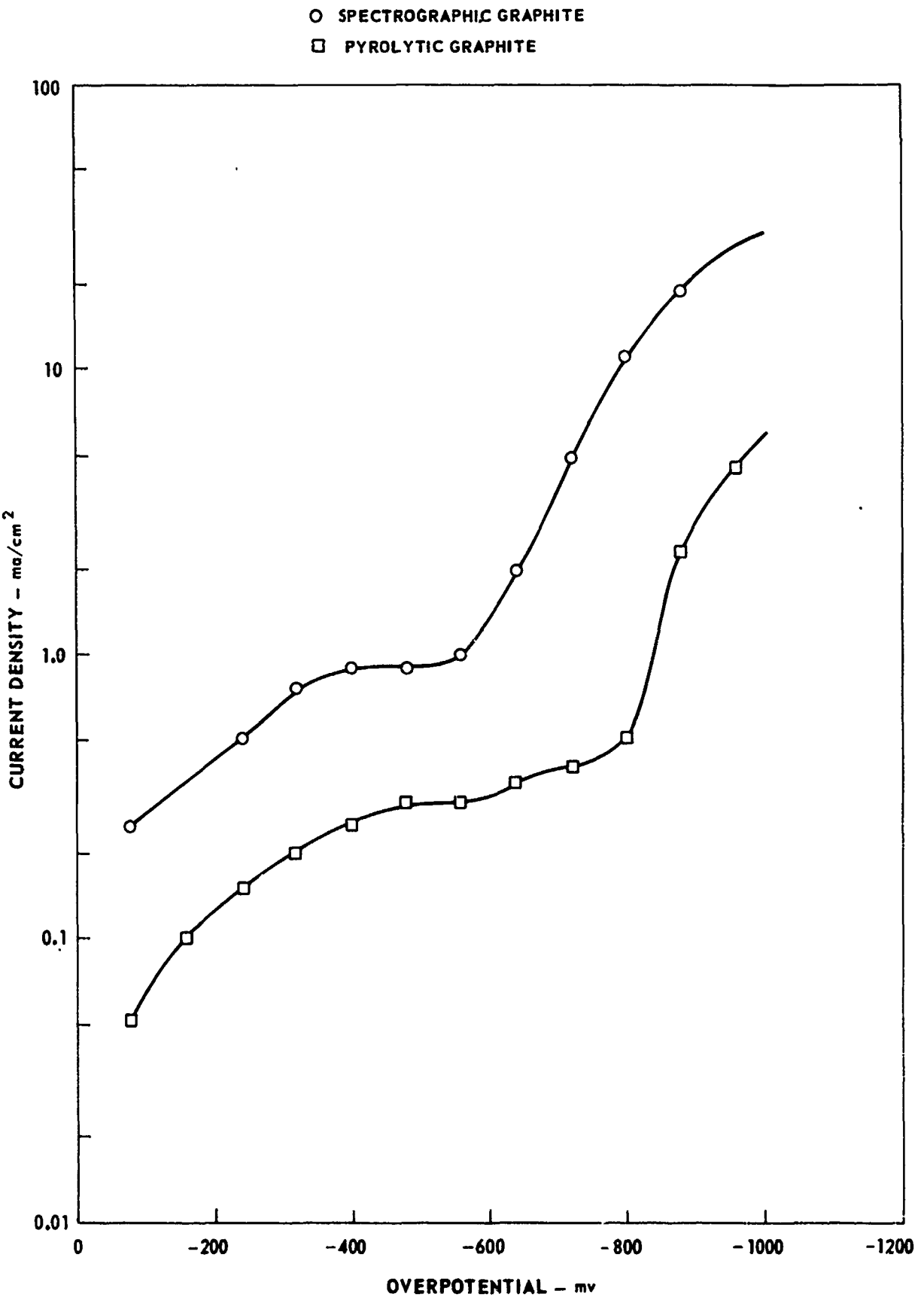

ANODIC POLARIZATION OF 304 SS AS A FUNCTION OF AZIDE CONCENTRATION

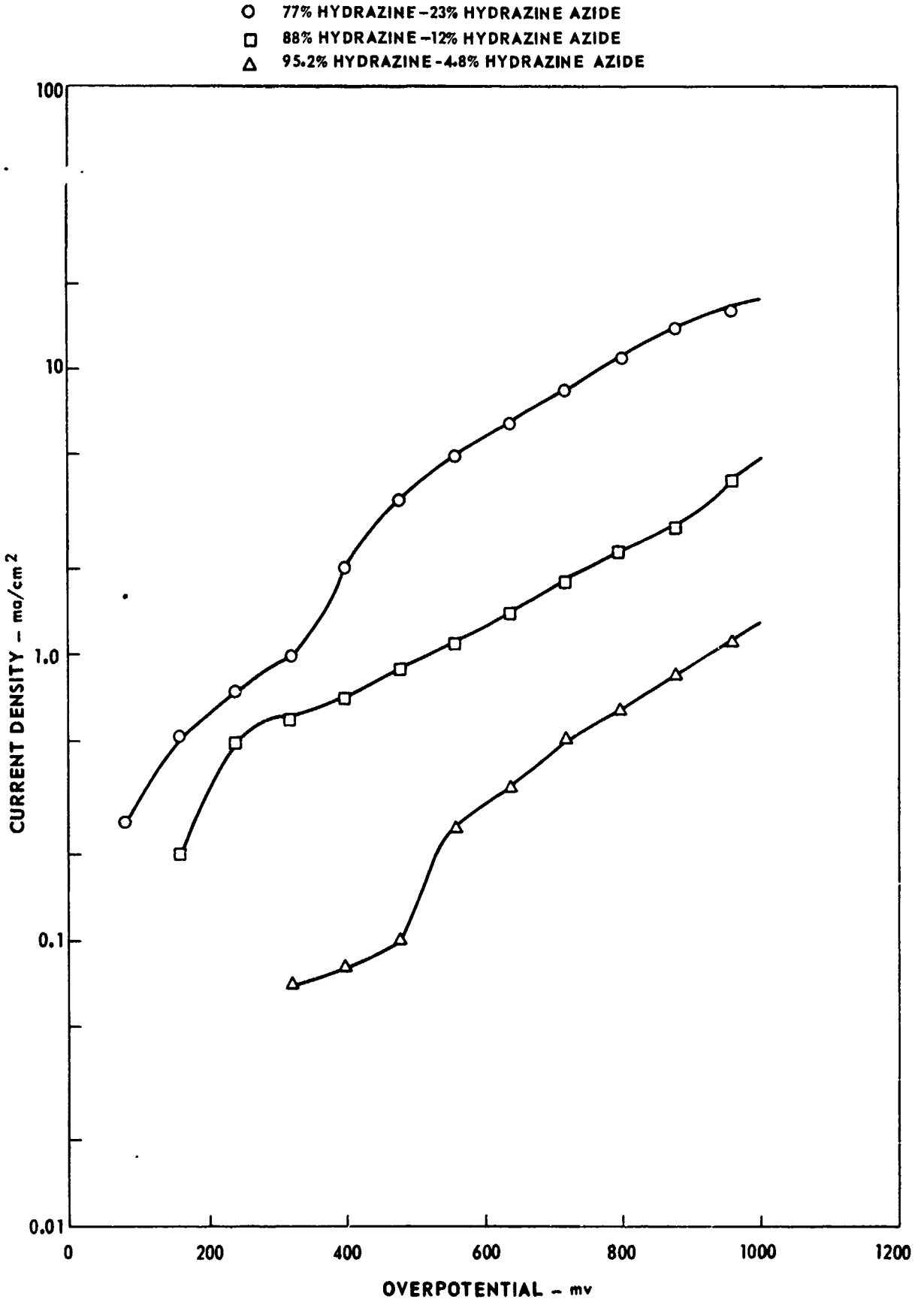

FIG. 27

ANODIC POLARIZATION OF AM 350 AS A FUNCTION OF AZIDE CONCENTRATION

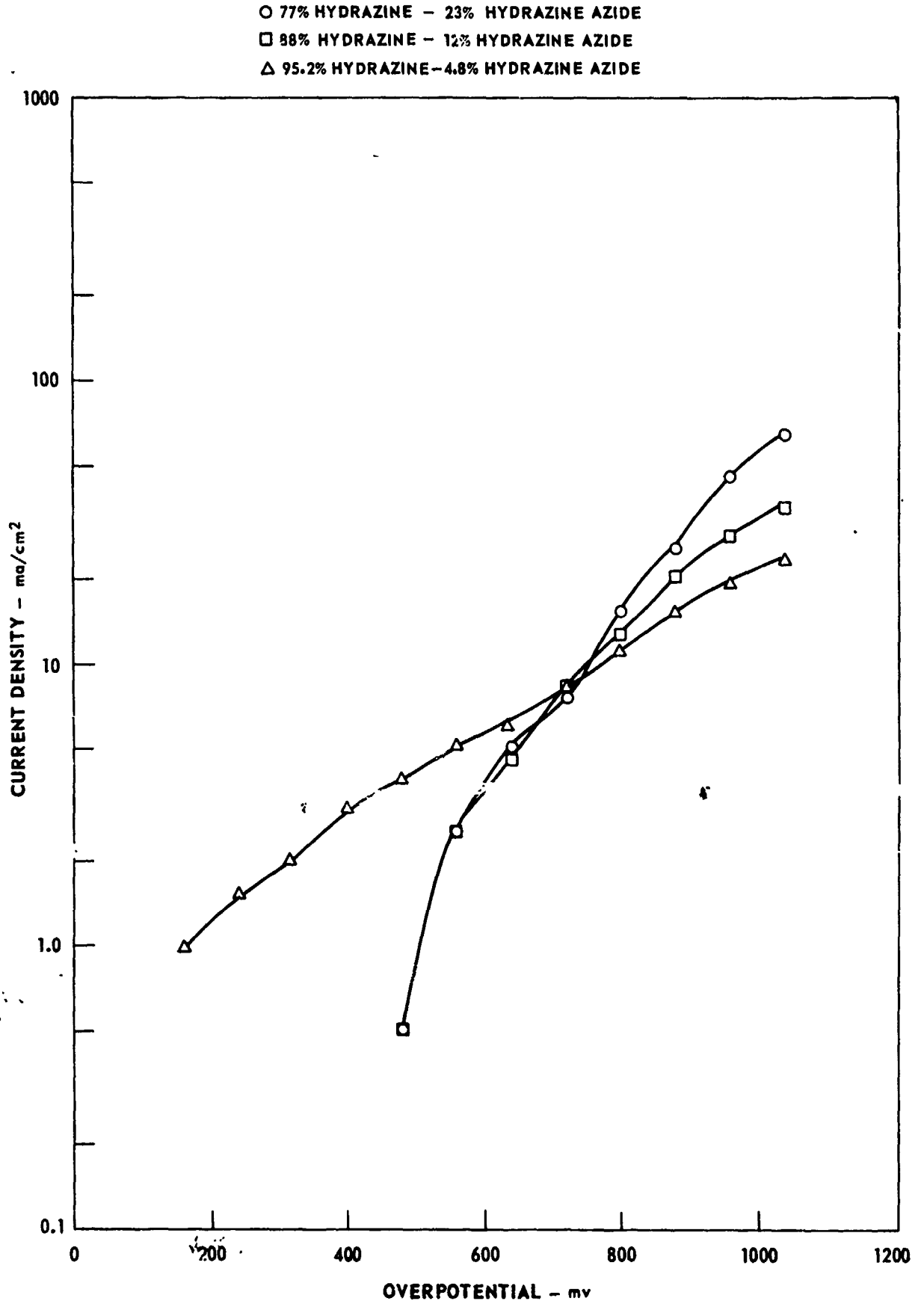

FIG. 28

ANODIC POLARIZATION OF PLATINUM AS A FUNCTION OF AZIDE CONCENTRATION

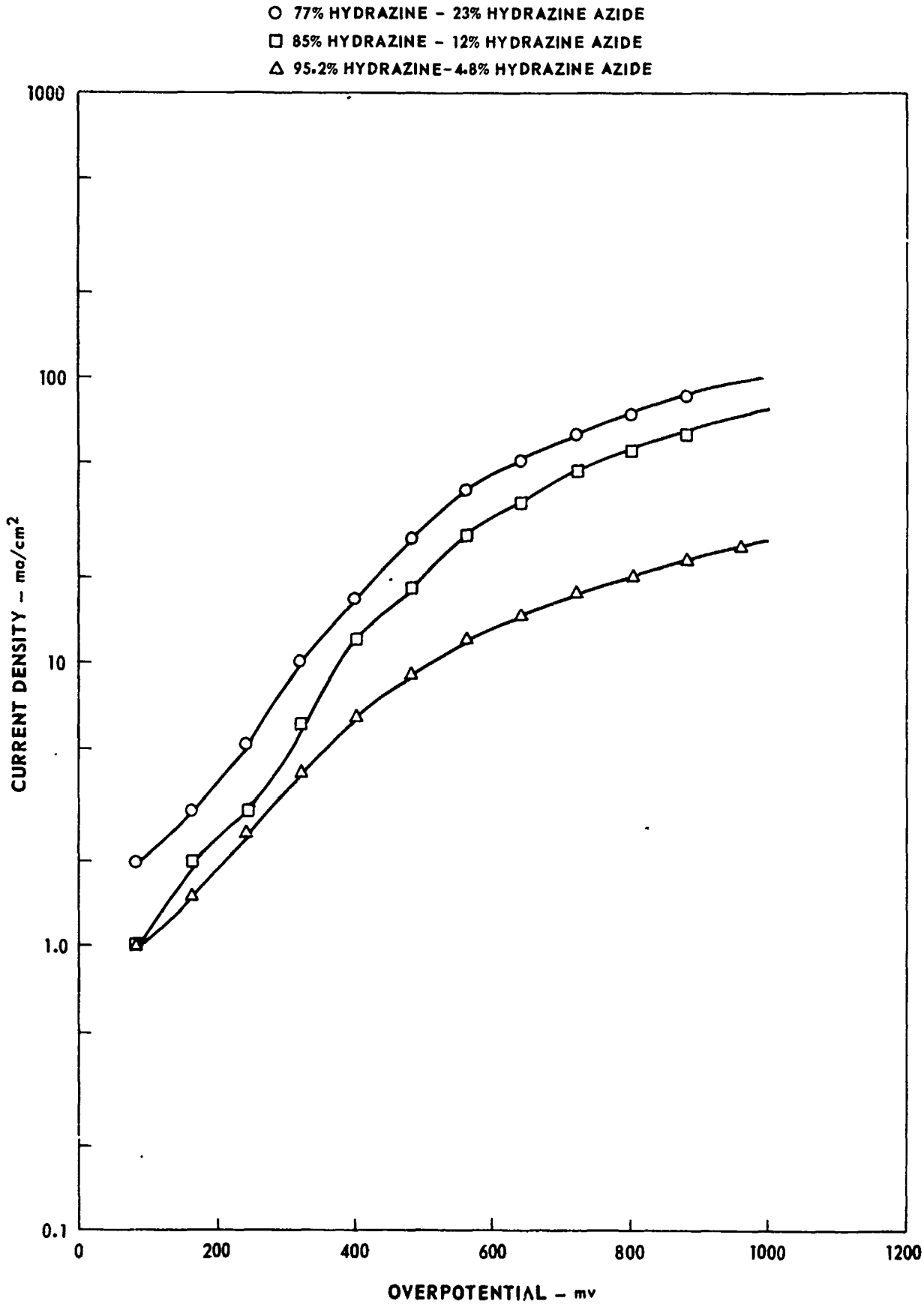

FIG. 29

ANODIC POLARIZATION OF PYROLYTIC GRAPHITE AS A FUNCTION OF AZIDE CONCENTRATION

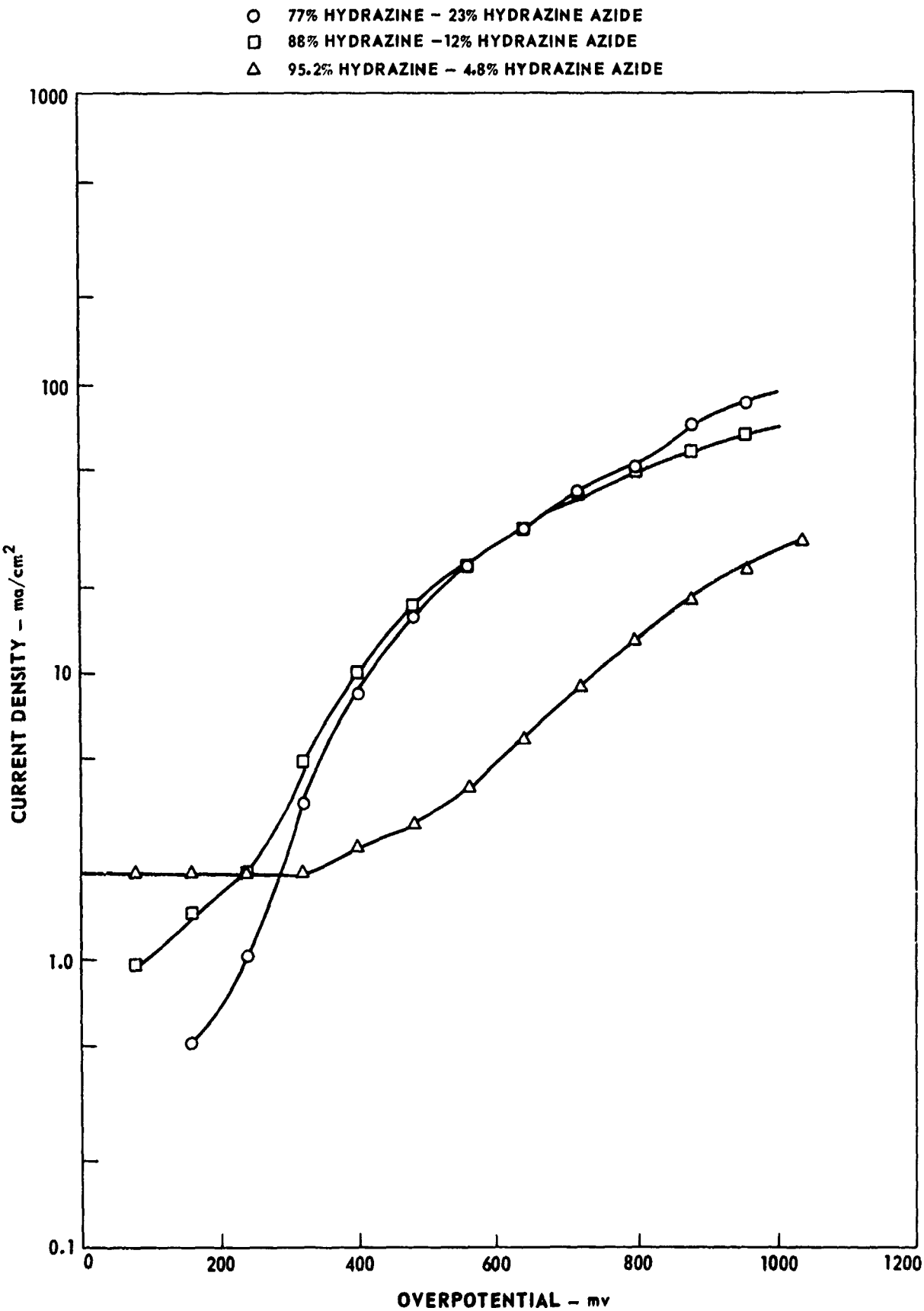

FIG. 30

CATHODIC POLARIZATION OF 304 SS AS A FUNCTION OF AZIDE CONCENTRATION

○ 77% HYDRAZINE – 23% HYDRAZINE AZIDE

□ 88% HYDRAZINE – 12% HYDRAZINE AZIDE

△ 95.2% HYDRAZINE – 4.8% HYDRAZINE AZIDE

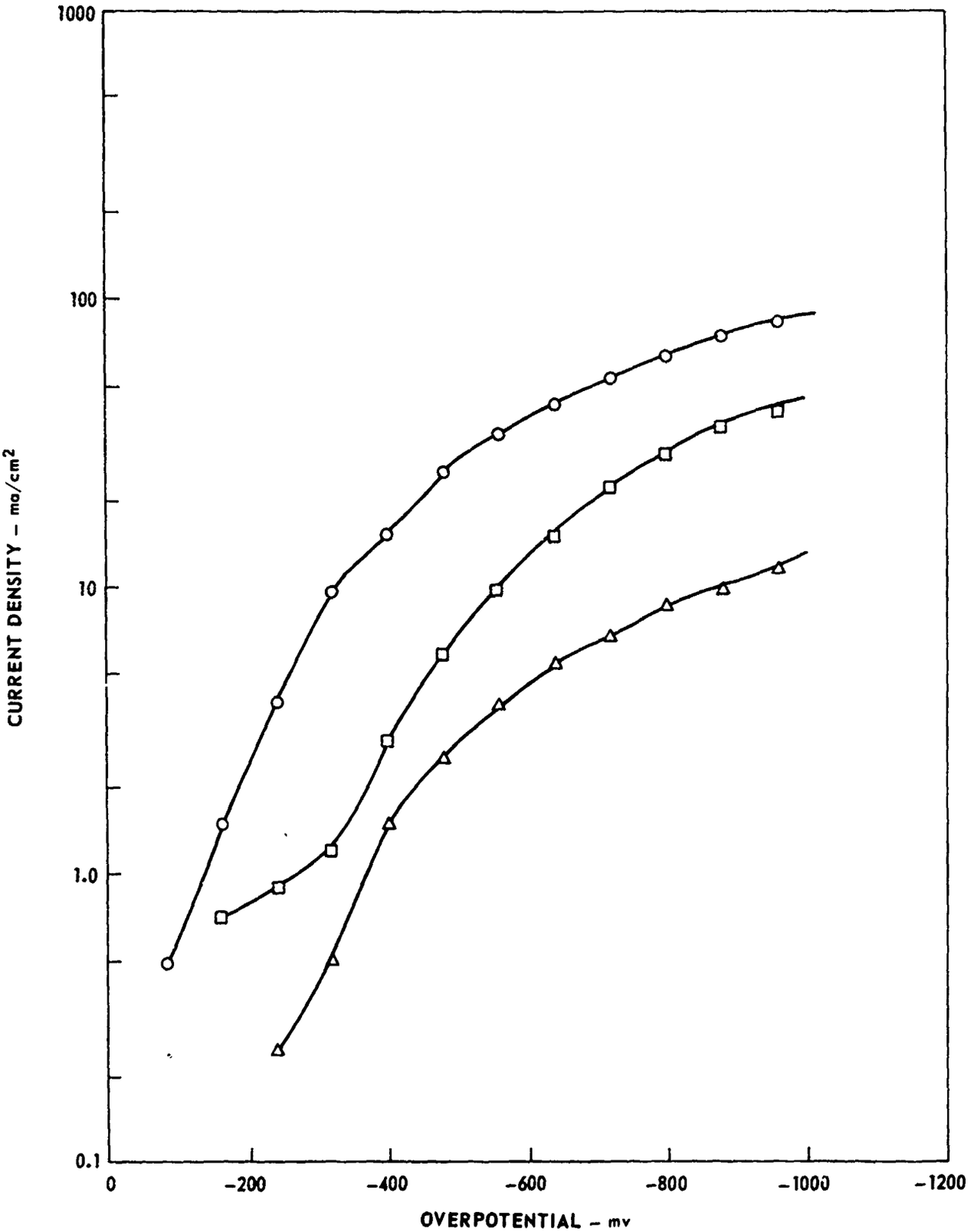

FIG. 31

CATHODIC POLARIZATION OF AM 350 AS A FUNCTION OF AZIDE CONCENTRATION

○ 77% HYDRAZINE – 23% HYDRAZINE AZIDE

□ 88% HYDRAZINE – 12% HYDRAZINE AZIDE

△ 95.2% HYDRAZINE – 4.8% HYDRAZINE AZIDE

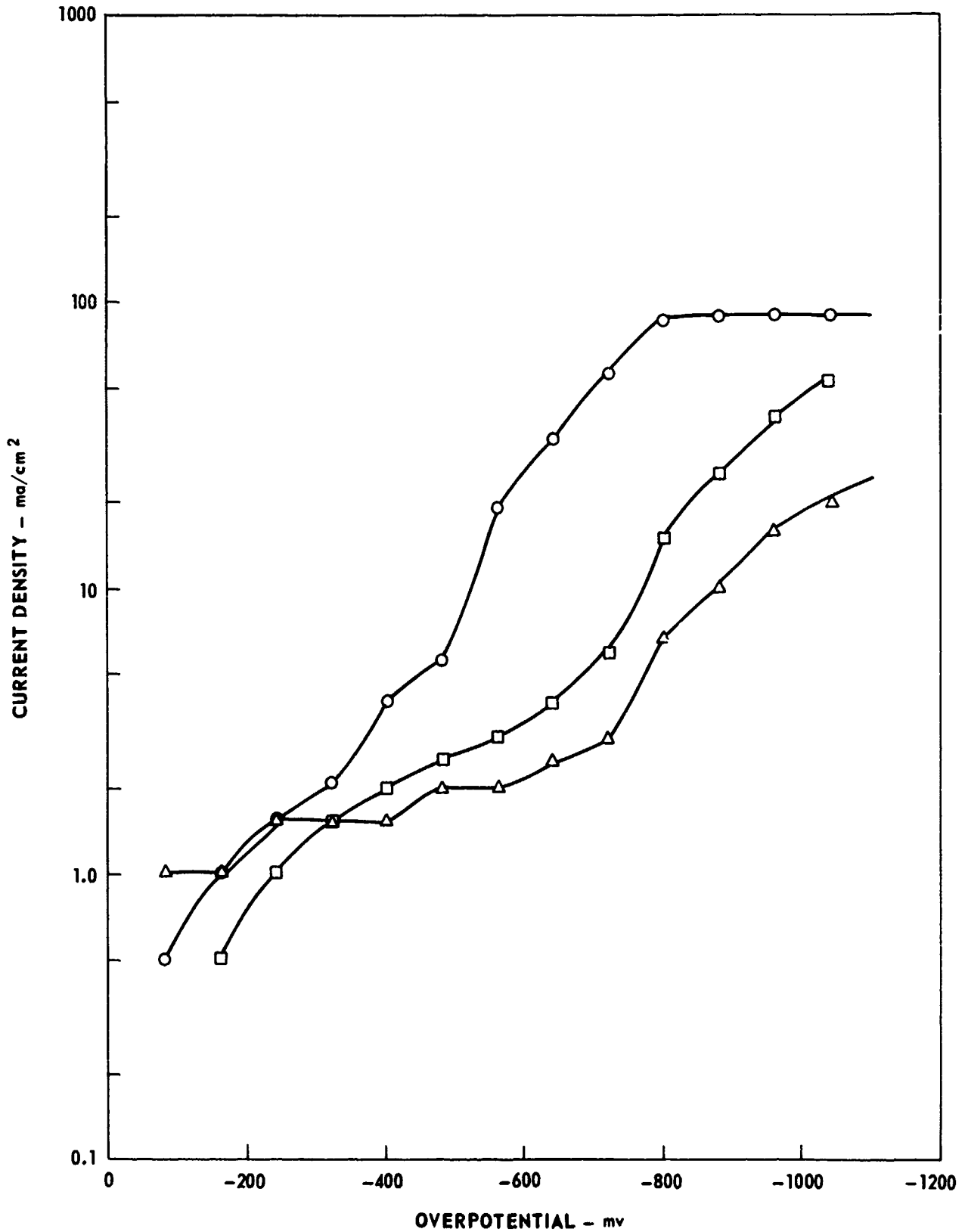

FIG. 32

CATHODIC POLARIZATION OF PLATINUM AS A FUNCTION OF AZIDE CONCENTRATION

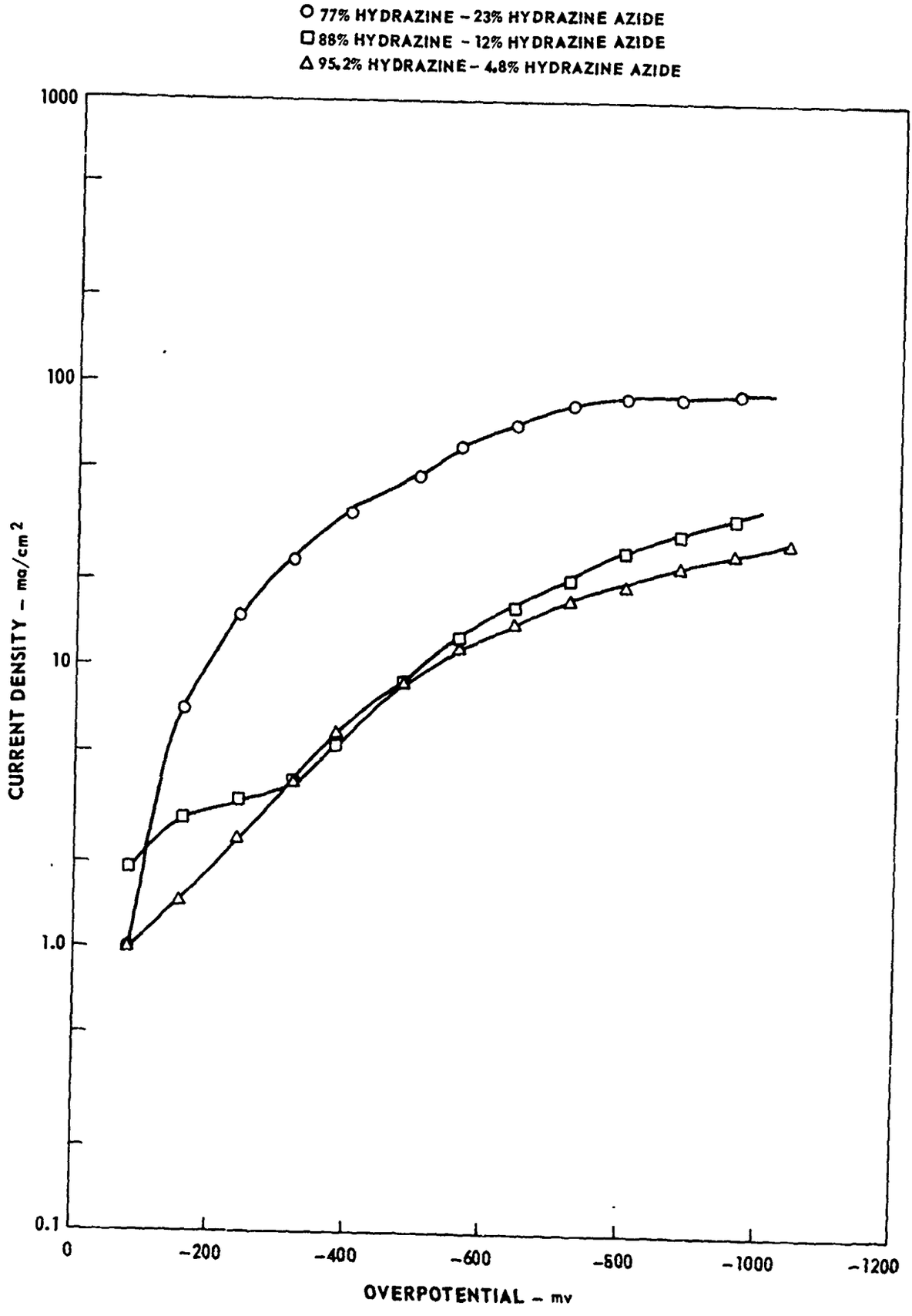

FIG. 33

CATHODIC CURRENT DENSITY VS AZIDE CONCENTRATION AT η = 1000 mv

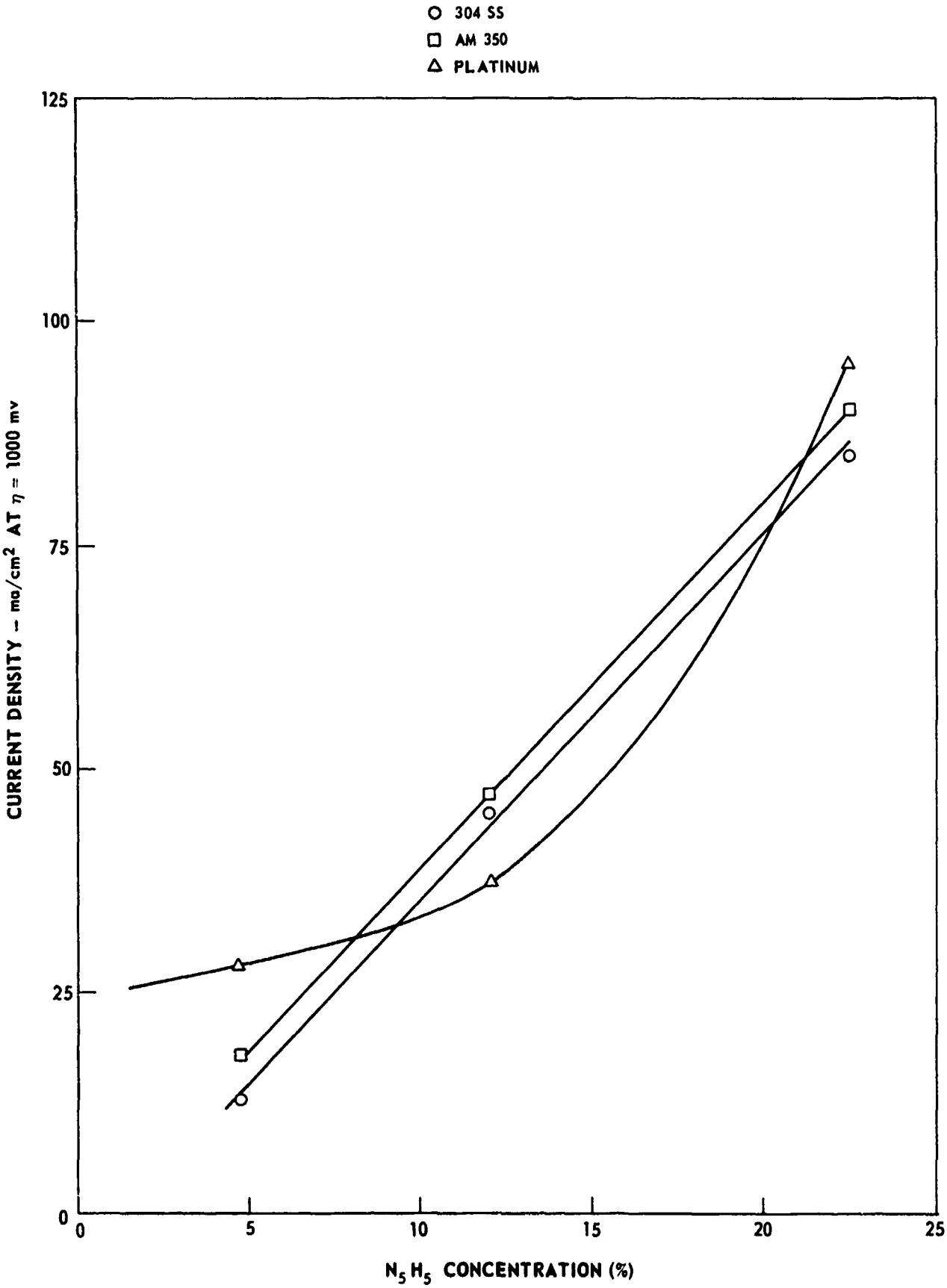

FIG. 34

ANODIC CURRENT DENSITY VS AZIDE CONCENTRATION AT η = 1000 mv

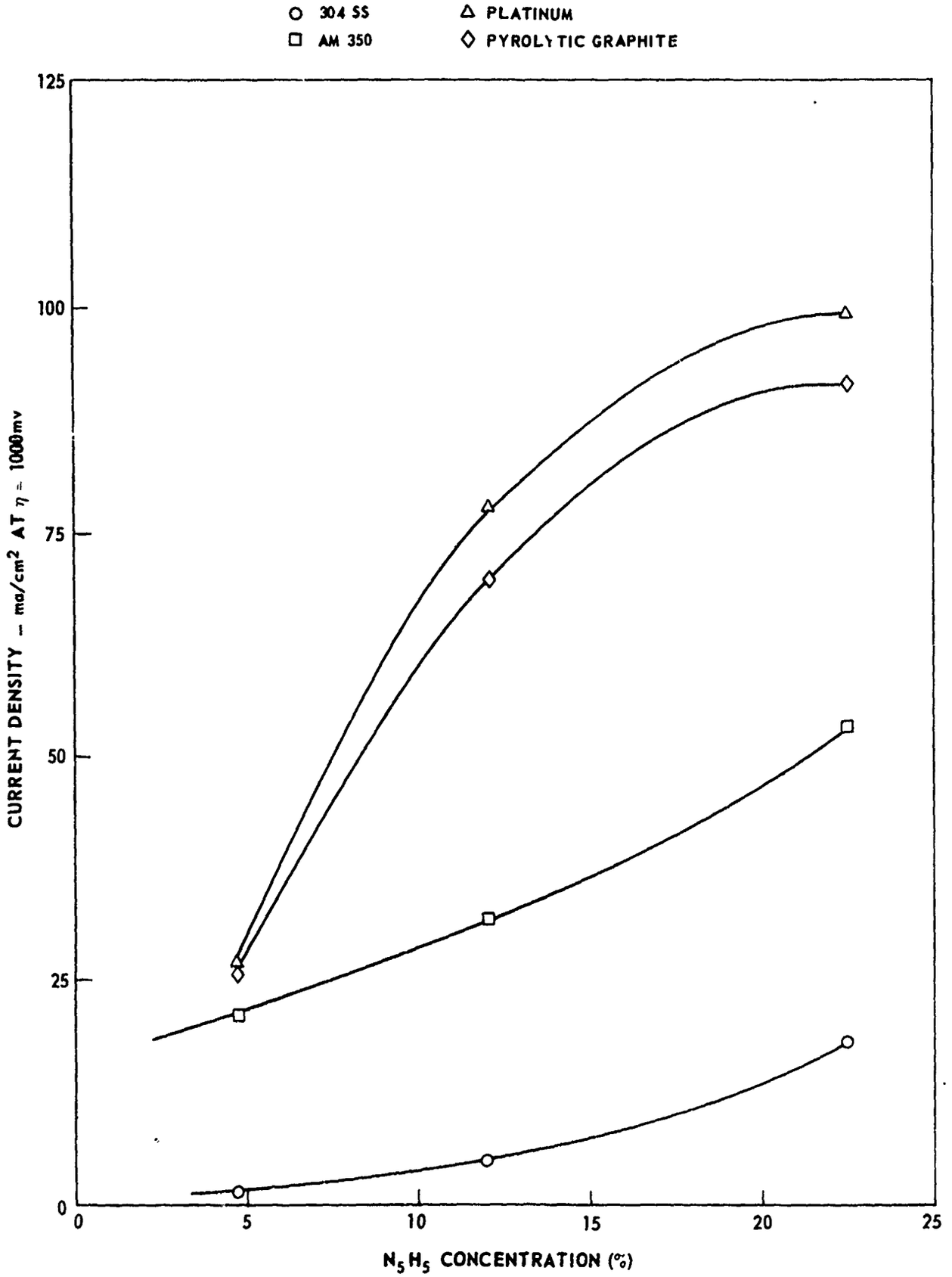

FIG. 35

ANODIC POLARIZATION OF 304 SS IN 6% HYDRAZINE NITRATE AND IN 4.8% HYDRAZINE AZIDE

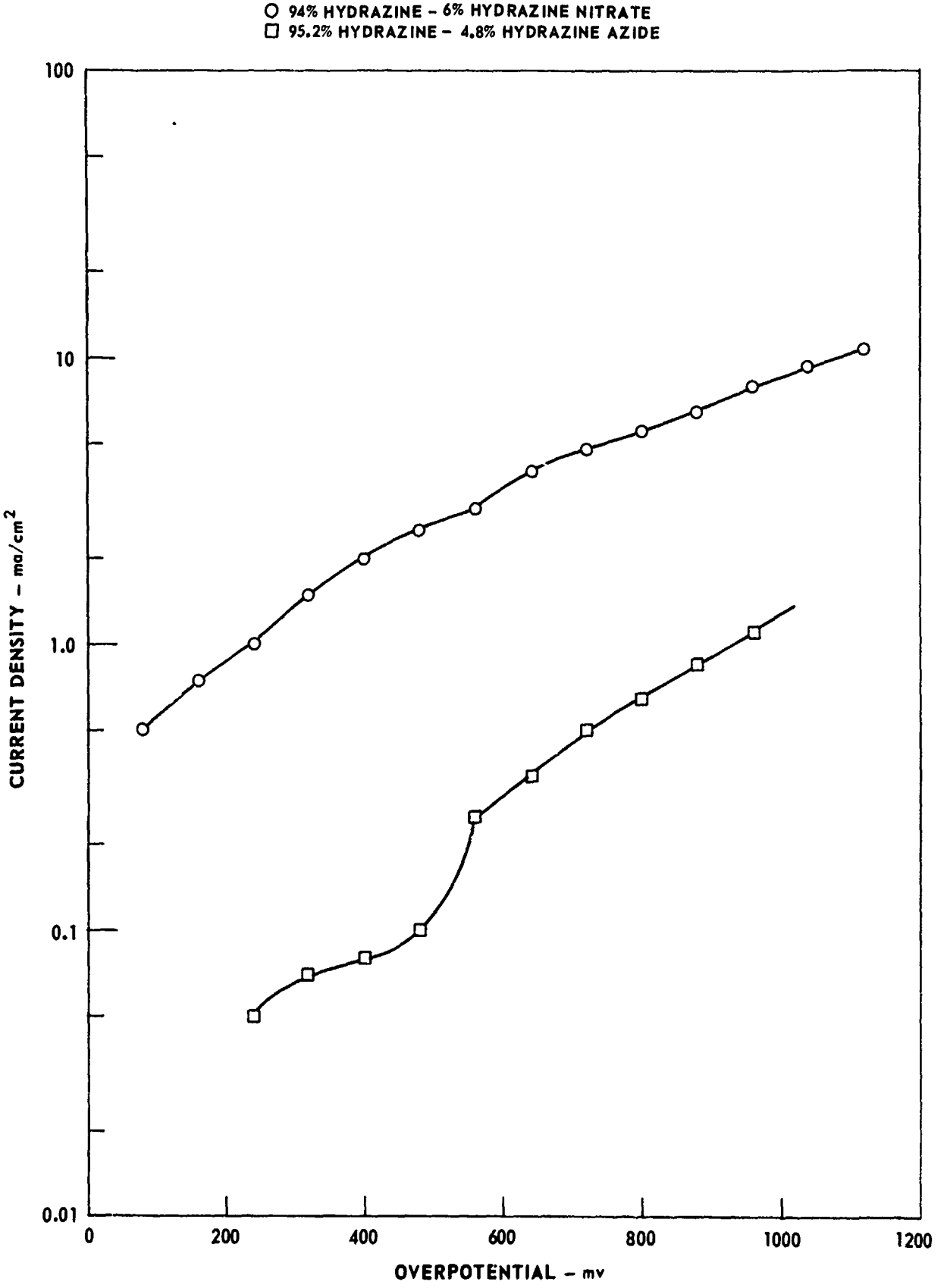

FIG. 36

ANODIC POLARIZATION OF AM 350 IN 6% HYDRAZINE NITRATE AND IN 4.8% HYDRAZINE AZIDE

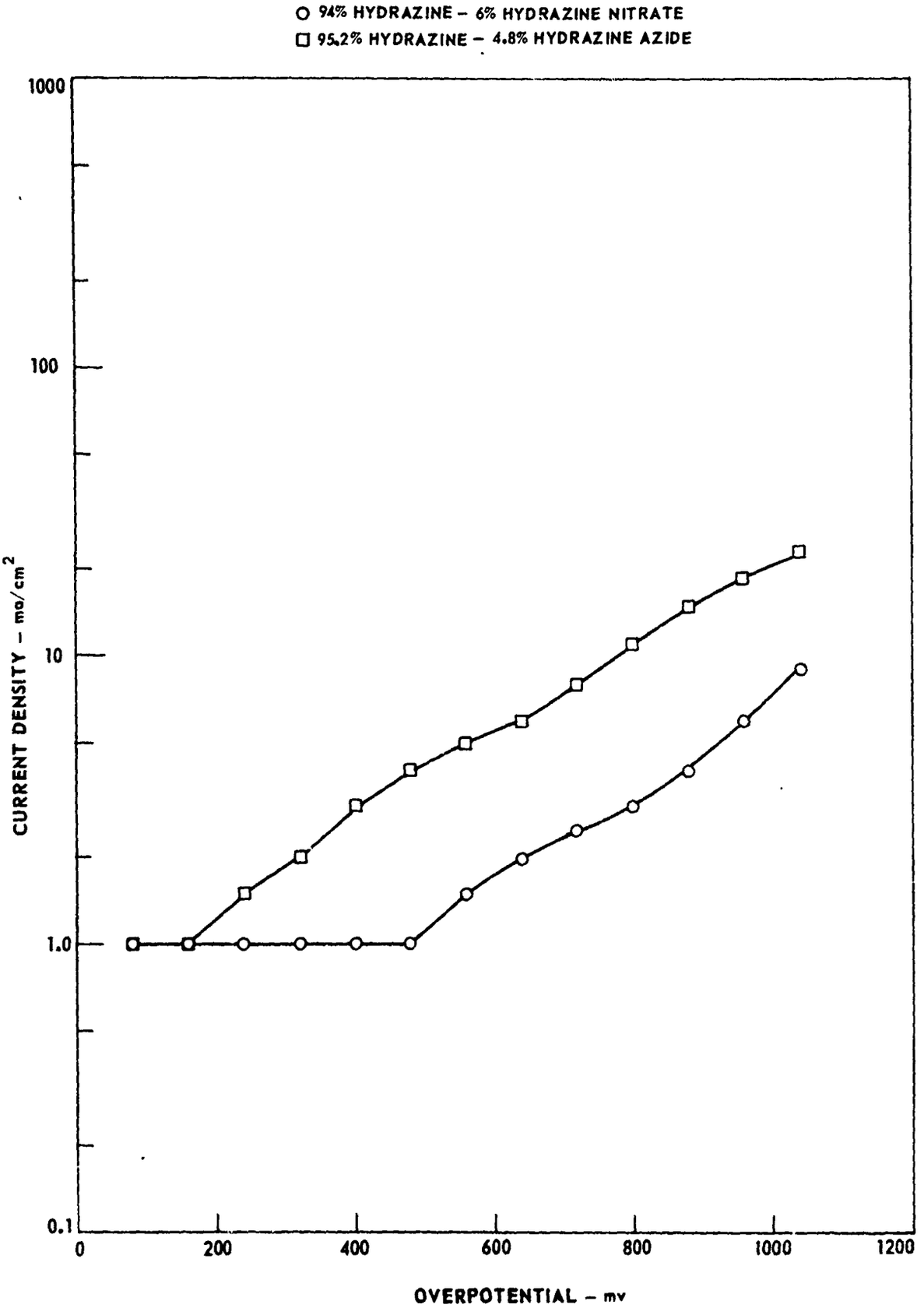

FIG. 37

ANODIC POLARIZATION OF PLATINUM IN 6% HYDRAZINE NITRATE AND IN 4.8% HYDRAZINE AZIDE

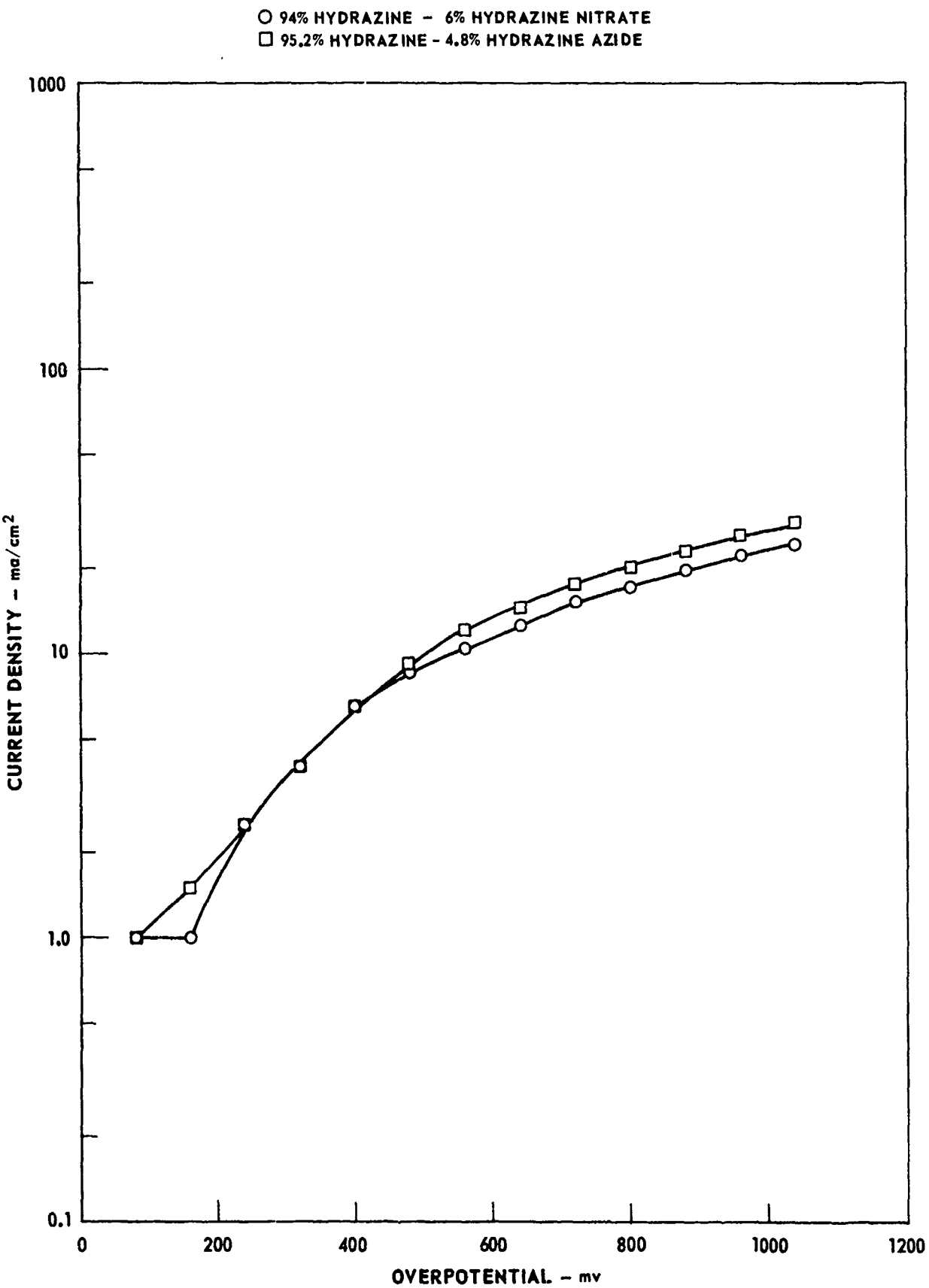

FIG. 38

ANODIC POLARIZATION OF PYROLYTIC GRAPHITE IN 6% HYDRAZINE NITRATE AND IN 4.8% HYDRAZINE AZIDE

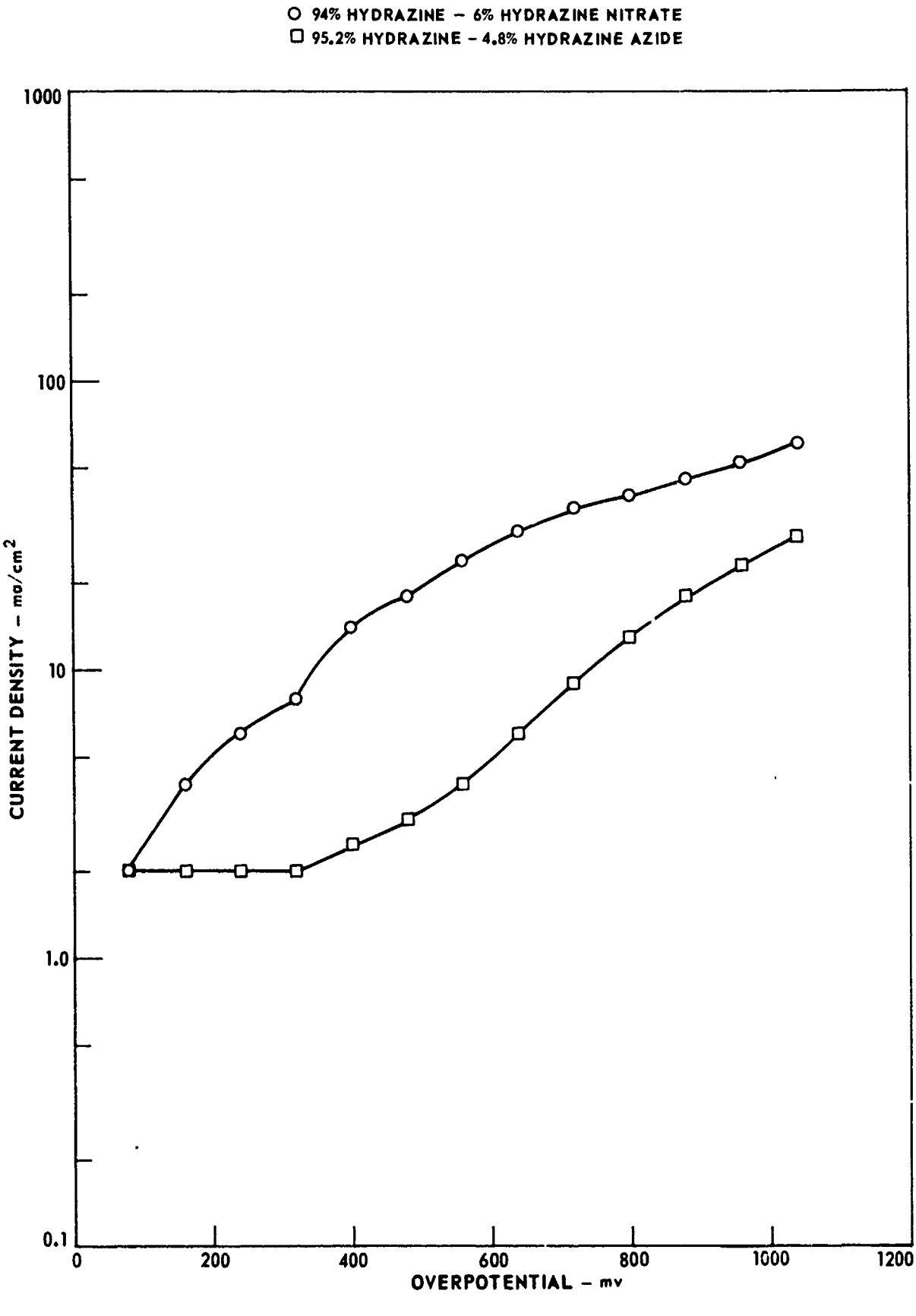

FIG. 39

CATHODIC POLARIZATION OF 304SS IN 6% HYDRAZINE NITRATE AND IN 4.8% HYDRAZINE AZIDE

○ 94% HYDRAZINE - 6% HYDRAZINE NITRATE

□ 95.2% HYDRAZINE – 4.8% HYDRAZINE AZIDE

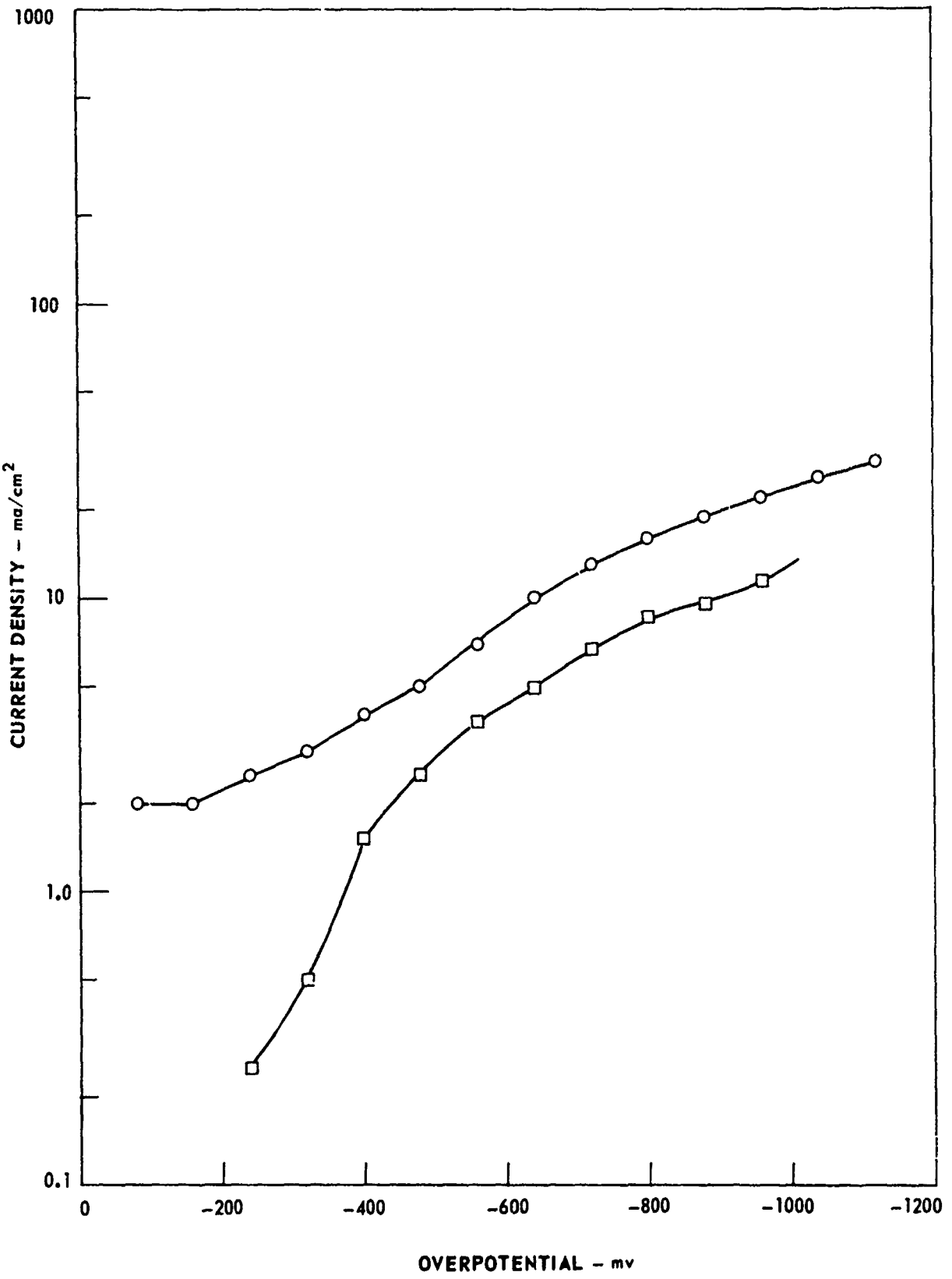

FIG. 40

CATHODIC POLARIZATION OF AM350 IN 6% HYDRAZINE AND IN 4.8% HYDRAZINE AZIDE

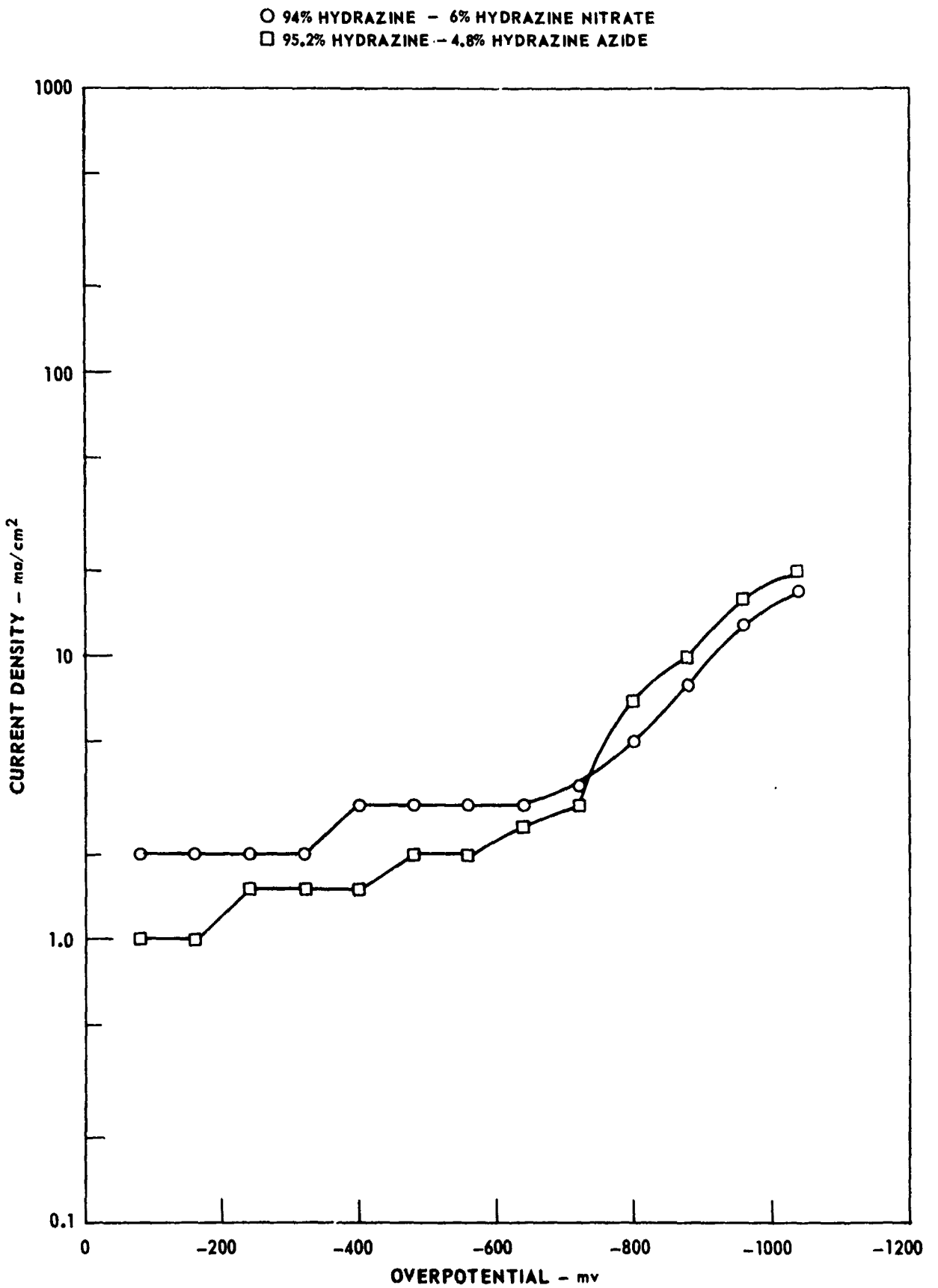

FIG. 41

CATHODIC POLARIZATION OF PLATINUM IN 6% HYDRAZINE NITRATE AND IN 4.8% HYDRAZINE AZIDE

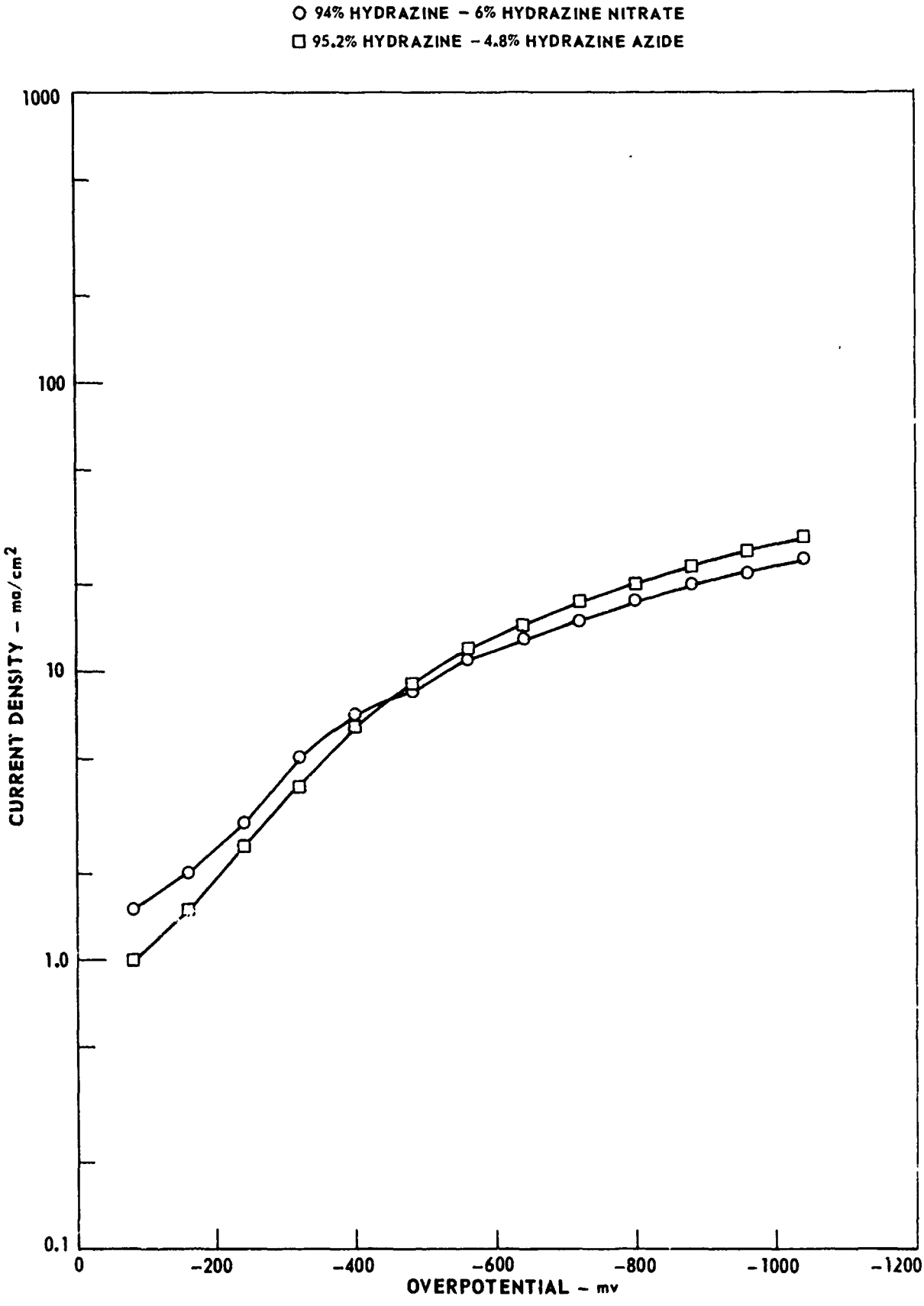

FIG. 42

POTENTIAL-TIME RELATIONSHIPS AT 100 ma IN 77% N_2H_4--23% N_5H_5

GRAPHITE-ANODIC

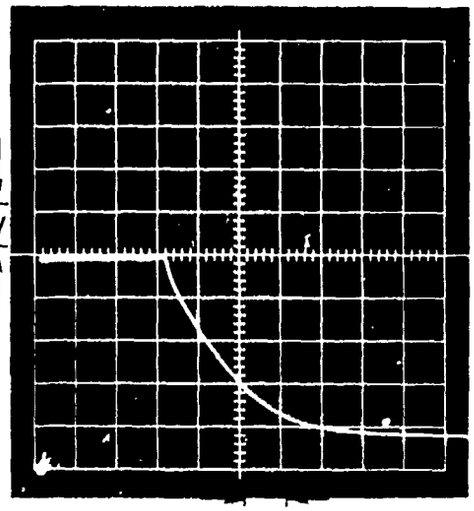

GRAPHITE-CATHODIC

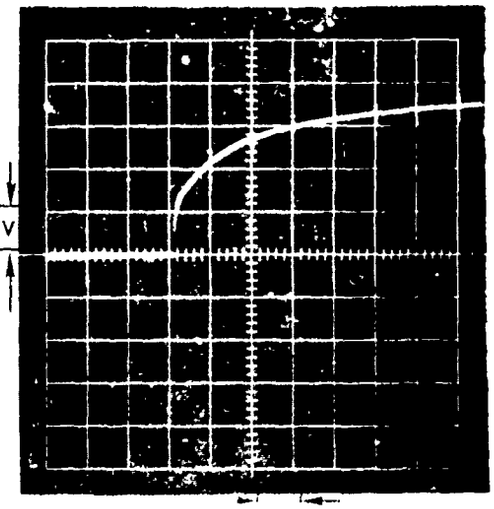

AM350-ANODIC

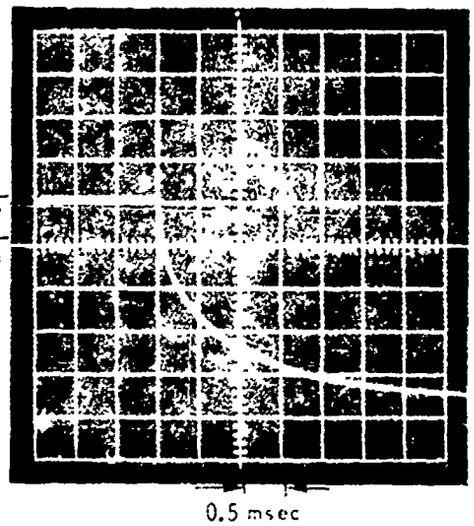

AM350-CATHODIC

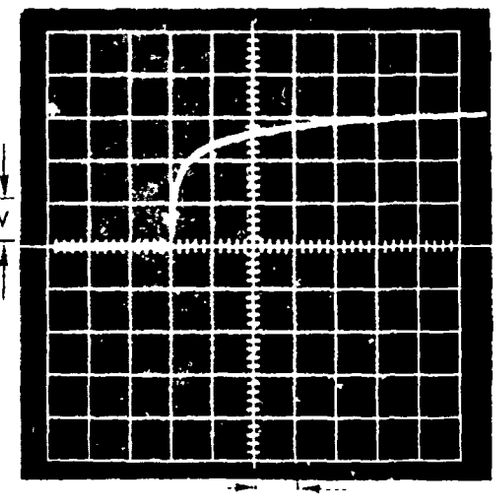

304SS-ANODIC

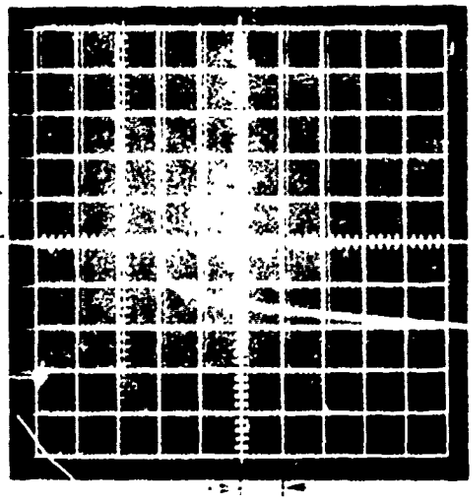

304SS-CATHODIC

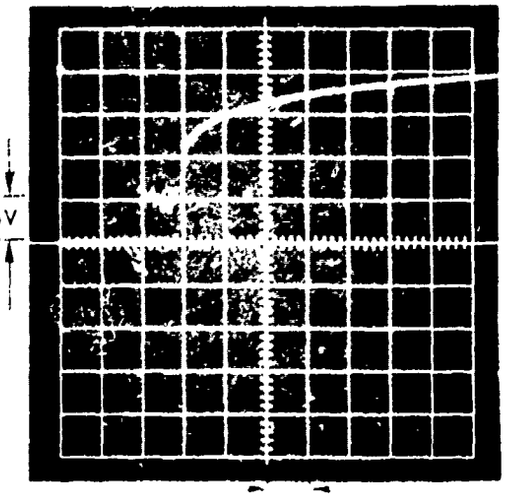

FIG 43

ELECTROLYSIS CELL

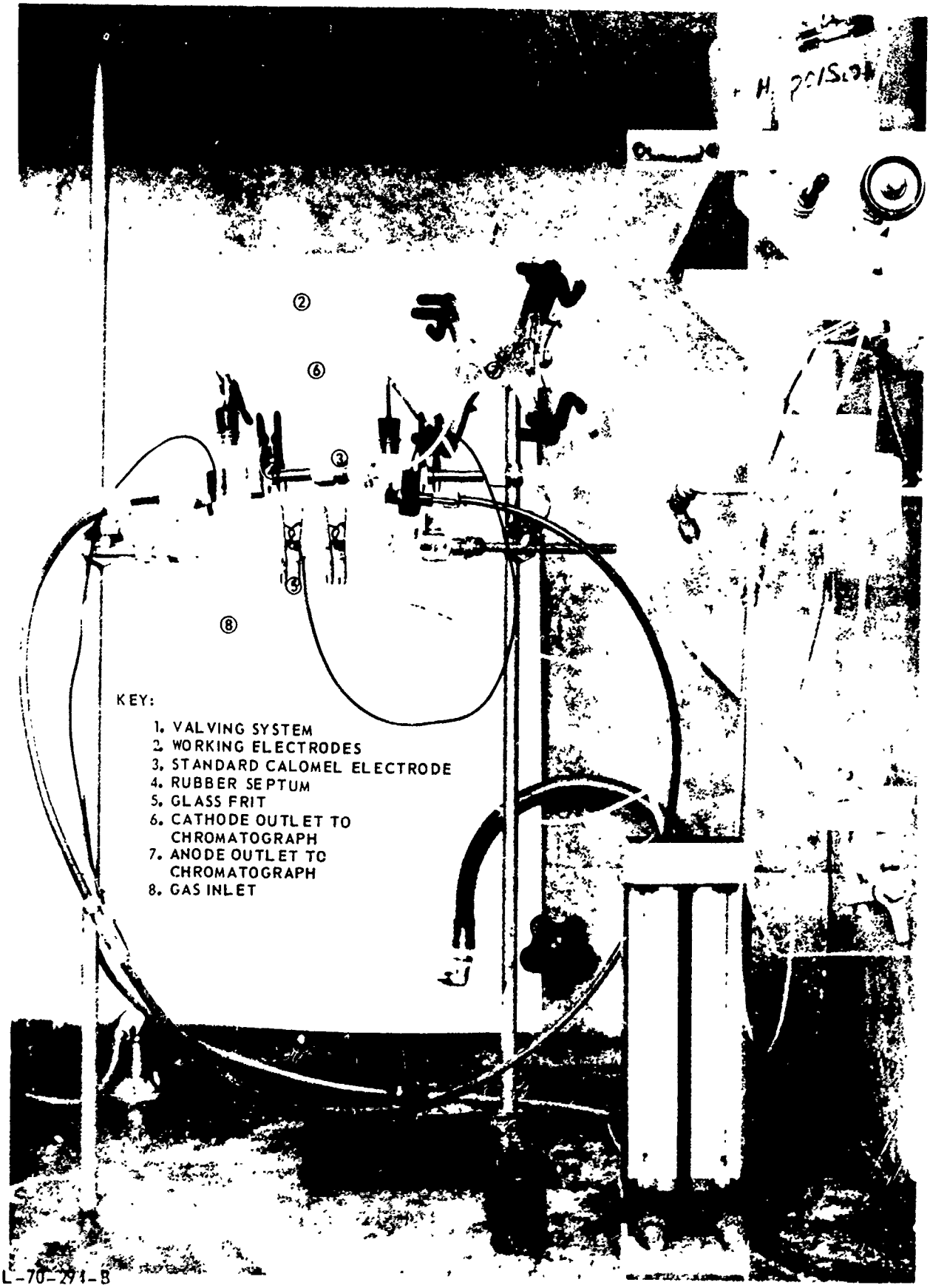

RL-70-271-B

FIG 44

CHROMATOGRAPHY APPARATUS

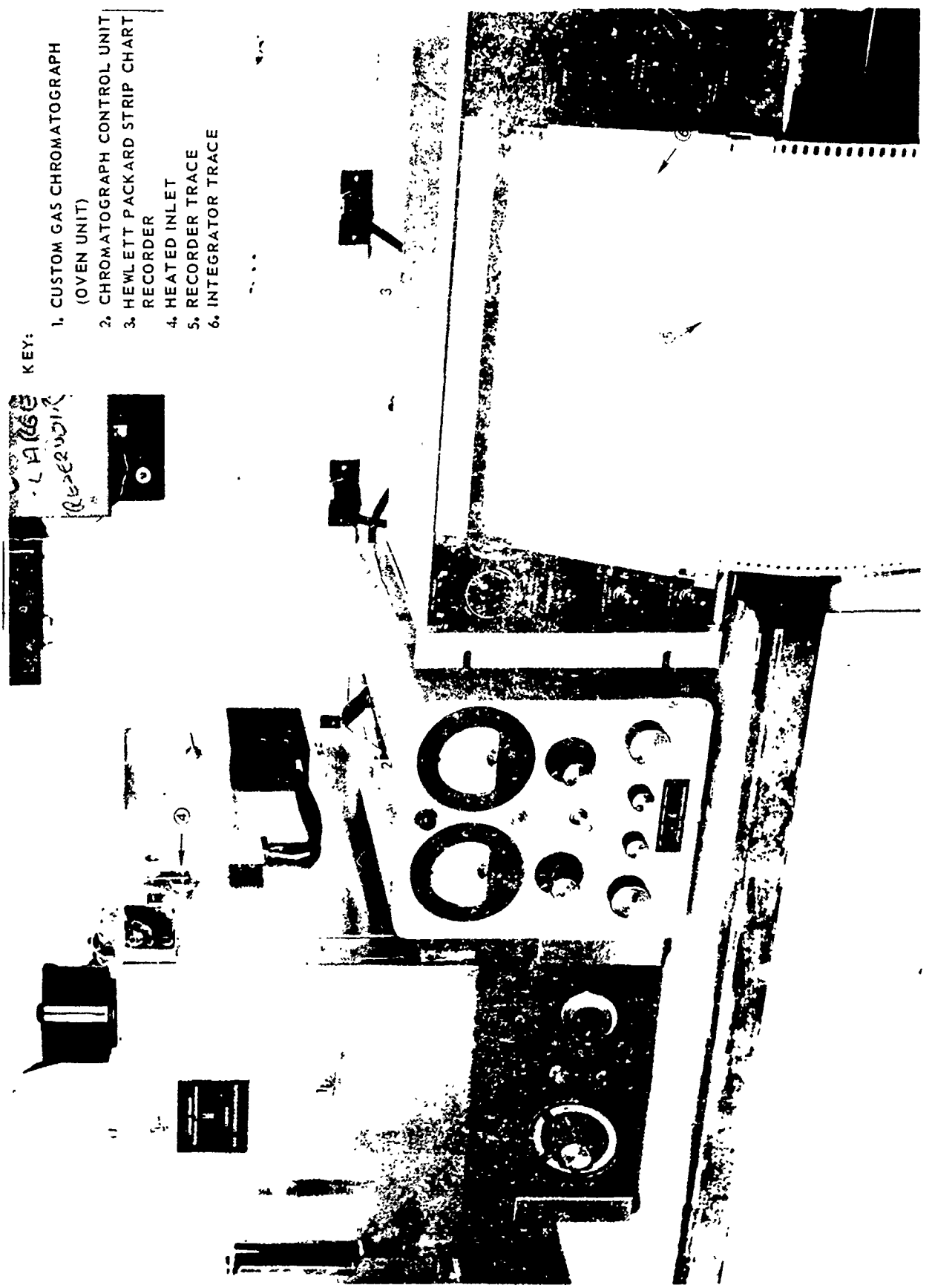

FIG. 45

HEATING RATES AS A FUNCTION OF ELECTRODE MATERIALS

(CURRENT – 6.0 AMPS)

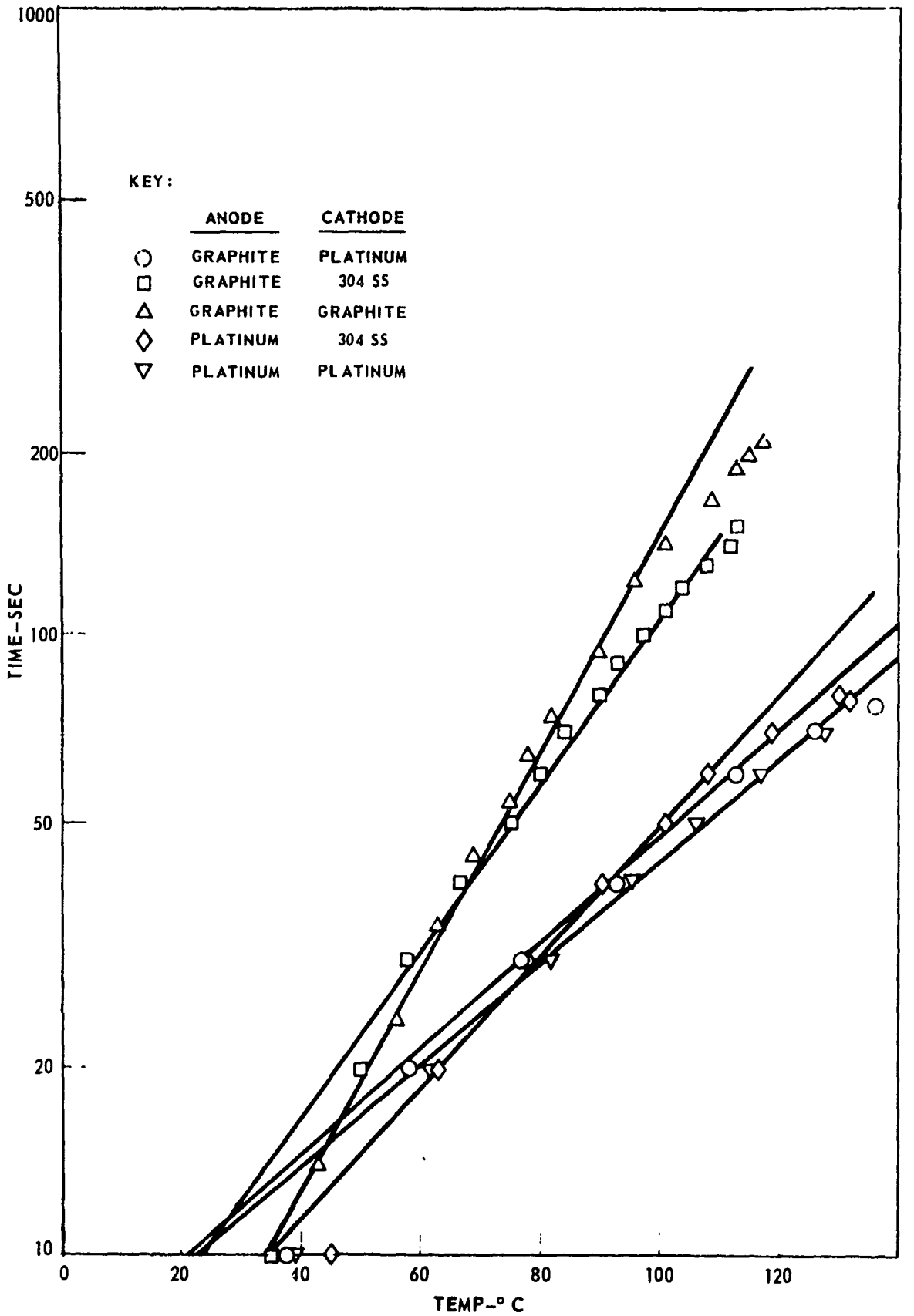

ELECTRODE CONFIGURATION NO. 1

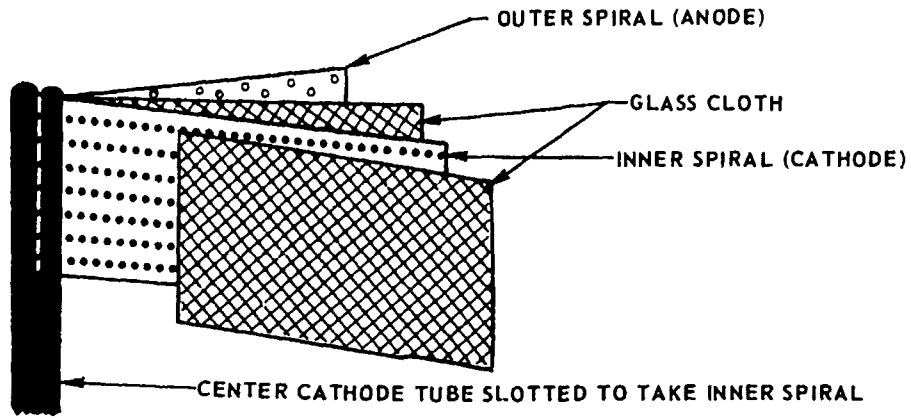

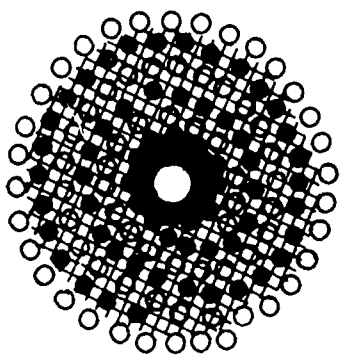

HORIZONTAL CROSS-SECTION

KEY:

- CATHODE SHELL
- CATHODE SCREEN
- ANODE SHELL
- ANODE SCREEN
- GLASS CLOTH

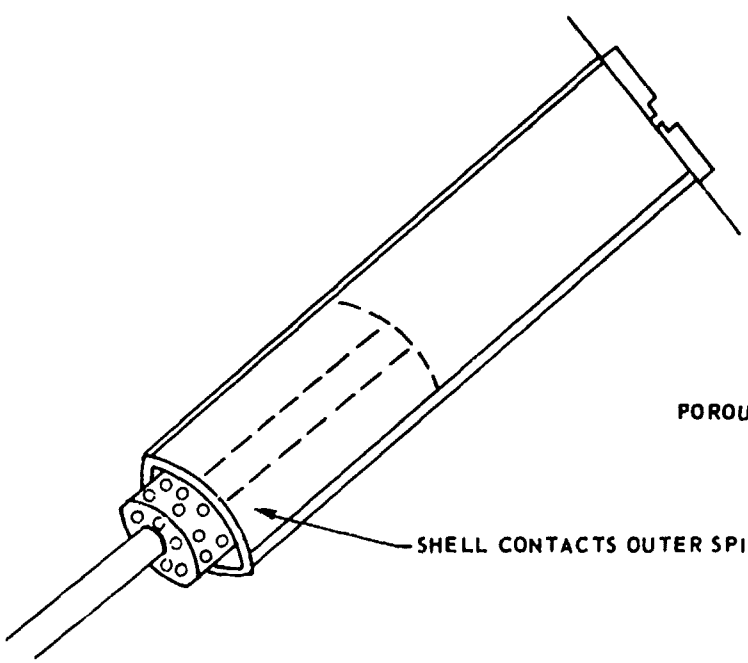

POROUS GLASS FRIT

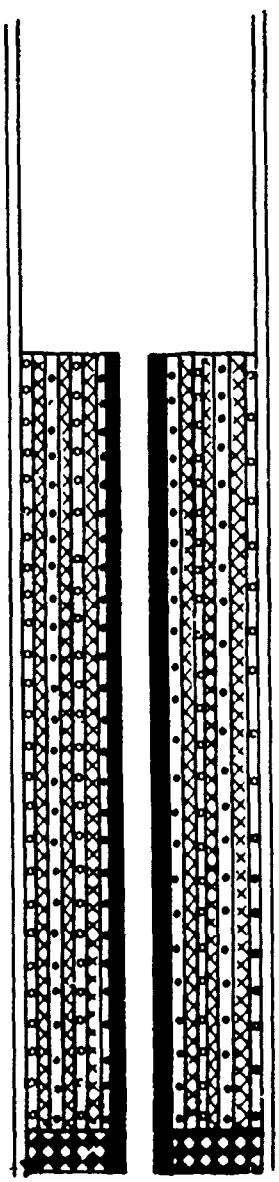

VERTICAL CROSS-SECTION

FIG. 47

ELECTRODE CONFIGURATION NO. 2

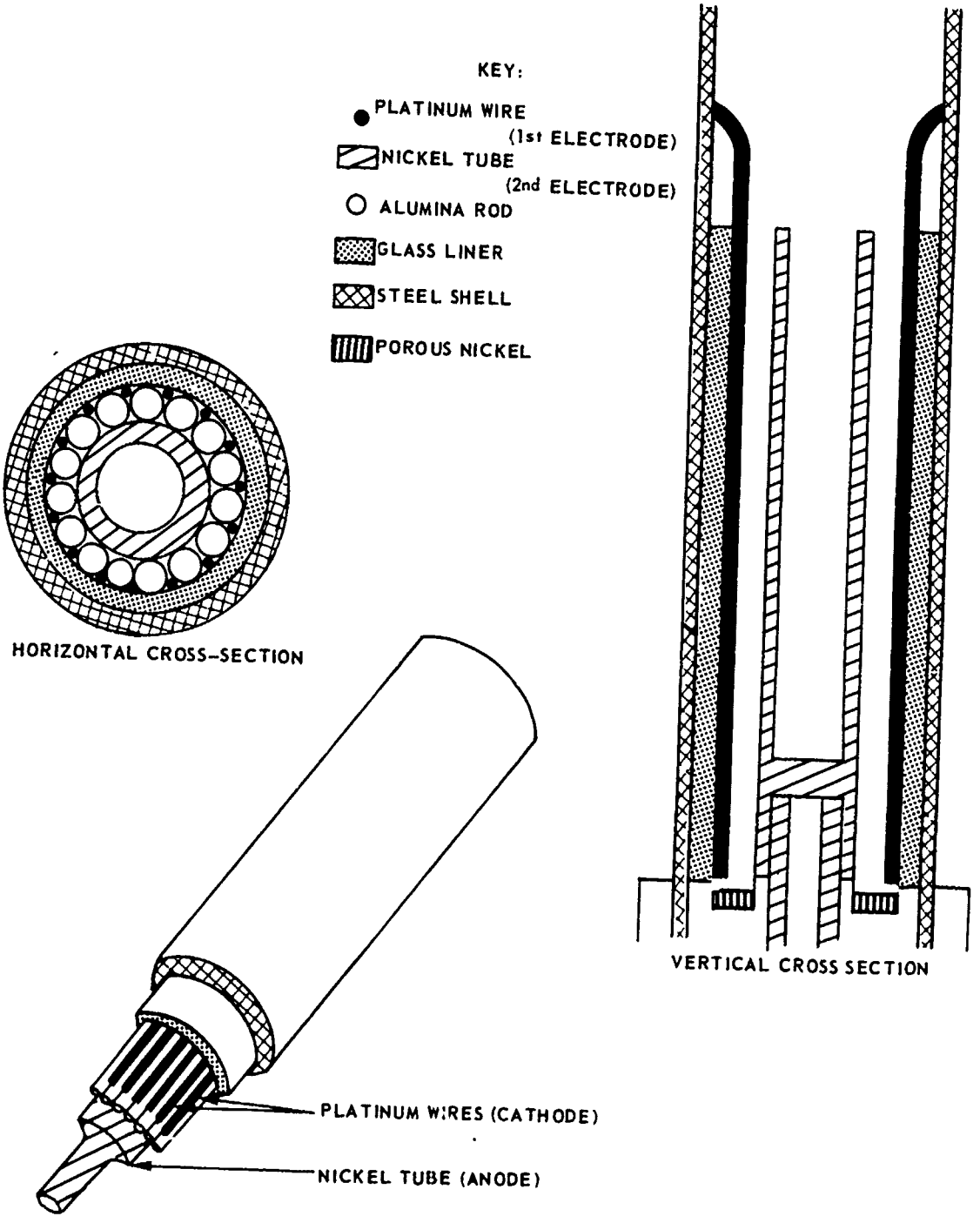

FIG. 47

ELECTRODE CONFIGURATION NO. 2

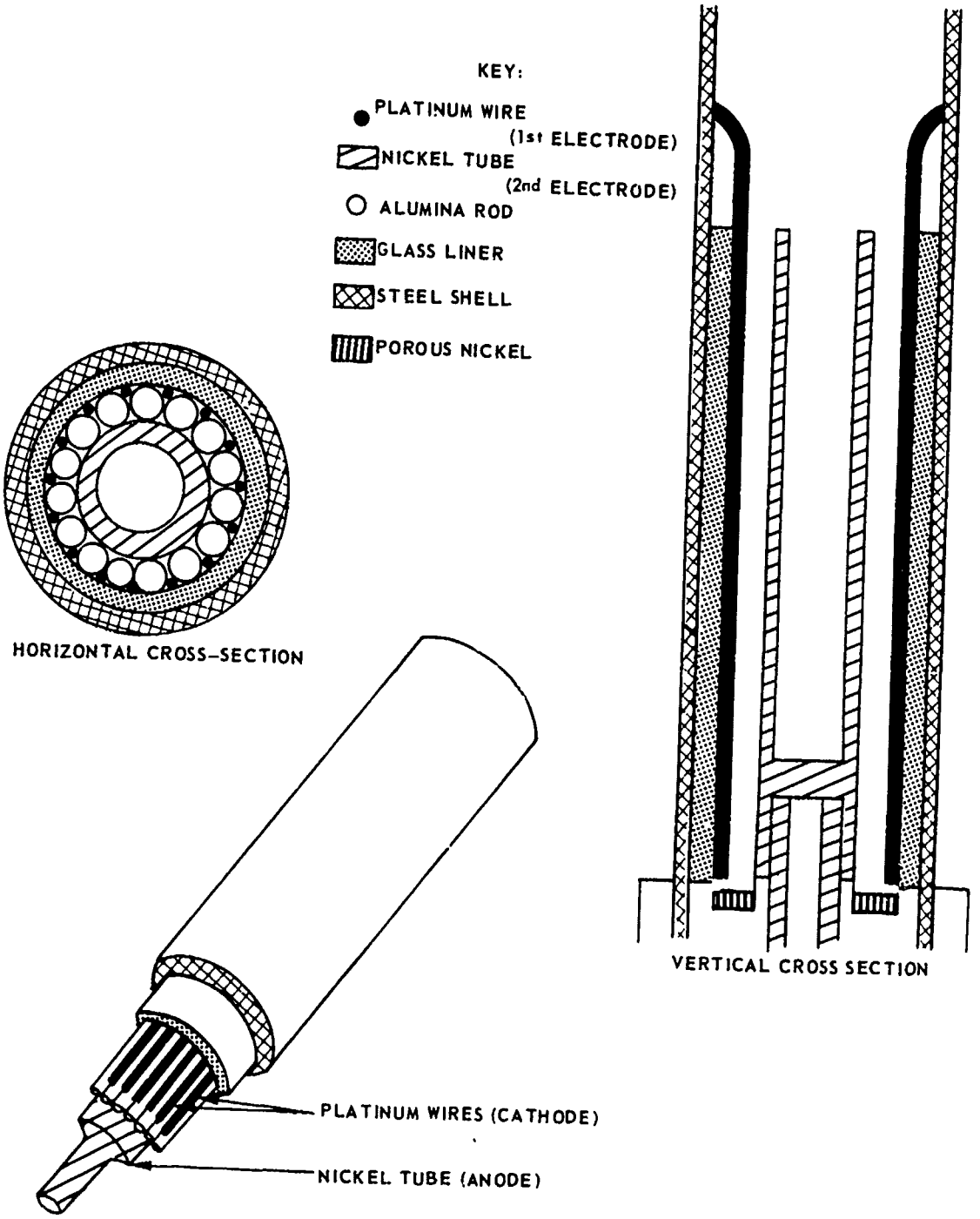

FIG. 48

ELECTRODE CONFIGURATION WITH HORIZONTAL FLAT SCREENS

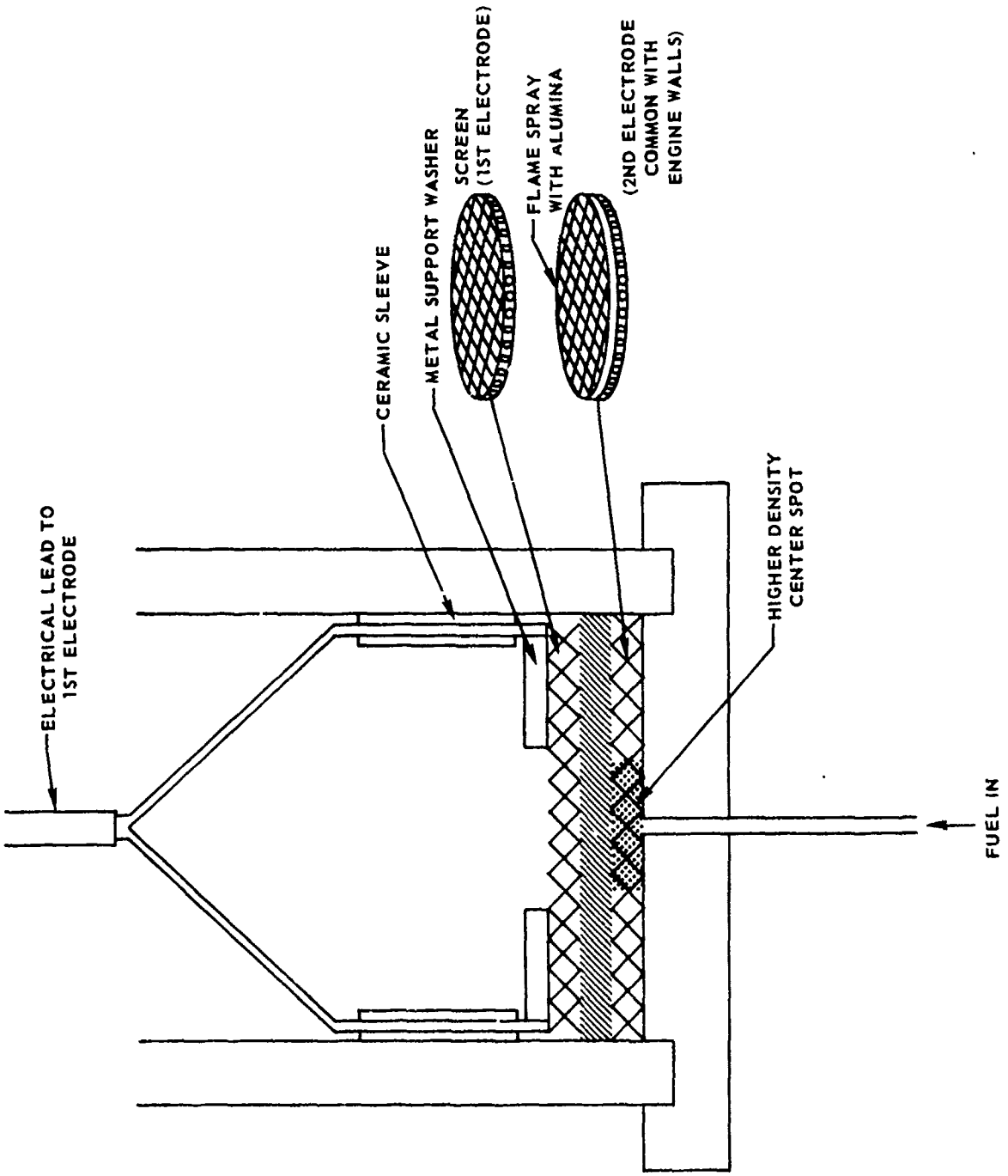

FIG. 49

ELECTRODE CONFIGURATION WITH PARALLEL VERTICAL PLATES

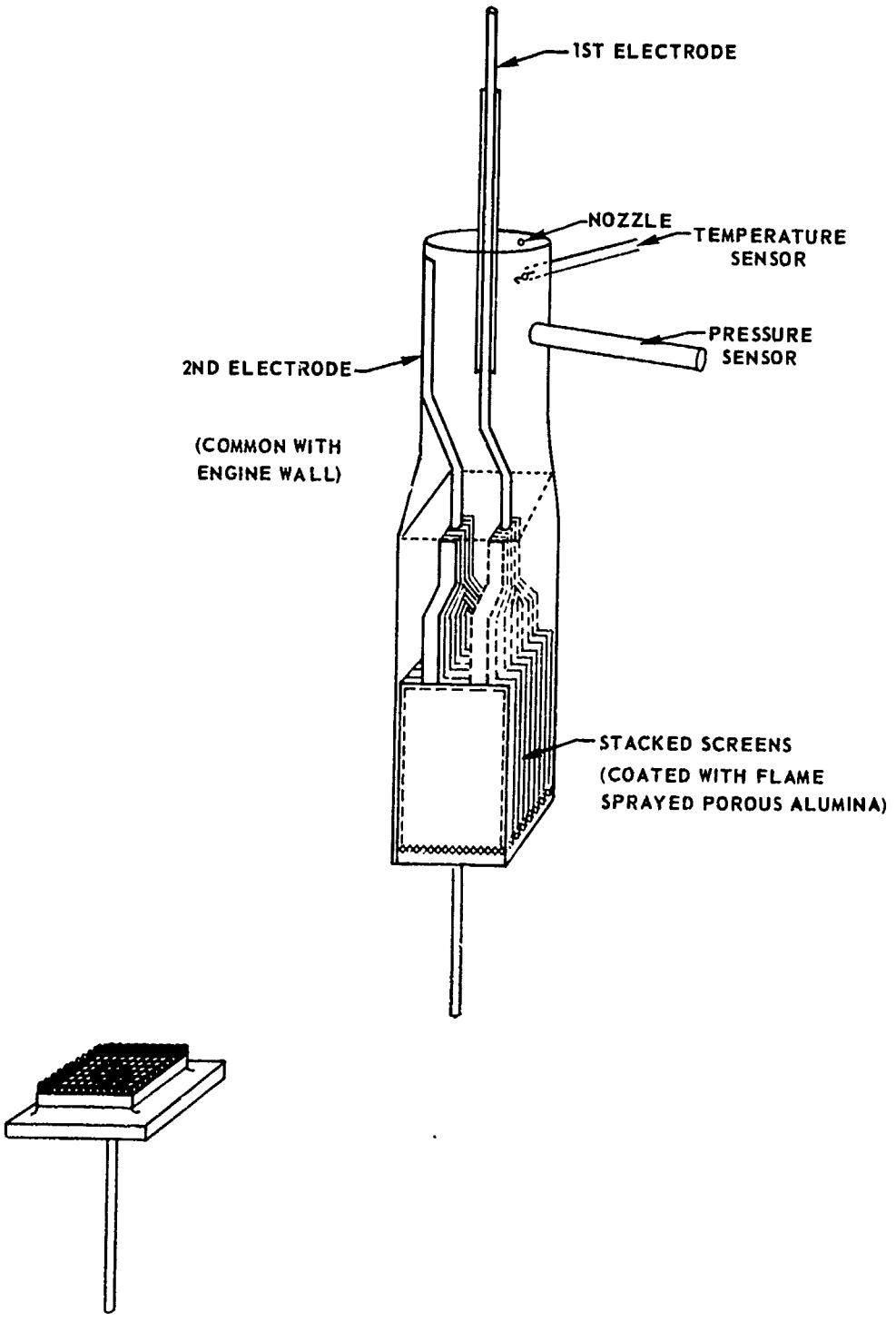

FIG. 50

ENGINE CONFIGURATIONS CS-1 AND CS-3

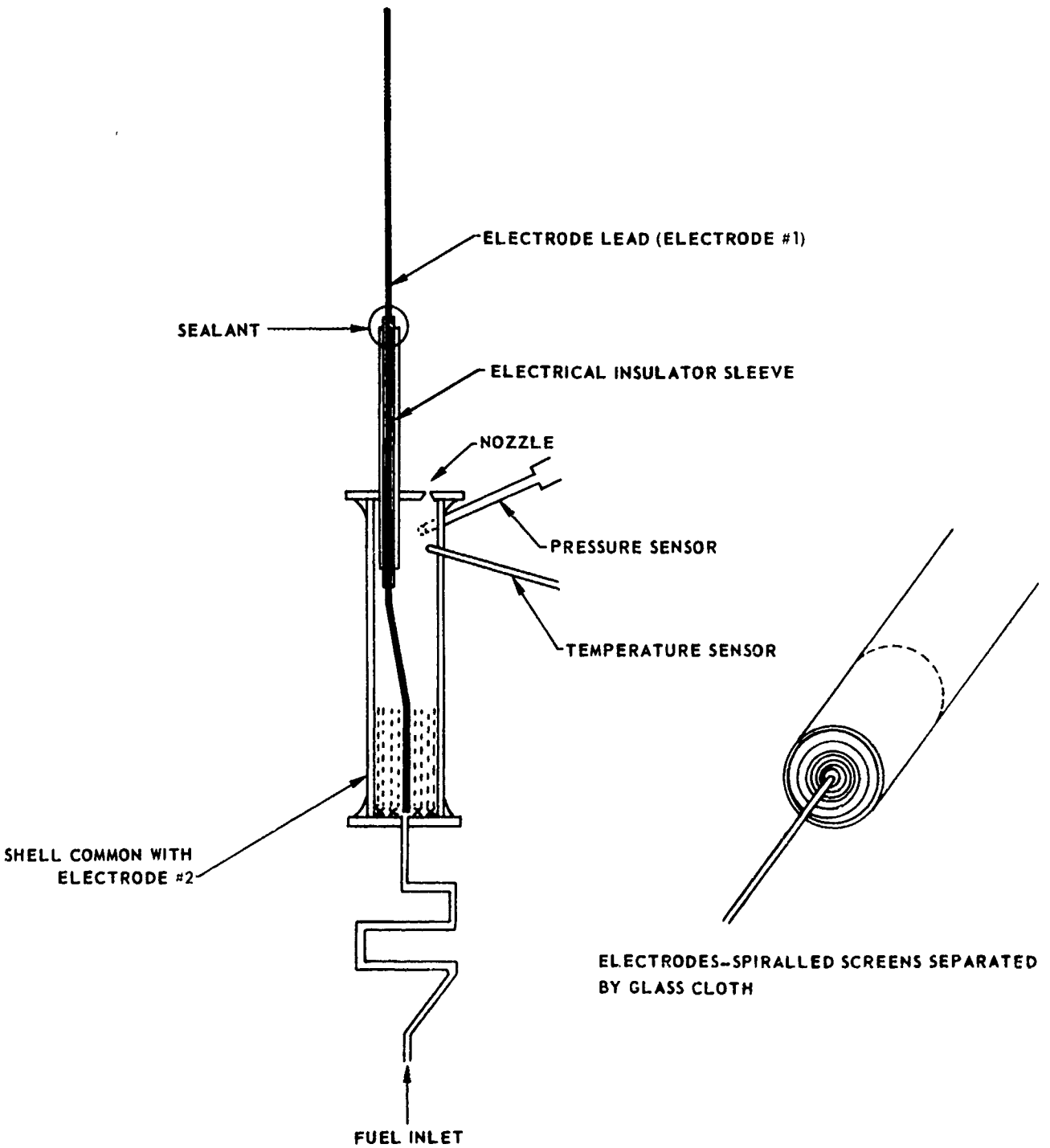

FIG.. 51

ENGINE CONFIGURATION CS-2TB

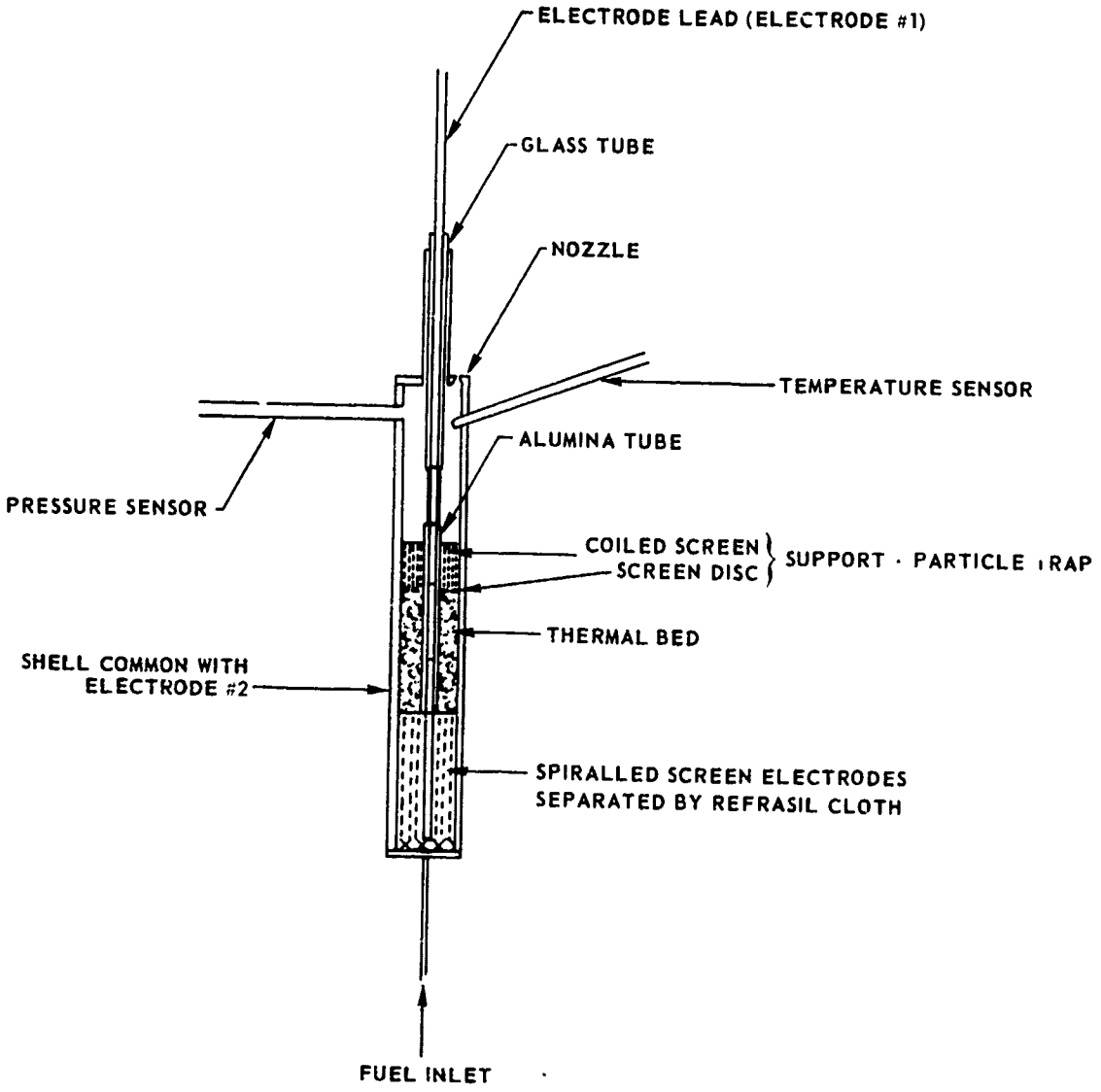

FIG. 52

FUEL DELIVERY SYSTEM

(WITH FLOW-MEASURING DEVICE)

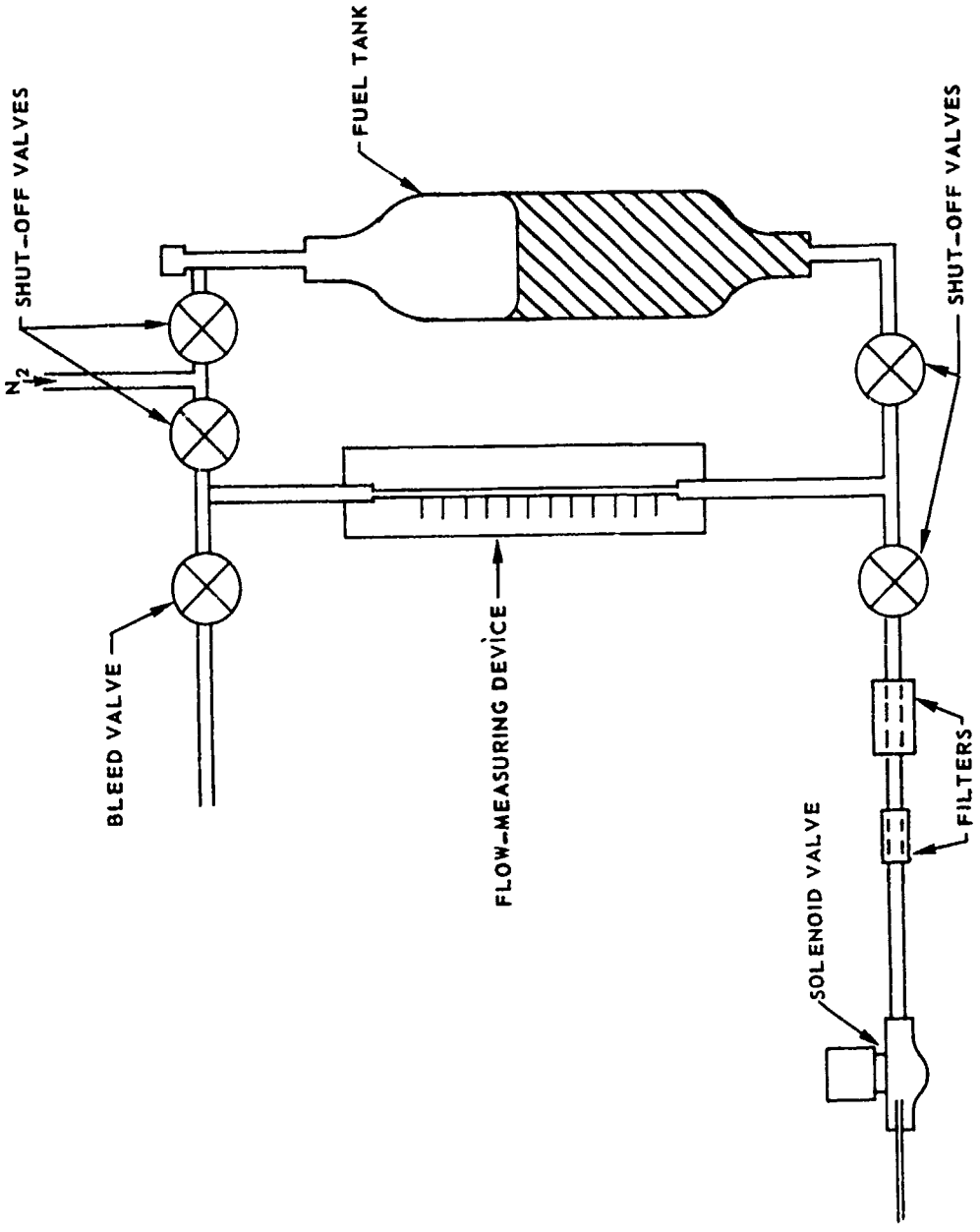

ENGINE TEST APPARATUS

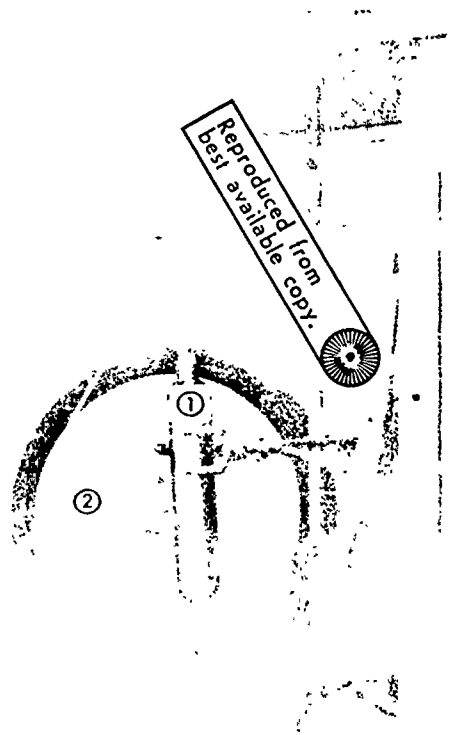

(1) FUEL TANK
(2) INLET PRESSURE GAUGE
(3) FUEL SIGHT GUAGE
(4) SOLINOID VALVE
(5) PRESSURE TRANSDUCER
(6) ENGINE
(7) VISICORDER
(8) SIGNAL AMPLIFIER
(9) TRANSDUCER AMPLIFIER

RL-72-58-A

FIG. 53

FIG. 54

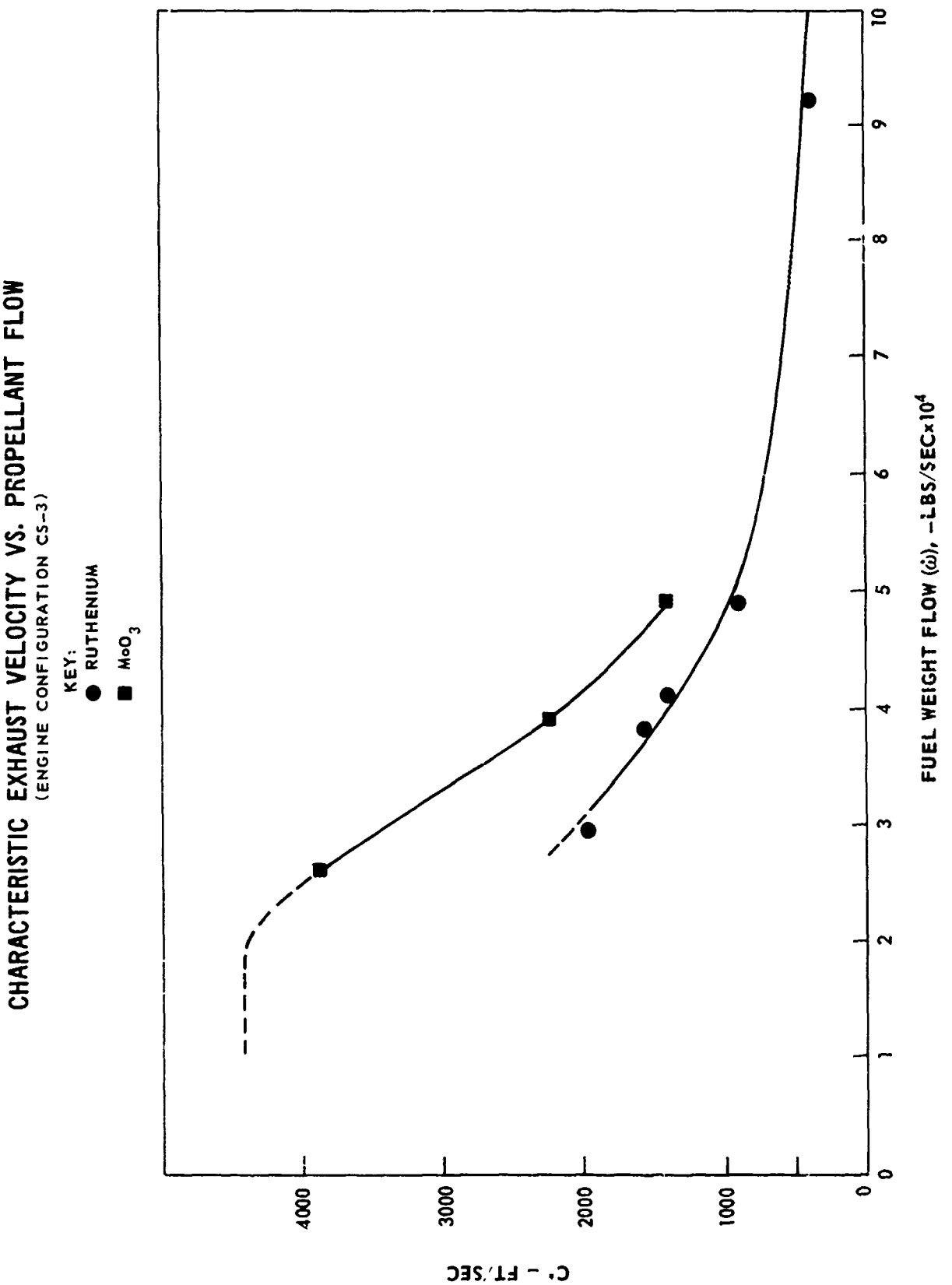
CHARACTERISTIC EXHAUST VELOCITY VS. PROPELLANT FLOW
(ENGINE CONFIGURATION CS-3)
KEY:
● RUTHENIUM
■ MoO_3
C* - FT/SEC
4000
3000
2000
1000
0
0
1
2
3
4
5
6
7
8
9
10
FUEL WEIGHT FLOW (ẇ), -LBS/SEC x 10^4

ENGINE CONFIGURATION WITH HORIZONTAL FLAT SCREENS AND THERMAL BED

(FP-1TB)

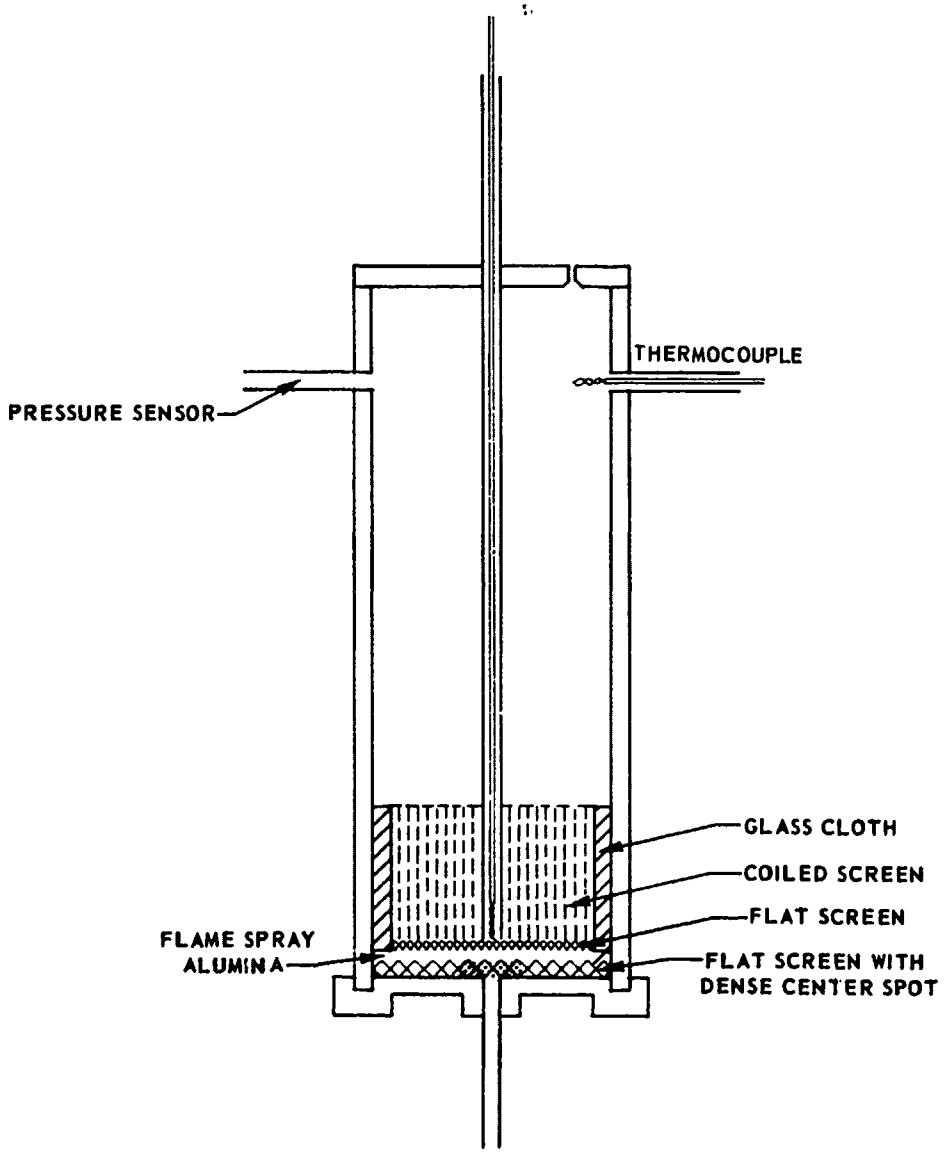

FIG. 56

ENGINE CONFIGURATION FP-2

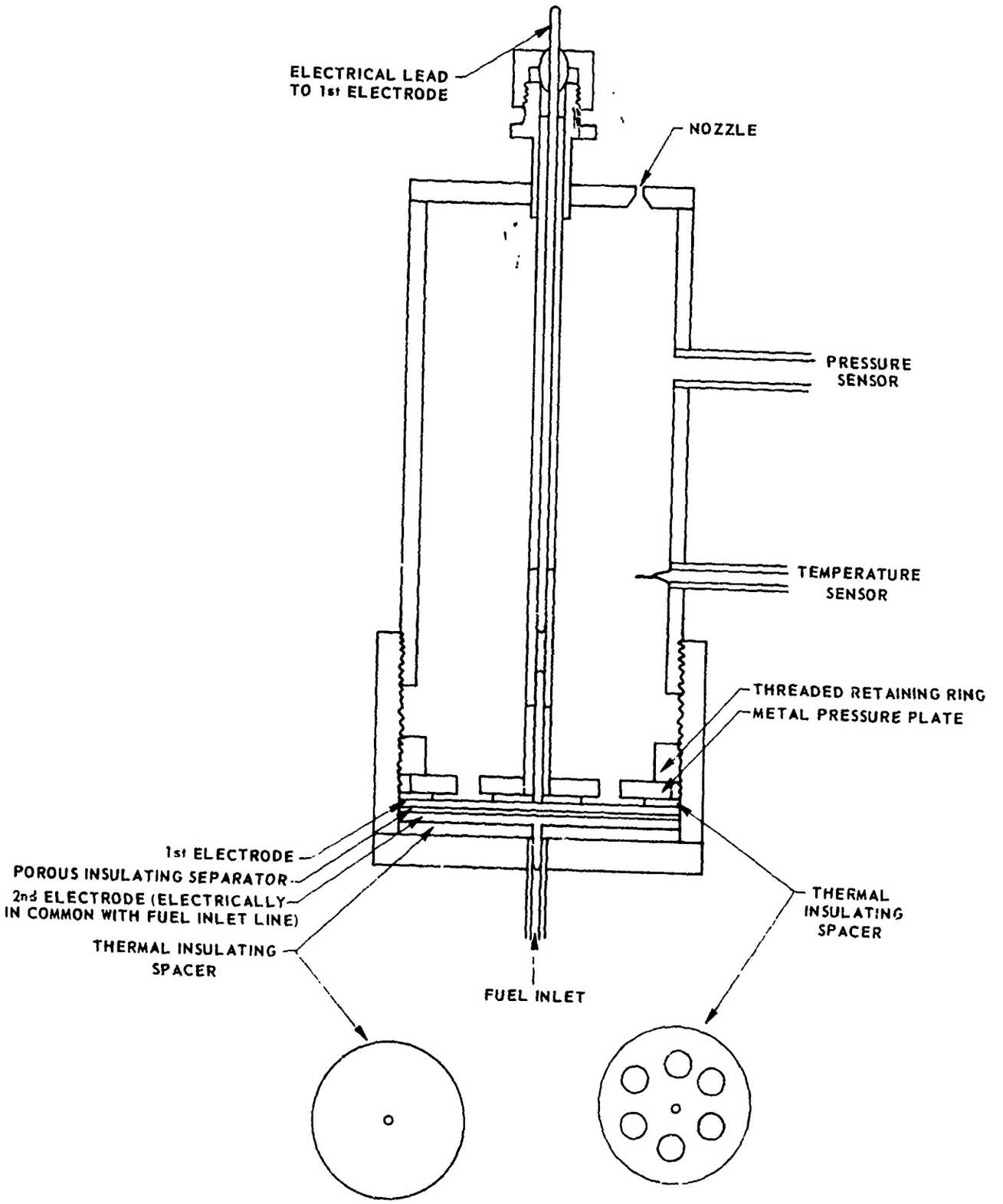

FIG. 57

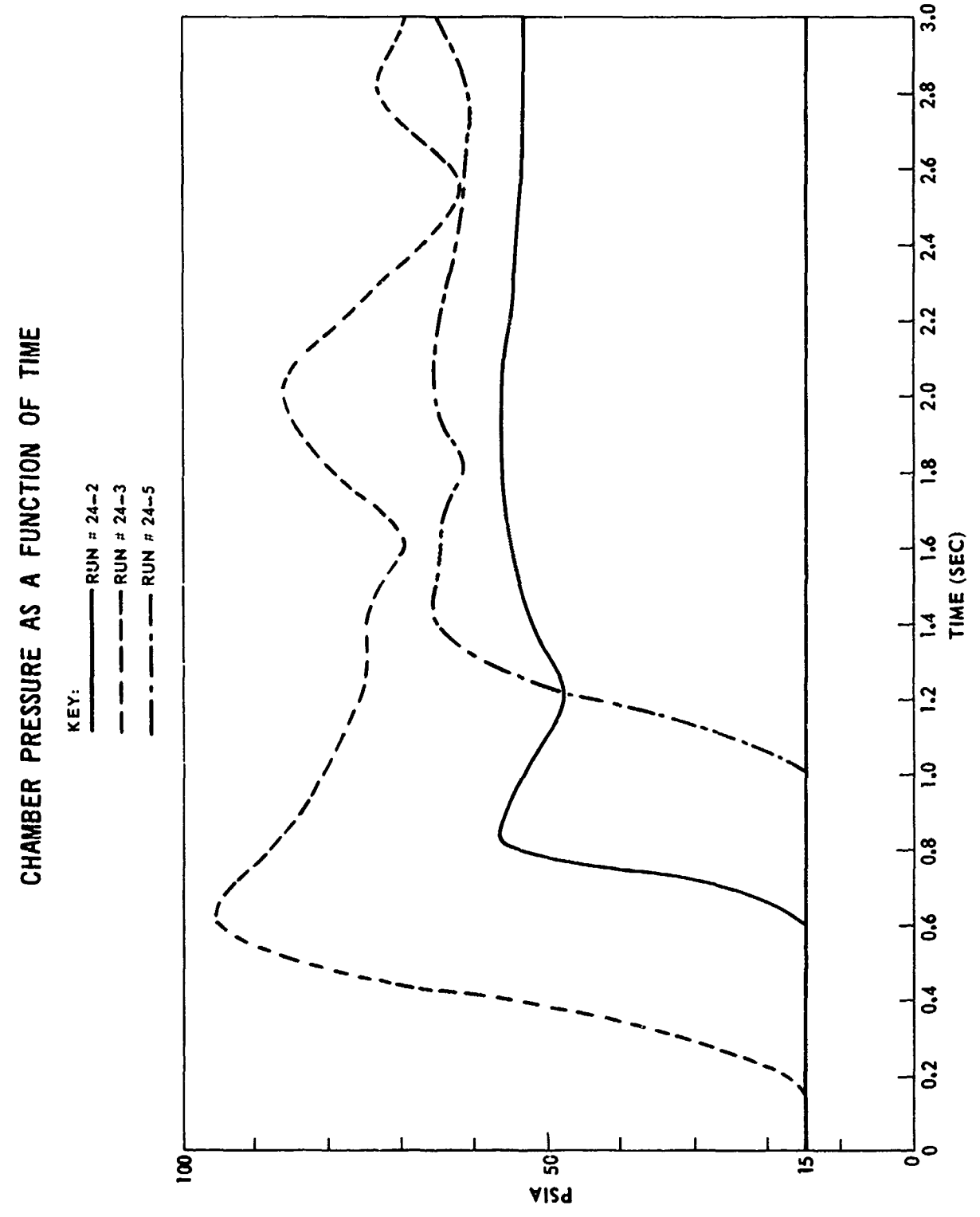
CHAMBER PRESSURE AS A FUNCTION OF TIME
KEY:
RUN # 24-2
RUN # 24-3
RUN # 24-5
100
50
15
PSIA
0
0.2
0.4
0.6
0.8
1.0
1.2
1.4
1.6
1.8
2.0
2.2
2.4
2.6
2.8
3.0
TIME (SEC)

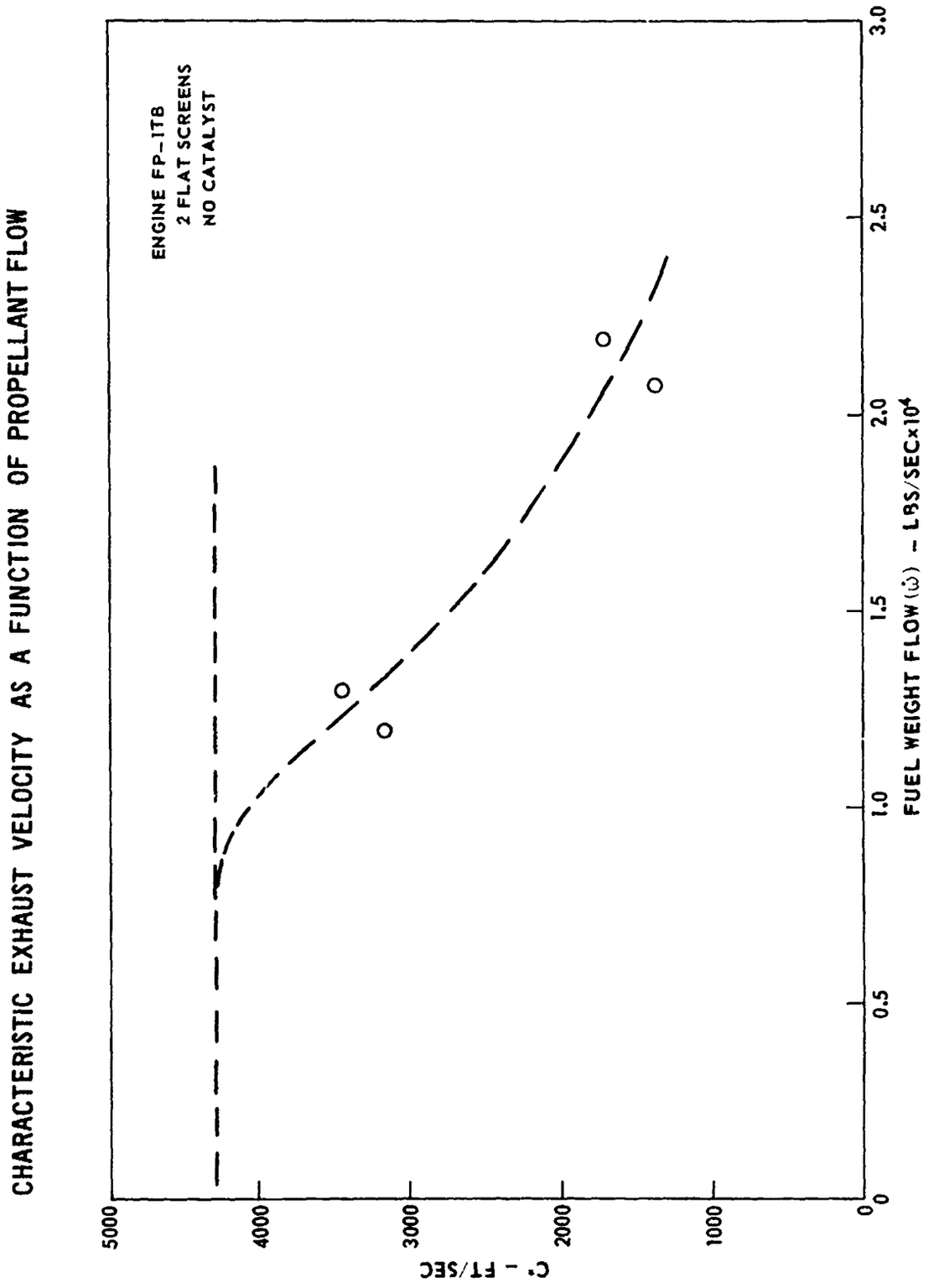
CHARACTERISTIC EXHAUST VELOCITY AS A FUNCTION OF PROPELLANT FLOW
ENGINE FP-1TB
2 FLAT SCREENS
NO CATALYST
C* - FT/SEC
5000
4000
3000
2000
1000
0
0.5
1.0
1.5
2.0
2.5
3.0
FUEL WEIGHT FLOW (ω) - LBS/SEC x 10⁴

FIG. 59

ENGINE CONFIGURATION FP-3

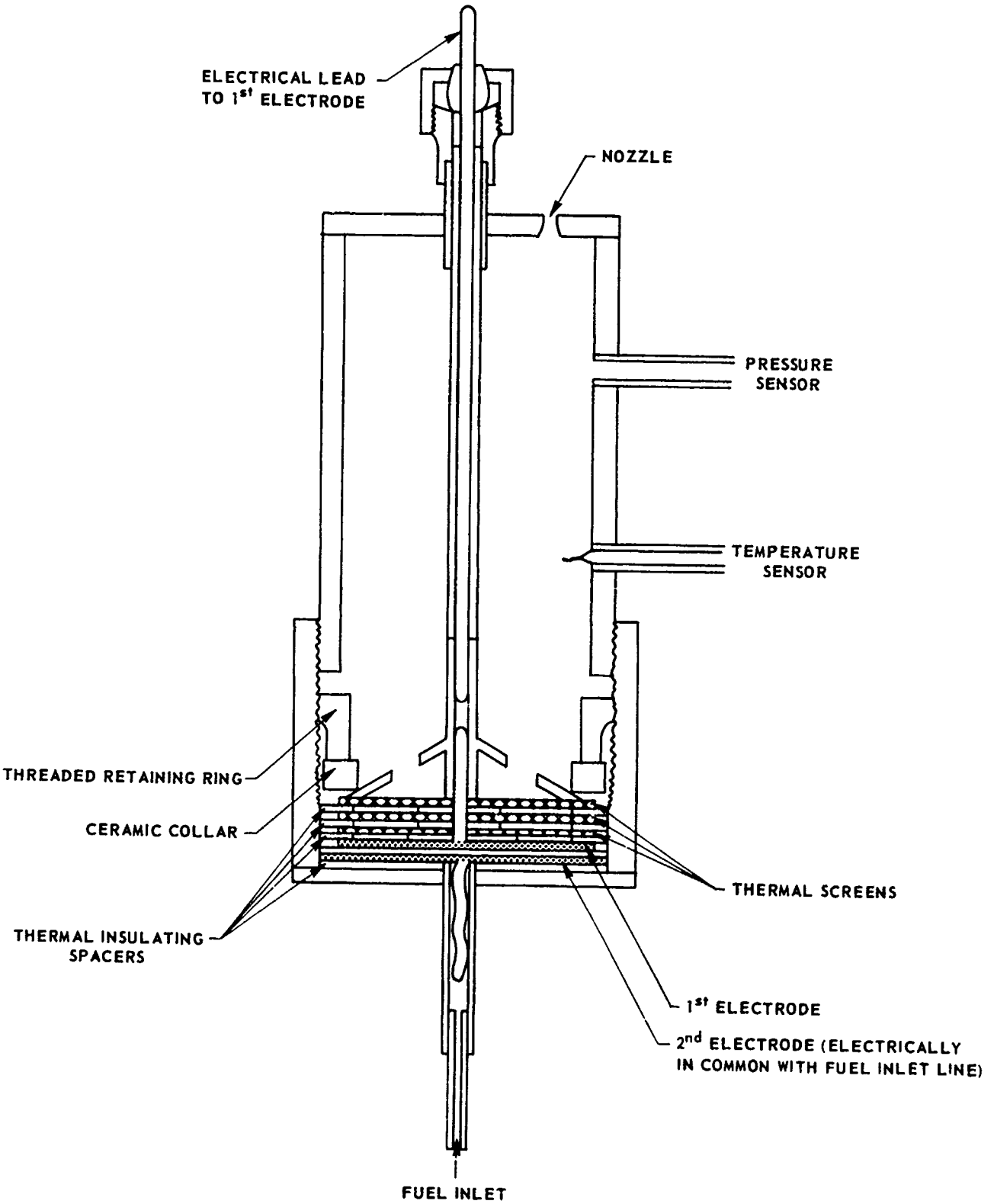

FIG. 60

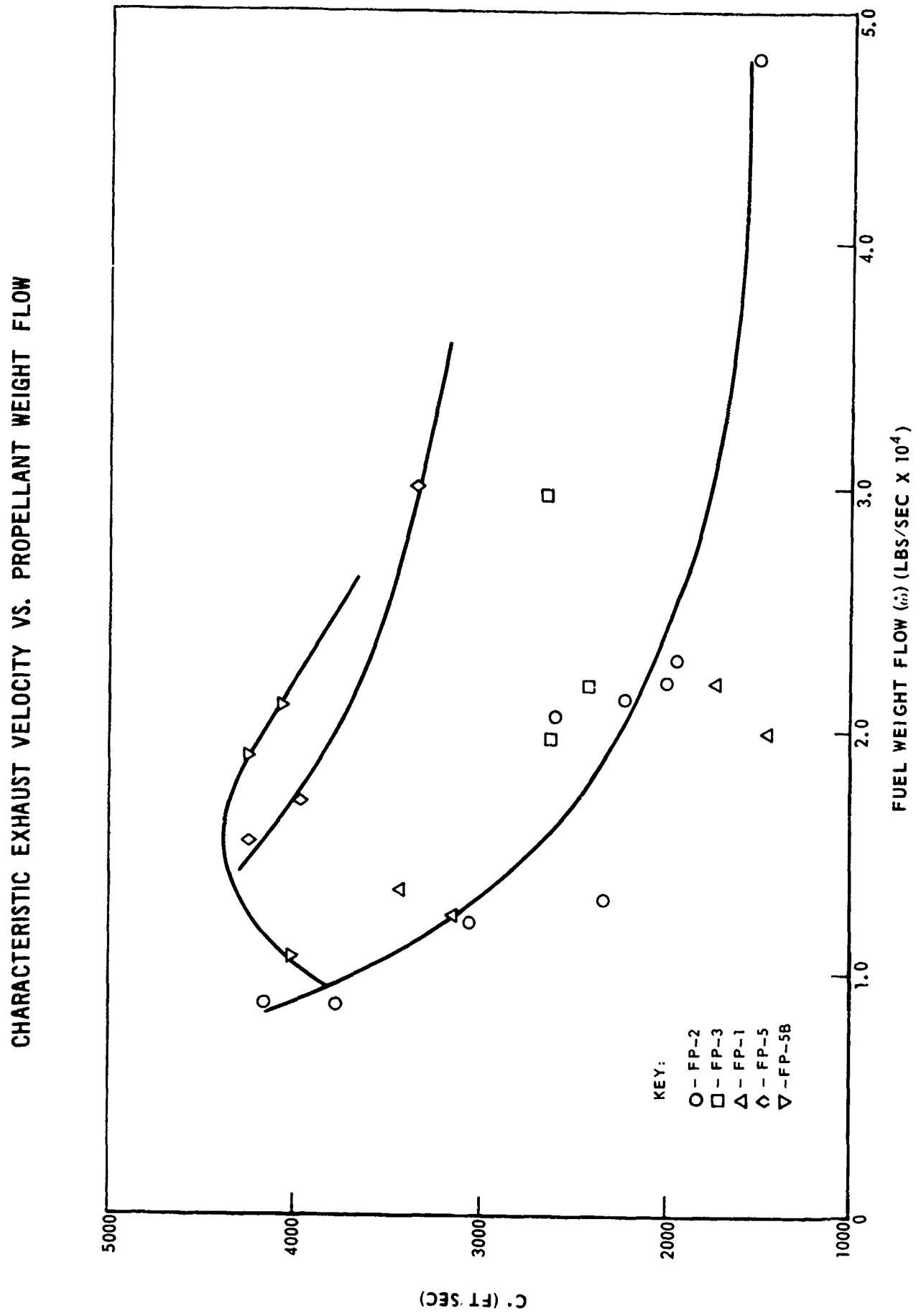
CHARACTERISTIC EXHAUST VELOCITY VS. PROPELLANT WEIGHT FLOW
C* (FT/SEC)
5000
4000
3000
2000
1000
0
FUEL WEIGHT FLOW (ṁ) (LBS/SEC X 10⁴)
5.0
4.0
3.0
2.0
1.0
KEY:
O - FP-2
□ - FP-3
△ - FP-1
◇ - FP-5
▽ -FP-5B

ELECTROLYTIC CELL

(CONFIGURATION FP-4)

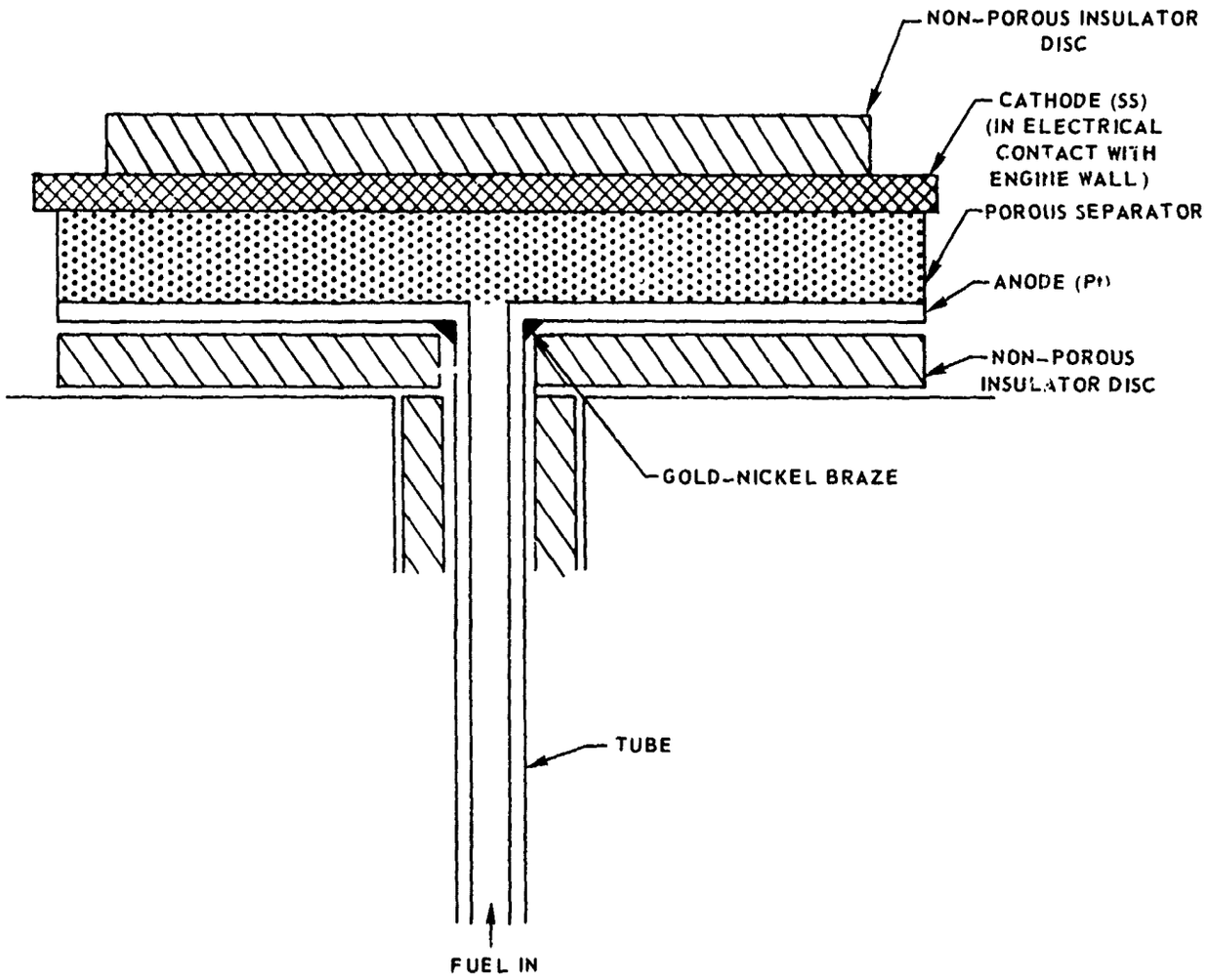

ENGINE CONFIGURATION FP-4

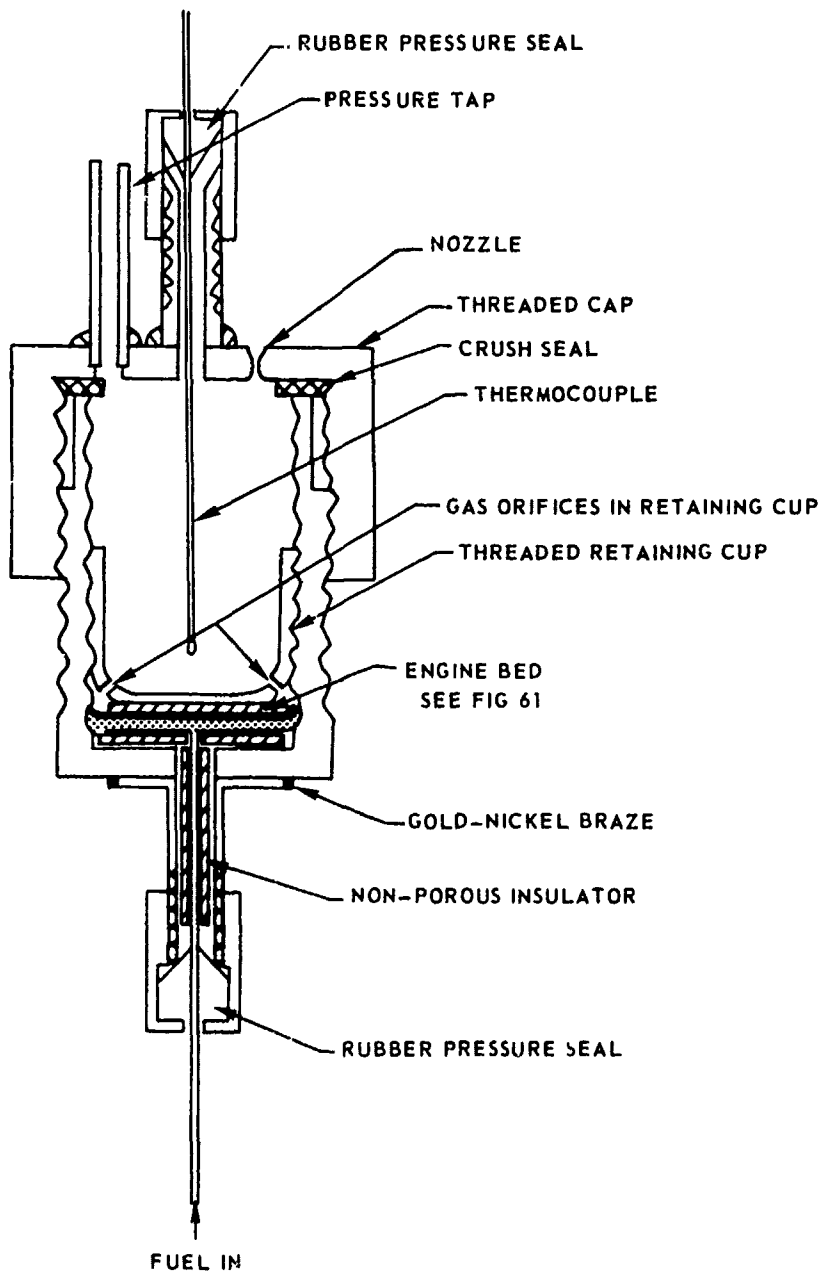

FIG. 63

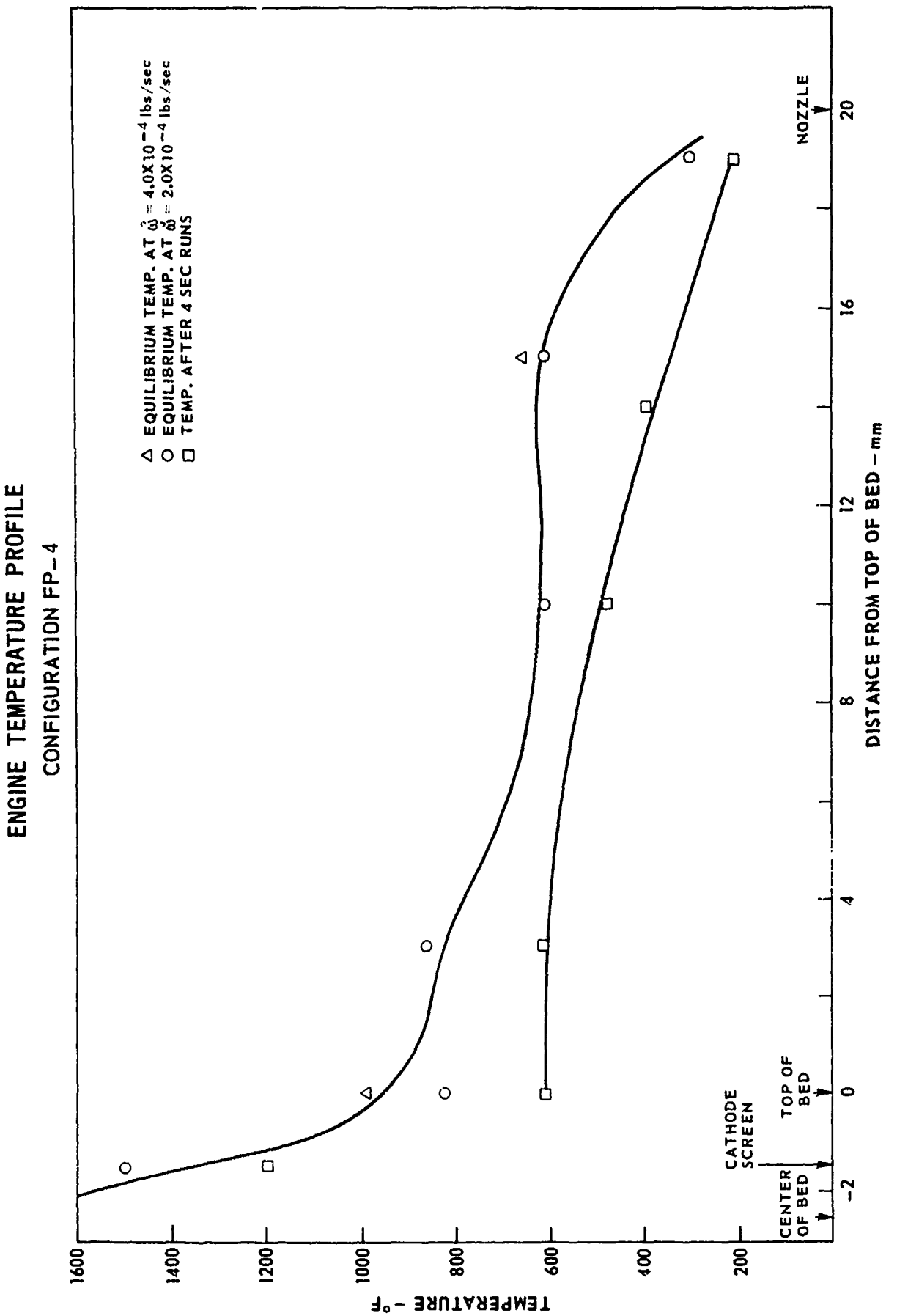
ENGINE TEMPERATURE PROFILE
CONFIGURATION FP-4
△ EQUILIBRIUM TEMP. AT $\dot{\omega} = 4.0X10^{-4}$ lbs/sec
○ EQUILIBRIUM TEMP. AT $\dot{\omega} = 2.0X10^{-4}$ lbs/sec
□ TEMP. AFTER 4 SEC RUNS
TEMPERATURE - °F
1600
1400
1200
1000
800
600
400
200
CENTER OF BED
CATHODE SCREEN
TOP OF BED
NOZZLE
-2
0
4
8
12
16
20
DISTANCE FROM TOP OF BED - mm

FIG. 64

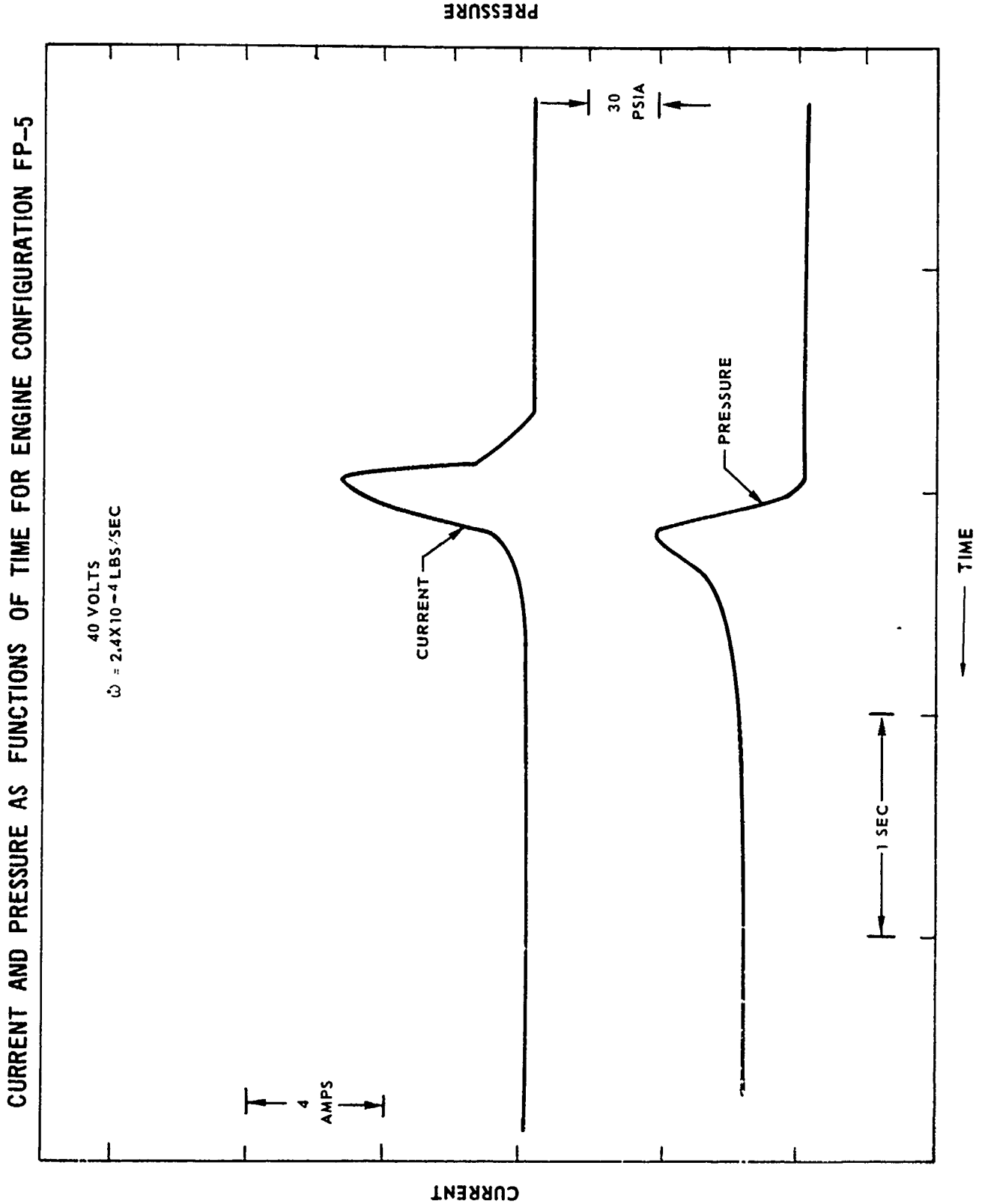
CURRENT AND PRESSURE AS FUNCTIONS OF TIME FOR ENGINE CONFIGURATION FP-5
40 VOLTS
ω = 2.4X10-4 LBS/SEC
CURRENT
PRESSURE
4 AMPS
30 PSIA
1 SEC
TIME

FIG. 65

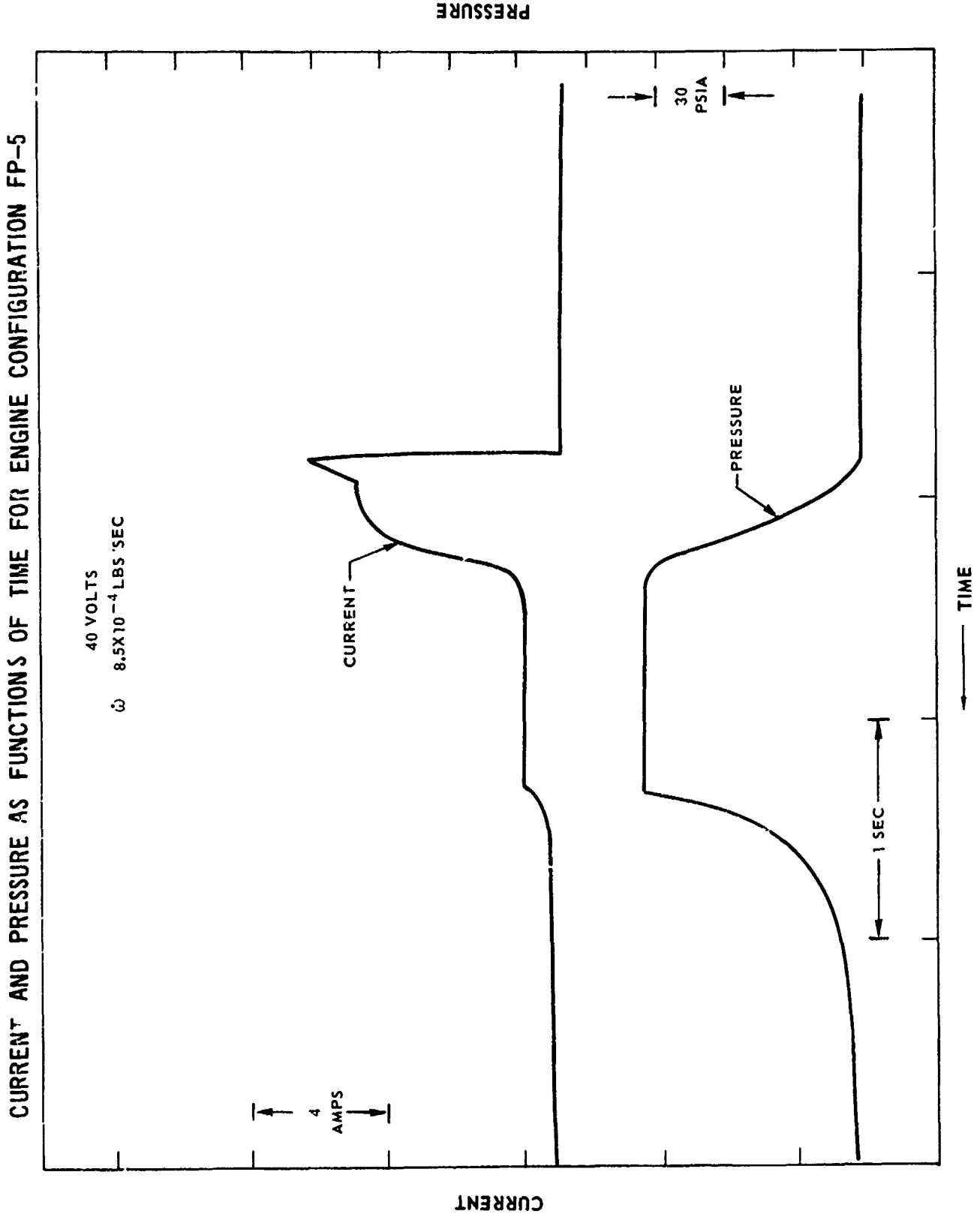
CURRENT AND PRESSURE AS FUNCTIONS OF TIME FOR ENGINE CONFIGURATION FP-5
40 VOLTS
ω 8.5X10⁻⁴ LBS SEC
CURRENT
PRESSURE
4 AMPS
30 PSIA
1 SEC
TIME
CURRENT
PRESSURE

FIG. 66

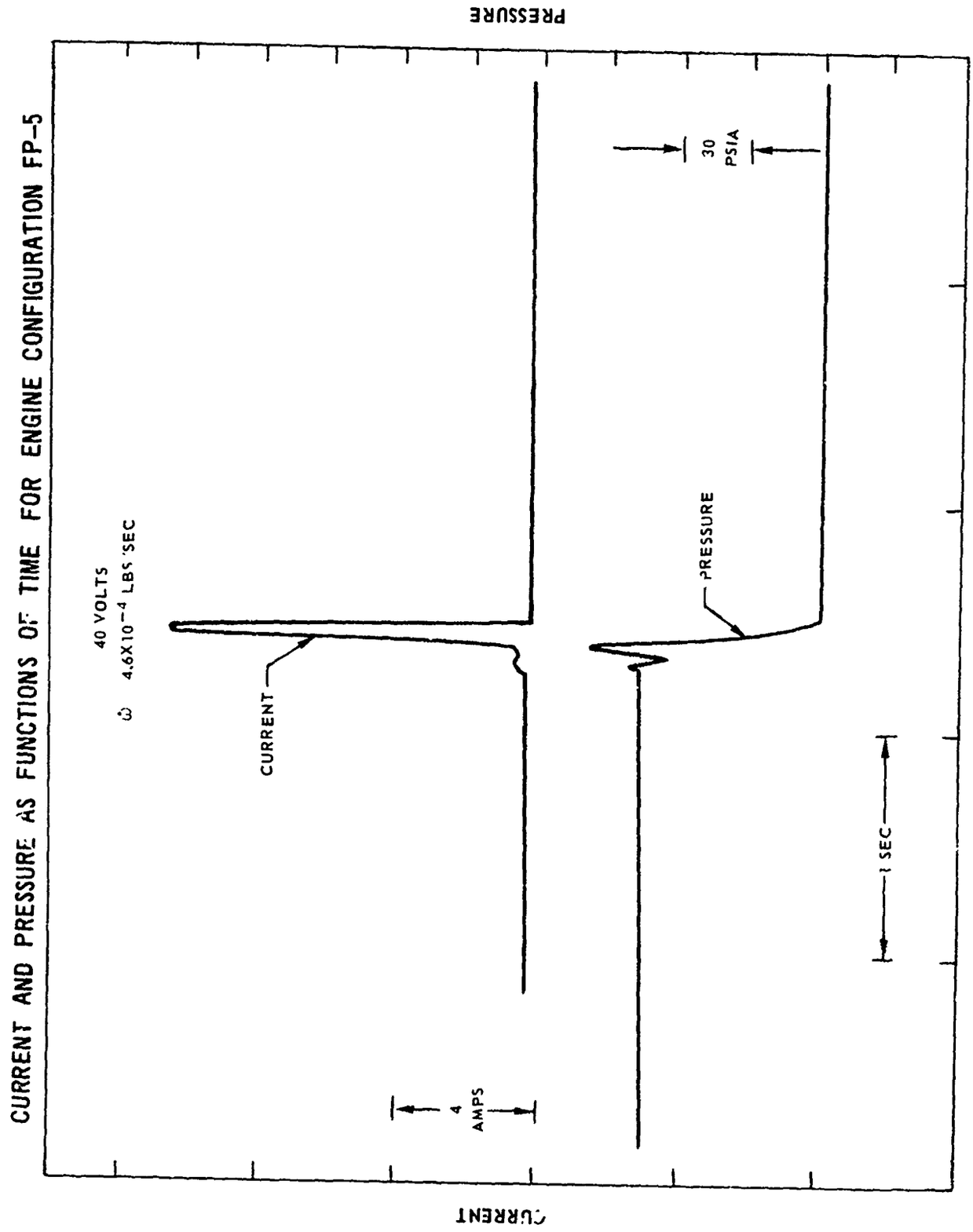
CURRENT AND PRESSURE AS FUNCTIONS OF TIME FOR ENGINE CONFIGURATION FP-5
PRESSURE
CURRENT
TIME
40 VOLTS
4.6X10⁻⁴ LBS/SEC
CURRENT
PRESSURE
4 AMPS
30 PSIA
1 SEC

FIG. 67

ENGINE CONFIGURATION FP-5

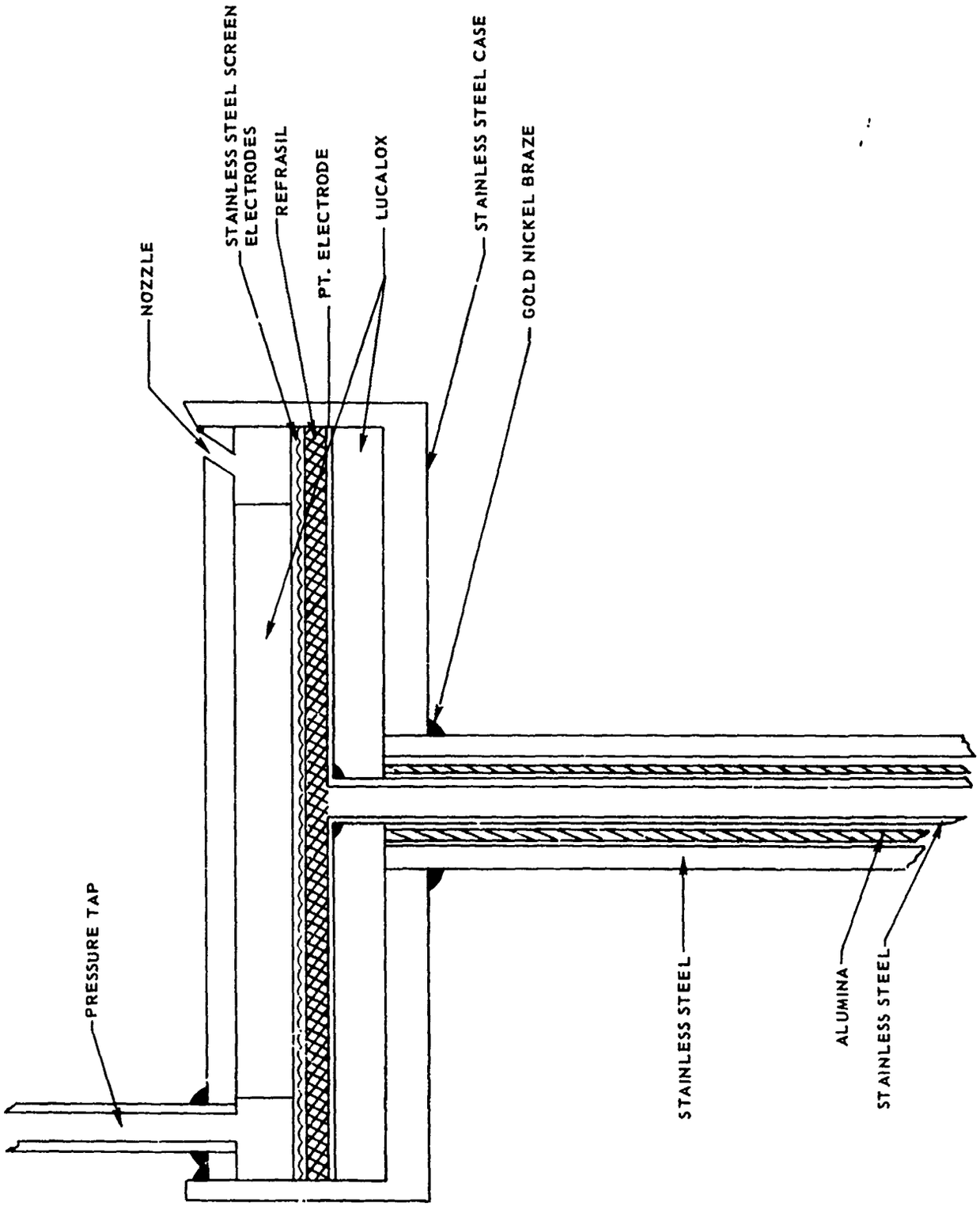

FIG. 68

PRESSURE-TIME RELATIONSHIP AS A FUNCTION OF TEMPERATURE

(ENGINE CONFIGURATION FP-5B)

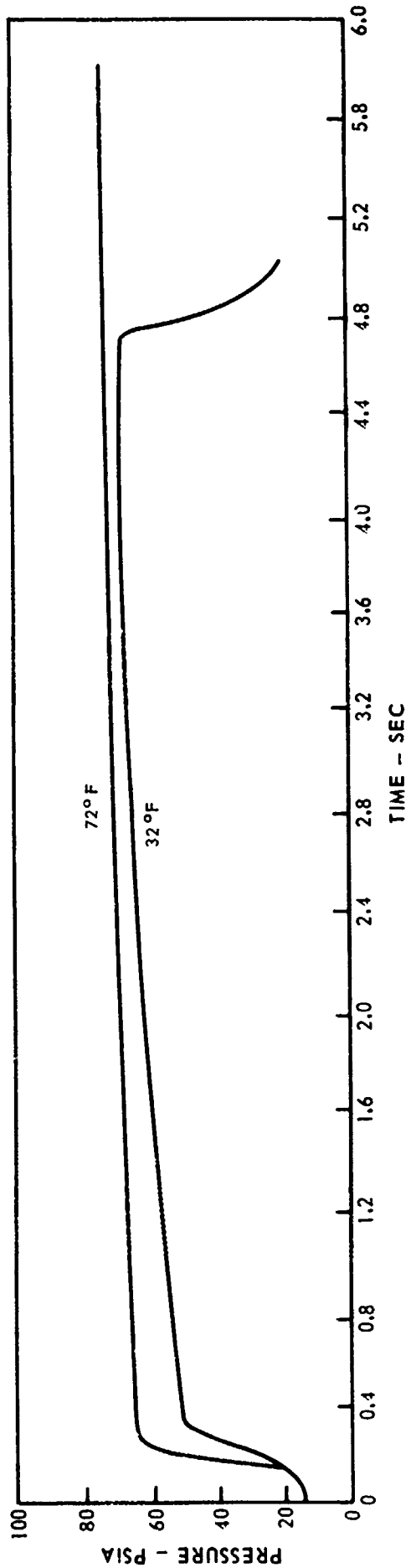

PRELIMINARY DESIGN FOR PROTOTYPE MILLIPOUND THRUSTER

(SCALE – 4X)

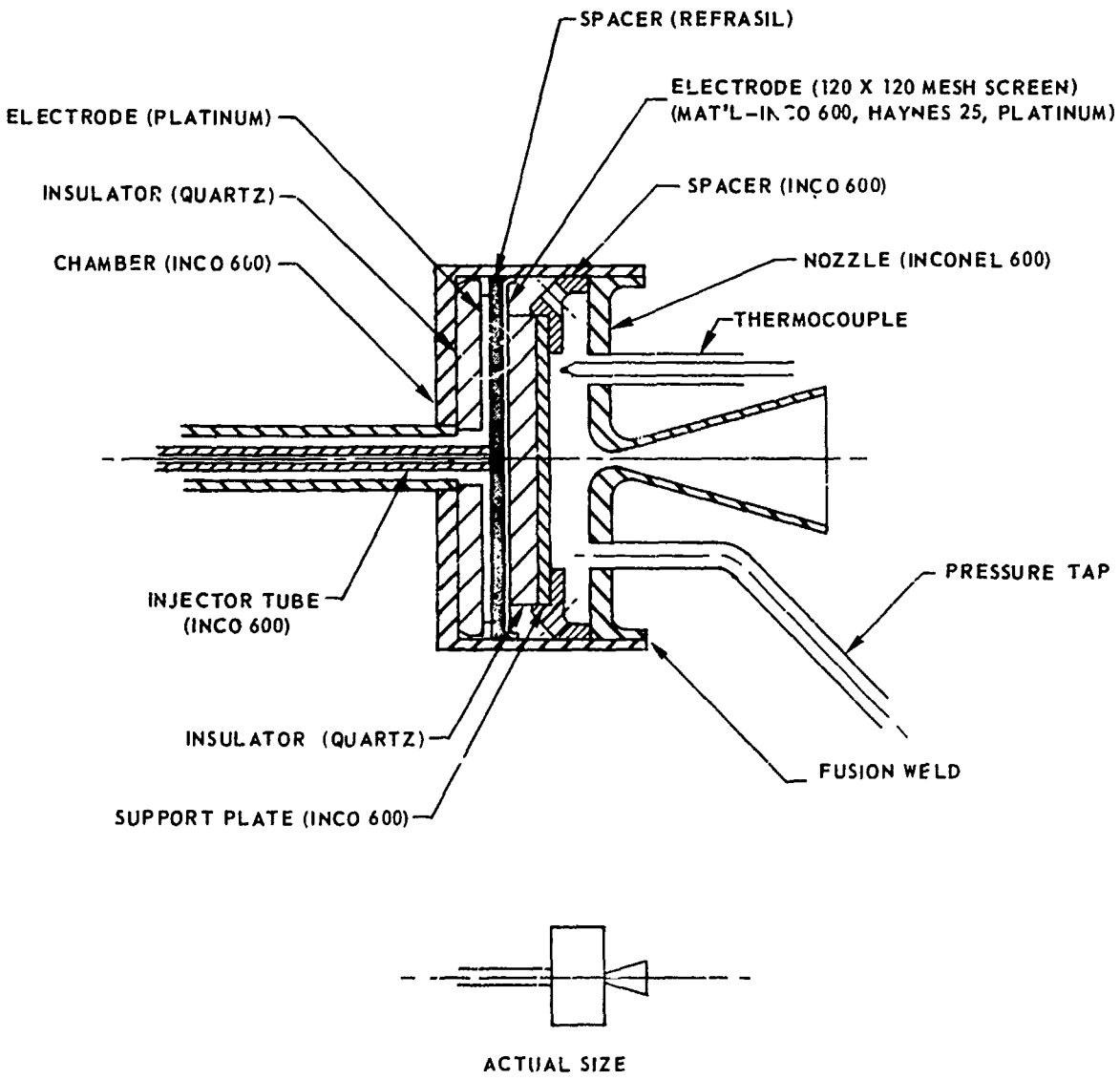

ACTUAL SIZE

FIG. 70A

MILLIPOUND THRUSTER-EXPLODED VIEW

FIG. 70 B

MILLIPOUND THRUSTER-EXPLODED VIEW

KEY

① ENGINE CHAMBER

② LOWER QUARTZ INSULATOR

③ INLET TUBE AND LOWER PLATINUM ELECTRODE (ANODE)

④ REFRASIL (GLASS) ELECTROLYTE MATRIX

⑤ RETAINER RING-QUARTZ AND UPPER PLATINUM ELECTRODE ASSEMBLY (CATHODE)

⑥ UPPER QUARTZ INSULATOR

⑦ UPPER PLATINUM ELECTRODE (CATHODE)

} ⑥, ⑦ AND RETAINING RING ARE PARTS CONSTITUTING ⑤

⑧ NOZZLE

⑨ INLET TUBE

⑩ LARGER TUBING ADAPTOR FITTED TO ⑨ TO MATCH INLET TO ID OF FITTING ⑬

⑪ LOWER PLATINUM ELECTRODE WITH HOLE FOR FUEL INLET

⑫ ALUMINA INSULATOR TO ELECTRICALLY INSULATE LOWER ELECTRODE ASSEMBLY FROM ENGINE BODY

⑬ INLET FITTING

⑭ GOLD-NICKEL BRAZING RINGS USED TO SEAL LOWER ELECTRODE AND ADAPTER ⑩ TO INLET TUBE ⑨

FIG. 71

MILLIPOUND THRUSTER

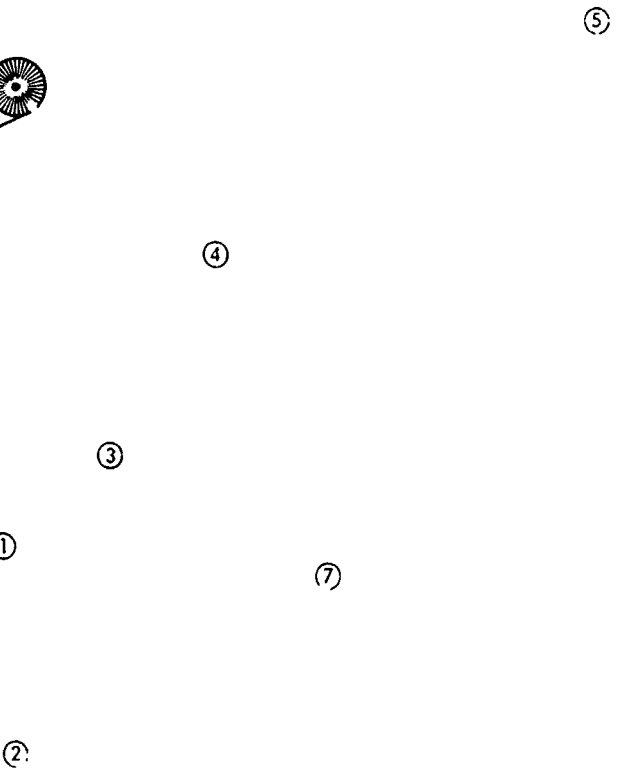

① ENGINE CASE AND NOZZLE
② INSULATED INLET
③ COMBUSTION CHAMBER THERMOCOUPLE
④ PRESSURE TAP
⑤ PRESSURE TRANSDUCER
⑥ SOLINOID VALVE
⑦ CHAMBER WALL THERMOCOUPLE

FIG 72

FIG. 73

BASE POINT PERFORMANCE DATA

ENGINE #3

(250 msec PULSES)

BASE POINT	P_C	t_{90}	t_{10}	C* (ft/sec)
#1 – 1ST PULSE	47	50	250	–
– 100TH PULSE	50	50	250	3680
#2 – 1ST PULSE	42	60	200	–
– 100TH PULSE	53	40	200	3980
#3 – 1ST PULSE	49	70	150	–
100TH PULSE	5ɔ	50	150	4330
#4 – 1ST PULSE	51	100	200	–
– 100TH PULSE	53	60	200	4060

——— 1ST PULSE

– – – 100TH PULSE

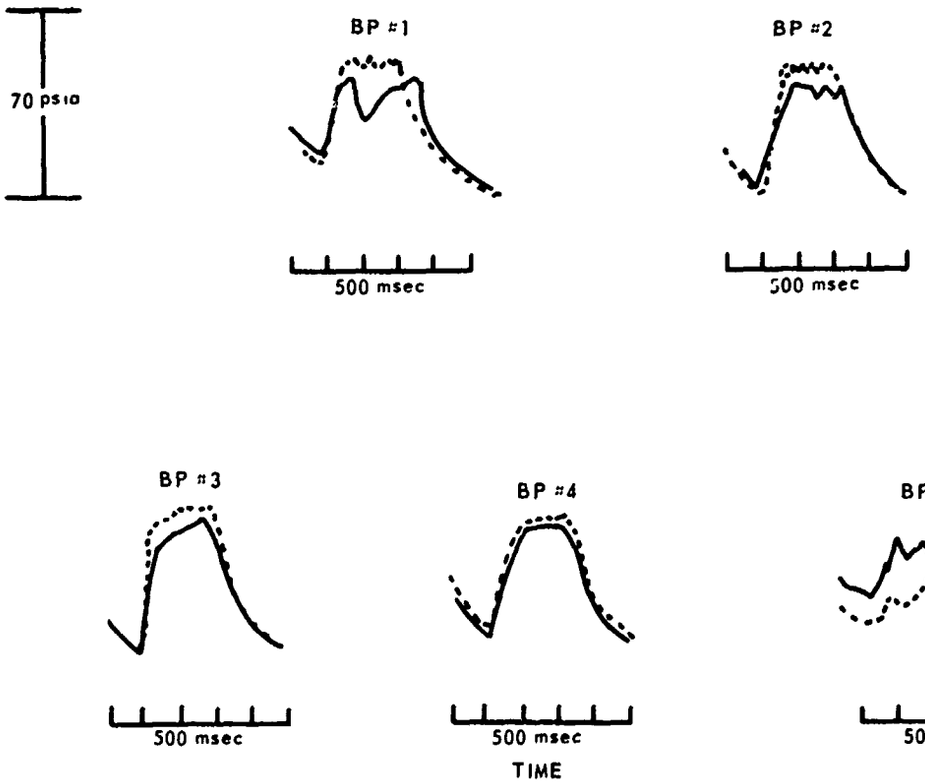

BASE POINT PERFORMANCE DATA

ENGINE #5

(250 msec PULSES)

BASE POINT	P_C (psia)	t_{90} (msec)	t_{10} (msec)	C* (ft/sec)
#1 – 1ST PULSE	48	30	250	–
– 100TH PULSE	53	30	250	3870
#2 – 1ST PULSE	49	50	250	–
– 43RD PULSE	49	50	150	3310

——— 1ST PULSE

– – – – 100TH PULSE

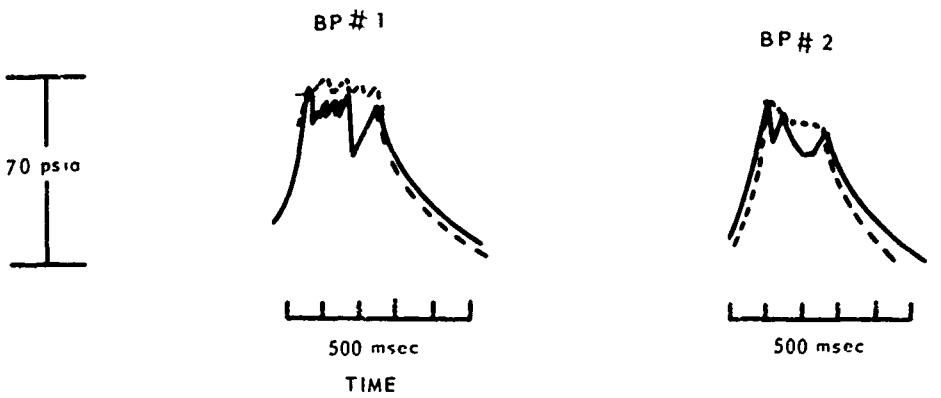

BASE POINT PERFORMANCE DATA

ENGINE #6

(250 msec PULSES)

BASE POINT	P_C (psia)	t_{90} (msec)	t_{10} (msec)	C* (ft/sec)	$\dot{\omega}$ (lbs/sec x 10^{-4})
#1 – 1ST PULSE	46	40	240	3760	1.95
– 100TH PULSE	48.5	40	260	3960	1.95
#2 – 1ST PULSE	44.5	40	170	3440	2.06
– 100TH PULSE	47.5	40	310	3670	2.06
#3 – 1ST PULSE	40	50	340	3210	1.98
– 100TH PULSE	46	50	400	3700	1.98
#4 – 1ST PULSE	43	30	160	3860	1.77
– 100TH PULSE	45.5	30	210	4090	1.77
#9 – 1ST PULSE	42	50	240	3900	1.71
– 100TH PULSE	44.5	50	180	4140	1.71